

Investigation of Cell Division Genes in *Streptomyces coelicolor*

Xiao Tan

100007765

A thesis submitted for the degree of Doctor of Philosophy

University of East Anglia

School of Biological Sciences

December 2018

This copy of the thesis has been supplied on condition that anyone who consults it is understood to recognise that its copyright rests with the author and that use of any information derived there from must be in accordance with current UK Copyright Law. In addition, any quotation or extract must include full attribution.

Abstract

Streptomyces coelicolor is a Gram-positive, filamentous, high G-C content bacterium with a complex developmental life cycle involving differentiation into distinct tissues, such as the vegetative hyphae, aerial hyphae and spores. Unlike in other bacteria, cell division in *Streptomyces coelicolor* is only required for sporulation rather than for viability. The key protein FtsZ, which assembles into Z-rings, marks the positions for future, regularly spaced septation that transforms the aerial hyphae into spores, is essential for septation during sporulation in *S. coelicolor*. The function of several genes, located between *ftsZ* (SCO2082) and *divIVA* (SCO2077) in the chromosome, have not been well characterised, despite the fact they are downstream of *ftsZ* in many Gram-positive bacteria, including *Streptomyces*. In this study we mainly focus on three genes *SCO2081*, *SCO2080*, *SCO2079* (*sepF*), located downstream of *ftsZ*. SepF was previously shown to tether the Z-ring to the membrane in *Bacillus subtilis* and promote FtsZ protofilament formation. Considering the chromosomal location, important roles in cell division or cell-wall synthesis were anticipated.

In this work, we generated knockout mutant strains by the deletion of these three genes and confirmed the mutant strains generated. We characterized the mutant phenotypes using macroscopic observations and extensive microscopic analysis focusing on possible effects on the division process and cell-wall synthesis. We also monitored the localisation of the SepF protein during development of *S. coelicolor* in order to explore its role during the Z-ring assembly and positioning. The severe defect of septum formation in the the *sepF* (SCO2079) knockout mutant suggested a key role for SepF in the early stages of cell division in *Streptomyces*, which is different to the role of the *B. subtilis* SepF in the late stages of septum formation. The gene knockouts of the surrounding genes *SCO2080* and *SCO2081* resulted in less severe, more subtle phenotype, nevertheless affecting the efficiency of septation and cell division in *Streptomyces*.

Acknowledgements

I would like to thank my supervisor Dr Gabriella Kelemen and my supervisory team members Dr Jonathan Todd and Dr Richard Bowater for their guidance and supports. Also, I am grateful to my group members Dr Michael Gillespie, Alan Lau, Sundeep Kaur Gamma Cassettari and Emily Alcock for their great helps with the laboratory work. Finally, especially thank my family who have given me love and encouragement all the time. I will never achieve this without their support. Thank my friends Sundeep Kaur, Rebecca Lo, Monika Zietek, Shiwen Liu, Yingxue Wang and my boyfriend Zhe Huang who gave me a lot of accompanies and encouragement.

Table of Contents

1 Introduction	1
1.1 Bacterial Cell Division	2
1.1.1 FtsZ and the Z-ring assembly	3
1.1.2 Regulation of Z-ring	4
1.1.2.1 Min System	5
1.1.2.2 Nucleoid Occlusion and SlmA	9
1.1.2.3 Stabilising the Z-ring	11
1.1.3 Maturation of the Z-ring	14
1.2 Bacterial Growth	16
1.2.1 Lateral growth	17
1.2.2 Polar growth	19
1.3 Chromosome segregation	22
1.4 <i>Streptomyces coelicolor</i>	23
1.4.1 Life cycle of <i>S. coelicolor</i>	25
1.4.1.1 Growth of <i>S. coelicolor</i>	27
1.4.1.2 DNA replication and segregation	30
1.4.1.3 Cell division in <i>S. coelicolor</i>	31
1.4.2 FtsZ and Septation in <i>S. coelicolor</i>	32
1.4.3 Cell division site regulation in <i>S. coelicolor</i>	35
1.4.4 Linear chromosome of <i>S. coelicolor</i>	39
2 Materials and Methods	42
2.1 Bacterial strains and plasmids	42
2.2 Media	44
2.3 Bacterial growth conditions and storage	45
2.4 General Molecular Biology Methods	47
2.5 Microscopy of <i>S. coelicolor</i>	55

3 SepF - an essential component for septum formation	56
3.1 Identification of SepF homologues in <i>S. coelicolor</i>	59
3.2 Generation of the <i>S. coelicolor sepF</i> mutant strain	68
3.3 Confirmation of the <i>S. coelicolor sepF</i> mutant strain	76
3.4 The <i>S. coelicolor sepF</i> mutant strain has a severe developmental phenotype	79
3.4.1 Analysis of the macroscopic phenotype of the <i>sepF</i> mutant strain	79
3.4.2 Analysis of the <i>sepF</i> mutant phenotype using microscopy	81
3.5 Complementation of the <i>sepF</i> mutant	87
3.5.1 Complementation using construct containing <i>sepF</i> and different upstream sequences	87
3.5.2 Complementation of the <i>sepF</i> mutant using construct <i>P-sepF</i>	95
3.6 Summary	99
4 Localisation of SepF protein <i>in vivo</i>	100
4.1 Localisation of SepF-EGFP using the knock in construct <i>sepF-egfp</i>	103
4.1.1 Generation of the knock-in construct in <i>E. coli</i>	103
4.1.2 Microscopic visualisation of SepF-EGFP in the wild-type strain	109
4.2 SepF-EGFP localisation by introducing <i>sepF-egfp</i> in trans	117
4.2.1 Generation of a <i>sepF-egfp</i> clone with a large upstream sequence including the coding region of <i>2080</i>	117
4.2.2 Complementation of the <i>sepF</i> mutant with pMS82/ <i>2080-sepF-egfp</i>	119
4.2.3 Monitoring SepF-Egfp using pMS82/ <i>2080-sepF-egfp</i>	121
4.2.4 Generation of a <i>sepF-egfp</i> clone with a shorter upstream sequence	129
4.3 Summary	137
5 Investigation of the role of <i>ftsZ</i> downstream genes, <i>SCO2080</i>	139
5.1 Bioinformatics analysis of <i>2080</i> , a putative racemase	141
5.2 Generation of the <i>2080</i> knockout mutant	146
5.3 Confirmation of the <i>2080</i> mutant	152
5.4 Analysis of the phenotype of the <i>2080</i> mutant	155
5.4.1 Macroscopic observations of the <i>2080</i> mutant	155
5.4.2 Microscopic analysis of the the <i>2080</i> mutant	157

5.5 Complementation experiments of the <i>2080</i> mutant	160
5.5.1 Complementation experiment of the <i>2080</i> mutant using constructs containing <i>2080</i> gene	160
5.5.2 Complementation experiments of the <i>2080</i> mutant using constructs containing <i>sepF</i> gene	177
5.6 Summary	185
6 Gene <i>2081</i> - Required for septation	187
6.1 Bioinformatics study of gene <i>2081</i>	188
6.2 Generation of the knockout <i>2081</i> mutant	191
6.3 Confirmation of mutant strain <i>2081</i>	196
6.4 Characterisation of the <i>2081</i> mutant phenotype	199
6.4.1 Macroscopic analysis of <i>2081</i> mutant	199
6.4.2 Microscopic analysis of <i>2081</i> mutant	200
6.4.3 Quantitative analysis of septum placement in the <i>2081</i> mutant	203
6.5 Summary	205
7 Discussion	206
References	216

1 Introduction

The bacterial cell cycle includes two major events, DNA replication and cytokinesis (septation). Studies in *E. coli* indicate that the regulatory that control these two events converge on two proteins, DnaA for DNA replication and FtsZ for cytokinesis (Figure 1.1). DnaA, which assembles into an oligomer on *oriC*, is required to unwind the DNA so that DnaB, the replicative helicase, can be loaded and the replication forks started (Bramhill and Kornberg 1988; Erzberger *et al.*, 2006). FtsZ assembles into the Z-ring, a cytoskeletal element that determines the site of

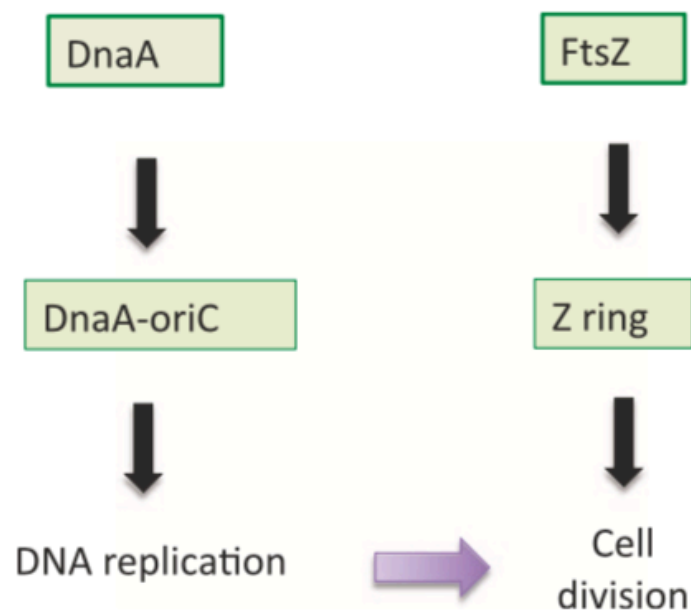


Figure 1.1. Regulatory of cell cycle control converge on two key proteins, DnaA and FtsZ. DnaA-ATP assembles on *oriC* to initiate DNA replication. FtsZ assembles into a Z ring that determines the division plane by organizing the machinery to synthesize the septum. Whereas DnaA-ATP assembles on the *oriC* template, the Z-ring does not have a landmark and is a self-organizing organelle that assembles where conditions are favorable (Lutkenhaus and Du, 2017).

cytokinesis and functions as a scaffold to recruit additional division proteins to synthesize septal peptidoglycan (PG) (Bi and Lutkenhaus, 1991). These two major events are not obligatorily coupled, since DNA replication and segregation can continue in the absence of cytokinesis (Lutkenhaus and Du, 2017).

1.1 Bacterial Cell Division

In bacteria, cells divide by binary fission which leads to physical cell separation achieved by the formation of a single septum between two replicated chromosomes at the mid-point of cells to produce two identical offsprings containing a single complete chromosome (Wu and Errington, 2012). Septum formation is driven by a macromolecular complex known as a divisome and various of bacterial cytoskeletal proteins (Adams and Errington, 2009). The divisome is assembled through the polymerisation of a key protein FtsZ, which initially localises at the mid-point of the cell to assemble protofilaments through polymerisation via head-to-tail interactions in a GTP-dependent manner (Bi and Lutkenhaus, 1991; de Boer *et al.*, 1992; RayChaudhuri and Park, 1992; Mukherjee *et al.*, 1993; Stricker *et al.* 2002; Jindal and Panda, 2013). These protofilaments are bundled together by non-uniform lateral interactions to form a ring-like structure, Z-ring (Michie *et al.*, 2006; Fu *et al.*, 2010). The Z-ring serves as a scaffold for the recruitment of other cytokinesis proteins and activates the divisome to synthesize a PG-based septum at the future division site (mostly in mid-point of cells) (Addinall and Lutkenhaus, 1996; Goehring and Beckwith, 2005; Osawa *et al.*, 2008; Adams and Errington, 2009; Egan *et al.*, 2015). The formation of the septum leads to invagination of the cytoplasmic membrane at the midpoint of the cells so that the progeny cells can separate (Lutkenhaus *et al.*, 1997; Chen *et al.*, 2005; Michie *et al.*, 2006; Gerding *et al.*, 2009; Fu *et al.*, 2010). To complete this complex process, many essential proteins are involved and an increasing number of nonessential proteins have partially overlapping functions (Goehring and Beckwith, 2005; Vicente and Rico, 2006; de Boer, 2010).

1.1.1 FtsZ and the Z-ring assembly

FtsZ has a tertiary structure that is considered to be the homologue of eukaryotic tubulin (Löwe and Amos, 1998; Nogales *et al.*, 1998). FtsZ was the first component of a prokaryotic cytoskeleton identified and consists of two globular domains, the N-terminal domain and C-terminal peptide domain (Erickson, 2001; Vaughan *et al.*, 2004). The N-terminal region contains a conserved globular core domain containing a GTP binding region and the T7 synergy loop required for GTP hydrolysis. The globular core domain is sufficient for interactions for FtsZ polymerisation. The C-terminal peptide region includes a C-terminal conserved region and a C-terminal variable region. These two regions are reported to directly interact with positive regulators of FtsZ (Rothfield, 1997; Lutkenhaus, 2012).

Assembly of the Z-ring at the division site is the earliest event in bacterial cytokinesis (Bi and Lutkenhaus, 1991). The Z-ring was the first cytoskeletal element to be described in bacteria and is assembled from FtsZ filaments formed by the polymerization of FtsZ (Ma and Margolin, 1999), the ancestral homologue of eukaryotic tubulin (Lowe and Amos 1998). It is a very dynamic structure (Chen and

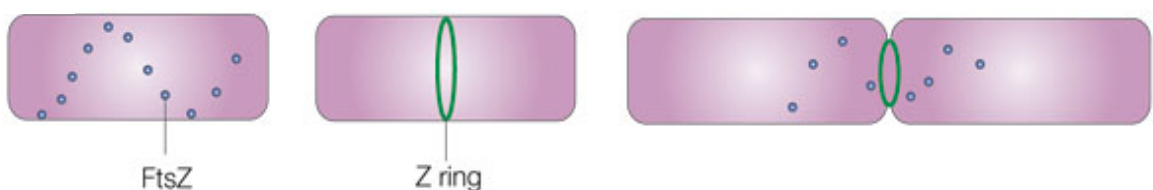


Figure 1.2. FtsZ formation in bacteria.

FtsZ initially forms spiral patterns, which eventually form the Z-ring mid-cell in a GTP dependent manner during division. The FtsZ ring contracts with the loss of FtsZ subunits from the ring as the cell divides. Taken from (Margolin, 2005)

Erickson, 2005), formed by the coalescence of FtsZ filaments attached to the membrane (Figure 1.2).

In rod-shape bacteria, such as *Escherichia coli* and *Bacillus subtilis*, FtsZ is essential for their viability. (Bi *et al.*, 1991; Wang *et al.*, 2001). The best studied example of FtsZ driving cell division is in *E.coli* where bacterial cytokinesis can be separated into three main stages (de Boer, 2010). The initial stage occurs with the assembly of a polymeric FtsZ to form a ring structure (Z-ring) at the future site of cell division (Bi and Lutkenhaus, 1991). Polymerisation of FtsZ is regulated by GTP in which filamentation occurs when FtsZ is in the GTP bound form before the polymers disassemble as GTP is hydrolysed into GDP (Erickson *et al.*, 1996). After a considerable lag, the Z-ring undergoes maturation through the recruitment of the other cell division proteins, many of which are essential, forming the complete divisome. Finally, the divisome begins to constrict concomitantly with the synthesis of a septum and splitting of septal peptidoglycan, resulting in invagination and division of the bacteria into two daughter cells (Gerding *et al.*, 2009; Goley *et al.*, 2011).

1.1.2 Regulating of Z-ring

The regulatory processes that act upon the Z-ring can be separated into two categories: the proteins that positively regulate Z-ring formation helping formation and tethering of the Z-ring onto membrane, and the negative regulators, such as the Min system and Nucleoid occlusion system that inhibit Z-ring formation near the poles or over chromosomes (Huang *et al.*, 2013). The positioning of FtsZ at future cell division site is negatively regulated by two distinct systems, Min system and nucleoid occlusion system (Adams and Errington, 2009; Harry *et al.*, 2006; Barák and Wilkinson, 2007; Wu and Errington, 2012).

1.1.2.1 Min System

The spatial regulation to ensure that the Z-ring is assembled at mid-cell, between segregated chromosomes is essential for cell division (Lutkenhaus, 2007). The Min system spatially regulates Z-ring positioning by an oscillation mechanism which limits FtsZ polymerisation in the cell poles. Absence of the Min system in *E.coli* leads to an increase in the frequency of Z-ring formation near the pole of cells and thus the formation of mini-cells lacking chromosomes. In *E. coli*, Min system consists of three cooperating proteins MinC, MinD and MinE, which cooperate to dominate FtsZ placement (Wu, 2011; Margolin, 2001). MinC is an antagonist of FtsZ assembly, which inhibits lateral interactions between FtsZ filaments which are crucial for the assembly of the Z ring and for its structural integrity. MinC is recruited to the membrane by a membrane-associated ATPase, MinD, which binds to the membrane by its C-terminus when bound to ATP (Barak and Wilkinson, 2007; Wu and Errington, 2012). MinD is evenly distributed on the membrane where it activates MinC inhibiting FtsZ polymerization close to the cell poles (De Boer *et al.*, 1989; Hu *et al.*, 1999; Raskin and De Boer 1999). This MinCD complex is regulated by MinE, which can allocate the Z-ring assembled at the mid-point of cell through its ability to stimulate the ATPase activity of MinD and the release of MinD from the membrane (Hu *et al.*, 2002; Shih *et al.*, 2003).

This system is not static and the Min proteins rapidly oscillate between the poles of the cell to dominate Z-ring forming at mid-point of cell (Meinhardt and De Boer, 2001). Pole to pole oscillation of Min system ensures that there is an increase in the concentration of the MinCD complex at cell poles in a time dependent manner and results in lower concentrations of the complex at mid-cell where cell division takes place (Dajkovic *et al.*, 2008). To establish this oscillation, MinD and MinC accumulate at one pole and are flanked by a MinE ring. As this ring moves closer to the pole, MinC and MinD are released and they re-assemble at the other pole, flanked again by a MinE ring (Fu *et al.*, 2001; Hale *et al.*, 2001) (Figure 1.3).

In *B. subtilis*, MinC and MinD proteins were identified by sequence homology to their *E. coli* counterparts (Levin *et al.*, 1992). The *B. subtilis* Min system is now known to consist of at least four proteins: MinC, MinD, MinJ and DivIVA (Figure 1.4). MinD localisation is not achieved by oscillation but rather through static localization to the poles of cell and newly synthesised division septa via the polar marking protein DivIVA. Like in *E. coli*, inhibition of FtsZ polymerisation at poles is carried out by MinC which is activated in an ATP dependent mechanism by MinD associated with the membrane bound MinD ATPase (Karoui and Errington, 2001; Barak and Wilkinson, 2007; Wu and Errington, 2012). However, while ATP binding is important for MinD activity, no regulatory mechanism for the ATPase activity of MinD, such as MinE in *E. coli*, has been shown in *B. subtilis*. Localisation of MinD to the pole is dependent on the localisation of DivIVA facilitated by the intermediary protein MinJ, which interacts with both DivIVA and MinD (Patrick and Kearns, 2008). While it was originally thought that localisation of DivIVA to the site of division was due to an interaction with the maturing divisome complex, it has instead been shown that this localisation is due to the initial constriction of the membrane during septum formation which generates the negative curvature that localises DivIVA (Ramamurthi and Losick, 2009; Ramamurthi and Losick, 2009; Eswaramoorthy *et al.*, 2011). Localisation of MinCD to the site of septum formation prevents any aberrant secondary FtsZ rings from forming close to the mid cell during or after division. *E. coli* lacks counterparts of the MinJ and DivIVA proteins and instead uses an amazing oscillating MinCD mechanism to prevent division at the cell poles (Lutkenhaus 2007).

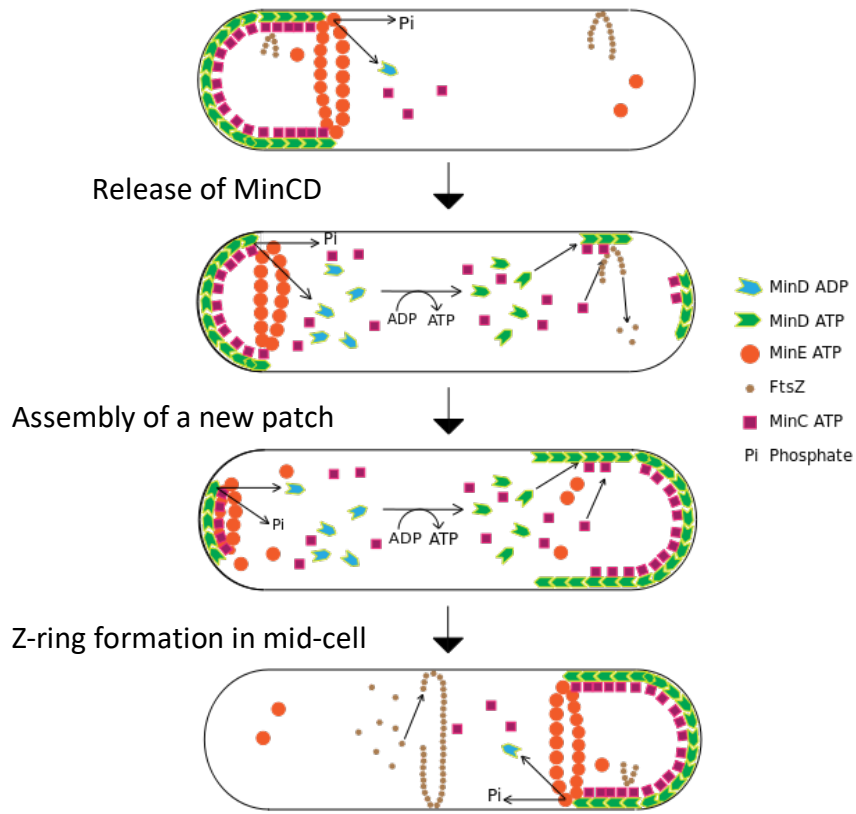


Figure 1.3. Inhibition of polar cell-division events by the Min system in *E. coli*. MinD, bound to the cell division inhibitor MinC, assembles on the cytoplasmic membrane, forming a cap-like polymeric layer that prevents FtsZ ring formation in the polar region of the cell. MinE is organized into a ring-shaped structure that gradually displaces MinCD from the membrane. Free MinC and MinD subunits reassemble at the opposite cell pole, thus establishing a new polar cap and restarting the cycle.

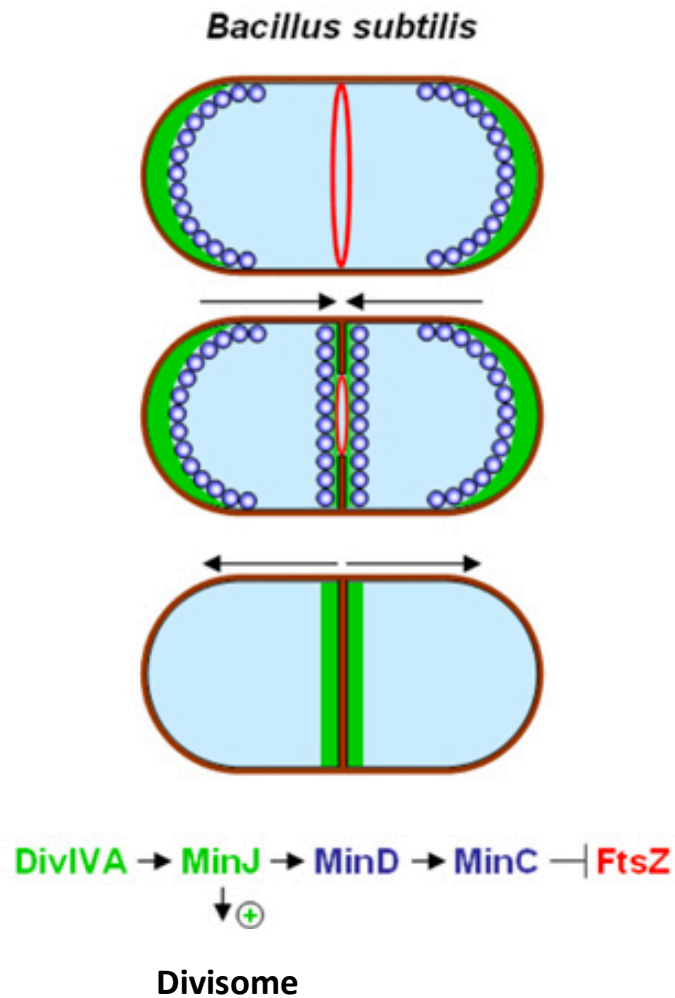


Figure 1.4. MinD localisation in *B. subtilis*.

In *B. subtilis*, MinD is statically localised to the pole by the polar localising protein DivIVA which recruits the intermediary MinJ. MinD then recruits MinC to the poles which inhibits FtsZ polymerisation at the poles. MinD is also localised to the mid-cell once the division membrane starts to form. This prevents secondary division events from occurring mid-cell. Image courtesy of Dr Marc Bramkamp.

Although Min system has a significantly effect on spatial control of assembly of Z-ring, other factors which makes positioning more accurate and precise in nucleated cells are important as well. The nuclear occlusion system, which prevents the formation of the Z-ring over the nucleoid, Noc (in *B.subtilis*) or SlmA (in *E.coli*), displays similar localization patterns, binding to the nucleoid with highest

concentration at the pole in cell (Wu and Errington, 2004; Bernhardt and de Boer, 2005). The absence of the Noc or SImA leads to the formation of septa in unsegregated cells.

1.1.2.2 Nucleoid occlusion and SImA

A variety of mechanisms prevent assembly of FtsZ filaments in the wrong places, to ensure positioning of the Z-ring on the membrane at mid-cell and also to help coordinate cell division with chromosome segregation. The negative regulators of FtsZ that we have discussed so far are involved in promoting mid-cell location of the FtsZ ring. While this is important, within itself it does not protect the chromosome from being guillotined during the formation of the septum. In fact, even chromosome segregation would not be enough to prevent this as usually the terminator region of the DNA is found within the closing septa and DNA translocases are required to transport these ends into the correct compartment before the septa fully closes (Touzain *et al.*, 2011). Actually, a long-standing observation in bacterial cell biology is that cytokinesis over the nucleoid, which would result in guillotining of the chromosome, is rarely observed (Woldringh *et al.*, 1990). To ensure that chromosomes are not guillotined during cell division, bacteria have developed the nucleoid occlusion mechanism exerted a negative effect on Z-ring assembly over the nucleoid (Figure 1.5) (Yu and Margolin, 1999; Hajduk *et al.*, 2016). This mechanism inhibits FtsZ ring formation from occurring over the DNA, and so far two proteins, SmlA in *E. coli* and Noc in *B. subtilis*, have been implicated in this system (Wu and Errington, 2004). In *E. coli*, the nucleoid occlusion factor SImA, interacts directly with FtsZ on the surface of each nucleoid, specially inhibits Z ring assembly nearby and thus protects the nucleoid from being bisected (Cho *et al.*, 2011; Tonthat *et al.*, 2013). In *B. subtilis*, however, the nucleoid occlusion protein Noc is functionally analogous but does not interact directly with FtsZ (Adams *et al.*, 2015).

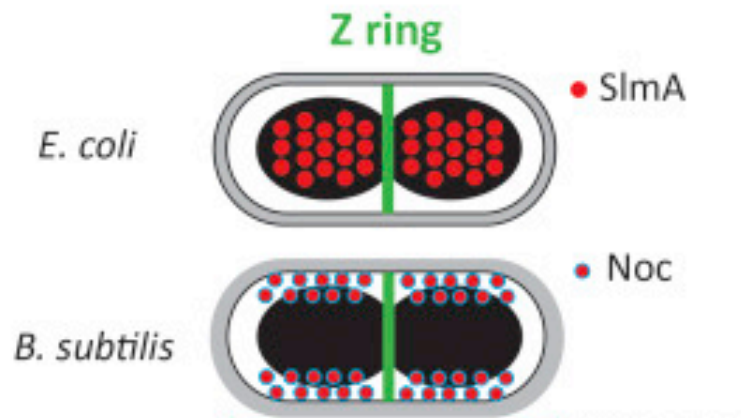


Figure 1.5. Nucleoid occlusion.

The nucleoid occlusion proteins SmlA (*E. coli*) and Noc (*B. subtilis*) inhibit FtsZ-ring formation from occurring over the chromosome. Taken from (Hajduk *et al.*, 2016).

While there is no sequence homology between these two proteins, with SmlA having no homologues of known function and Noc belonging to the ParB family of proteins with 40% identity to Spo0J, both proteins share similar characteristics (Sievers *et al.*, 2002). They both bind to specific region of the chromosome, SmlA binding sites (SBS) and Noc binding sites (NBS), which are distributed around the chromosome everywhere except for the region surrounding the terminus (Cho *et al.*, 2011; Wu *et al.*, 2009; Du and Lutkenhaus, 2014). The binding pattern of these two proteins would support the idea that as the chromosomes are segregated during division, a process driven from the origin, the areas covered by these nucleoid occlusion proteins would vacate the mid-cell first, leaving the uncoated terminal regions at the site of division. FtsZ can then form over this uncoated terminal region of the chromosome and begin the process of septum formation. Then, as mentioned, the terminus region of the chromosome can be removed from the closing septum by DNA translocases (Wu and Errington, 2004).

In *E. coli*, there are two proposed models for the action of SmlA. The first suggestion is that when SmlA binds to SBS sites around the chromosome, SmlA is able to bind to the C-terminal tail of FtsZ where it competes for binding with the other

regulatory proteins of FtsZ, such as ZapD, MinC, FtsA and even other FtsZ molecules. This would not only promote further interactions of SmlA with FtsZ but eventually lead to the breakdown of FtsZ protofilaments (Du and Lutkenhaus, 2014). The second suggestion is that SmlA spreads along DNA as a dimer of dimers forming higher order nucleoprotein complexes which sequester FtsZ preventing its formation into Z-Rings (Tonthat *et al.*, 2013). Both of these models would indicate a negative regulation of FtsZ polymerisation that is independent of the GTPase activity of FtsZ (Cabre *et al.*, 2015). In contrast to SmlA, Noc is not thought to have any direct interaction with FtsZ. Instead, Noc acts by binding the chromosome to the membrane along the lateral wall and physically occupying the space that FtsZ requires in order to polymerise into the Z ring (Adams *et al.*, 2015). Noc is a site-specific DNA-binding protein with recognition sites (NBS) distributed all over the chromosome, except in the replication terminus region, where binding sites are scarce (Wu and Errington, 2004; Wu *et al.*, 2009).

1.1.2.3 Stabilising the Z-ring

Positive regulators of the Z-ring consist of proteins that actively promote stabilisation of the Z-ring and anchor it to the membrane at sites of future cell division. Gram-negative bacteria, such as *E. coli*, achieve this through the presence of one of the two trans-membrane proteins FtsA and ZipA both of which interact directly on FtsZ and provide the membrane connection necessary to complete division (Pichoff and Lutkenhaus, 2002). These two proteins interact at the earliest stage of Z-ring formation and are essential for recruitment of the next set of proteins of divisome (Pichoff and Lutkenhaus, 2005).

While ZipA is only found among Gram-negative bacteria, FtsA homologues are also found among numerous Gram-positive bacteria. In fact besides FtsZ, FtsA is the most widely conserved member of the divisome found across bacteria (Haeusser and Margolin, 2016). FtsA is an actin-like protein and able to form actin-like

protofilaments (Szwedziak *et al.*, 2012). It links FtsZ filaments to the plasma membrane and also to the other components of the divisome in many bacteria, although other FtsZ membrane anchors exist (Haeusser and Margolin, 2016). FtsA is known to interact with a number of proteins encoded by genes that are located downstream of *ftsA* (Karimova *et al.*, 2005). In *E. coli*, Z-ring can form with either FtsA or ZipA providing the membrane connection (Pichoff and Lutkenhaus, 2002).

Of these two proteins, FtsA plays a more important role in divisome assembly, since mutations in *ftsA* can bypass ZipA (Geissler *et al.*, 2003). The *ftsA* mutations that bypass ZipA were found to reduce the ability of FtsA to self-interact, therefore it led to a model in which FtsA monomer are the form of FtsA active in the recruitment of the downstream proteins (Pichoff *et al.*, 2012). In *E. coli*, ZipA has some overlapping functions with FtsA in tethering the Z-ring to the membrane. ZipA interacts with FtsZ at the C-terminus of ZipA, while the N-terminus contains a membrane embedded domain which helps to anchor the Z-ring, reinforcing its placement (Ohashi *et al.*, 2002; Pichoff and Lutkenhaus, 2002). However, in mutant strains with depleted ZipA filaments, Z-rings, while still being able to assemble, do so less frequently and more variably than wild-type *E. coli* (Hale and de Boer, 1999).

In *B. subtilis*, FtsA was identified by its conserved location immediately upstream of and adjacent to FtsZ (Beall *et al.*, 1988). Unlike *E. coli*, *ftsA* mutants of *B. subtilis* are viable, though they are substantially deficient in division (Beall and Lutkenhaus, 1992). The *ftsA* mutations demonstrate a loss of function suggesting that polymerisation is required for the recruitment of divisome related proteins encoded by genes that are located downstream of *ftsA* (Szwedziak *et al.*, 2012). This has led to uncertainty as to the exact role of FtsA polymerisation in cytokinesis, particularly surrounding its mechanism for recruiting other proteins to the divisome (Huang *et al.*, 2013). In addition, due to lack of ZipA homologues in *B. subtilis*, SepF partially carried out the role of ZipA. Ishikawa *et al.* (2006) detected the formation of a SepF-SepF self-interaction and SepF interaction with FtsZ using yeast 2-hybrid experiments. Meanwhile, Hamoen *et al.* (2006) identified *sepF* as a candidate cell division gene from its conserved position (in Gram-positive bacteria) between *ftsZ* and *divIVA* and

found that deletion of *sepF* gene resulted in cell defects and aberrant septum formation (Hamoen *et al.*, 2006; Ishikawa *et al.*, 2006). In addition, overexpression of SepF counters division defects seen in *ftsA* mutants, indicating an overlapping of function, while *ftsA-sepF* double mutants are synthetically lethal and are unable to form Z-rings (Ishikawa *et al.*, 2006). SepF localises to the division site in *B. subtilis*, which is dependent upon its interaction with FtsZ (Hamoen *et al.*, 2006; Ishikawa *et al.*, 2006). It is essential for correct septum formation with *sepF*-depletion strains, showing a deformed septum which does not fully close (Hamoen *et al.*, 2006). Recent data suggests that SepF promotes the correct formation of FtsZ polymers required for proper cell division (Gundogdu *et al.*, 2011). As demonstrated by transmission electron microscopy (TEM), SepF *in vitro* assemble into large rings with a diameter of 50 nm. These rings are able to bundle FtsZ protofilaments into long tubular structures (Figure 1.6). This suggests that SepF rings act to bundle FtsZ protofilaments probably to aid in the formation of the FtsZ rings (Gundogdu *et al.*, 2011).



Figure 1.6. SepF bundling of FtsZ protofilaments.

SepF rings (red) bundle FtsZ protofilaments (grey) in order to help promote FtsZ- ring formation. Taken from (Gundogdu *et al.*, 2011)

1.1.3 Maturation of the Z-Ring

Once the FtsZ ring has been successfully formed and tethered to the membrane at the division site, maturation of the ring can begin. In the two most widely studied bacteria, *E. coli* and *B. subtilis*, maturation of the Z-ring occurs in a slightly different fashion, although with many of the same proteins being involved. In *E. coli* this is a linear process whereby each protein or protein complex is required to be localised before the next protein can be localised (Figure 1.7). In *B. subtilis* however, divisome formation could be considered to be a two stage process in which stabilisation of the Z-ring occurs, after which the proteins responsible for maturation all localise interdependently forming the divisome (Harry *et al.*, 2006).

In *E. coli* the first protein recruited to the FtsZ ring after it is tethered to the membrane is the DNA translocase protein FtsK, which is conserved across bacteria (Margolin, 2000). FtsK is involved in cell division through the recruitment of the next protein required for maturation and in chromosome segregation. At the same time the C-terminus of the protein has been implicated in the resolution of sister chromosomes into their respective daughter cells thus linking both cell division and chromosome segregation (Aussel *et al.*, 2002; Bigot *et al.*, 2004). The *B. subtilis* homologue of FtsK, SpoIIIE has thus far only been found to play a role in DNA translocation during sporulation (Sharp and Pogliano, 2003).

Post FtsK localisation in *E. coli* the next proteins involved in Z-ring maturation are FtsQ, FtsL and FtsB, which form a protein complex, and as shown using co-immunoprecipitation of FLAG-tagged proteins, formation of the FtsQLB complex occurs prior to septal localization (Buddelmeijer and Beckwith, 2004). These are represented in *B. subtilis* by the homologues DivIB, FtsL and DivIC respectively. All of these proteins are very similar in structure with a short cytoplasmic region, a single transmembrane segment, and a larger periplasmic domain. Although the function of FtsQ/DivIB is unknown, crystal structure data reveals that it has an α -domain with similarity to polypeptide transport-associated domains (van den Ent *et al.*, 2008) and

is essential for cell survival in *E. coli* (Storts *et al.*, 1989) but only at high temperatures in *B. subtilis* (Beall and Lutkenhaus, 1992; Katis *et al.*, 2000). Further data on FtsL suggests that it may play a role in regulating Z-ring constriction in *B. subtilis* through recruitment regulation of later acting division proteins to allow constriction (Kawai and Ogasawara, 2006). FtsB/DivIC are known to be essential genes for cell survival in their respective bacteria, although their function is still unknown (Buddelmeijer and Beckwith, 2004; Levin and Losick, 1994).

The next protein recruited to the divisome in *E. coli* is FtsW which is a transporter of lipid-linked precursors for peptidoglycan synthesis, such as lipid II, across the membrane (Mohammadi *et al.*, 2011). FtsI and its homologue PBP2B (Penicillin-Binding Protein 2B) are both located just downstream of *ftsW* in their respective organisms. They are involved in the final stages of PG synthesis and were identified through their ability to bind penicillins (Goffin and Ghuyssen, 1998). FtsN is not a well-conserved protein and is only found in enteric bacteria and *Haemophilus spp.* (Errington, 2003). In *E. coli*, FtsN localises in a ring pattern at the septum late in the division cycle. It is an essential gene with depletion mutants losing viability after forming long filaments (Dai *et al.*, 1993). More recent data has suggested that it interacts with PBPIB (Penicillin Binding Protein 1B), stimulating its murein synthesis activity (Muller *et al.*, 2007; Ursinus *et al.*, 2004). The final protein localised to the maturing Z-ring in *E. coli* is the amidase AmiC, an enzyme involved in cleaving murein crosslinks, which is required for septal cell wall degradation and hence cell separation (Bernhardt and de Boer, 2003; Weiss, 2004).

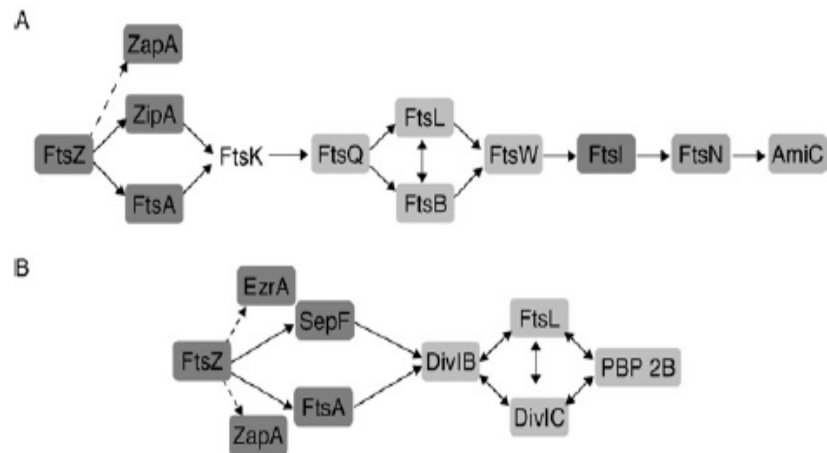


Figure 1.7. Stabilisation and maturation of the Z-ring.

After stabilisation of the Z-ring with the localisation of FtsZ, FtsA, ZipA and SepF the Z-ring undergoes maturation. (A) In *E. coli* this is a linear process where the recruitment of proteins is sequential and dependent upon localisation of the previous protein. (B) In *B. subtilis* maturation is a single step process whereby all proteins required for maturation localise concurrently in an interdependent manner (Harry *et al.*, 2006).

1.2 Bacterial Growth

Beside the most common site of growth that occurs during cell division at mid-cell driven by FtsZ (Carballido-Lopez and Errington, 2003; Cabeen and Jacobs-Wagner, 2005). There are another two mechanisms of growth both contributing to bacterial cell elongation for their shape. The first one is the lateral growth that occurs along the lateral wall, found in *B. subtilis* and *E. coil*. This is driven by MreB, the bacterial homologue of eukaryotic actin. The second mechanism of bacterial growth found mainly in *Actinomycetes*, is polar growth which occurs at the poles. This form of growth is driven by DivIVA, a protein that currently is not currently considered to

be a homologue of any class of eukaryotic protein (Flardh, 2003a). After growth in both lateral and polar locations, rod-shape bacteria then undergo the same FtsZ-dependent division event (Cabeen and Jacobs-Wagner, 2005).

1.2.1 Lateral growth

For lateral growth of bacteria, one of the first proteins identified to contribute to this mode of growth are the MreB proteins, which were first described in *E. coli* and *B. subtilis* (Levin *et al.*, 1992; Wachi *et al.*, 1987). The distribution of these proteins correlates to the shape of the organism, with most rod shape bacteria containing at least one MreB homologue, while the vast majority of spherical bacteria lack a homologue of this protein (Cabre *et al.*, 2015; Daniel and Errington, 2003). Across most bacteria containing an MreB homologue, the gene encoding this protein is found in a gene operon containing *mreC* and *mreD*, creating the *mreBCD* operon (Carballido-Lopez and Errington, 2003; Doi *et al.*, 1988; Levin *et al.*, 1992; Varley and Stewart, 1992). The role of these other genes in the operon are yet to be determined although, in *E. coli*, they are required for correct localisation of MreB and are assumed to form a complex with MreB based upon interactions between all three proteins, MreB, MreC and MreD (Kruse *et al.*, 2005). Further searches for homologues of MreB have thus far revealed that some bacteria contain multiple MreB proteins with two, Mbl (MreB-like) and MrebH (MreB homologue), being found in *B. subtilis* (Jones *et al.*, 2001; Varley and Stewart, 1992). Studies on these proteins have shown that all are required to form a rod shape. However, the effect on shape of the absence of each protein is unique, suggesting that they interact with different components of the cell wall synthesis machinery (Carballido-Lopez *et al.*, 2006; Defeu Soufo and Graumann, 2006; Dominguez-Cuevas *et al.*, 2013; Kawai *et al.*, 2009). Initial localisation of MreB and Mbl, using immunofluorescence of an epitope-tagged MreB and detection of Mbl-GFP fusion, in *B. subtilis* revealed that they form helical filaments that wrap around the cell wall longitudinally from pole to pole (Jones *et al.*,

2001). This localisation pattern suggested that the proteins had an actin-like function within bacteria which was confirmed when the structure of MreB was solved and found to be a structural homologue of the eukaryotic actin (van den Ent *et al.*, 2001a; van den Ent *et al.*, 2001b). Localisation of the sites of cell wall insertion in *B. subtilis* showed that this also occurs in a helical pattern suggesting that MreB proteins contribute to the control of location of cell wall synthesis in bacteria (Daniel and Errington, 2003). The initial localisation pattern of these proteins were challenged by data observing MreB filaments using electron cryotomography (ECT) which suggested that in fact MreB localises as discrete disconnected patches that follow a helical path through the cell and are moved through coupling to the cell wall synthetic machinery (Dominguez-Escobar *et al.*, 2011; Garner *et al.*, 2011; Swulius *et al.*, 2011; van Teeffelen *et al.*, 2011). More recently, data observing MreB *in vitro* has tilted the model of MreB localisation back towards the initial helical filaments. MreB has been shown to form antiparallel filaments that interact extensively with membranes (Salje *et al.*, 2011; van den Ent *et al.*, 2014). In addition, observations of MreB localisation using high-end microscopy methods such as structured illumination microscopy (3D-Sim) have shown helical filaments once again in actively grown cells (Olshausen *et al.*, 2013; Reimold *et al.*, 2013). All of this data leads to the current suggested model (Figure 1.8) in which MreB filaments associate to the membrane and elongate upon a uniform and favourable cylindrical shape, where they recruit multiple cell wall synthetic complexes. These complexes create new peptidoglycan strands which are guided by the motion of the MreB helices (Errington, 2015).

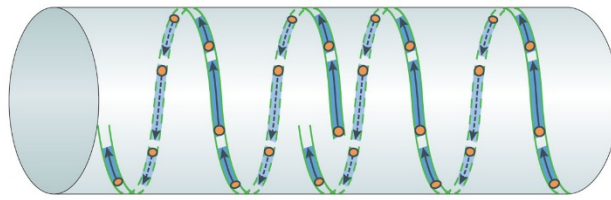


Figure 1.8. Model for the role of MreB in shape determination

MreB filaments (solid and dashed lines) elongate along the cell wall due to the cylindrical shape of the bacteria. The filaments are able to recruit peptidoglycan synthetic complexes (orange circles) which in turn generate new peptidoglycan strands. Taken from (Errington, 2015).

1.2.2 Polar growth

While lateral growth is the predominant form of growth in the bacteria that have thus far been characterised, a significant number of bacteria exhibit an alternative form of growth – polar growth. This mode of growth is especially prevalent in the Gram-positive Actinobacteria and the Gram-negative *Rhizobium* and *Agrobacterium* genera (Brown *et al.*, 2012; Daniel and Errington, 2003). The first protein implicated in driving polar growth was DivIVA, which was found in both *S. coelicolor* and *Brevibacterium lactofermentum* and is an essential protein (Flardh, 2003a; Ramos *et al.*, 2003). Homologues of DivIVA have since been shown to be essential for growth in other Actinobacteria, including the pathogenic *Mycobacterium tuberculosis* (Kang *et al.*, 2008; Nguyen *et al.*, 2007). DivIVA was originally identified in *B. subtilis*, where it plays a role in division (Cha and Stewart, 1997). In this organism, DivIVA is located to the poles where it recruits MinD via the intermediary protein MinJ (Patrick and Kearns, 2008). As I will discuss later, MinD is part of the septum-site determining Min system (Margolin, 2001). As DivIVA in *S. coelicolor* was identified due to its homology

with the division associated DivIVA protein from *B. subtilis*, it was named accordingly (Cha and Stewart, 1997; Flardh, 2003a). Although DivIVA has two functions in different bacteria e.g. division in *B. subtilis* and growth in *S. coelicolor*, in all cases the protein is localised to the poles (Flardh, 2003a; Marston *et al.*, 1998). This suggests that DivIVA homologues all share similar characteristics from which bacteria has adapted their function whether in growth or division. In *Actinobacteria*, DivIVA is thought to localise key components of the cell wall synthesis machinery and has been shown to make direct contact with penicillin-binding protein 3 (PBP3) in *Mycobacterium* (Mukherjee *et al.*, 2009). Interestingly, while partial complementation of the *divIVA* null mutant in *Corynebacterium glutamicum* by DivIVA homologues from other *Actinobacteria* was possible, DivIVA homologues from the *Firmicutes*, such as *B. subtilis*, failed to sustain viability in *C. glutamicum* suggesting an evolutionary divergence among DivIVA homologues (Letek *et al.*, 2008). More recently the use of super-resolution microscopy has suggested that in *Mycobacterium* growth is not occurring right at the tip, but at a sub-polar location that is just behind the pole (Meniche *et al.*, 2014). It remains to be seen whether sub polar growth is a feature of all bacteria that show polar growth or is specific to *Mycobacteria* and most likely other *Actinobacteria*. While DivIVA has been implicated in numerous *Actinobacteria* in driving growth, there are no homologues of DivIVA found in Gram-negative bacteria (Oliva *et al.*, 2010). Thus far in Gram-negative bacteria that exhibit polar growth, there is no mechanism identified that controls polar growth (Oliva *et al.*, 2010). Across bacteria that have polar growth there is great diversity in how growth at different poles is regulated to produce a variety of shapes and nuances to growth (Figure 1.9), with the filamentous *Streptomyces*, the bi-directional growth of *Corynebacterium*, the asymmetrical bi directional growth of *Mycobacterium* and the uni-directional growth of *Agrobacterium* (Aldridge *et al.*, 2012; Allan and Pearce, 1983; Brown *et al.*, 2012; Meniche *et al.*, 2014; Sieger *et al.*, 2013).

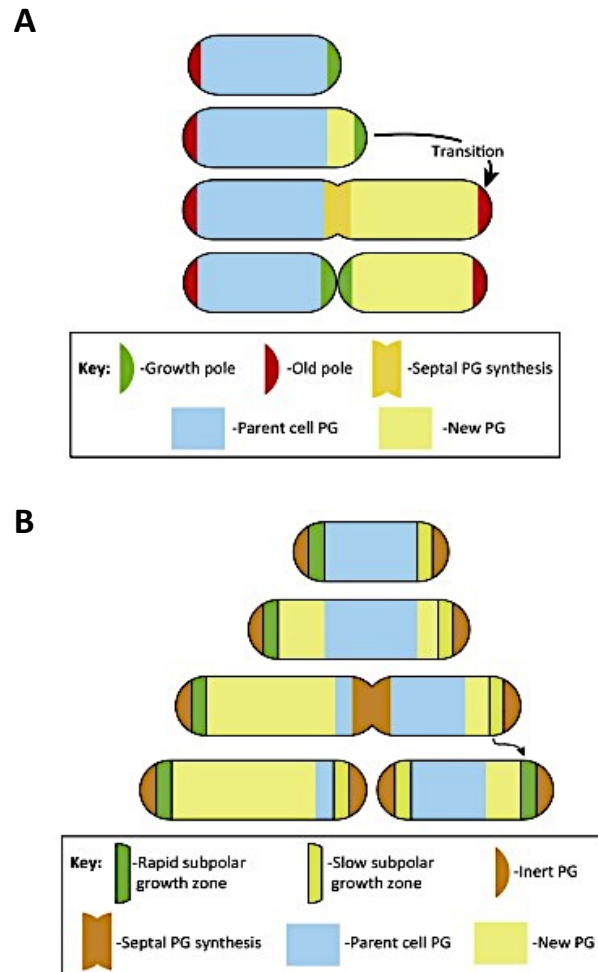


Figure 1.9. Polar growth in bacteria.

Bacteria that exhibit polar growth do so in a variety of mechanisms such as in (A) *Agrobacterium* where only the newly generated cell pole grows during the next cell cycle (unidirectional growth) and (B) *Mycobacterium*, where there is slower growth at the newly generated cell pole compared to the rate of growth seen at the old pole (bi-directional asymmetric growth). Taken from (Cameron *et al.*, 2015).

1.3 Chromosome segregation

So far, we have discussed the importance of FtsZ in the formation of bacterial septa as well as the process that cells use to create a stable Z-ring that will allow division to occur. While septum formation is important for generating progeny, in itself it is not sufficient to in generating identical progeny. To achieve identical progeny two events must be coordinated, the segregation of chromosomes and placement of the septa mid cell such that the chromosomes are not guillotined during division. Given the coordination required between these two processes in order that efficient division can occur, it is not surprising that both of these processes are performed by a single superfamily of proteins; the ParA/MinD superfamily (Lutkenhaus, 2012). Beyond the obvious functional similarity of this family, all ParA/MinD proteins share a deviant walker ATPase motif characterised by the amino acid sequence GXGGXHKTS, which is located within a nucleotide-binding P-loop near the N-terminus of the protein (Koonin, 1993). This superfamily can broadly be assigned to two subgroups based upon the function of the individual protein (Lutkenhaus, 2012). That is, those involved in chromosome segregation, the Par proteins, and those involved in septum positioning, the Min proteins (Lutkenhaus, 2012). Even within these subgroups we find enormous diversity in how mechanistically the proteins carry out their function. This is likely to be due to the unique environmental factors that different bacteria have been exposed to, which has given rise through evolution to adaptations that increase the reproductive fitness of the bacteria. While this is clearly the case, we have very limited understanding of why these different mechanistic processes developed (Lutkenhaus, 2012).

In order for viable daughter cells to be produced during cell division, correct segregation of the chromosome prior to construction of the Z-Ring is essential. Originally it was thought that the chromosome was tethered to the cell membrane and segregation driven by cellular elongation, dragging the chromosome into the daughter cell (Jacob and Brenner, 1963). However, with advances in understanding,

that cell elongation occurs throughout the cell and the inability of cell growth to match the speed at which chromosomes move in the cell, it became clear that a different regulatory system was responsible (Nanninga, 1998; Viollier *et al.*, 2004). The first system of protein driven DNA segregation in bacteria came with the discovery of the Type 1 plasmid partitioning system. This plasmid partitioning system, which has been most widely studied in *E. coli*, generally consists of three components, a cis-acting centromeric DNA site; either *parS* or *parC*, a Walker Box ATPase; ParA or ParA-like protein, and a DNA binding; ParB or SopB (Davis *et al.*, 1992; Ebersbach and Gerdes, 2001; Mori *et al.*, 1989; Viollier *et al.*, 2004; Watanabe *et al.*, 1989). The ParAB system is built upon several characteristics, which appear to be present in all of these systems characterised thus far, and defines the ParA subfamily of proteins. The ParA protein in these systems is a very weak ATPase whose activity is upregulated through interaction with the ParB protein. This interaction requires the presence of ATP bound form of ParA, with ParA mutants deficient for ATP binding unable to interact with ParB. The ParA forms a dimer in the presence of ATP and a monomer after hydrolysis of ATP has occurred. This creates a mechanism by which dimerisation or oligomerisation of ParA is regulated by the presence of ParB.

1.4 *Streptomyces coelicolor*

After discussing the proteins which provide the mechanism for the bacterial life cycle we will now turn our attention to introducing *Streptomyces coelicolor*, a model organism for filamentous growth from the *Actinobacteria* phylum and the subject organism of this study.

S. coelicolor is a high G-C content, Gram-positive, soil dwelling, filamentous bacterium, which belongs to a genus of the phylum *Actinobacteria*. It is a good model organism for a genus that produces many biologically active secondary metabolites including antibiotics, anticancer agents and immunosuppressants, as well as

industrial enzymes (Kieser *et al.*, 2000; Hopwood, 2007). *Streptomyces* play a significant role in medicine because they produce over two-thirds of the naturally derived antibiotics in current use (Kurtuboke 2012, Tauqeer *et al.*, 2011) and many other pharmaceuticals such as anti-tumour agents and immunosuppressants (Jakimowicz, 2005; van Wezel, 2012). In addition, their broad range of metabolic processes make a highly valuable contribution to carbon recycling (Bentley *et al.*, 2002). *S. coelicolor* is the most studied *Streptomyces* (Bentley *et al.*, 2002) and it has unique mycelial and sporulating life cycle involving complex regulation of gene expression resembling that of other differentiated and multicellular organisms, which makes it a good “model organism” and a tool for fundamental knowledge studying, such as studying of the functions, interactions and spatial and temporal expression of regulatory genes controlling aerial mycelium formation and the metamorphosis of aerial hyphae into spore chains. Moreover, *Streptomyces* genetics and developmental biology can be applied to improve Mycobacterium genetics and to understand its resting stage physiology, with applications for the understanding and possible control of diseases such as tuberculosis and leprosy.

Unlike most other bacteria *Streptomyces* have linear chromosomes (Lin *et al.*, 1993), with *S. coelicolor* containing 7,825 genes and 20 possible gene clusters coding for secondary metabolites within its 8 Mbp chromosome (Bentley *et al.*, 2002). The chromosome consists of a central core region containing many of the primary metabolic genes and the replication origin (*oriC*) which is flanked by two unstable terminal arm regions containing non-essential genes, often implicated in secondary metabolism (Bentley *et al.*, 2002). Predictions suggest that approximately 12.5% of genes encode regulatory proteins including putative sigma factors, two component systems and DNA binding proteins reflecting its complexity of development (Bentley *et al.*, 2002).

1.4.1 Life cycle of *S. coelicolor*

Unlike most other bacteria that divide by binary fission, *S. coelicolor* undergoes a far more complex life cycle and its growth resembles that of filamentous fungi (Flardh and Buttner, 2009) (Figure 1.10). The life cycle of *Streptomyces* starts from a

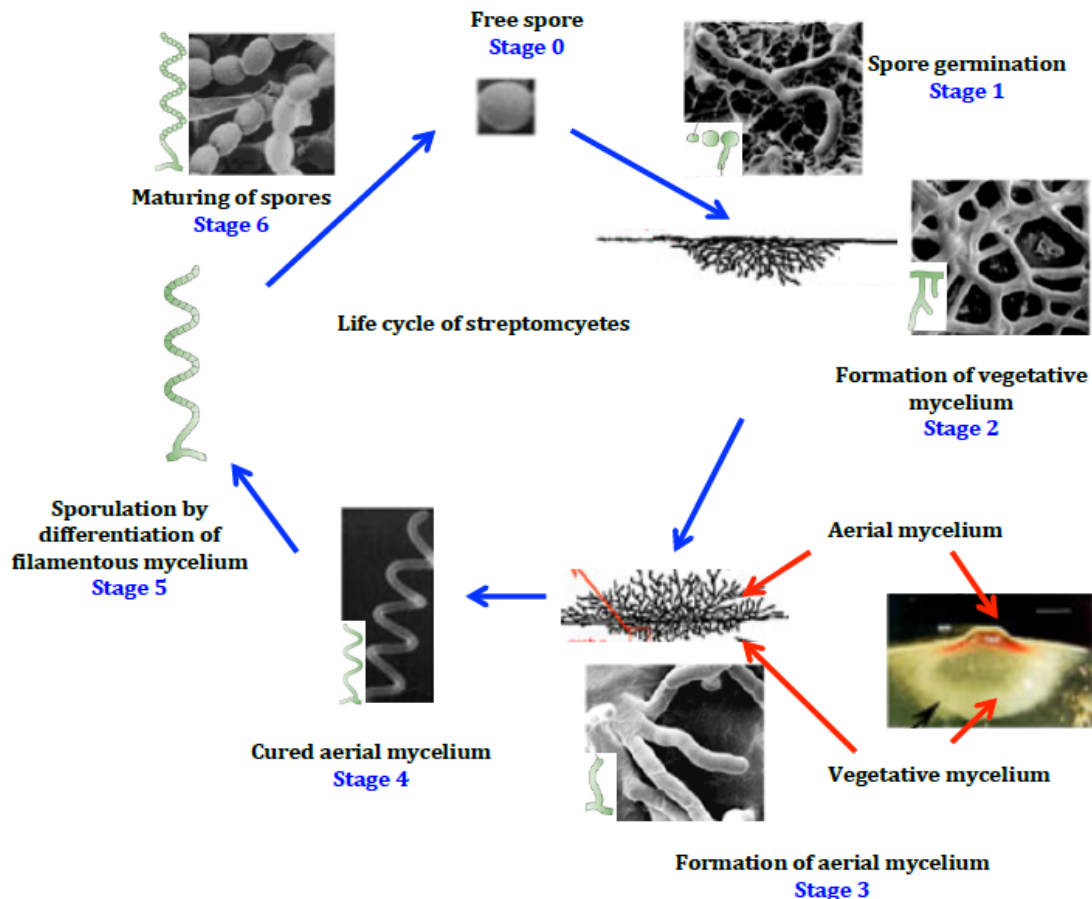


Figure 1.10. The life cycle of *S. coelicolor*. A spore germinates branching hyphae and grow into a solid medium ("vegetative mycelium", step 0-2). Then the developed vegetative mycelium break the surface and grow toward the surface ("aerial mycelium", step 3-4). The aerial mycelium spirals (step 5), and then the polynucleated aerial filaments are partitioned (step 6). The resulting sheaths will become spores, and the cycle continues. The secondary metabolites including antibiotics are secreted during the generation of aerial hyphae from the vegetative mycelium.

single uni-genomic spore which germinates with the production of either one or two germ tube under favourable conditions and nutrient-rich environment (Jyothikumar *et al.*, 2008). This subsequently develops into a network of vegetative mycelium allowing for the uptake of nutrients which grow in a polar manner through tip extension and branching events that occur along the lateral wall of the hyphae in a similar fashion to filamentous fungi (Chater and Losick, 1997; Errington *et al.*, 2003). These branching events allow for the increase in growth rate which is also proportionate to the rate of DNA replication (Chater, 1993; Flardh, 2003b).

During vegetative growth in *S. coelicolor*, cell division is suspended with the placement of cross walls that separate the hyphae into connected compartments rather than full cell-cell separation, whereby each compartment contains multiple copies of the chromosome (Claessen *et al.*, 2014). In the suspended cell division, new poles are not generated at the hyphal septa. Instead, tips are generated at lateral hyphal locations, usually far behind an existing growing tip, which in turn extend as branches of the original filament. Thus, exponential growth can only be achieved through the increase in number of growing tips and branching (Claessen *et al.*, 2014). This makes *Streptomyces* a rare example of a multicellular bacterium. At this stage of growth, colonies display the classic bald phenotype and are shiny in appearance on nutrient medium. Under the depletion of environmental nutrients, a signaling cascade is initiated, which results in the erection of aerial hyphae that break the surface tension of the media to rise towards the air (Kelemen and Buttner, 1998). The production of antibiotics is temporally correlated to this phase of the *Streptomyces* life cycle (Bibb, 2005; van Wezel and McDowall, 2011). Aerial hyphae grow as single multi-genomic individual hyphae with less branching and appear as fuzzy white colonies as seen in colonies blocked at this stage of development.

During the next stage, a chain of spores is formed by the differentiating apical compartment which arrests aerial hyphae extension and initiates sporulation (Flardh *et al.*, 1999). After that, sporulation septation is induced by protein FtsZ, which assembles into cytokinetic structure Z-ring that can recruit cell-division proteins to allow cytokinesis (McCormick *et al.*, 1994; Margolin, 2005). Completion of the septa

is followed by the maturation of spores involving spore wall assembly. Pre-spores are rounded up by thick lysozyme-resistant spore wall. Mature spores are held together in chain shape and then develop a characteristic grey pigment as they mature (Mazza *et al.*, 2006).

1.4.1.1 Growth in *S. coelicolor* – TIPOC

In *S. coelicolor*, polar growth is achieved by extending the hyphal filaments at their tip ends, which is opposed to lateral cell wall extension, a mechanism widespread in most rod-shaped bacteria (Flardh, 2003). Polar growth in *S. coelicolor* is driven by the multiprotein assembly that constitutes the Tip Organising Centre (TIPOC), otherwise known as the polarisome, which is present at the tip of all actively growing hyphae (Flardh *et al.*, 2012; Holmes *et al.*, 2013). This polar complex includes the positional marker DivIVA, the molecular organizer Scy (*Streptomyces* Cytoskeletal element) and the intermediate filament-like protein FilP, which have been implicated in growth and branching (Holmes *et al.*, 2013). These cytoskeletal proteins all share a similar basic coiled-coil structure and bioinformatics analysis reveals some interesting structural domains.

DivIVA was the first of these proteins to be characterised in *S. coelicolor*, named as a homologue of the division associated protein DivIVA in *B. subtilis* (Flardh, 2003a). In *S. coelicolor*, coiled-coil DivIVA has an indispensable role which has a profound impact on tip extension, branching and cell shape (Flardh, 2003). Partial depletion of DivIVA produces irregular hyphae and branching while overproduction affects tip extension and results as hyphae branching (Hempel *et al.*, 2008). These observations strongly imply that DivIVA is necessary to cell-wall assembly in apical extension in *S. coelicolor* (Letek *et al.*, 2008). DivIVA may act as a signal protein which recruits the cell-wall biosynthetic machinery directly or indirectly to new sites (Flardh and Buttner, 2009). Moreover, recent studies suggest that Scy protein together with DivIVA localize to the extended hyphae tip and also to the lateral sites positioning the

future branches and new cell wall assembly (Holmes *et al.*, 2013). Furthermore, special compositional cues of membrane might also act as site-specific markers for tip extension. While DivIVA consists of two classical heptad coil-coiled domains flanking a long linker region, both Scy and FilP share an unusual domain structure consisting of N-terminal heptad coiled-coils, a linker, and a C-terminal 51mer coiled-coil (Walshaw *et al.*, 2010). The DivIVA homologue in *S. coelicolor* is found to localise to the poles, and its function, as determined by the manipulation of its expression levels, is in tip growth and branching. Low expression levels of DivIVA results in irregular shaped short hyphae with branching close to existing tips. While, higher level DivIVA expression induces hyperbranching and leads to swollen tips that lyse (Flardh, 2003a). Moreover, in *S. coelicolor* DivIVA is an essential gene, which combined with the fact that cell division is a dispensable process in this organism underlines its importance to growth rather than division, although DivIVA has been localised to vegetative cross walls. Time lapse imaging techniques also demonstrate that DivIVA localises to sites of branching long before the emergence of new tips, which when DivIVA is overexpressed localises as discrete foci along the length of the hyphae where hyperbranching occurs (Hempel *et al.*, 2008; Richards *et al.*, 2012). This was established after monitoring tip localised DivIVA-EGFP patches which appear to break of and localise at sites of future branching. (Flardh *et al.*, 2012; Hempel *et al.*, 2012; Saalbach *et al.*, 2013).

The second protein to make up the TIPOC is Scy (*Streptomyces* cytoskeletal protein), a large alanine/glutamate (1326 amino acids) protein with homologues found exclusively amongst filamentous *Actinomycetes*. Scy is also found to localise to tips during active growth in *S. coelicolor* suggesting it has a role in growth (Holmes *et al.*, 2013). This is evident in the *scy* mutant strain which produces smaller colonies compared to the wild-type, is developmentally delayed and exhibits an over-branching phenotype. Moreover, overexpression of Scy also results in hyperbranching suggesting that, like DivIVA, Scy is important for the proper placement of branch sites and normal growth. In fact, manipulation of Scy expression levels in *S. coelicolor* shows that in the presence of elevated Scy levels, DivIVA

localisation is perturbed with localisation comparable to that seen when DivIVA is overexpressed and in fact co-localises with Scy at these ectopic locations. Moreover, with Scy and DivIVA interaction shown through both pelleting assays, bacterial two hybrid and co-elution experiments, it is clear that the two proteins act together, possibly forming a complex assembly, to ensure that correct growth and branching occurs. Interestingly, the *scy* mutant also shows perturbed spore formation with irregular spore size, aberrant DNA segregation and branched aerial hyphae suggesting that aberrant growth has either an indirect effect on division or there is a mechanistic regulation between growth and division via Scy (Ditkowski *et al.*, 2013; Holmes *et al.*, 2013).

The final protein to make up the TIPOC is the intermediate filament-like protein, FilP. Originally, FilP was identified in *S. coelicolor* when the genome was mined for proteins containing a similar domain architecture to crescentin in *Caulobacter crescentus*, a protein that is responsible for the signature curvature of the organism. It was not however, the first *Streptomyces* homologue for that gene to be described. Originally that gene locus was characterised in *Streptomyces reticuli* and was identified due to its affinity to avicel, a crystalline form of cellulose and the property that led to its name avicel binding protein (AbpS) (Walter *et al.*, 1998). The homologue in *S. coelicolor* was characterised through its relationship to growth and its cytoskeletal properties, including its similarity to crescentic, and thus its name was changed to filamentous Intermediate-like protein (FilP) (Bagchi *et al.*, 2008). FilP was originally found to localise to the tip and to inner hyphal curvatures forming long cables when expressed with a fluorescent tag, although more recent immunolocalisation suggests that it forms a network which extends along the hyphae from just behind the tip (Bagchi *et al.*, 2008; Fuchino *et al.*, 2013). While its role in growth and branching still remains a mystery, with the mutant strain showing no obvious effect on this process, it has been suggested that FilP could play a role in both the strength of the wall behind the growing tip and establishing new polarity centres in response to osmotic pressures (Bagchi *et al.*, 2008; Fuchino *et al.*, 2017).

1.4.1.2 DNA replication and segregation

Bacterial development requires accurate scheduling of the expression of different sets of genes for among others metabolism, morphogenesis, cell division and DNA replication. Chromosome replication needs to be synchronized with cytokinesis to guarantee that each daughter cell obtains a single copy of the chromosome. The initiation of chromosome replication is tightly controlled with the life cycle. In bacteria, chromosome replication starts with binding of DnaA (*trans*-acting element) to DnaA boxes (*cis*-regulatory element) in the *oriC* region (Fuller *et al.*, 1984; Kaguni, 2006; Katayama *et al.*, 2010; Leonard and Grimwade, 2010). Streptomyces have a large linear and GC-rich chromosome and the *oriC* region has 19 DnaA boxes instead of the five found in *E. coli* (Majka *et al.*, 1999; Majka *et al.*, 2001; Jakimowicz *et al.*, 1998). The spacing, orientation and position of these 19 DnaA boxes are conserved among *Streptomyces* spp (Wolański *et al.*, 2014). In contrast to DnaA of *E. coli*, the DnaA protein-mediated unwinding of *Streptomyces oriC* has not been detected (Jakimowicz *et al.*, 1998), perhaps due to the absence of an AT-rich region within the *oriC* region (Jakimowicz *et al.*, 1998). To make sure that chromosome replication only occurs once per cell cycle, the availability and activity of both *oriC* region and DnaA need to be strictly controlled. ATP hydrolysis is the most common strategy to inactivate ATP-DnaA (the active form of DnaA) (Zakrzewska-Czerwińska *et al.*, 2007).

In *Streptomyces* hyphal compartments, multiple chromosomes remain uncondensed until the final stages of sporulation, and replication in both vegetative and aerial hyphae seems asynchronous (Ruban-Ośmiałowska *et al.*, 2006). Little is known of DNA segregation during normal growth, but replicating chromosomes follow the growing hyphal tip (Wolanski *et al.*, 2011). A dynamic *oriC* partitioning system was identified, called the Par system (Abeles *et al.*, 1985). This system is widely distributed, since over 70% of all bacteria contain *par* loci on their genomes (Livny *et al.*, 2007). Par system includes the ParA and ParB proteins, and the *cis*-acting

centromere-like site(s) *parS* sites. ParA and ParB protein likely play a role in the control of chromosome replication. Indeed, ParA directly affects DnaA function in *B. subtilis* (Murray and Errington, 2008; Scholeld *et al.*, 2012). It is yet unclear if similar interactions occur in *Streptomyces*.

In *S. coelicolor*, *parA* and *parB* form an operon and in total 24 *parS* sites were found in the region near *oriC* (Jakimowicz *et al.*, 2002). ParB specifically recognizes *parS* sites, and ParA is a Walker-type ATPase, which likely provides the energy required for ParB-mediated chromosome segregation (Jakimowicz *et al.*, 2002; Jakimowicz *et al.*, 2005; Leonard *et al.*, 2005a; Leonard *et al.*, 2005b). Surprisingly, deletion of *parAB* does not cause major defects in chromosome segregation during vegetative growth of *Streptomyces*, which may be explained by the fact that the large multinucleoid hyphal compartments contain many non-segregated chromosomes (Jakimowicz *et al.*, 2005). However, in the absence of *parAB*, aberrant chromosome segregation was observed in the spores (Dedrick *et al.*, 2009; Jakimowicz *et al.*, 2005). Unlike in rod-shaped bacteria, where ParB drives origin regions to the poles of the dividing cell, in *Streptomyces* ParB complexes align the chromosomes regularly along the aerial hyphae to ensure that each of the many prespore compartments receives a single copy of the chromosome (Jakimowicz *et al.*, 2005; Jakimowicz and van Wezel, 2012; Dedrick *et al.*, 2009).

1.4.1.3 Cell division in *S. coelicolor*

The cell cycle of *S. coelicolor* involves a highly complicated and a number of carefully coordinated complex processes involving cell-wall assembly, cell division and chromosome segregation. Unlike the other rod-shaped bacteria, cell division is only essential for sporulation but not for the whole growth and viability of *Streptomyces* (Jakimowicz and Van Wezel, 2012). During the vegetative growth phase of *S. coelicolor* development, crosswalls are formed in an irregular pattern in an FtsZ-dependent manner similar to the septa formed during sporulation. However, these

crosswalls fail to undergo the cell-cell separation stage of cell division (Grantcharova *et al.*, 2005). In *S. coelicolor*, the aerial hyphae differ substantially from vegetative hyphae. One major difference is that aerial hyphae of wild-type cells do not branch, are nearly twice as wide as vegetative hyphae and undergo rapid growth and concomitant chromosome replication. The process of cell division is also completely different: while cross walls divide the vegetative hyphae into multi-genomic compartments, during sporulation-specific cell division in aerial hyphae many septa are formed nearly simultaneously, followed by formation of spore compartments and cell fission, which then results in chains of spores that each contain a single copy of the chromosome. The study of cell division in *Streptomyces* is particularly interesting for several reasons. The switch from vegetative to aerial division is a crucial step in the developmental pathway leading to sporulation.

1.4.2 FtsZ and Septation in *S. coelicolor*

Like rod-shape bacteria, cell division in *S. coelicolor* is driven by protein FtsZ which leads to the formation of bacterial septum that allows division to occur. Unlike majority of bacteria, *ftsZ* is not an essential gene for viability in *Streptomyces* and in fact *S. coelicolor* is still viable in the absence of division (McCormick *et al.*, 1994). While viable, in the sense that the strain can be passaged, not only is the strain inhibited in sporulation and therefore unable to produce spores but the crosswalls in vegetative hyphae do not grow. This lack of compartmentalisation in vegetative hyphae leads to colonies that are severely impaired in growth compared to the wild-type strain. Therefore, while cross-wall formation in vegetative hyphae is not essential to growth, compartmentalization of the hyphae is required in order to maintain healthy colonies (McCormick *et al.*, 1994). The fact that cell division is a dispensable process in *S. coelicolor* makes it an important organism in which to study this process. Cell division proteins that are essential in other bacteria, and thus harder

to characterise, are not essential in *Streptomyces* creating the opportunity for gaining insights into their mechanisms.

During late development in *S. coelicolor* FtsZ has been shown to form a series of classical Z-rings, a precursor to septum formation, that are evenly spaced along the length of aerial hyphae in what is often termed a ladder-like formation (Schwedock *et al.*, 1997). In order to generate such an even spacing of approximately 1.3 μm , FtsZ has been shown to develop rings through a series of intermediary localisation patterns which begin in late development with an upregulation of *ftsZ* gene expression. The *ftsZ* gene is transcribed from three distinct promoters, which regulate its expression levels throughout the life cycle of *S. coelicolor* (Flardh *et al.*, 2000). The first promoter, P1, is expressed during vegetative growth while the third promoter, P3 is constitutively expressed throughout the life cycle. The second promoter, P2, is developmentally regulated, with a strong upregulation in aerial hyphae prior to the onset of the division process (Flardh *et al.*, 2000). At the onset of the division process, an FtsZ ring is localised to the base of the aerial hyphae, which gives rise to a basal septum which compartmentalizes the hyphae into a sporogenic hyphae and the sub-apical stem compartment (Dalton *et al.*, 2007; Kwak *et al.*, 2001). After upregulation, FtsZ initially forms into spiral-like intermediates from a dispersed pattern. The spirals then condense into helical filaments, before further condensation results in the many, 20-50 Z-rings which form along the length of the hyphae marking the future sites of septation (Grantcharova *et al.*, 2005). The compartmentalisation of the aerial hyphae into sporogenic hyphae and the sub apical stem is important for containment of the elevated FtsZ levels and promote its condensation into Z-rings. The Z-rings only occur transiently before giving way to the rise of septa (Grantcharova *et al.*, 2005). Time lapse imaging revealed that Z-rings are also present, as expected, in the vegetative hyphae, which give rise to the cross-walls that compartmentalises the vegetative hyphae. Here, while the spiral intermediates are seen, the helical filaments are not, possibly due to the more dispersed formation in vegetative hyphae (Jyothikumar *et al.*, 2008).

In *S. coelicolor*, the transition of the multi-genomic hyphae into uni-genomic pre-spore compartments is a highly-orchestrated but poorly-understood process (Flardh and Buttner, 2009; Jakimowicz and van Wezel, 2012; McCormick and Flardh, 2012). This is followed by the re-organisation of the chromosomes and the appearance of regularly positioned FtsZ rings, generating the so-called FtsZ “ladder” that marks the positions of the division machinery, the divisome, where cross-walls are built. Once septation is completed, each pre-spore compartment carries a single chromosome (Figure 1.11). During filamentous growth cell division is suspended, therefore, it is not surprising that components of the divisome, including the key division protein, FtsZ, are not essential for growth in *Streptomyces*. Knockout mutants of divisome components effect on septation but not hyphal growth (McCormick *et al.*, 1994; Schwedock *et al.*, 1997; Jakimowicz and van Wezel, 2012; McCormick and Flardh, 2012). This is in stark contrast to uni-genomic bacteria, where deletion of components of the divisome is lethal. Composition of the divisome itself is also different in *Streptomyces*, lacking either FtsA or ZipA that are important for the membrane association of the FtsZ ring in *E. coli* or *B. subtilis* (Hale and de Boer, 1997; Raychaudhuri, 1999; Donachie *et al.*, 1979; Pichoff and Lutkenhaus, 2002; Szwedziak *et al.*, 2012; van den Ent and Lowe, 2000).

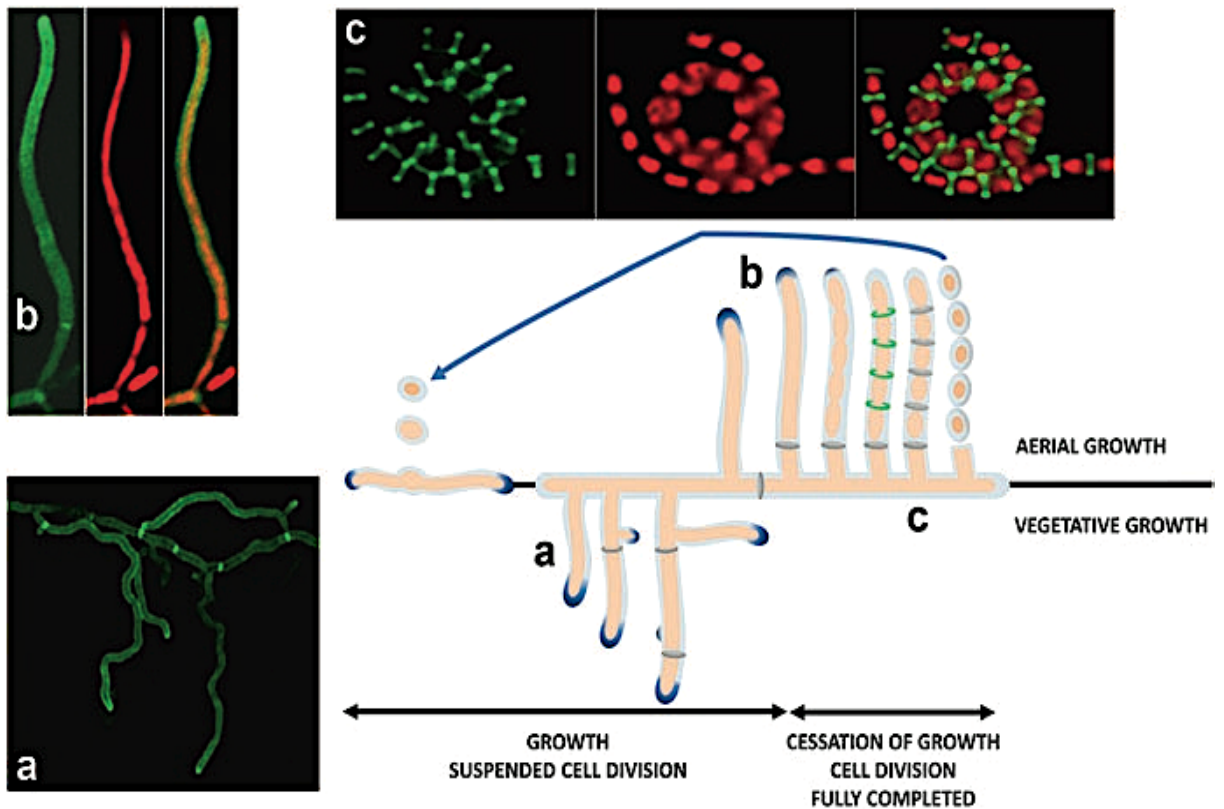


Figure 1.11. Septum formation during the life cycle of *S. coelicolor*.

During vegetative growth *S. coelicolor* produces irregular septum that compartmentalise hyphae (a). These septa do not undergo cell-cell separation typical of cell division. When aerial hyphae form a single basal septum forms in order to compartmentalise aerial hyphae (b). During sporulation many septa are placed along the length of aerial hyphae that do undergo the cell-cell separation seen in division (c). (Kelemen, 2017)

1.4.3 Cell division site regulation in *S. coelicolor*

The cell division machinery itself is generally well conserved in *Streptomyces* when compared to bacteria that undergo binary fission, but the control of division-site selection and FtsZ recruitment in the long and multinucleoid hyphae is entirely different. In the multi-genomic filaments of *Streptomyces*, the coordinated polymerisation of FtsZ at regular intervals during sporulation require a complex

organisation that is not yet fully understood. No direct homologs of MinC are found in *S. coelicolor*, and MinD-like proteins that are there have not yet been characterised and are not thought to play a role in the control of cell division (Jakimowicz and van Wezel, 2012). DivIVA is present in *S. coelicolor*, but instead of playing a role in the regulation of cell division, the protein is required to drive tip growth, and is therefore essential for viability (Flardh, 2003a). In addition, sporulation septa formation precedes full chromosome segregation (Flardh and Buttner, 2009), so a nucleoid occlusion mechanism, in the strictest sense, is unlikely in *S. coelicolor*.

Importantly, a significant increase in cellular FtsZ levels is required for the synchronous septation of aerial hyphae, which is achieved via the activation of one of the *ftsZ* promoters by the transcription factors, WhiA and WhiB (Bush *et al.*, 2016). On the other hand, FtsZ positioning in *S. coelicolor* is proposed to be under positive regulation through an FtsZ partner protein SsgB, which in turn depends on SsgA (Willemse *et al.*, 2011). SsgA and SsgB are small, 130–145 amino acid long, proteins that are exclusive to the morphologically more complex Actinomycetales (Noens *et al.*, 2005; Traag and van Wezel, 2008).

Previous studies showed that null mutants lacking these proteins were blocked at a stage preceding the onset of sporulation specific cell division, indicating a role in control of this process (Keijser *et al.*, 2003; van Wezel *et al.*, 2000). The progression towards fully formed FtsZ rings begins with the localisation of SsgA starting at the hyphal tips followed by evenly spaced distinct foci which occur the length of the young aerial hyphae. SsgA then recruits SsgB to the side wall in an evenly spaced manner alternating between the two sides of the hyphae in early division stage. FtsZ then forms long spiral-like filaments along the length of the hyphae interacting with the alternately placed SsgB. At this point small SsgB foci are seen on the opposite side wall of the hyphae from the SsgA recruited SsgB. FtsZ then co-localises with SsgB as distinct foci along the hyphal length forming foci on opposite sides of the hyphae. FtsZ and SsgB then co-localise as rings with both forming the classical laddering seen in FtsZ localisation. SsgA localises before the appearance of

the other two proteins suggesting that its localisation is not dependent on FtsZ or SsgB.

Indeed, SsgA was shown to correctly localise in an *ftsZ* mutant background. FtsZ on the other hand failed to localise correctly in either the *ssgA* or *ssgB* null mutants suggesting that its localisation is dependent on both of these proteins. Interestingly, in these mutant strains, FtsZ forms sparsely spaced ring-like structures which are similar to the distribution of septa in vegetative hyphae, and show the same lack of constriction associated with these non-dividing septa suggesting that at least part of the difference in septa formation between vegetative and aerial hyphae is the presence of SsgA and SsgB. While, SsgB is not able to localise correctly in a *ssgA* mutant background, which does not form regular foci on the lateral wall to Z-ring formation. What SsgB is not able to do it is correctly form the rings associated with the formation of FtsZ rings (Willemse *et al.*, 2011). And finally, of all the proteins that are involved in Z-ring assembly and stabilization, only SepF is present in *Streptomyces*. This raises the question as to how division site selection is controlled in *Streptomyces* in the absence of the canonical control systems (Figure 1.12).

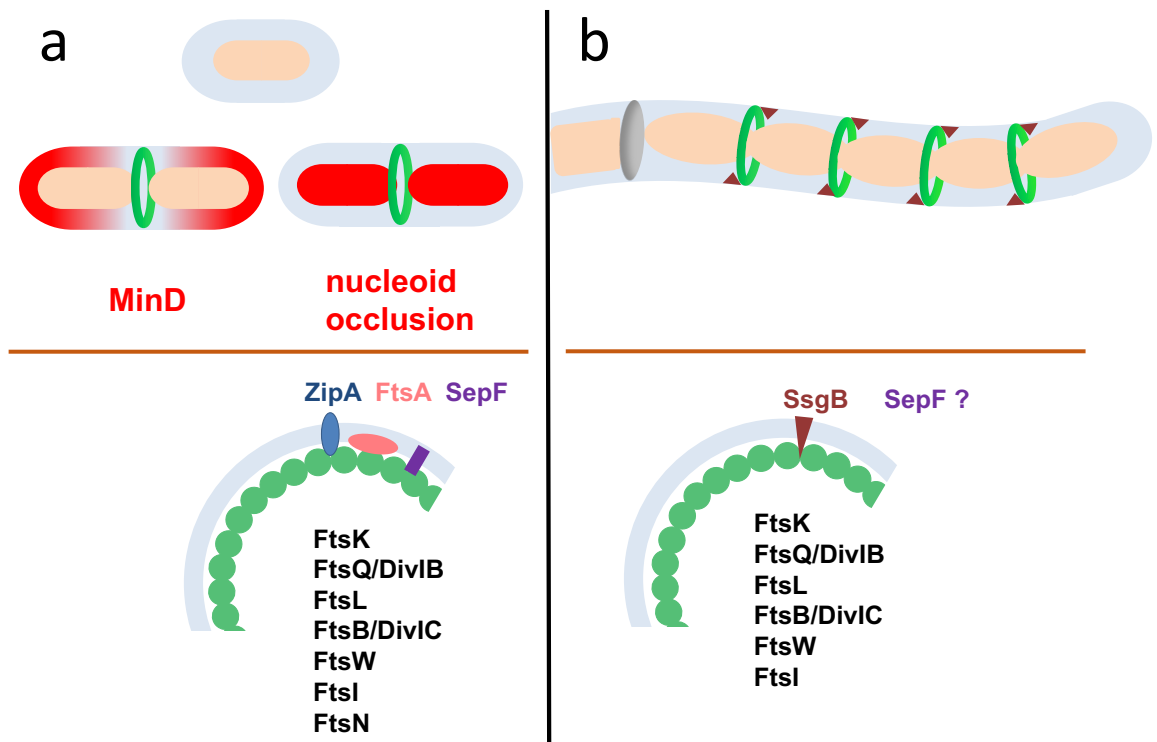


Figure 1.12. Controlling FtsZ-ring formation.

(a) Polymers of FtsZ at mid-cell of the rod-shaped *E. coli* or *B. subtilis* rely on both nucleoid occlusion where proteins that are associated with the chromosomes (red) block FtsZ (green) assembly at sites that are occupied by DNA and the negative regulation of FtsZ assembly by MinD (red), which interacts with the division inhibitor MinC and sequesters it to the cell poles, allowing FtsZ polymerisation at the mid-cell position. (Wu and Errington, 2003; Lutkenhaus, 2012).

(b) In the multi-genomic laments of *S. coelicolor*, the co-ordinated polymerisation of FtsZ at regular intervals during sporulation requires a complex organisation that is not yet fully understood. *S. coelicolor* has no obvious MinC homologue nor a nucleoid occlusion mechanism, in the strictest sense. Instead, FtsZ positioning is proposed to be under positive control by an FtsZ partner protein SsgB (Willemse *et al.*, 2011). Comparison of the divisome compositions demonstrates that *Streptomyces* lacks some of the key proteins known for FtsZ stabilisation on the membrane (Jakimowicz and van Wezel, 2012; McCormick and Flardh, 2012). As shown in the figure, many other FtsZ positive regulation proteins including FtsK, FtsQ/DivIB, FtsL etc. are conserved in *S. coelicolor*.

1.4.4 Linear chromosome of *S. coelicolor*

The strain *Streptomyces coelicolor* A3 (2) which we used as a study material is the genetically most characterized representative of the genus and is one of the largest completely sequenced bacterial genomes at 8.67 Mbp. In 2002, Bentley *et al.* sequenced and annotated the genome of a plasmid-free prototrophic derivative strain M145 (SCP1, linear, 365 kb, and SCP2, circular, 31 kb, which have been separately sequenced). The sequenced genome has revealed the single linear chromosome of 8,667,507 bp and 7,825 predicted genes. This was the largest number of genes discovered in a bacterium at that time. This complex genome is almost twice the size of *Bacillus subtilis* (Kunst *et al.*, 1997) and *Escherichia coli* (Blattner *et al.*, 1997). The genome of *S. coelicolor* consists of three regions: a central core region, left arm region and right arm region (Figure 1.13). The core region

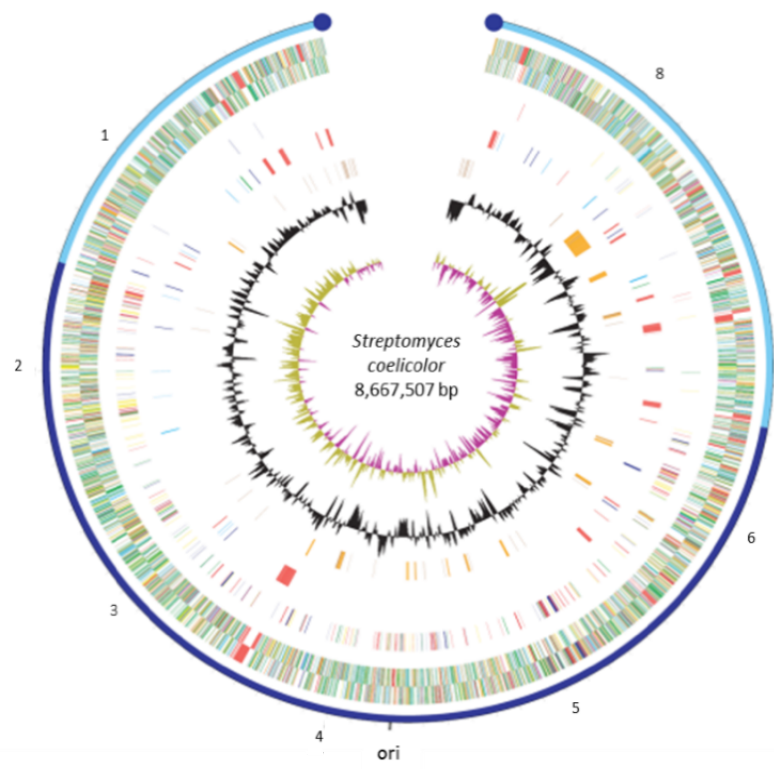


Figure 1.13. Circular representation of the *Streptomyces coelicolor* genome. The core region and the arms regions of the chromosome are shown as dark blue and light blue respectively (Bentley *et al.*, 2002).

comprises of approximately half the chromosome and appears to extend from around 1.5 Mb to 6.4 Mb, thus giving uneven arm lengths of approximately 1.5 Mb (left arm) and 2.3 Mb (right arm) (Bentley *et al.*, 2002).

The essential genes involved in cell division, such as DNA replication, transcription and translation, are located within the core. Sequencing has revealed over 20 potential gene clusters that might encode secondary metabolites, including the pigmented antibiotics actinorhodin and undecylprodigiosin, and the polyketide synthase which produces the grey pigment associated with mature spore production (Bentley *et al.*, 2002). Studies of many *Streptomyces* have showed that extensive deletions and amplifications of more than a million base pairs of DNA at either end of the chromosomes does not compromise viability under laboratory conditions (Voff and Altenbuchner, 1998), which suggests that essential genes are conserved in the core region (Friend and Hopwood, 1971).

Aims

S. coelicolor has a complex life cycle which culminates in the compartmentalisation of multiple aerial hyphae into uni-genomic spores. Many of the genes involved in cell division and cell-wall synthesis are located in the *dcw* (division and cell wall biosynthesis) cluster. The gene order and many of the components of the *dcw* cluster are quite well conserved in different bacteria, whereby the genes can be classified into those encoding components of the divisome and those that encode cell-wall biosynthetic enzymes (Mingorance *et al.*, 2004; Tamames *et al.*, 2001).

A key question of cell division is how the GTP-induced polymerisation of FtsZ is orchestrated in the three-dimensional space of a bacterial cell. In rod-shaped *E. coli* or *B. subtilis*, the formation of a ring of FtsZ polymers at mid-cell relies on two mechanisms, each involving negative regulation of FtsZ assembly: (1) nucleoid occlusion, where proteins associated with the chromosomes block FtsZ assembly at

sites that are occupied by DNA, or (2) the negative regulation of FtsZ assembly, MinD, in complex with the inhibitor protein MinC; these proteins, when sequestered to the cell poles, allow FtsZ polymerisation only at the mid-cell position (Wu and Errington 2003; Lutkenhaus 2012). But in *Streptomyces*, neither Min system or NO system was found. Therefore, we attempt to address several major questions: What are the specific proteins to control the positioning of the septum formation temporally and spatially in aerial hyphae? And how do they avoid the damage to the chromosomes during synchronous multiple cell division in multi-nucleoid hyphae? One interesting place in *S. coelicolor* to investigate is the *dcw* cluster which contains genes related to cell wall synthesis and cell division. The function of several genes between *ftsZ* (*SCO2082*) and *divIVA* (*SCO2077*) have not been well characterised, despite the fact they are downstream of *ftsZ* in many Gram-positive bacteria, including *Streptomyces*. In this study we mainly focus on three genes *SCO2081*, *SCO2080*, *SCO2079* (*sepF*). SepF was previously shown to tether the Z-ring to the membrane in *B. subtilis* and promote FtsZ protofilaments formation (Hamoen *et al.*, 2006; Ishikawa *et al.*, 2006). In addition, the genes *SCO2081* and *SCO2080* are located adjacently downstream of *ftsZ*. Considering this location, important roles in cell division or cell-wall synthesis were anticipated.

In this work, we will generate the knockout mutant strains by deletion of these three genes respectively, to characterize the phenotype and identify their effects on the division process and cell-wall synthesis. We also plan to localise the protein SepF to explore its activity during the Z-ring assembly and positioning.

2 Materials and Methods

2.1 Bacterial strains and plasmids

Table 2.1: *E. coli* strains used in this study.

Strain	Genotype	Growth temperature
DH5α (Hanahan, 1983)	F ⁻ λ ⁻ <i>endA1 glnV44 thi-1 recA1 relA1 gyrA96 deoR nupG Φ80dlacZΔM15 Δ(lacZYA- argF)U169 hsdR17(rk⁻ mk⁺)</i>	37°C
BW25113/pIJ790 (Datsenko and Wanner, 2000)	λ ⁻ Δ(<i>araD-araB</i>)567 Δ <i>lacZ</i> 4787(:: <i>rrnB-4</i>), <i>lacI</i> p- 4000(<i>lacI</i> ^R) <i>rpoS</i> 369(<i>Am</i>) <i>rph-1</i> Δ(<i>rhaD- rhaB</i>)568 <i>hsdR</i> 514	30°C
ET12567 (MacNeil <i>et al.</i> , 1992)	F- <i>dam</i> ::Tn9 <i>dcm6 hsdM hsdR</i>	37°C
DH5α/BT340	DH5α/pCP20	30°C

Table 2.2: *Streptomyces* strains used in this study.

Strain	Genotype
M145 (Hopwood <i>et al.</i> , 1985)	SCP1 ⁻ SCP2 ⁻ Pgl ⁺
Δ <i>sepF</i>	M145 <i>sepF</i> :: <i>ApraR</i>
Δ2080	M145 2080:: <i>ApraR</i>
Δ2081	M145 2081:: <i>ApraR</i>
Δ <i>sepF</i> /pMS82/ΔP- <i>sepF</i>	M145 <i>sepF</i> :: <i>ApraR</i> containing <i>sepF</i> gene
Δ <i>sepF</i> /pMS82/P- <i>sepF</i>	M145 <i>sepF</i> :: <i>ApraR</i> containing <i>sepF</i> gene under the control of its promoter
Δ <i>sepF</i> /pMS82/2080- <i>sepF</i>	M145 <i>sepF</i> :: <i>ApraR</i> containing <i>sepF</i> gene and 2080 gene
Δ <i>sepF</i> /pMS82/P- <i>sepF</i> - <i>egfp</i>	M145 <i>sepF</i> :: <i>ApraR</i> containing <i>sepF</i> gene under the control of its native promoter and <i>egfp</i> fusion
Δ <i>sepF</i> /pMS82/2080- <i>sepF</i> - <i>egfp</i>	M145 <i>sepF</i> :: <i>ApraR</i> containing 2080 gene <i>sepF</i> gene and <i>egfp</i> fusion
Δ2080/pMS82/P ₂₀₈₀ -2080	M145 2080:: <i>ApraR</i> containing 2080 gene and its putative promoter

$\Delta 2080/pMS82/P_{ftsZ-2080}$	M145 <i>2080::ApraR</i> containing <i>2080</i> gene and putative promoters of gene <i>ftsZ</i>
$\Delta 2080/pMS82/P_{2080+ftsZ-2080}$	M145 <i>2080::ApraR</i> containing <i>2080</i> gene and putative promoter of gene <i>2080</i> and promoters of gene <i>ftsZ</i>
$\Delta 2080/pMS82/\Delta P-sepF$	M145 <i>2080::ApraR</i> containing <i>sepF</i> gene
$\Delta 2080/pMS82/P-sepF$	M145 <i>2080::ApraR</i> containing <i>sepF</i> gene under the control of <i>sepF</i> promoter
$\Delta 2080/pMS82/2080-sepF$	M145 <i>2080::ApraR</i> containing <i>sepF</i> gene and <i>2080</i> gene

Table 2.3: Plasmid/Cosmid DNA used in this study.

Plasmid	Genotype
pIJ773 (Gust <i>et al.</i> , 2003)	<i>aac(3)IV oriT bla apramycin resistant</i>
pIJ790 (Gust <i>et al.</i> , 2003)	<i>araC-P_{araB}, γ, β, exo, cat, repA101ts, oriR101</i>
4A10	Supercos Cosmid with a 50 Kbp chromosomal fragment with cell division genes used in this study.
4A10/ <i>sepF::aac(3)IV</i>	Cosmid 4A10 with <i>sepF::ApraR</i> allele
4A10/ <i>2080::aac(3)IV</i>	Cosmid 4A10 with <i>2080::ApraR</i> allele
4A10/ <i>2081::aac(3)IV</i>	Cosmid 4A10 with <i>2081::ApraR</i> allele
4A10/ <i>ftsZ-2081::ApraR2</i>	Cosmid 4A10 with <i>ftsZ-2081 (long)::ApraR</i> allele
4A10/ <i>ftsZ-2081::ApraR3</i>	Cosmid 4A10 with <i>ftsZ-2081 (short)::ApraR</i> allele
4A10/ <i>ftsZ-2081::Scar2</i>	Flipped Cosmid 4A10 with <i>ftsZ-2081 (long)::ApraR</i> allele, leaving a 81 bp scar
4A10/ <i>ftsZ-2081::Scar3</i>	Flipped Cosmid 4A10 with <i>ftsZ-2081 (short)::ApraR</i> allele, leaving a 81 bp scar
pMS82 (Gregory <i>et al.</i> , 2003)	<i>ori pUC18, hyg, oriT RK2, int ΦBT1, attP</i>
pMS82/ <i>P₂₀₈₀₋₂₀₈₀</i>	pMS82 derivative containing <i>2080</i> gene under the control of its putative promoter
pMS82/ <i>P_{ftsZ-2080}</i>	pMS82 derivative containing <i>2080</i> gene under the control of <i>ftsZ</i> promoters
pMS82/ <i>P_{2080+ftsZ-2080}</i>	pMS82 derivative containing <i>2080</i> gene under the control of <i>ftsZ</i> promoter and <i>2080</i> putative promoter
pMS82/ $\Delta P-sepF$	pMS82 derivative containing <i>sepF</i> gene

pMS82/ <i>P-sepFp</i>	pMS82 derivative containing <i>sepF</i> gene under the control of its native promoter
pMS82/ <i>2080-sepF</i>	pMS82 derivative containing <i>sepF</i> gene and <i>2080</i> gene
pMS82/ <i>P-sepF-egfp</i>	pMS82 derivative containing <i>sepF</i> gene under the control of its native promoter and <i>egfp</i> fusion
pMS82/ <i>2080-sepF-egfp</i>	pMS82 derivative containing <i>sepF</i> gene <i>2080</i> gene and <i>egfp</i> fusion

2.2 Media

Solid Media

SFM (Soya Flour Mannitol): For general growth and phenotypic analysis of *S. coelicolor* strains.

Mannitol 60 g

Tap Water 3000 ml

The mannitol was dissolved in Tap water while 6 g soya flour and 6 g agar was measured into 500 ml Duran bottles. The dissolved mannitol media was dispensed in 300 ml aliquots into Duran bottles and twice autoclaved.

Lennox Broth (LB) Agar (Kieser *et al.*, 2000): For growing of *E. coli* strains and spore titres of *S. coelicolor* strains.

Tryptone 16 g

Yeast Extract 8 g

NaCl 8 g

Glucose 1.6 g

dH₂O up to 1600 ml

The above ingredients were dissolved in dH₂O, while 4 g of agar was measured into 500 ml Duran bottles. The dissolved media was dispensed in 400 ml aliquots into Duran bottles and autoclaved.

Liquid Media

Lennox Broth (LB) (Kieser *et al.*, 2000): For growing *E. coli* strains.

Tryptone	10 g
Yeast Extract	5 g
NaCl	5 g
Glucose	1 g
dH ₂ O	up to 1000 ml

Once dissolved, the media was dispensed, either in 10 ml aliquots into universals or in 50 ml aliquots into 250 ml conical flasks, and autoclaved.

SOB (Super Optimal Broth) : For growing *E. coli* BW25113/ pIJ790.

Tryptone	10 g
Yeast Extract	2.5 g
NaCl (5 M)	1 ml
KCl	0.093 g
MgCl ₂ (1 M)	5 ml
MgSO ₄	3 g
dH ₂ O	up to 500 ml

Once dissolved, the media was dispensed in 10 ml aliquots into universals and autoclaved.

2.3 Bacterial growth conditions and storage

S. coelicolor strains

S. coelicolor strains were grown on SFM containing the appropriate antibiotics and incubated at 30°C until the required developmental stage. For storage (spore preparation), *S. coelicolor* spores were streaked on a single SFM plate to generate a confluent lawn and incubated at 30°C until mature spores developed. Spores were harvested by rubbing spores in a layer of water using a cotton bud. The spore suspension was collected in a 15 ml falcon tube using a pastor pipette. The spores were centrifuged for 10 minutes at 4500 g at 4°C and the supernatant removed. The spores were re-suspended in approximately 1 ml 20% glycerol and stored at -20°C in a 2 ml microcentrifuge tube with a screw cap. The viable spore concentration was determined by plating out a dilution series on LB agar plates containing the appropriate antibiotics (Table 2.4).

E. coli strains

E. coli strains were grown in either LB solid or liquid media and incubated at 37°C, except for BW25113/pIJ790, which was grown at 30°C due to the presence of a temperature sensitive plasmid (pIJ790). Glycerol stocks were generated by making a 1:1 mixture of culture to 100% glycerol, and stored at -20°C.

Table 2.4: Antibiotic concentrations used in this study.

Antibiotic	Stock (mg/ml)	<i>Streptomyces</i> final concentration (µg/ml)		<i>E. coli</i> final concentration (µg/ml)	
		SFM	LB	SFM	LB
Ampicillin	100	-	-	100	100
Apramycin	100	50	-	50	50
Chloramphenicol	25	-	-	25	25
Hygromycin	50	50	-	50	50
Kanamycin	100	50	-	50	50
Nalidixic Acid	25	25	-	-	-

2.4 General Molecular Biology Methods

Plasmid DNA isolation from *E. coli*

Solution 1: 50 mM Tris/HCl, 10 mM EDTA pH 8

Solution 2: 200 mM NaOH, 1% SDS

Solution 3: 3 M potassium acetate pH 5.5

A single colony of DH5 α (or BW25113 for cosmids after cassette targeting) containing the desired plasmid DNA was inoculated into 50 ml LB supplemented with the appropriate antibiotic. The inoculum was grown overnight at 37°C (shaking 250 rpm). The overnight growth was collected in a 50 ml falcon by centrifugation for 5 minutes at 5000 g at 4°C. The cells were washed in 40 ml Solution 1 and centrifuged for 5 minutes at 5000 g at 4°C. The supernatant was discarded and cells re-suspended in 1 ml Solution 1 before the addition of 2 ml Solution 2. The cells were mixed gently by turning the falcon tube and incubated for 4 minutes on ice. After incubation 1.5 ml Solution 3 was added and the lysate shaken vigorously. The lysate was incubated for 10 minutes on ice before centrifugation for 10 minutes at 5000 g at 4°C. The supernatant was transferred to a 15 ml falcon and mixed with 500 μ l of 1:1 phenol:chloroform. The extract was vortexed for 30 seconds and centrifuged for 5 minutes at 5000 g. After centrifugation the aqueous phase was collected in a fresh 15 ml falcon and 7 μ l of 30 mg/ml RNase was added. The extract was incubated for 1 hour at 37°C. After incubation another phenol: chloroform extraction was performed as before. After collecting the aqueous phase the DNA was precipitated by mixing 1:1 with isopropanol kept at -20°C, the solution was mixed by inversion and incubated on ice for 30 minutes. The precipitated DNA was centrifuged for 15 minutes at 5000 g at 4°C. The supernatant was discarded and the DNA pellet washed with 2 ml 70% ethanol kept at -20°C. The DNA was centrifuged for 5 minutes at 5000 g at 4°C and the supernatant was discarded. The DNA pellet was allowed to air dry for 5 minutes before re-suspension in 200-400 μ l sterile dH₂O. DNA was stored at -20°C.

Agarose gel electrophoresis of DNA

50x TAE: 2M Tris acetate, 50 mM EDTA pH 8

10x Loading dye: 50 mM Tris, 50 mM EDTA, 50% Glycerol pH 7.4 -Autoclave- 0.05% Xylene Cyanol, 0.05% Bromophenol Blue

Agarose gels were cast using the Bio-Rad Mini-Sub and Sub-cell trays. Gels were made in a range between 0.7% and 1% agarose in 1x TAE buffer with the addition of 0.5 µg/ml ethidium bromide. DNA was mixed with 1x loading dye a run in gels submerged in 1x TAE buffer. Gels were imaged with UV light using a Bio-Rad trans-illuminator. A size marker of λ DNA digested with *HindIII*, and *EcoRI* was used to estimate band sizes.

PCR

All PCR reactions were performed using a BioRAD DNA Engine® Peltier Thermal Cycler.

Hi-Fidelity PCR using Phusion High-Fidelity DNA Polymerase (Thermofisher)

Used for the generation of PCR fragments used for cloning

Reaction conditions: 1x Phusion GC Buffer, 200 µM of each of the four dNTPs, 1.5 mM MgCl₂, 3% DMSO, 1 µM of each primer, 0.02 U/µl Phusion DNA polymerase.

Conditions:

1. Initial Denaturation 98°C for 2 minutes
2. Denaturation 98°C for 20 seconds
3. Primer Annealing x*°C for 30 seconds
4. Extension 72°C for x** seconds
5. Repeat steps 2-4 with 25 cycles
6. Final Extension 72°C for 5 minutes
7. Cool down 20°C for 5 minutes

* Primer annealing temperature set according to melting temperature calculator at www.thermoscientific.com/pcrwebtools. Calculated temperature was adjusted down 5°C due to addition of DMSO.

** Extension time was proportional to the length of the product calculate at 30 seconds per 1 Kbp.

Low-Fidelity PCR using Go Taq DNA Polymerase (Invitrogen)

Used for diagnostic purposes and for the generation of disruption cassettes.

Reaction conditions: 1 x Go Taq polymerase buffer, 200 µM of each of the four dNTPs, 2.5 mM MgCl₂, 5% DMSO, 1 µM of each primer, 0.02 U/µl Go Taq DNA polymerase.

Conditions:

1. Initial Denaturation 96°C for 5 minutes
2. Denaturation 98°C for 20 seconds
3. Primer Annealing 55°C* 30 seconds
4. Extension 72°C for x** seconds
5. Repeat steps 2-4 for 30 cycles
6. Final Extension, 72°C for 5 minutes
7. Cool down 20°C for 5 minutes

*Primer annealing temperature was initially set at 55°C, but altered if no product visible.

** Extension time was proportional to the length of the product calculate at 30 seconds per 500 bp.

Conditions for generation of disruption cassette:

1. Initial Denaturation 94°C for 2 minutes
2. Denaturation 94°C for 45 seconds

3. Primer Annealing 50°C 45 seconds
4. Extension 72°C for 90 seconds
5. Repeat steps 2-4 for 10 cycles
6. Denaturation 94°C for 45 seconds
7. Primer Annealing 55°C 45 seconds
8. Extension 72°C for 90 seconds
9. Repeat steps 6-7 for 15 cycles
10. Final Extension, 72°C for 5 minutes
11. Cool down 20°C for 5 minutes

Table 2.5: Oligonucleotide sequences

Primer	5'-3' Sequence
SepF KO FRW	GTCAGCAGATCCACCACAGAGCGGAGGACTCAGAGCATG
SepF KO2 REV	ACACCAAACCGGCCGCAAAGTCGACAAGTCGCTTCGCAT
SepF XbaBgl Prom FRW	GATCACTCTAGATCTCGGGTAACGTCGCCAAGAAGTCG
SepF 3' END	GCCTTGCCGGGTTGCCACGAGC
SepFp2 XbaBgl FRW	GATCACTCTAGATCTGACCGTGGCCCCGCTCAGCGG
SepF FWR	CAAGGCCCGTATCGCAGAGGGCGGGTTCTTCAACCAGAG CCCGGTCGCCACCGTGAGCAAGG
SepF REV	GTCCCGGGCCCGTGTCTTGTCTGTACCGGTAGTGCGTC CATATGTGTAGGCTGGAGCTGC
FP Eco REV	GGATCGAATTCTTACTTGTACAGCTCGTCCATGCCG
mCherry Eco REV	GGATCGAATTCTTACTTGTACAGCTCGTCCATG
2080 KO FRW	CGGCTCGCGGGCTATGTGTGGCTGGACTGATGGGGCATG ATTCCGGGGATCCGTCGACC
2080 KO REV	CCATATTTTCTGCTGTGGTCCGACTTCTTGGCGACGTTATG TAGGCTGGAGCTGCTTC
2080 Bgl Prom FRW	GATCACAGATCTGCGGCCGGTGCTACGAGGTGC
2080 3' END	TCGGGTTCCGGGTCCAGTTCGG
2080 XbaI Nde FWR	CGGGCGACACGTAACCTCGAGGCGAGAGGCCTTCGACGTG ATTCCGGGGATCCGTCGACC
2080 Nde REV	GATCACCATATGCCCCGAGCCTGGGTCCGACTCC
2081 KO2 Apra REV	CACCTCGGCGCGCATCTCCTCGGGCACCTCGTAGCACCGT GTAGGCTGGAGCTGCTTC
2081 KO REV	CGCGGCGAGTTCGTGCTTACGGTCCGTCATGCCCCATCAT GTAGGCTGGAGCTGCTTC

2081 Nde REV	GATCACCATATGCCCCGAGCCTGGGTCGGACTCC
2081 KO2 FRW	GGCCGAGGAACTGGACGTGCCGGACTTCCTGAAGTGATA ATTCCGGGGATCCGTCGACC
2081 KO2 REV	CGCGGCGAGTTCGTGCTTACGGTCCGTCATGCCCCATCAT GTAGGCTGGAGCTGCTTC
FtsZ KO FRW	CGCGGCGAGTTCGTGCTTACGGTCCGTCATGCCCCATCAT GTAGGCTGGAGCTGCTTC
FtsZ XbaNde FRW	GGATCATCTAGAGCATATGGCAGCACCGCAGAACTACC
Apra 5' REV	CGCACCTGGCGGTGCTCAACG

Restriction digest

Table 2.6. Concentration and restriction sites of enzymes used in these experiments.

Restriction enzyme	Concentration (U/ μ l)	Restriction site
<i>EcoRI</i>	10	5'..G↓AATTC..3' 3'..CTTAA↑G..5'
<i>XbaI</i>	10	5'..T↓CTAGA..3' 3'..AGATC↑T..5'
<i>EcoRV</i>	10	5'..GAT↓ATC..3' 3'..CTA↑TAG..5'

Restriction digests for the analysis of plasmids containing recombinant DNA and cosmids successfully mutagenised were carried out in 20 μ l. DNA was digested with 10 U of the appropriate restriction enzyme from Roche in 1x of the recommended digestion buffer. Digests were incubated for 4 hours (plasmids) or overnight (cosmids) at 37°C. Reactions were stopped by heating to 65°C for 10 minutes before the digested DNA was cooled on ice before loading onto agarose gel and analysed by electrophoresis.

Isolation of DNA fragments by agarose

After the separation of fragments generated by a preparative restriction digest, the gels were visualised using long-wavelength UV light (310 nm). Desired fragments were excised using a razor blade and purified using the Qiagen QIAquick Gel Extraction kit. Fragments were stored in sterile dH₂O and stored at -20°C.

Ligation of DNA fragments

Linearised vector and insert fragments were mixed in approximately 1:3 molar ratio in 11.5 μl volume made up with sterile dH_2O . The fragments were mixed and incubated for 2 minutes at 65°C. After cooling on ice, 3 μl of 5x ligation buffer and 0.5 μl of T4 DNA ligase from Invitrogen was added. The ligation was incubated on ice overnight at 4°C. Ligations were desalted using a self-made G75 sephadex column prior to transformation by electroporation.

Transformation of competent *E. coli* cells by electroporation

A single colony of the appropriate *E. coli* strain was inoculated into 10 ml LB supplemented with the appropriate antibiotics and grown overnight with shaking at either 30°C or 37°C depending on the strain. After overnight growth, the culture was subcultured, using 1% of the volume of the fresh media, into either 10 ml or 50 ml LB supplemented with the appropriate antibiotics. The fresh culture was incubated at the appropriate temperature with shaking until it achieved an OD₆₀₀ ~0.7. The cells were collected by centrifugation for 5 minutes at 5000 g at 4°C. The supernatant was removed and the cells washed twice in 10% glycerol centrifuging for 5 minutes at 5000 g at 4°C. The pellet was re-suspended to a final volume between 100 μl and 250 μl in 10% glycerol. For transformation 50 μl of cells were mixed with either 1 μl of plasmid or cosmid DNA, or 5 μl of ligation. Electroporation was carried out in an ice cold 0.2 cm electroporation cuvette using a BioRad Gene Pulser 2 set to 200 Ω , 25 μF and 2.5 kV. After electroporation, cells were mixed with 1 ml ice cold LB and allowed to recover during a 1 hour incubation at either 30°C or 37°C before plating onto LB agar plates supplemented with the appropriate antibiotics. Plates were incubated overnight at either 30°C or 37°C.

Transformation of competent *E. coli* cells by chemical competence

A single colony of the appropriate *E. coli* strain was inoculated into 10 ml LB supplemented with the appropriate antibiotics and grown overnight with shaking at either 30°C or 37°C depending on the strain. After overnight growth the cells were

subcultured by transferring 500 µl into fresh 50 ml LB supplemented with the appropriate antibiotics. The fresh culture was incubated at the appropriate temperature with shaking until it achieved an OD₆₀₀ ~0.4-0.6. The cells were collected by centrifugation for 5 minutes at 5000 g at 4°C. The supernatant was removed and the cells washed with 10 mM NaCl centrifuging for 5 minutes at 5000 g at 4°C. The pellet was re-suspended in 30mM CaCl₂, 10 mM RbCl₂ and incubated on ice for 1 hour at 4°C. After incubation the cells were centrifuged for 5 minutes at 5000 g at 4°C before the pellet was re-suspended with 500 µl and 250 µl of 30mM CaCl₂, 10 mM RbCl₂. For transformation 50 µl of cells were mixed with either 1 µl of plasmid or cosmid DNA, or 5 µl of ligation and incubated for 30 minutes on ice. The cells were then heat shocked at 42°C for 1 minute before being placed immediately in ice. After heat shock, the cells were mixed with 1 ml LB and allowed to recover during a 1 hour incubation at either 30°C or 37°C before plating onto LB agar plates supplemented with the appropriate antibiotics. Plates were incubated overnight at either 30°C or 37°C.

Conjugation into *S. coelicolor*

Conjugation of vectors containing *oriT* into *S. coelicolor* was achieved using the *E. coli* strain ET12567/pUZ8002. A single colony of ET12567/pUZ8002 containing the desired plasmid or cosmid for conjugation was inoculated into 10 ml LB containing kanamycin, chloramphenicol and the antibiotic for which the plasmid or cosmid confers resistance, and grown overnight with shaking at 37°C. After overnight growth the cells were subcultured by transferring 100 µl into fresh 10 ml LB supplemented with the appropriate antibiotics. The fresh culture was incubated with shaking at 37°C until it achieved an OD₆₀₀ ~0.4-0.6. The cells were collected by centrifugation for 5 minutes at 5000 g at 4°C. The supernatant was removed and the cells washed twice with 10 ml LB centrifuging for 5 minutes at 5000 g at 4°C. The pellet was re-suspended in 250 µl LB and kept on ice. Approximately 10⁸ spores of the desired *S. coelicolor* strain were added to 500 µl LB and germination activated by heating at 50°C for 10 minutes before cooling on ice. After cooling the germinating spores were mixed with re-suspended ET12567/pUZ8002 cells containing the plasmid/cosmid and

centrifuged for 2 minutes at 16,000 g at 4°C. The supernatant was removed and the pellet re-suspended in 300 µl sterile dH₂O. A dilution series was set up in which three 10x dilutions were made. The stock and 3 dilutions were then plated into SFM containing 10 mM MgCl₂ and incubated at 30°C. After overnight incubation the plates were overlaid with 500 µl sterile dH₂O containing nalidixic acid and the appropriate antibiotics. The plates were then incubated at 30°C until the appearance of colonies which had developed mature spores (5-8 days). Successful ex-conjugants were selected streaked for single colonies on SFM supplemented with nalidixic acid and the appropriate antibiotics and grown at 30°C until spores were produced. Spore preparations of the strain were then generated, originating from a single colony of the streaked plate.

Replica plating

Determination of double crossover ex-conjugants during the generation of mutant strains of *S. coelicolor* was achieved through replica plating. Double crossover events lead to strains that are apramycin resistant but kanamycin sensitive. Spores were transferred from the SFM conjugation plate to first an LB plate containing kanamycin and nalidixic acid and then immediately an LB plate containing apramycin and nalidixic acid using a single sterile velveteen cloth such that both LB plates become a replica of the original SFM plate. The replica plates were incubated for 2 days at 30°C before being analysed for colonies present on the apramycin containing plate that were absent from the kanamycin containing plate. These colonies were identified on the original SFM conjugation plate and picked and streaked for single colonies on SFM supplemented with nalidixic acid and apramycin and grown at 30°C until spores were produced. Another round of replica plating was performed on the streaks once they had produced spores, after which spore preparations were generated for the successful double crossover strain.

2.5 Microscopy of *S. coelicolor*

Coverslip microscopy

Approximately 10^5 spores of an *S. coelicolor* was plated in a 1 cm² confluent patch (0.5 cm by 2 cm) on SFM containing the appropriate antibiotics. A glass coverslip, 22 x 22 mm with a thickness of 0.13-0.17 mm, was inserted into the patch at an approximate angle of 70° to the horizontal plain of the medium. Plates were incubated at 30°C with coverslips removed at regular intervals after approximately 45 hours growth in order to visualise the developmental stages of *S. coelicolor*.

Coverslip staining

Plates containing coverslips were allowed to dry for 30 minutes in order to ensure that aerial hyphae stuck to the surface of the coverslip. Coverslips were removed from the media and placed on filter paper with the sample face up. The sample was fixed with 100% methanol (kept in the freezer) for 1 minute, after which the excess methanol was removed and the remainder allowed to evaporate. The sample was stained with the application of WGA-Alexa Fluor 488 conjugate (50 µg/ml) and propidium iodide (25 µg/ml) to each coverslip on the growth line. The samples were incubated for 30 minutes in total darkness at room temperature. The coverslips were washed 4 times by pipetting 1 ml PBS onto the surface before allowing the slides to dry. After drying the slides were mounted face down onto microscope slides (76 x 26 mm (thickness 1.0 – 1.2 mm) with an 8 µl drop of 20% glycerol on the surface. Excess liquid was removed from the edge of the coverslip before it was sealed with a fine coat of nail varnish applied around the edge.

Visualisation of microscope slides

Samples were visualised using an Axioplan 2 Imaging E (Carl Zeiss) Universal microscope with an AxioCamMR camera. A Plan Apochromatic 100x/1.40 Oil (440780) objective was used in combination with FS 38 GFP and FS 45 TxR filters. AxioVs40x64 V 4.9.1.0 software was used for image capture and measurement of distances between septa.

Chapter 3 SepF - an essential component for septum formation

Introduction

The protein SepF was first identified by Hamoen *et al.* (2006) and Ishikawa *et al.* (2006) and found to be essential for the completion of cell division in *B. subtilis*. SepF is conserved among Gram-positive bacteria and has been best characterized in *B. subtilis*. The *B. subtilis sepF* null mutant displays a cell division defect in which septa are formed slowly, aberrantly and ultimately fail to fully close. In addition, SepF has been shown to self-interact forming polymers that assemble into rings of ~50 nm when the overexpressed and purified protein is visualized by transmission electron microscopy (Figure 3.1) (Hamoen *et al.*, 2006; Ishikawa *et al.*, 2006; Duman *et al.*

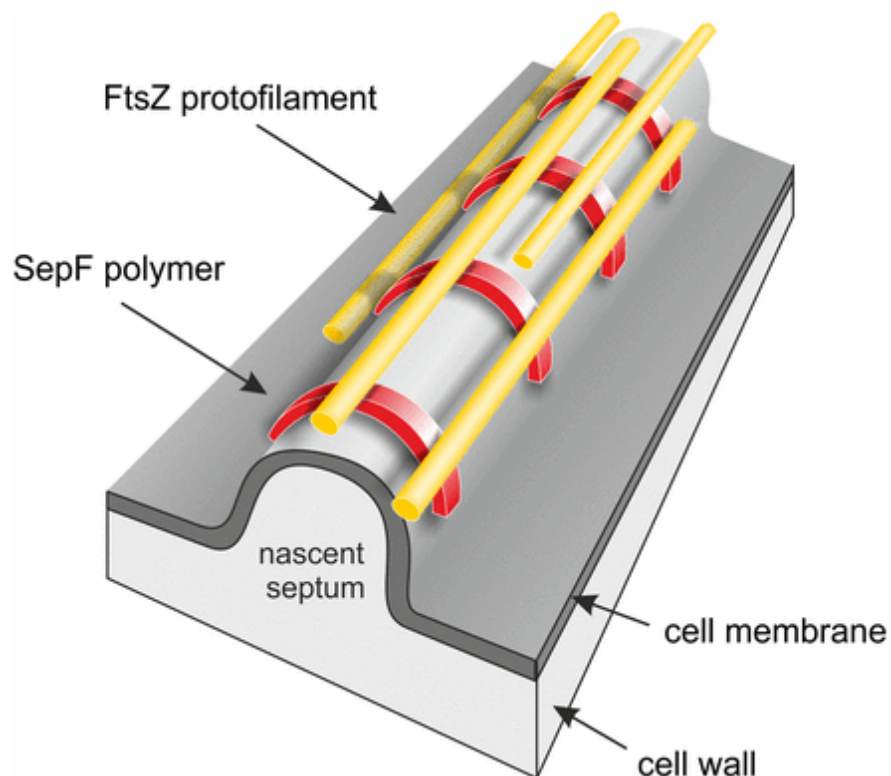


Figure 3.1. Current model of SepF function in *B. subtilis*. The SepF protein (red) polymerises on the membrane at the time of membrane invagination at the division site. SepF polymers aid the membrane anchoring of FtsZ (yellow). Taken from Duman *et al.*, 2013.

2013). The N-terminus of SepF has also been discovered to interact with the cell membrane whilst the C-terminus of SepF was shown to interact with the C-terminal end of FtsZ and is responsible for the correct localization and ring formation of FtsZ (Duman, 2013). In *E. coli*, the FtsZ filaments are anchored to the cell membrane by the FtsA and ZipA proteins. In *B. subtilis*, in addition to FtsA and ZipA, SepF is involved in anchoring FtsZ to the membrane. In fact, an FtsA knockout of *B. subtilis* was rescued by the overexpression of SepF (Ishikawa *et al.*, 2006). However, Actinomycetes, including *Streptomyces* lack FtsA. According to the proposed model, SepF might take the role of FtsA of *E. coli* and is proposed to be involved in the anchoring of FtsZ polymers to the cell membrane. Interestingly, SepF has been found in those archaea, which possesses FtsZ, but lacks FtsA (Makarova and Yutin, 2010). This might suggest that SepF is the archeotype of FtsZ anchoring proteins. SepF has been partially characterized in the Gram-positive bacterium *Streptococcus pneumoniae* and two cyanobacteria as well. The *S. pneumoniae sepF* null mutant strain displayed a similar phenotype compared to the *B. subtilis sepF* null mutant: cells of various sizes and shapes as well as multiple and thinner septa forming during an early stage of constriction (Fadda *et al.*, 2003). In cyanobacteria, SepF (previously named Cdv2 for Cell Division Protein 2) was found to be essential, and depletion of SepF in *Synechococcus elongatus* (rod-shaped) and *Synechocystis* Strain PCC6803 (spherical) led to cell filamentation and giant cells, respectively (Miyagishima *et al.*, 2005; Marbouty *et al.*, 2009). SepF also localises to the *Synechocystis* septum at mid-cell site and stimulates the assembly of FtsZ protofilaments (Marbouty *et al.*, 2009). In *B. subtilis*, SepF promotes the assembly and bundling of FtsZ protofilaments. Existing as a dimer, SepF can be seen uniformly distributed along the protofilaments, stabilizing lateral interactions of FtsZ. It is also thought to decrease the critical concentration of FtsZ assembly, prevent dilution-induced disassembly of FtsZ and suppress FtsZ GTPase activity which promotes disassembly (Singh *et al.*, 2008). SepF forms complexes with many divisome proteins such as FtsA, EzrA and ZapA, as well. Over expression of the *sepF* gene can compensate for the absence of other divisome stabilizing proteins, such as FtsA, highlighting the redundancy of some of the divisome proteins. However, *sepF* mutants exhibit abnormally thick septa and partial impairment of cell division in *B. subtilis*. Z-rings have been shown to assemble in the

absence of SepF but fail to initiate septum synthesis, resulting in the production of elongated cells due to the delay in cell division suggesting that SepF acts downstream of FtsZ localization (Adams and Errington, 2009; Singh *et al.*, 2008).

SepF was characterized in *Mycobacterium*, where it was shown to be an essential component of cell division (Gola *et al.*, 2015; Gupta *et al.*, 2015). SepF of *M. smegmatis* was shown to interact with FtsZ and was localized to the developing septum, forming a ring, similar to the FtsZ rings. Depletion of SepF resulted in the formation of elongated filaments that did not complete cell division (Gola *et al.*, 2015; Gupta *et al.*, 2015).

S. coelicolor produces both vegetative crosswalls, which are responsible for compartmentalization of vegetative hyphae and sporulation septa, which are crucial for the formation of spores. It is therefore surprising that several divisome homologues, such as ZipA and FtsA, are absent from the genome in *S. coelicolor* (McCormick, 2009; Bentley *et al.*, 2002). The C-terminal domain of FtsZ contains highly conserved sequences and has been shown to contain a binding site for several division proteins, including SepF in *B. subtilis*. Compared to most characterised bacteria, *Streptomyces* have been found to be viable upon deletion of *ftsZ*, with the mutant exhibiting severely impaired vegetative growth and failing to generate spores (Adams and Errington, 2009). This is because *Streptomyces* does not rely on cell division for its filamentous growth. During hyphal growth FtsZ is dispensable and it is only essential during sporulation, where a synchronous septation event takes place. Intriguingly, the *S. coelicolor* chromosome encodes three SepF homologues, one of which is encoded in the same gene cluster that carries the *ftsZ* and *divIVA* genes.

In this chapter we present the initial characterisation of *sepF* and its role in septation in *S. coelicolor*.

- First, we identified potential SepF homologues in *S. coelicolor* using bioinformatics.
- We used the “REDIRECT” technology to generate a knockout *sepF2* mutant in *S. coelicolor*.
- We confirmed the knockout mutants generated.

- We characterized the phenotype of the knockout mutant using macroscopic observations, followed by epi-fluorescent microscopy and confocal microscopy.

3.1 Identification of SepF homologues in *S. coelicolor*

In order to identify potential SepF homologues encoded in the *S. coelicolor* genome we performed a Blast search (Figure 3.2) using the SepF amino acid sequence from *B. subtilis* (UniProt O31728) and StrepDB (<http://strepdb.streptomyces.org.uk>) a *Streptomyces* database that allows access to gene sequence data for several *Streptomyces* species. In *S. coelicolor*, we found three SepF homologues, encoded by genes *SCO1749*, *SCO2079* and *SCO5967*, which are given the names as *sep1*, *sepF2* and *sepF3*, respectively. When the genome sequencing of *Streptomyces* was completed (Bentley *et al.*, 2002), gene annotation assigned a SCO number to each

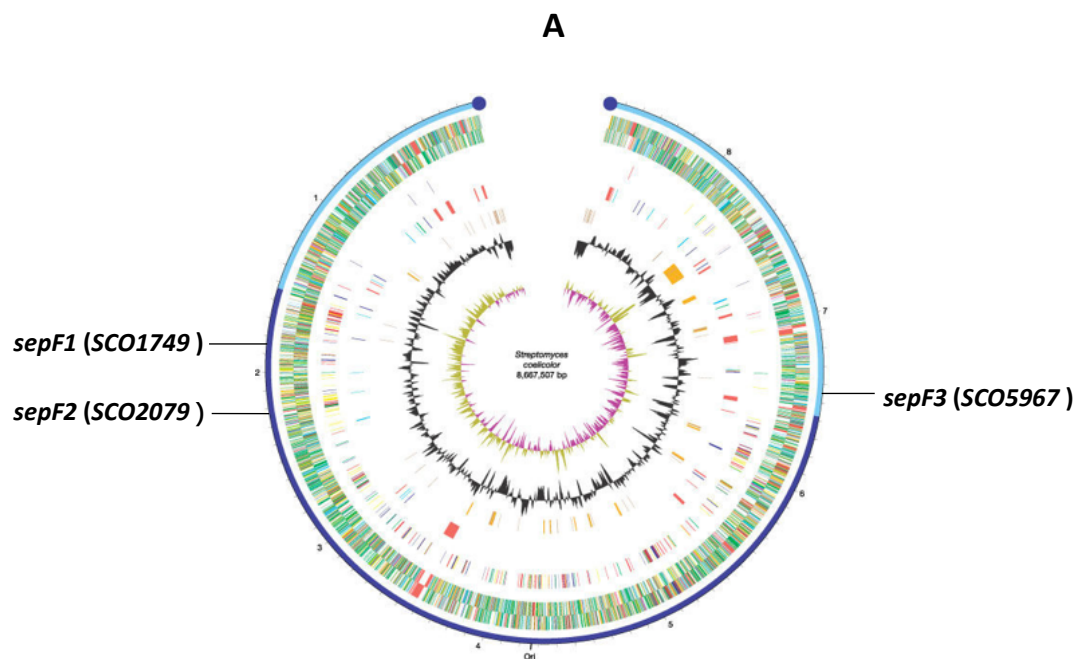
Sequences producing significant alignments:						Score (bits)	E Value
SCO2079	SCO2079, SC4A10.12c	SCO2079	CAB51988.1	SC4A10.12c	SCO2...	66	2e-12
SCO1749	SCO1749, 2SCI34.02	SCO1749	CAC12922.1	2SCI34.02	SCO174...	52	2e-08
SCO5967	SCO5967, SCBAC16H6.02	SCO5967	CAC44581.1	SCBAC16H6.02	...	52	4e-08

Figure 3.2. Homologues of SepF encoded in the *S. coelicolor* genome.

The amino acid sequence of SepF (UniProt O31728) from *B. subtilis* was used in a BlastP search against the translated *S. coelicolor* genome. There are three SepF homologues found encoded in the *S. coelicolor* genome.

gene, starting numbering from one end of the chromosome to the other. Therefore, these SCO numbers also indicate chromosomal locations of genes. In this thesis, I often use these SCO numbers without the SCO prefix. The 213 amino acids long *S. coelicolor* SepF2 (2079) exhibited the greatest level of sequence identity with the *B. subtilis* SepF (151 amino acids), despite the fact that SepF1 (1749) and SepF3 (5967) have a similar amino acid length (151 amino acids; Figure 3.2).

Gene *sepF1* (1749) and *sepF2* (2079) are located in the core region of *S. coelicolor* chromosome and *sepF3* (5967) is located in the arm region (Figure 3.3). *S. coelicolor* has a very large genome that contains many duplicated genes, therefore it is not surprising that there are multiple *sepF*-like genes. However, we did not find multiple copies of the key cell division genes such as *ftsZ* and *divIVA* in *S. coelicolor*



Gene	SCO number	Number of nucleotides	Number of amino acids	GC content %
<i>sepF1</i>	1749	441	146	68.48
<i>sepF2</i>	2079	642	213	63.86
<i>sepF3</i>	5967	411	146	70.56

Figure 3.3. The *S.coelicolor* genome (Bentley *et al.*, 2002) highlighting the position of the three *sepF* genes.

(A) Gene *sepF1* (SCO1749) and *sepF2* (SCO2079) are located in the core region of *S. coelicolor* chromosome (dark blue) and *sepF3* (SCO5967) is located in the arm region (light blue). (B) Comparisons of the three SepFs of *S. coelicolor*.

chromosome. In addition, *sepF2* (2079) is located in the cell division gene cluster containing the essential cell division gene *ftsZ*. This might suggest that the role of

SepF2 potentially is more linked to the role of FtsZ assembly during cell division. We carried out sequence alignment between the three SepF homologues encoded within *S. coelicolor* genome sequence from StrepDB (strepdb.streptomyces.org.uk) and SepF from *B. subtilis* (Table 3.1) using the software Clustal Omega (<https://www.ebi.ac.uk/Tools/msa/clustalo/>). SepF1 encoded by 1749 shares 50.6% identity with *S. coelicolor* SepF2 encoded by 2079 while SepF3 encoded by 5967 shares less identity with SepF2, that is 32.35%. SepF1 and SepF2 share the highest

```

sepF3      -----VKSGEPV-NSHDVTDEQW
sepF2      MAGAMRKMAVYLGLVEDDGYDGRGFDPDFDDDFEPELDPEPERDHRHE PAHQSHGAHQSQR
sepF1      -MGSVRKASAWLGLVDDNDDERYDDDYSEGPESGDA-----

sepF3      E-GLAQVVPLRGRDAWPS-----AVGHRAMPEA-ETE
sepF2      DEEVRVVQPPAQREMPRAASLAAESSRPARIAPVASITQERASLEKSAPVIMPKVVSER
sepF1      ---WV-----TDPRVKVASDVAEE
                                         : . .

sepF3      RRRRFVVLRLNINVADAREVAETLMAGI PVLLDLTSAEGEVAKRVLDFSTGVVFGLASGMH
sepF2      E PYRI T LHPRTYNEARTI GEHFREGT PVIMNLTEMDDTDAKRLVDFAAAGLVFGLHGS IE
sepF1      KGRRIATVT PDSFRDARAI GELFRDGVFVIVNLTAMEGTDAKRVDFAAGLIFGLRGS IE
.  *:::  : : ** :.* : * **::**  :.  ***::***::***  ...

sepF3      RVDNRVFLLLTPAGTEVNLME SAAGVPGV*----
sepF2      RVTQKVFLLSPANVDVT AEDKAR IAEGGF FNQS *
sepF1      RVSTRVFLLLSPADTQVI SGESAAHRSDGFFNQS *
**  .***:***:*. . . :  *

```

Figure 3.4. Protein sequence alignment of the three SepF homologues from *S. coelicolor*. (*) indicates positions which have a conserved residue, (:) represents conservation between groups of amino acids with strongly similar properties, and (.) indicates conservation between groups with weakly similar properties. The sequence alignment was generated using Clustal Omega

(<http://www.ebi.ac.uk/Tools/msa/clustalo/>). Residues AK and F that are implicated in the interaction with FtsZ are highlighted (Gupta *et al.*: 2015)

level of sequence identity amongst the three *S. coelicolor* homologues (Figure 3.4; Table 3.1). Interestingly, the residues that are involved in the interaction with FtsZ are conserved amongst all three SepFs of *S. coelicolor* (Figure 3.4). The SepF homologue with the greatest sequence identity to the *B. subtilis* SepF is *S. coelicolor* SepF2 (2079) with 29.8% identity (Figure 3.5; Table 3.1).

```

sepF2      MAGAMRKMAVYLGLVEDDGYDGRGFDPDDDFEPELDPEPERDHRRHPEAHQSHGAHQSOR
B. su      -MSMKNKLNKFFS-MEDEEY-----EYEYIET-----ERESHEEHEQK-
           .  .* :  :. :*: *                * *                ::* *:.

sepF2      DEEVRVVQPPAQREMPRAASLAAESSRPARIAPVASITQERASLEKSAPVIMPKVVSER
B. su      -----EKPA-----YNGNKPAGKQNVV-----SLQSQVQ
           :  **                :. :** * .                .: * :

sepF2      EPYRITLHPRTYNEARTIGEHFREGTPVIMNLTEDDTDAKRLVDFAAGLVFGLHGSIE
B. su      KSSKVVLEPRVYAEAEQEIADHLKNRRVVVNLQRIQHDQAKRIVDFLSGTVYAIGGDIQ
           :  :. .**.* **: *.:*:::  *::** .:. :***:*** :* *:. :*:.

sepF2      RVTQKVFLLSPANVDVTAEDKARIAEGGFFNQS*
B. su      RIGSDIFLCTPDNVDVSGTISELISEDEHQRW--
           *: .:.* :* *****. . *:* . .

```

Figure 3.5. Protein sequence alignment of the SepF homologues from *B. subtilis* (*B. su*) and SepF2 (*SCO2079*) from *S. coelicolor* (*sepF2*). (*) indicates positions which have a conserved residue, (:) represents conservation between groups of amino acids with strongly similar properties, and (.) indicates conservation between groups with weakly similar properties. The sequence alignment was generated using Clustal Omega (<https://www.ebi.ac.uk/Tools/msa/clustalo/>). Residues that are involved in FtsZ binding are highlighted (Gupta *et al.*, 2015; Duman *et al.*, 2013).

Table 3.1. Sequence identity resulting from the amino acid sequence alignments between SepF homologues identified in *S. coelicolor* (*sepF1*, *sepF2* and *sepF3*) and *sepF* in *B. subtilis*.

	<i>sepF2</i>	<i>sepF1</i>	<i>sepF3</i>	<i>B. subtilis</i>
<i>sepF2</i>	100%	50.00%	32.35%	29.80%
<i>sepF1</i>	50.00%	100%	33.33%	23.74%
<i>sepF3</i>	32.35%	33.33%	100%	21.32%
<i>B. subtilis</i>	29.80%	23.74%	21.32%	100%

The comparison of the three *S. coelicolor* SepFs highlighted areas of conservation (Figure 3.4). The residues that are involved in the interaction between FtsZ and SepF have been described in *B. subtilis* and in *Mycobacterium smegmatis* (Duman *et al.*, 2013; Gupta *et al.*, 2015). Interestingly, these residues are conserved in all three *Streptomyces* SepFs suggesting that all three SepFs might be able to interact with FtsZ.

Next, we were looking for the genes surrounding the *sepF* genes. In bacteria gene density is very high and genes that are involved in the same biological process often form operons and are located adjacent to each other in the chromosome. The gene *sepF2* (2079) is located in the conserved position within the cell division gene cluster between *ftsZ* and *divIVA* (Figure 3.6). Upstream of *sepF2* is 2080, which encodes a protein that shares a high level of homology with alanine racemases, finally 2081, which encodes a laccase, and 2082, which encodes FtsZ. Downstream of *sepF2* is 2077, which encodes DivIVA, a cytoskeletal protein involved in polar growth and branching (Flardh, 2003), and 2078, encoding a small hypothetical membrane protein (Figure 3.6A). Analysis of the gene organisation around *sepF1* identified upstream of *sepF1*, 1746 encoding a secreted serine protease, 1747 encoding a conserved hypothetical protein and 1748 encoding a probable transcriptional regulator. Downstream of *sepF1* is 1750 encoding a probable acyl-CoA dehydrogenase and 1751 encoding a putative transmembrane transport protein.

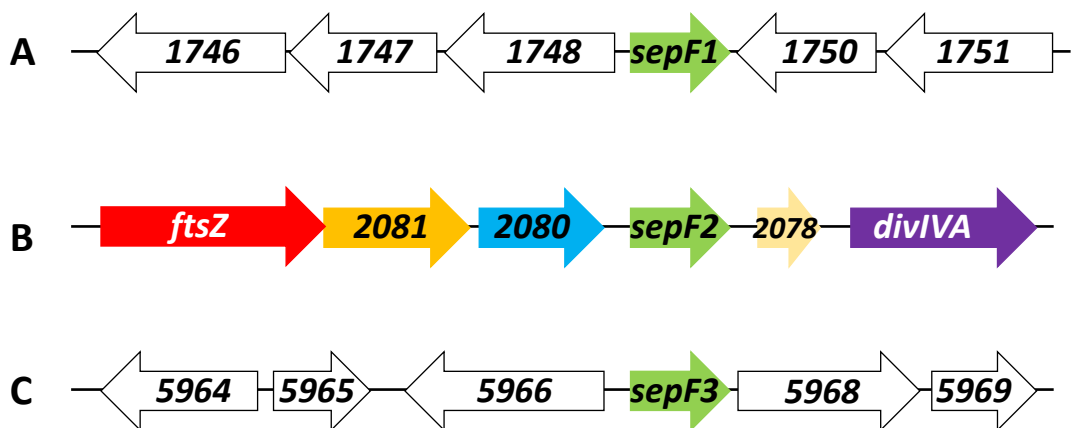


Figure 3.6. Gene organisation containing three *sepFs* and their surrounding genes.

A. Gene organization of *sepF1*(1749) and its surrounding genes. Gene *sepF1* is located on the reverse strand of core region in chromosome, shortly downstream of *sepF2*.

Gene organization of *sepF2*(2079) and its surrounding genes with their respective lengths (bp), which is involved in targeting studying in this thesis. *sepF2* gene is situated on the reverse strand of the core region in chromosome of *S. coelicolor*.

C. Gene organization of *sepF3*(5967) and its surrounding genes. Gene *sepF3* is situated on the forward strand of the right arm of chromosome.

These five surrounding genes all maintain a reverse orientation compared to *sepF1* (Figure 3.6 B). Upstream of *sepF3* is 5964 which encodes a putative membrane protein, 5965 which encodes a putative integral membrane protein and 5966 encoding a putative oxidase. Downstream of *sepF3* is 5968, which encodes a putative *bldA*-regulated nucleotide binding protein and 5969 encoding a conserved hypothetical protein. Among these five surrounding genes of *sepF3*, 5068 and 5069 are in the same orientation as *sepF3*, so these including *sepF3* might form an operon (Figure 3.6 C). None of the genes surrounding *sepF1* or *sepF2* have been characterised. As *sepF2* is encoded in the gene cluster that includes the cell division gene *ftsZ* and the gene for the cytoskeletal polarity determinant protein, DivIVA, we decided to focus our work on *sepF2*.

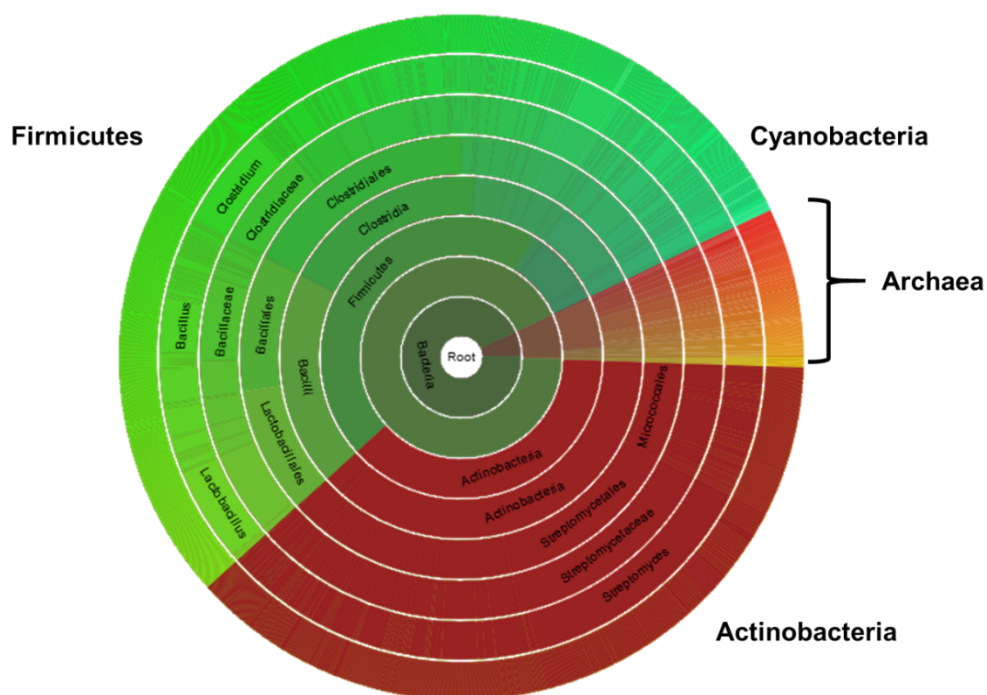


Figure 3.7. The distribution of SepF proteins amongst prokaryotes. SepF is well represented amongst the Phylae Firmicutes, Actinobacteria and Cyanobacteria according to the PFAM search (<https://pfam.xfam.org/family/PF04472.1>). Interestingly, SepFs are also found amongst Archaea.

Intriguingly, although SepF is widely represented amongst some bacterial phyla such as the Actinobacteria and Firmicutes, it is also absent in some, such as Proteobacteria. Interestingly, SepF is present amongst Archaea (Figure 3.7). We then compared the three SepFs of *S. coelicolor* with some SepF proteins of the Actinobacteria phylum, where *Streptomyces* also belongs. Sequence alignment for selected SepFs showed quite poor conservation amongst these actinomycete sequences (Figure 3.8), which is a bit surprising. SepF1 and SepF2 from *S. coelicolor* have more similarity to each other than SepF3 (Table 3.1). In this research, we focused on the SepF protein encoded by *sepF2* in the *ftsZ – divIVA* cell division gene cluster.

In addition, the percentage of identity increased when we omitted the *Bifidobacterium* and *Corynebacterium* sequences (Figure 3.9). The sequence identity between SepF2 of *S. coelicolor* and *M. tuberculosis* is 40.59% that is expectedly much higher than between the *Streptomyces* SepF2 and SepF of *B. subtilis* (29.80%). In this work I characterised only one of the *sepF* genes, *sepF2*, therefore in future descriptions I simply refer to *sepF* rather than *sepF2*.

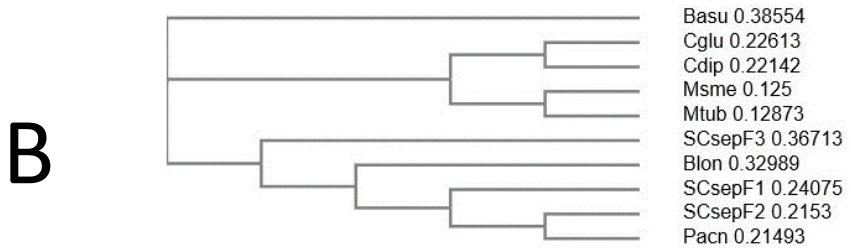
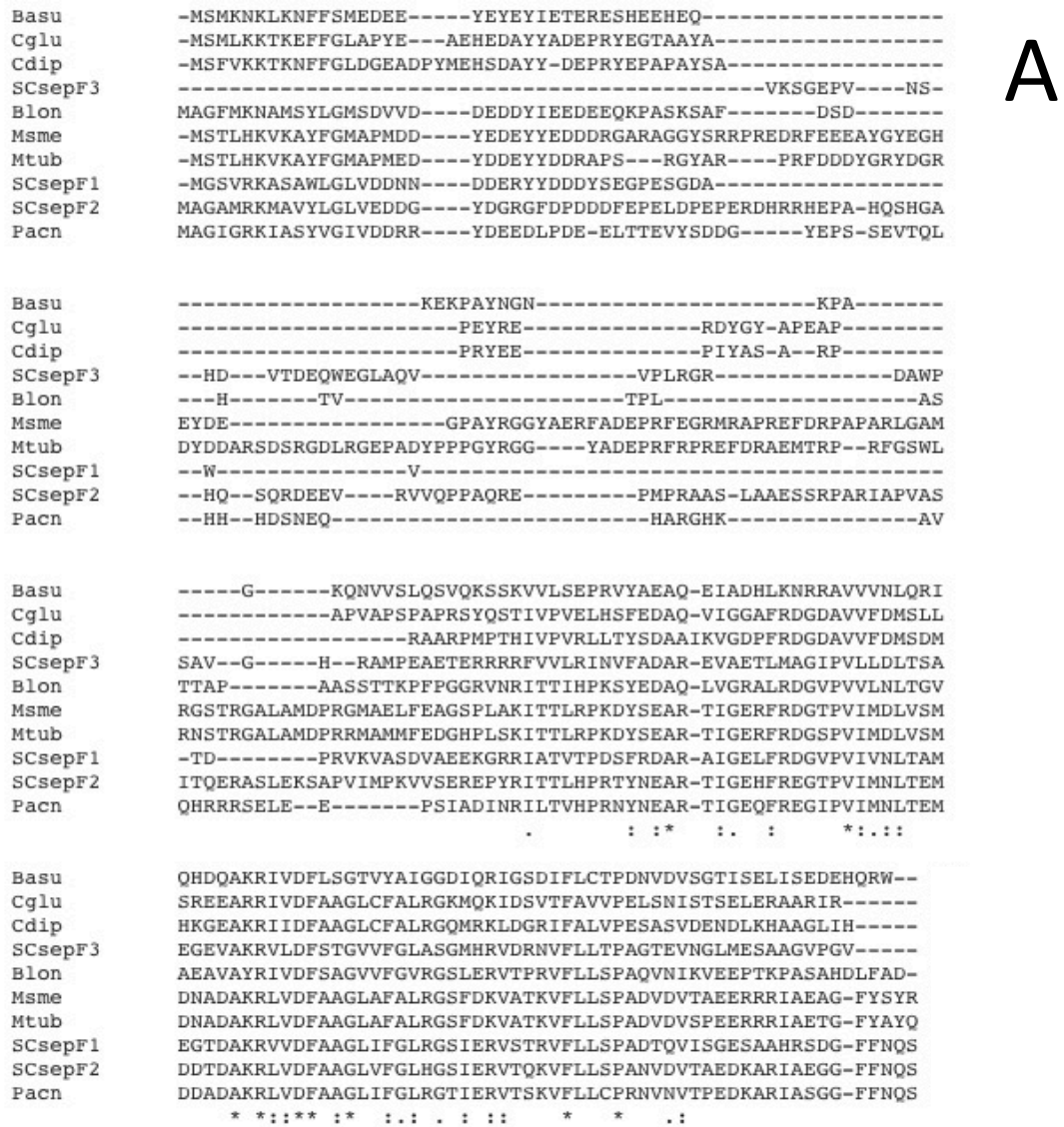


Figure 3.8. Sequence alignment of actinobacterial SepFs. The sequences shown, together with the uniprot numbers in brackets, are the following: SCsepF1, *Streptomyces coelicolor* (Q9EWX7); SCsepF2, *Streptomyces coelicolor* (Q9S2X2); SCsepF3, *Streptomyces coelicolor* (Q93JG0); Msme, *Mycobacterium smegmatis* mc2 (A0R008); Mtub, *Mycobacterium tuberculosis* H37Rv (P9WGJ5); Cglu, *Corynebacterium glutamicum* (Q8NNN6); Cdip, *Corynebacterium diphtheriae* (Q6NGD3); Pacn, *Propionibacterium acnes* (Q6A9P7); Blon, *Bifidobacterium longum* (Q8G7W6); Basu, *B. subtilis* (O31728). (A) The sequence alignment was generated using Clustal Omega (<https://www.ebi.ac.uk/Tools/msa/clustalo/>). (*) indicates positions which have a conserved residue, (:) represents conservation between groups of amino acids with strongly similar properties, and (.) indicates conservation between groups with weakly similar properties. (B) Simple phylogenetic tree generated using the same software (Clustal Omega).

```

Msme      -MSTLHKVKAYFGMAPMDDYEDEYYEDDDRGARAGGYSRRPREDRFEEAYGYEGHEYDE
Mtub      -MSTLHKVKAYFGMAPMEDYDDEYYDDRAPS---RGYAR----PRFDDDYGRYDGRDYDD
Scoe      MAGAMRKMAVYLGLEVEDDGYDGRGFDPPDD-----FEPELDPEPERDHRH
Pacn      MAGIGRKIASYVGIVDDRRYDEEDLPDE-E-----LTTEVYSDDG-----
          .  *:  *.*:  *:  .                :  :

Msme      -----GPAYRGGYAERFADEPRFEGMRAPREFDRPAPARLG
Mtub      --ARSDSRGDL---RG-EPADYPPPGYRGG----YADEPRFRPREFDRAEMTRP--RFGS
Scoe      HEPAHQSHGAHQSQRDEEVRVQPPAQRE-----PMPRAAS-LAAESSRPARIAPV
Pacn      YEPSSEVTQLHHHDSNEQ-----HARGHK-----
          .

Msme      AMRGSTRGALAMDPRGMAELFEAGSPLAKITTLRPKDYSEARTIGERFRDGTVPVIMDLVS
Mtub      WLRNSTRGALAMDPRMAMMFEDGHPLSKITTLRPKDYSEARTIGERFRDGSVPVIMDLVS
Scoe      ASITQERASLEKSAPVIMPKVVSEREPYRITTLHPRTYNEARTIGEHEFREGTVPVIMNLTE
Pacn      AVQHRRRSELE--E-----PSIADINRILTVHPRNYNEARTIGEQFREGI PVIMNLTE
          *  *                : * *::*: * .*****: ** : *  ** : * ..

Msme      MDNADAKRLVDFAAGLAFALRGSFDKVATKVFLLSPADVDVTAEEERRR IAEGFYSYR
Mtub      MDNADAKRLVDFAAGLAFALRGSFDKVATKVFLLSPADVDVSPEERRR IAETGFYAYQ
Scoe      MDDTDAKRLVDFAAGLVFGLHGSIERVTQKVFLLS PANVDVTAEDKARIAEGGFNQS
Pacn      MDDADAKRLVDFAAGLIFGLRGTIERVTSKVFLLCPRNVNVTPEDKARIAEGGFNQS
          **: :***** * .*: : : : * : ***** * : * : * : * : * : * :

```

Figure 3.9. Sequence alignment of actinobacterial SepFs. The sequences shown, together with the uniprot numbers in brackets, are the following: Scoe, *Streptomyces coelicolor* (Q9S2X2); Msme, *Mycobacterium smegmatis* mc2 (A0R008); Mtub, *Mycobacterium tuberculosis* H37Rv (P9WJ5); Pacn, *Propionibacterium acnes* (Q6A9P7).

The sequence alignment was generated using Clustal Omega (<https://www.ebi.ac.uk/Tools/msa/clustalo/>). (*) indicates positions which have a conserved residue, (:) represents conservation between groups of amino acids with strongly similar properties, and (.) indicates conservation between groups with weakly similar properties.

We also tested the gene organization around the *sepF* gene in different bacteria that possess *sepF* gene. We used BLAST searches and also the KEGG database (<http://www.genome.jp/kegg/>) for establishing gene synteny amongst the microorganisms (Figure 3.9). Amongst the Actinobacteria, the gene order and organization between *ftsZ* and *sepF* was highly conserved, with two genes in between, encoding an alanine racemase and a putative copper binding protein, encoded by *SCO2080* and *SCO2081*, respectively in *S. coelicolor*. Not surprisingly, in *B. subtilis* the gene organization is somewhat diverged. However, even here the arrangement of *sepF* and the two upstream genes are maintained, with the *ftsZ* gene located 7 genes more upstream and with an additional gene downstream of *sepF* (Figure 3.10).

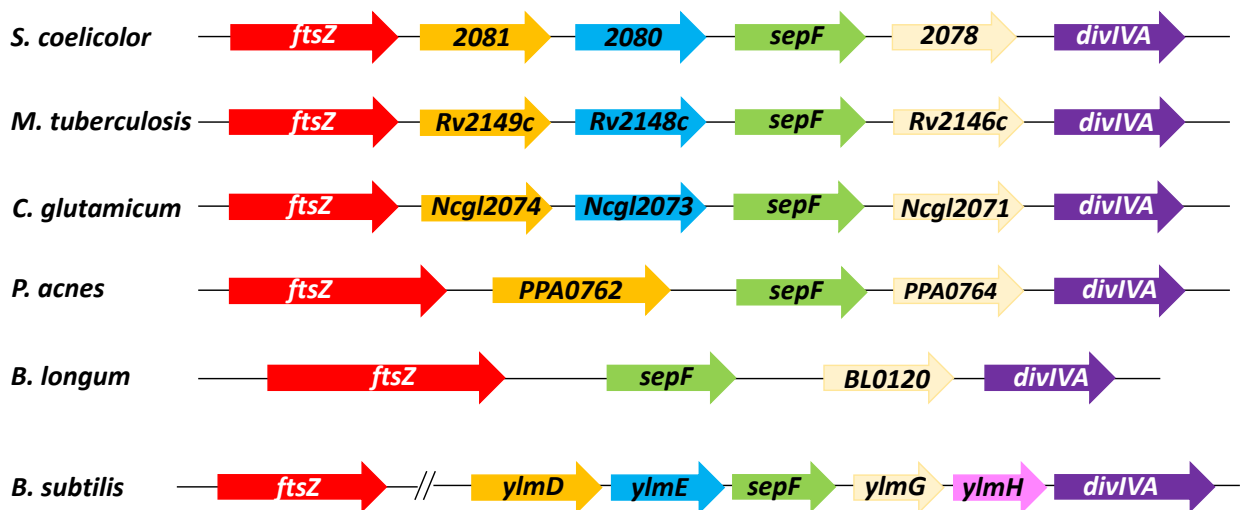


Figure 3.10. Gene organization of *S. coelicolor*, *M. tuberculosis*, *C. glutamicum*, *P. acnes*, *B. longum* and *B. subtilis*. Identical colour represents homologous protein products as identified using BLAST searches and the KEGG database.

3.2 Generation of the *S. coelicolor* *sepF* mutant strain

The *sepF* mutant strain was generated using REDIRECT[®] PCR-directed mutagenesis (Gust *et al.*, 2002). The gene *sepF* was knocked out by replacing it with an apramycin resistance disruption cassette. To generate a *sepF* gene knockout mutant, an apramycin resistance cassette containing 40 bp flanking regions that are homologous to the flanking regions of *sepF* gene can be used to disrupt the target gene (Figure 3.11). Once the disruption cassette was generated using PCR, it was used to replace the *sepF* gene with the apramycin resistance gene via homologous

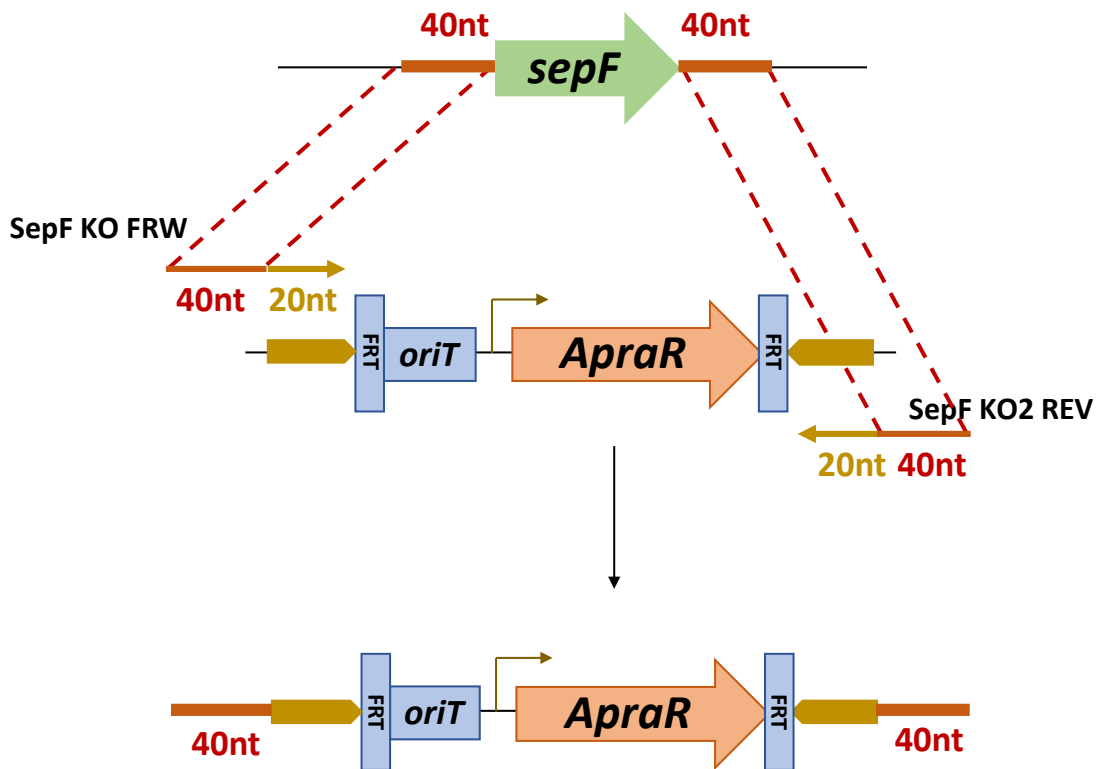


Figure 3.11. PCR amplification of the apramycin resistant cassette from PIJ773 for gene 2080 knockout using primers SepF KO FRW and SepF KO2 REV. The apramycin resistant cassette contained an *oriT* site, an apramycin resistance gene, and FLP recognition targets (FRT) required to excise the resistance marker. Primers were used containing DNA complementary to the DNA sequences (20 nt) of the template and DNA complementary to sequences flanking the region of DNA we wanted to replace (40 nt). PCR was used to create the disruption cassettes with appropriate combinations of primers (Gust, *et al.*, 2002).

recombination between the PCR generated cassette and the appropriate cosmid DNA that carried *sepF* and its surrounding genes in *E. coli*. The homologous recombination is promoted by the lambda RED recombinase. After the recombination event the cosmid that now contained the *sepF* null allele was introduced to *Streptomyces* using conjugation. As the cosmid itself cannot replicate in *Streptomyces*, it can only recombine with the chromosomal DNA generating a double crossover, full gene knock out (Figure 3.12).

The apramycin resistant cassette with *oriT* from plasmid pIJ773 was excised from pIJ773 using restriction enzymes *EcoRI* and *HindIII* and then purified from 0.7%

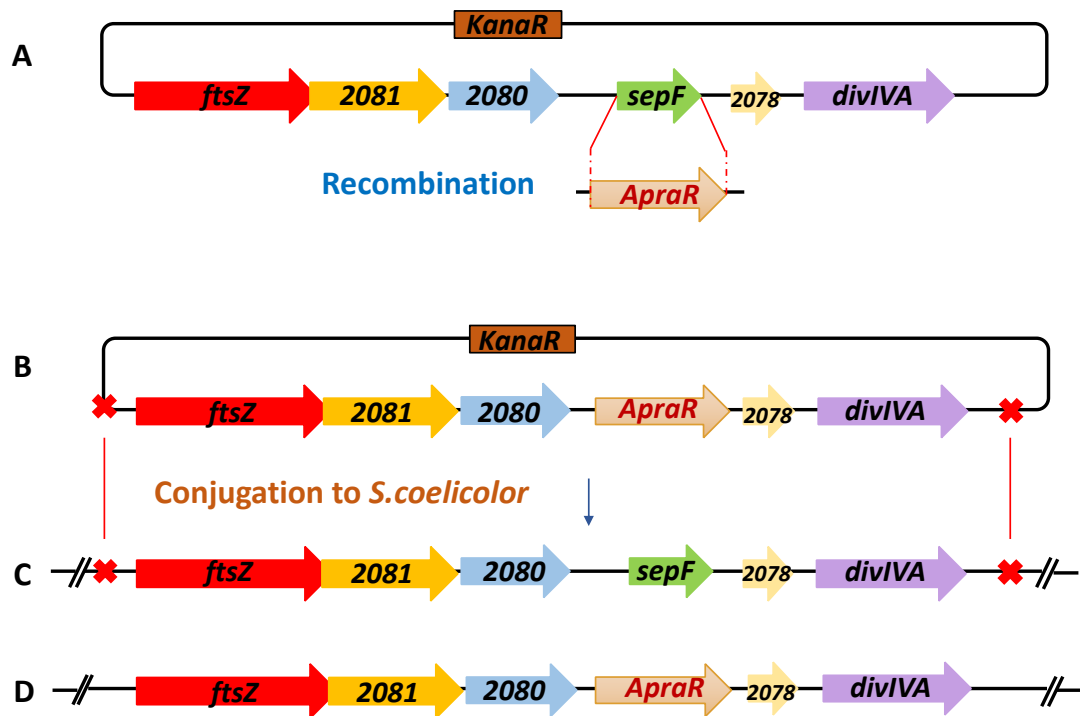


Figure 3.12. Knock out design for the generation of the *sepF* null mutant in *S. coelicolor*. In a cosmid containing *sepF* and its flanking genes, the *sepF* gene was replaced with an apramycin resistance cassette (Apra R) (A). Then the resulting cosmid (B) was conjugated into *S. coelicolor* (C). The apramycin resistance cassette replaced the *sepF* gene in *S. coelicolor* chromosome (D) after a double crossover event (B-D).

agarose gel using gel extraction. This apramycin resistance disruption cassette (~1.3kb) from pIJ733 was PCR amplified using the primers SepF KO FRW and SepF KO2 REV which are complimentary to the flanking sequences of target for knockout gene *sepF* (Figure 3.11). The resulting PCR product was then desalted using a self-made mini gel filtration column. This PCR product of apramycin cassettes produced for the knockout of *sepF* was analysed on a 0.7% agarose gel (Figure 3.13) which confirmed that PCR reactions resulted in correct amplification of the expected ~ 1.3 kb extended apramycin cassette.

The cosmid 4A10, containing *S. coelicolor* chromosomal DNA that carried the *sepF* (*sepF2*) gene and its surrounding genes, was used to target the apramycin resistance disruption cassette. The cosmid 4A10 was transformed into the *E. coli* strain BW25113 carrying pIJ790 plasmid, which encoded the phage lambda RED recombinase (λ RED) genes *gam*, *bet* and *exo* which are transcribed by the L-arabinose inducible promoter Para_{BAD} . The λ RED recombinase allows the homologous recombination between the flanking regions of the extended apramycin resistance cassette and flanking regions of target gene in order to replace the target gene with the cassette (Datsenko and Wanner, 2000).

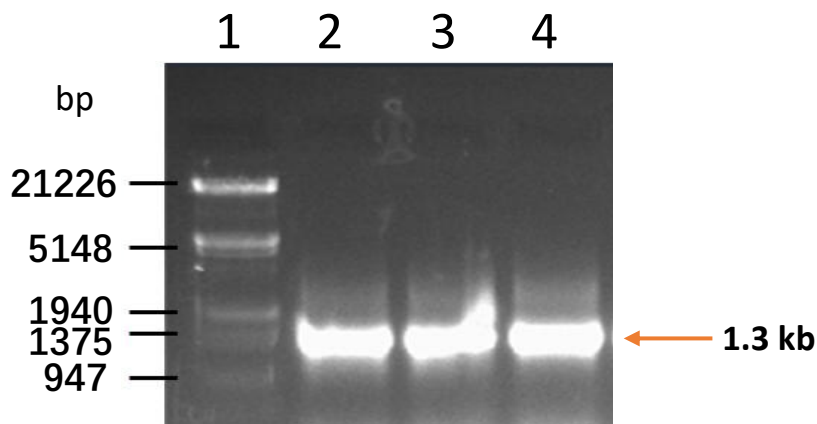


Figure 3.1.3. A. Amplification of apramycin disruption cassette using primers SepF KO FRW and SepF KO2 REV for knockout of gene *sepF*.

Gel analysis of the PCR amplification of apramycin disruption cassettes for the targeted knockout of *sepF2* (lane 4) using lambda DNA cut with *EcoRI* and *HindIII* as a molecular weight marker (lane 1). For this chapter, the product in lane 4 was produced using primers SepF KO FRW and SepF KO2 REV. Lanes 2 and 3 are not relevant here.

The apramycin resistance disruption cassette was then electroporated into the *E. coli* strain BW25113 carrying the *S. coelicolor* cosmid 4A10. The addition of L-arabinose to the media growing the *E. coli* BW25113 cells causes expression of the recombinase enzyme which initiates a homologous recombination event between the flanking regions of the apramycin resistance cassette and the reciprocal sequence

flanking the gene *sepF*. The plasmid pIJ790 contains a temperature sensitive origin of replication which results in its loss when the BW strain is grown at temperatures higher than 30°C. Therefore, after the disruption cassette was transformed into the BW25113, cells containing the 4A10 cosmid obtained from the transformation were plated onto LB containing apramycin, to select for successful recombination events and grown at 37°C to induce the loss of pIJ790. We picked several single apramycin resistant transformants, extracted the cosmid DNA from the cultured single colony using large scale cosmid extraction to obtain the cosmid DNA that had been disrupted.

To confirm the replacement of the *sepF* gene by the apramycin cassette in the cosmid, a restriction digest of the extracted cosmid DNA was conducted using *EcoRI* and *XbaI* enzymes. An “in-silico” restriction digest map was generated (Figure 3.14) using ARTEMIS (Rutherford *et al.*, 2000) highlighting the fragment sizes (Table 3.2). The *in silico* design confirmed that if the mutant cosmid was successfully generated, using *EcoRI* and *XbaI* enzymes we expected the wild-type ~20 kb fragment to be replaced by three fragments of ~12 kb, 7.8 kb and 1.3 kb in the mutant cosmid. The wild-type 4A10 cosmid digest generated four fragments between 5-20 kb, which corresponded to the sizes determined by the restriction map (Figure 3.15). According to the restriction maps the 20 kb fragment should be absent in the knockout gene cluster whilst the 6.7 kb, 8 kb and 14 kb fragments should remain uniform. This was confirmed in the knockout cosmid indicating that the apramycin cassette had been successfully incorporated within the targeted gene cluster. In the mutant cosmid the 20 kb fragment was replaced by four new fragments, three of which were visible on the gel. A 1.3 kb fragment, representing the apramycin cassette, could be seen further confirming its incorporation into the cosmid (Figure 3.15).

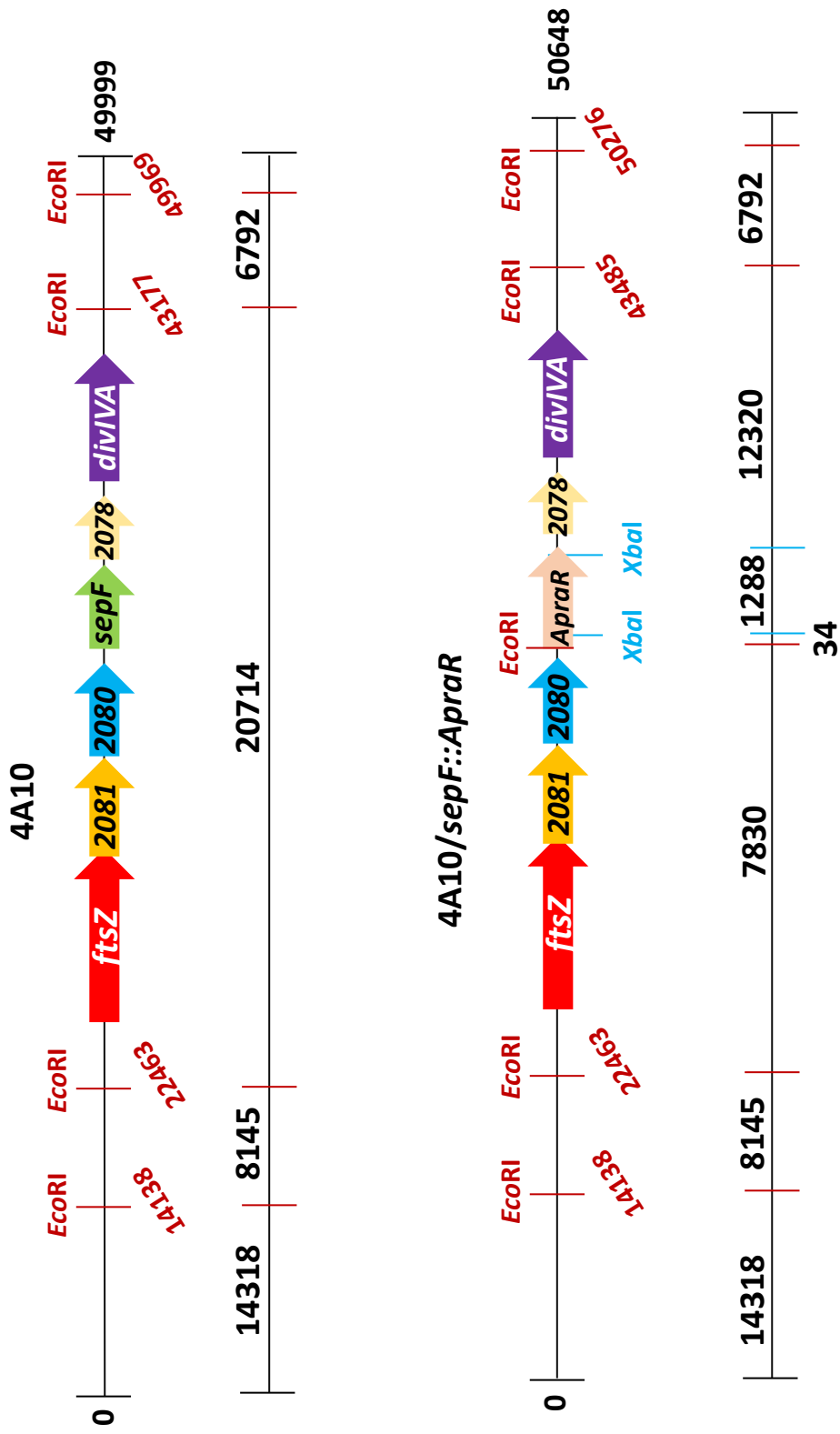


Figure 3.14. The gene map of the 4A10 cosmid and the 4A10/*sepF*::*ApraR* cosmid highlighting the position of *EcoRI* and *XbaI* restriction enzyme cleavage sites and the subsequent fragment sizes generated by a restriction digest (bold red). The tilted numbers represent the location of the restriction sites using the cosmid numbering. The horizontal numbers represent the size of each restriction fragments (bp).

Table 3.2. The expected fragments that are generated by restriction digest using endonucleases *EcoRI* and *XbaI* of the wild-type 4A10 cosmid and 4A10/*sepF::ApraR* cosmid. Shaded fragments represent those that remain the same in both cosmid digests.

4A10	4A10/ <i>sepF::ApraR</i>
20714	-
14318	14318
-	12320
8145	8145
-	7830
6792	6792
-	1288
-	34

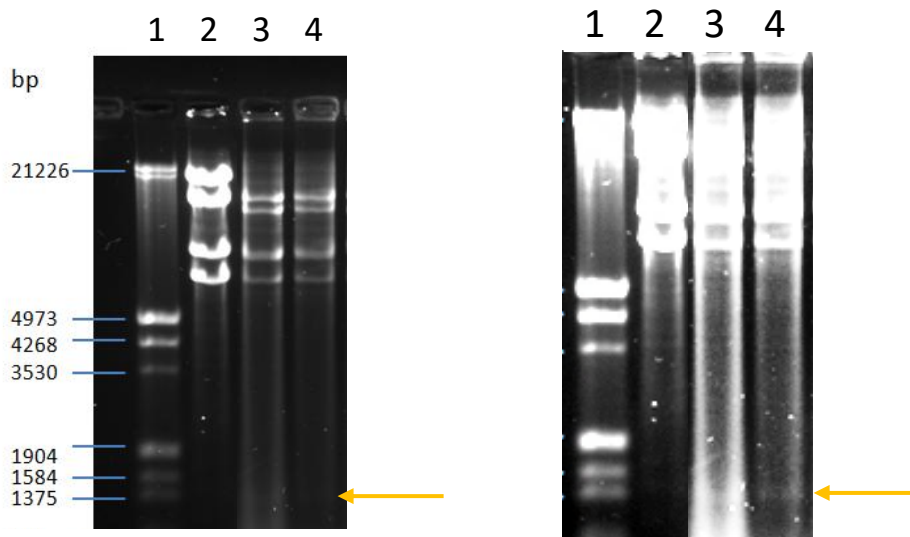


Figure 3.15. Confirmation of the mutant cosmid 4A10/*sepF::ApraR* using restriction digest with *EcoRI* and *XbaI*. The restriction digest of the extracted cosmids were run on a 0.7% agarose. The wild-type 4A10 cosmid (lane 2) and two 4A10/*sepF::ApraR* cosmids (lane 3 and 4) were digested with *EcoRI* and *XbaI* and the digests were analysed on a 0.7% agarose gel. Lambda DNA cut with *EcoRI* and *HindIII* was used as a molecular weight marker (Lane 1), sizes shown in bp. The 1.3 kb fragment carrying the apramycin resistance cassette is shown by the orange arrow. The gel images represent the same gels. The bands with an arrow were too weak to be visible, so I over exposed the gel in the image on the right to detect this band.

After confirmation of the cosmid 4A10/*sepF::ApraR*, it was transformed into a methylation-deficient *E. coli* strain ET12567/pUZ8002 and then conjugated into the wild-type *S. coelicolor* strain, M145 (Figure 3.15 B). Selection of exconjugants containing the apramycin cassette was achieved by overlaying the plates using apramycin to which the mutant strain is resistant. We also used nalidixic acid to kill the *E. coli* bacteria. However, the selection using apramycin was not able to differentiate between the desired double crossover event and single crossover event. The double crossover event generates a single copy of the gene cluster including the knockout mutation and the single crossover event results in two copies of the gene locus, one wild-type and the other carrying the knockout mutation. To distinguish colonies that had undergone a double crossover event and thus contain a single copy of the gene cluster without the *sepF* gene, we used replica plating to identify colonies that were sensitive to kanamycin but resistant to apramycin. It was very difficult to identify double crossover recombinants, as the presumed *sepF* mutants did not produce enough spores and therefore could not be transferred well using replica plating. Instead, we picked colonies from the primary conjugation plates that did not transfer during replica plating and streaked them onto SFM plates with apramycin and tested them also on SFM plates with kanamycin. The selected colonies identified as potential double crossovers were streaked on SFM medium with a cellophane layer on top and streaked for making stock for future analysis. As the potential *sepF* mutants were sickly and appeared not to sporulate, we did not attempt to collect spores, instead we collected whole cells from the top of the cellophane after 5-6 days growth and stored the mycelia in a special storage medium at -20°C.

3.3 Confirmation of the *S. coelicolor sepF* mutant strain

To confirm whether the *sepF* gene was successfully replaced with the apramycin resistant disruption cassette in the chromosome of *S. coelicolor*, we performed PCR tests using different primer pairs using chromosomal DNA from wild-type and the *sepF* mutant strains. We extracted chromosomal DNA from cells grown on the surface of cellophane on SFM medium. In the PCR test we also included the original cosmid 4A10 and the mutant cosmid 4A10/*sepF::ApraR* as controls.

Firstly, we used two external flanking primers of the *sepF* gene, one (SepF XbaBgl Prom FRW) located upstream of the *sepF* gene and the other (SepF 3' END) situated downstream of the *sepF* gene. With these two primers, a PCR product will be generated using both wild-type and the $\Delta sepF$ mutant chromosome extracts but with different sizes. The size of the apramycin disruption cassette (~1.3kb) is larger than size of *sepF* (642bp) therefore the PCR product generated from the chromosome or cosmid of the *sepF* mutant (1773bp) will be larger than the PCR product generated from chromosome or cosmid from the wild-type (922 bp) (Table 3.3 and Figure 3.16). In the second PCR, we used SepF KO2 REV, which was used to generate the knockout, which means that it can prime at the 3' end of the apramycin resistant cassette (Table

Table 3.3. The expected sizes of PCR fragments using selected oligo pairs in wild-type strain and *sepF* mutant strain.

Oligos	Size in wild-type	Size in $\Delta sepF$ mutant
SepF XbaBgl Prom FRW SepF 3'END	922 bp	1773 bp
SepF XbaBgl Prom FRW SepF KO2 REV	-	1518 bp

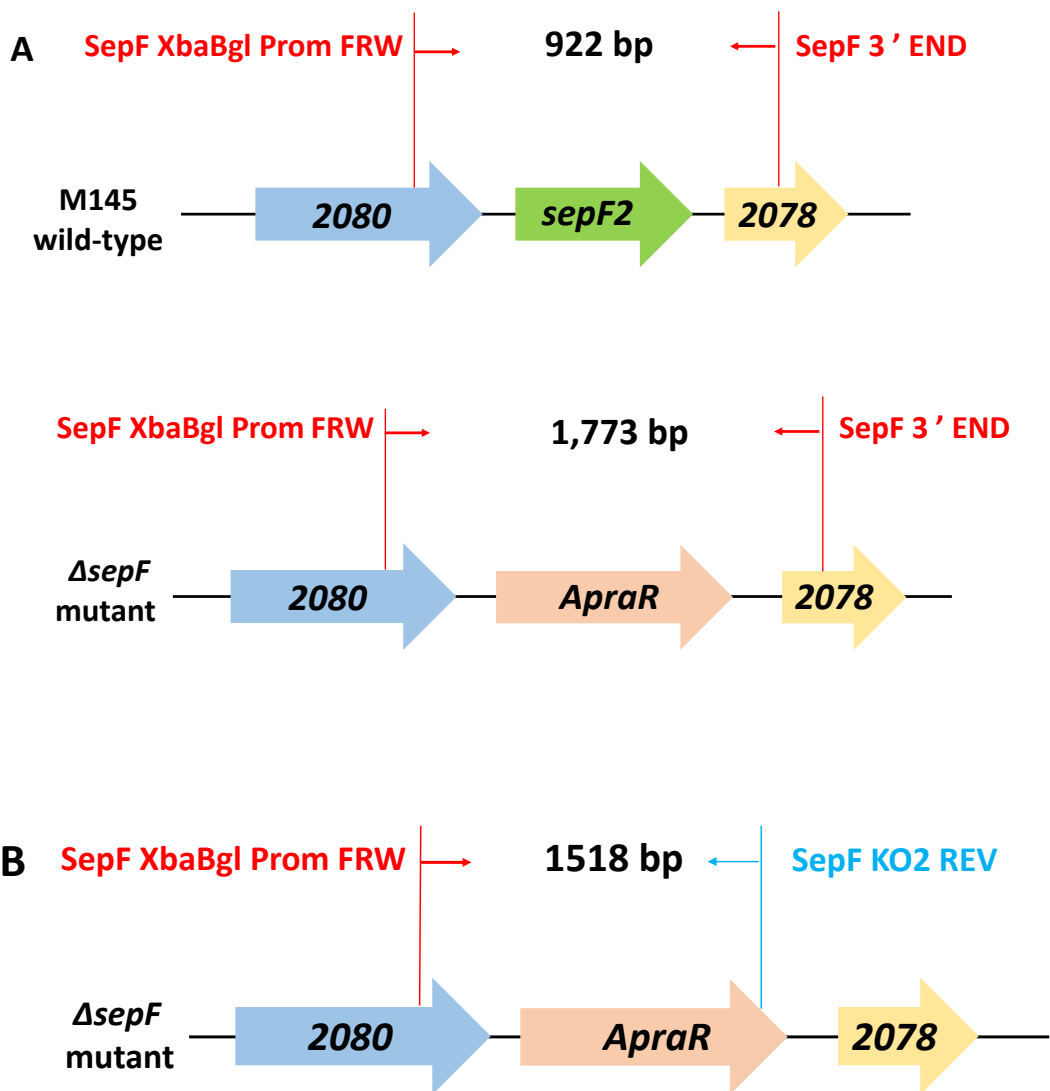


Figure 3.16. Confirmation of the *sepF* mutant using PCR.

(A) The primer SepF XbaBgl Prom FRW and *sepF* 3' END were used to generate PCR products to test whether the *sepF* gene was successfully replaced with the apramycin resistant disruption cassette in the chromosome of *S. coelicolor*. The expected sizes of PCR products showed difference in wild-type strain M145 and *sepF* mutant strain due to the replacement of apramycin resistant cassette (*Apra R* cassette). (B) The primers SepF XbaBgl Prom FRW and SepF KO2 REV will generate a PCR product only in the *sepF* mutant.

3.3 and Figure 3.16). The pairs SepF XbaBgl Prom FRW and SepF KO2 REV were used to generate PCR product only in the Δ *sepF* mutant strain. The expected size of PCR fragments are shown in Table 3.3. The PCR products were run on a 0.7% agarose gel (Figure 3.17).

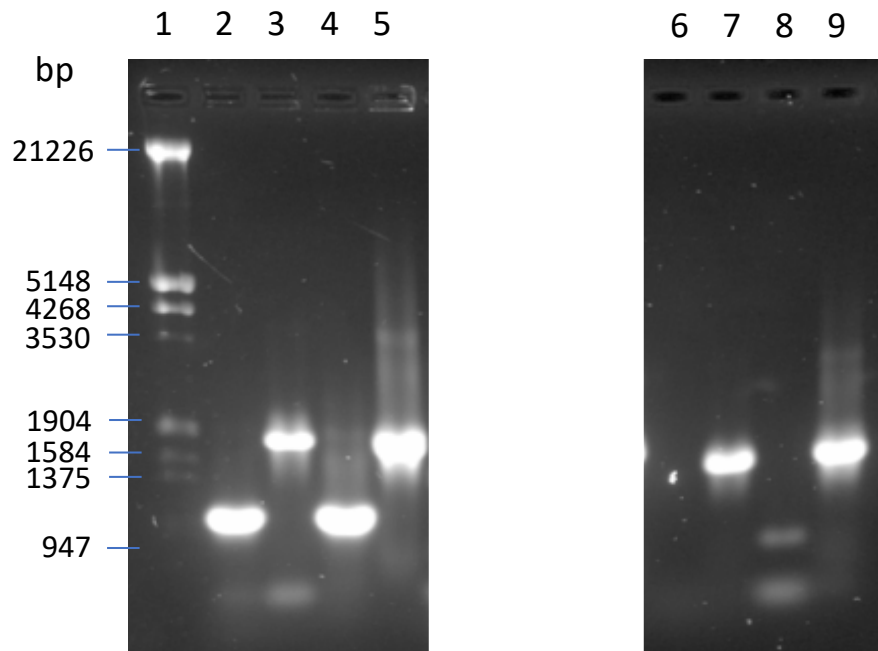


Figure 3.17. Confirmation of the *sepF* knockout mutant. Chromosomal DNA and relevant cosmid DNA was used as templates in PCR reactions.

Lane 1: Lambda DNA digested with *EcoRI* and *HindIII*, sizes shown in bp. Lane 2 and lane 6: wild-type M145 chromosome; Lane 3 and lane 7: Δ *sepF* mutant chromosome; Lane 4 and lane 8: 4A10 cosmid; Lane 5 and lane 9: 4A10/*sepF*::*ApraR* cosmid. Lanes 2-5 were tested using primers SepF XbaBgl Prom FRW and SepF 3'END. Lanes 6-9 were tested using primers SepF XbaBgl Prom FRW and SepF KO2 REV.

When using the flanking primers, SepF XbaBgl Prom FRW and SepF 3' END we generated two distinct PCR products corresponding to the expected sizes (Figure 3.17 lanes 2-5 and Table 3.3) depending whether wild-type or mutant DNA was used as templates. Importantly, there were no wild-type sized PCR products using the mutant DNAs confirming that the knockout strain does not contain the wild-type allele. When using the primers SepF XbaBgl Prom FRW and SepF KO2 REV, we only generated PCR product of the expected size when mutant DNA was used as a template (Figure 3.17 lanes 6-9 and Table 3.3). This is expected as the SepF KO2 REV primer will anneal to the apramycin resistance cassette that is only present in the mutant DNA.

3.4 The *S. coelicolor sepF* mutant strain has a severe developmental phenotype

3.4.1 Analysis of the macroscopic phenotype of the *sepF* mutant strain

To determine the macroscopic phenotype of the *sepF* mutant strain, it was plated onto SFM medium along with the wild-type control, M145. The spores were plated in a triangle shape with all the triangles of equal size to ensure that development was unaffected by the plating. Development is linked to nutrient depletion so it is important to make sure that each confluent triangle has access to the same nutrients. The plate then was grown at 30°C and it was observed daily (Figure 3.18). After one day (~24hrs), we can observe the matt appearance layer of the bacteria which corresponded to the development of vegetative hyphae of both the wild-type and the *sepF* mutant strains. After two days (~48-50hrs) of development, the colonies of both strains showed a developed fuzzy and white morphology which was consistent with growth of aerial hyphae. In this stage, the wild-type M145 strain exhibited faster growth than the *sepF* mutant strain and started to show divergence in development. After three days (~72hrs), the *sepF* mutant strain and wild-type M145 strain had obvious difference in development. The wild-type M145 strain presented classic grey pigment associated with mature spores that is produced at the end of the life cycle. After three days (~72hrs), similar to the most severe division mutants, the *sepF* mutant presented a white phenotype, which suggests that the *sepF* mutant was blocked for sporulation. After four days, the *sepF* mutant produced large amounts of the blue pigmented antibiotic, actinorhodin that typically is secreted into the surrounding medium in the wild-type strain. However, the *sepF* mutant not only secreted blue actinorhodin into the medium but it produced blue aerial hyphae suggesting that the actinorhodin was either produced in the aerial hyphae or it is diffused there. The fact that the *sepF* mutant failed to become grey even after 5-6 days incubation suggested that the *sepF* mutant failed to produce spores in the final stages.

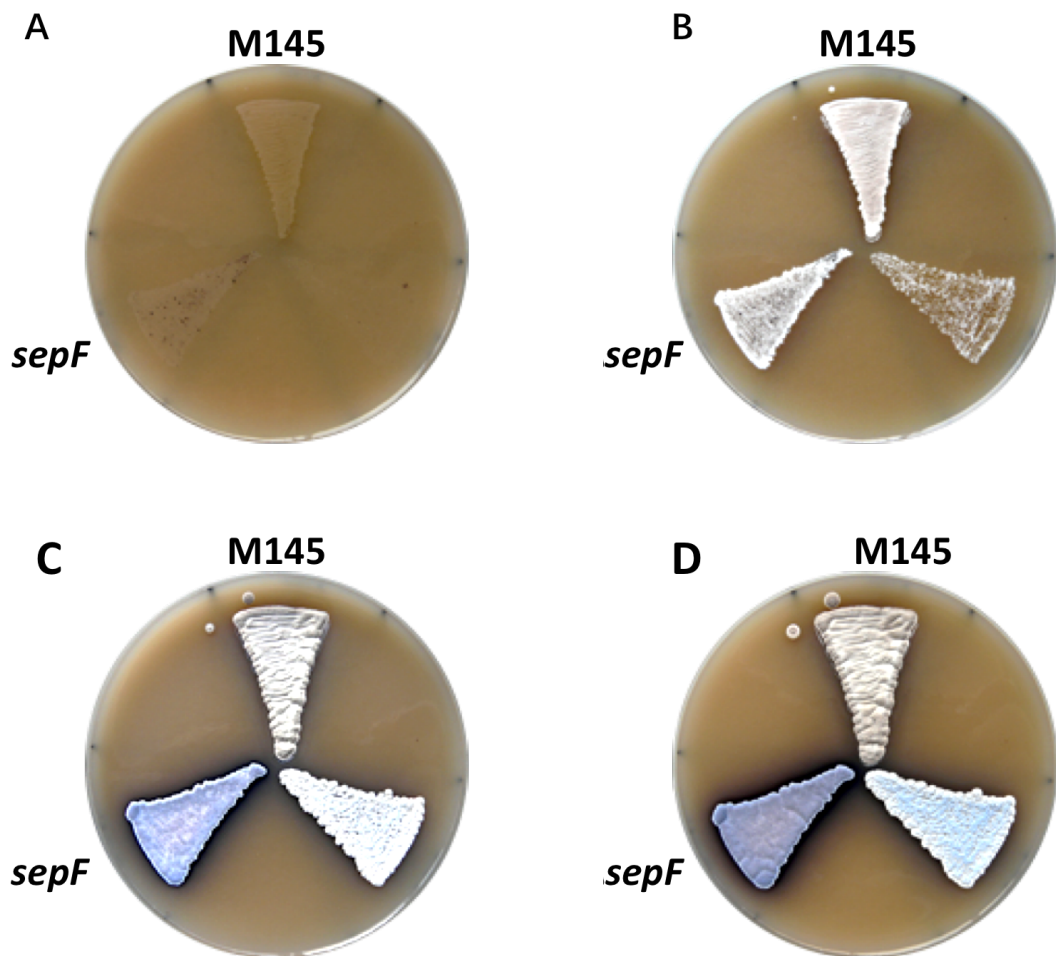


Figure 3.18. Macroscopic phenotype analysis of the *sepF* mutant strain. Wild-type M145 and the *sepF* mutant strain were plated in a triangle patch on a plate using SMF medium. The plate was incubated and monitored at regular time intervals (A) 1 day, (B) 2 days, (C) 3 days and (D) 4 days. It was observed that wild-type developed faster than the *sepF* mutant and produced grey pigment associated with spore maturation. The *sepF* mutant failed to become grey suggesting that it failed to sporulate. Unlabelled strain is not related to this experiment.

3.4.2 Analysis of the *sepF* mutant phenotype using microscopy

To confirm that the *sepF* mutant failed to sporulate we performed microscopy analysis of the wild-type M145 strain and *sepF* mutant. We monitored hyphal morphology during vegetative growth and we particularly focussed on the developmental stage when the aerial hyphae transform into spore chains. The microscopic phenotype of wild-type M145 strain acted as a control representing the different developmental stages from vegetative growth, aerial growth and sporulation. The spores of wild-type M145 strain were inoculated as patches onto SFM plates. Then we embedded sterilized glass coverslips at a 70° angle from horizontal plain of the medium into the inoculation streak line and grew the plates at 30°C. In order to monitor different stages of growth during cell differentiation in *S. coelicolor*, we stained the samples that adhered to the coverslips collected at different time points during growth and then detected the phenotype using epifluorescence microscopy. To properly visualise the formation of septa and segregation of chromosomes, we stained the cells using two dyes: wheat germ agglutinin (WGA) Alexa Flour® 488 and propidium iodide (PI). Wheat germ agglutinin (WGA) Alexa Flour® 488 emits green fluorescence when excited at 488nm and it has affinity to the cell wall, particularly newly synthesized cell wall stains more intensely. Propidium iodide is a DNA intercalator and its emission is at ~530nm, generating red fluorescence. Wild-type strain was monitored microscopically to act as a comparison. The first sample was collected and stained using WGA and PI after 42 hours of inoculation. At this early stage, we detected branching hyphal growth of wild-type M145. Using the staining we can detect vegetative crosswall formation in the vegetative hyphae, which separates compartments within the hyphae (Figure 3.19). The PI stained chromosomes (red) show continuous signal that is interrupted at the site of crosswall formation. The even staining of the chromosomes does not allow us to distinguish individual chromosomes within the hyphae (Figure 3.19).

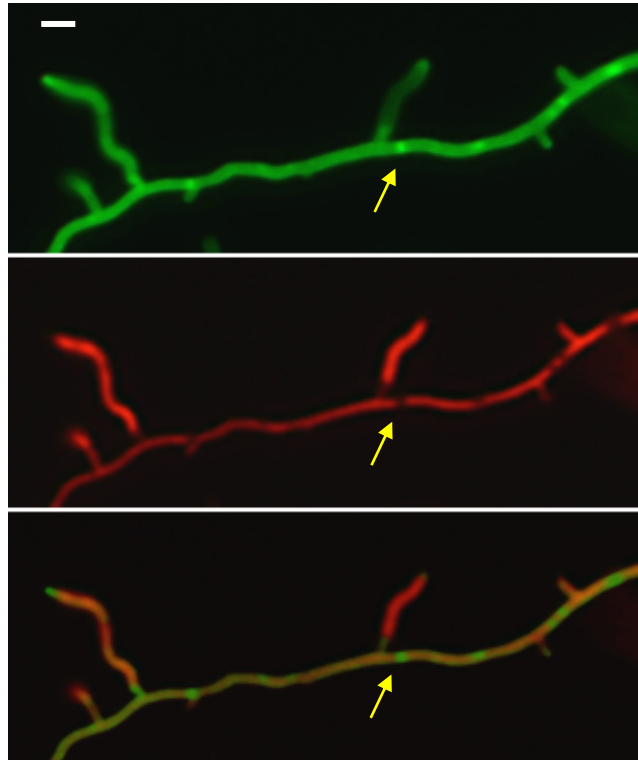


Figure 3.19. Microscopy of vegetative hyphae of the wild-type M145 strain. Spores of the wild-type strain M145 were plated on SFM medium and incubated at 30°C before staining with PI (red-DNA) and WGA-Alexa 488(green-cell wall). The vegetative hyphae grew to straight style with slightly curves and developed branches hyphae. We can see vegetative cross-wall appearing in the vegetative hyphae, which then disrupt the chromosomal DNA staining. Size bar represents 1µm.

After two days (48hrs - 50hrs) of growth, the wild-type strain developed aerial hyphae that can be recognised by non-branching and curly hyphae (Figure 3.20 A). The early aerial hyphae have even DNA staining (Figure 3.20 A) suggesting that the individual chromosomes were not separated. Later, there is some sign of DNA organisation as the DNA stain displays small packages of red staining. At this stage there is no septation yet and the cell wall stain is less effective in staining the cell wall. This might be because of changes in the cell wall of the aerial hyphae that becomes covered by a hydrophobic coat, including the chaplins and rodmins. These aerial hyphae then underwent sporulation septation together with chromosome segregation into the developing pre-spore compartments. The multiple septa, which were detected using the WGA-Alexa 488 stain, were laid down in the aerial hyphae

as ladder-like structure. At the same time, the chromosomes have undergone complete segregation with clear gaps between each individual DNA and each single chromosome were enclosed within a single pre-spore compartment (Figure 3.20 C and D). Synthesis of the new septum starts as a ring which is seen in the confocal microscopy image shown in Figure 3.4.2.2D. The pre-spore compartments underwent maturation to produce mature spores with thickened cell wall (not shown). As we were focusing on the event of the initiation of septation, we did not characterise late septation.

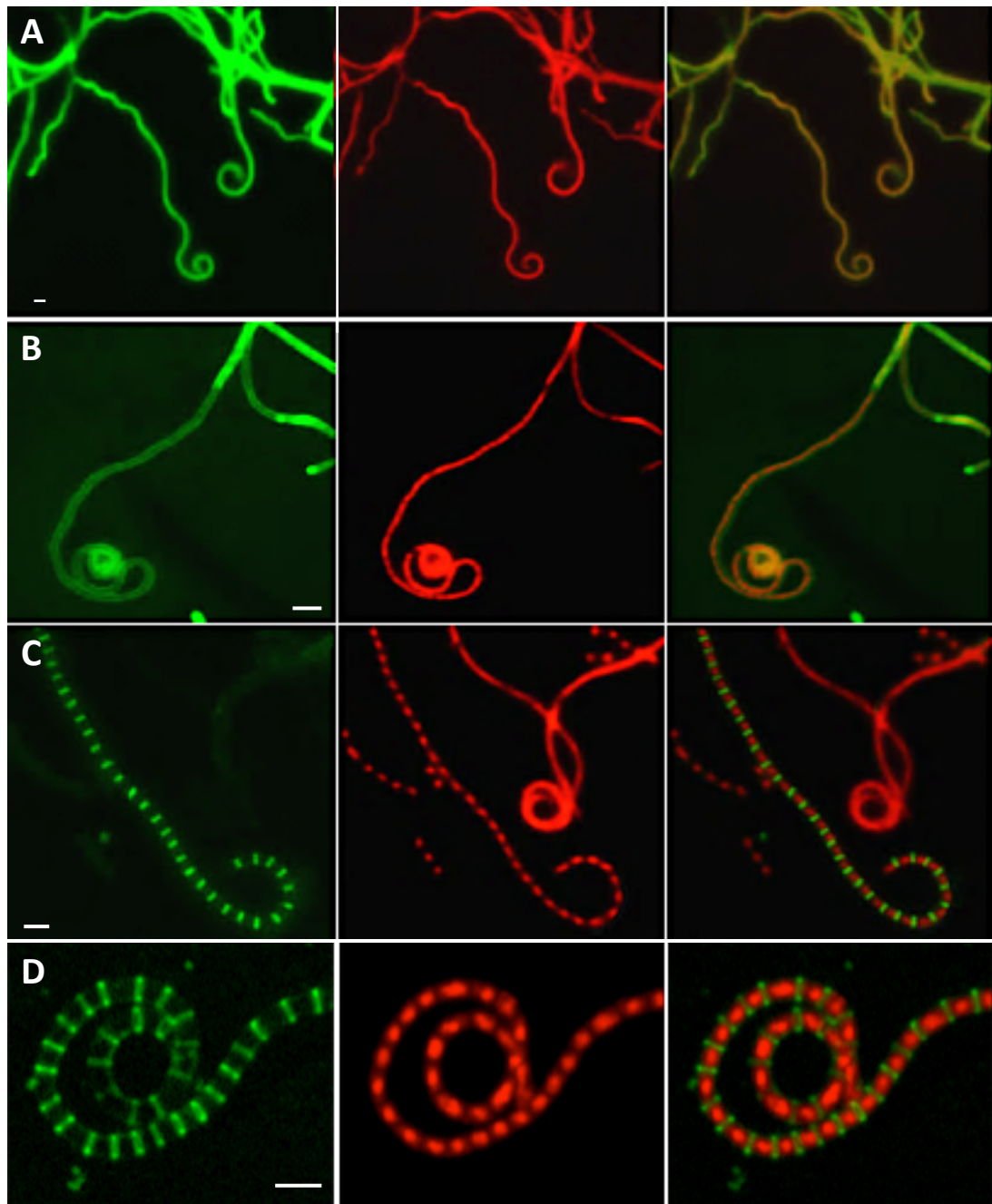


Figure 3.20. Fluorescent microscopy showing the developmental stages when the aerial hyphae transformed into spore chains in the wild-type strain M145.

Spores of the wild-type strain M145 were plated on SFM medium and incubated at 30°C before staining with PI (red-DNA) and WGA-Alexa 488 (green-cell wall). Size bar represents 1µm.

(A) Stage 1. Growth of the aerial hyphae with coiling tips; (B) Stage 2. The chromosomes start to condense but not yet fully separated; (C-D) Stage 3. The regular septa placed in the hyphae separating individual chromosomes. (A-C) epi-fluorescence microscopy; (D) confocal microscopy.

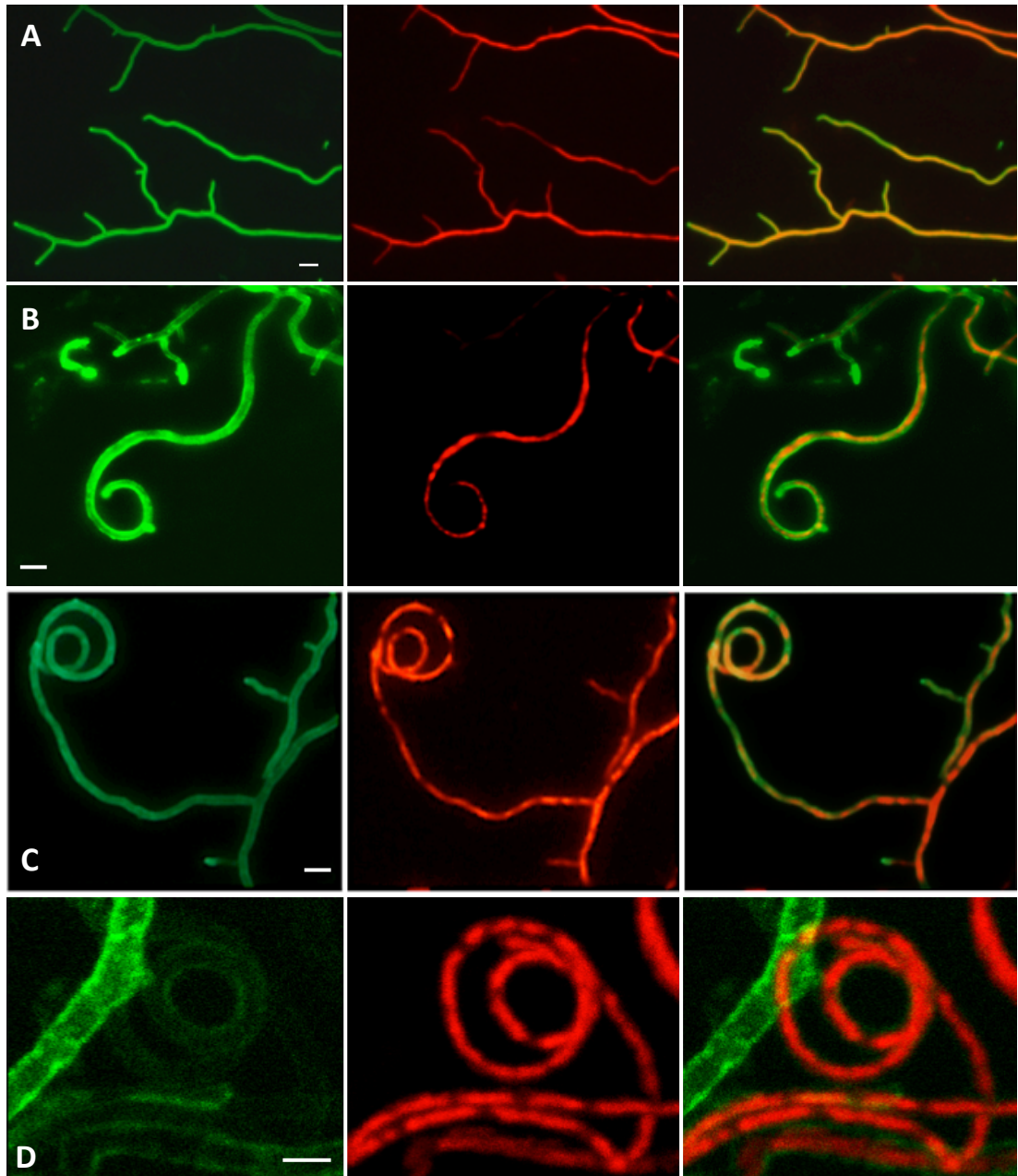


Figure 3.21. The phenotype of the *sepF* mutant.

The *sepF* mutant was plated on SFM medium and incubated at 30°C before staining with PI (red-DNA) and WGA-Alexa 488 (green-cell wall). Size bar represents 1µm.

(A) Vegetative hyphae including branching but no sign of cross-wall formation. (B-D) Aerial hyphae of the *sepF* mutant lack septation but chromosome condensation and segregation are detectable.

To assess the *sepF* mutant phenotype, we stained cells of the *sepF* mutant strain after 40 hours of growth using WGA Alexa 488 and PI and observed it using fluorescent microscopy. We found that the *sepF* mutant was severely blocked in

crosswall formation at the stage of vegetative growth (Figure 3.21 A), when we can easily detect vegetative crosswalls in the wild-type strain (Figure 3.19). We did not find any crosswalls after testing ~20 independent slides. However, after 48 hours we did find that vegetative hyphae are compartmentalised. We do not know whether this means that the *sepF* mutant can, even if inefficiently, generate some crosswalls eventually or whether what we observed as crosswalls were generated by a different mechanism. At 48 hours after inoculation, the wild-type M145 strain exhibited sporulation where single chromosomes condensed into pre-spore compartments and separated by septa. The *sepF* mutant strain exhibited only DNA condensation and partial segregation in aberrant shapes (Figure 3.21 B and C) but did not form sporulation septa. Old samples of 3-5 days did produce deformed spore-like

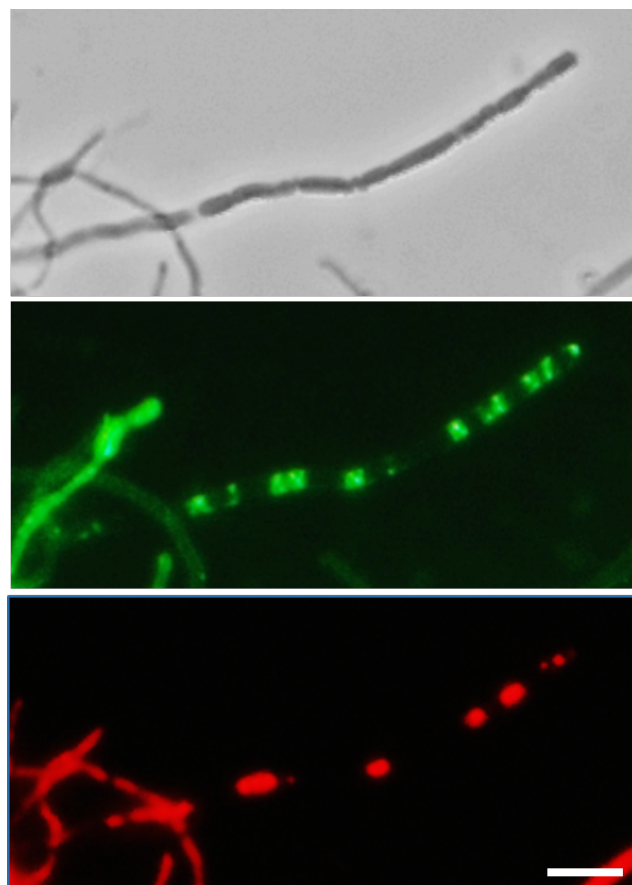


Figure 3.22. Spore-like structures of old samples of the *sepF* mutant. 5 days old samples grown on SFM medium were stained and visualised using fluorescence microscopy. Top: phase contrast image; Middle: WGA-alexa 488 staining of cell wall; Bottom: DNA staining using PI. Size bar represents 1 μm .

structures (Figure 3.22), with longer spore compartments than the wild-type strain. Interestingly, the septa that was stained in these spore-like chains were spiral shaped, unevenly positioned and very irregular (Figure 3.22). This confirms that SepF is a key contributor of normal septum development and lack of SepF prevents normal septum formation in *Streptomyces*.

In summary, microscopic analysis of the *sepF* mutant strain revealed that its ability to generate septa is severely affected, which is consistent with the white appearance of its macroscopic phenotype. However, the absence of sporulation septation did not block chromosome segregation in the aerial hyphae, which suggests that chromosome segregation does not rely on septum formation.

3.5 Complementation of the *sepF* mutant strain

3.5.1 Complementation using construct containing *sepF* and different upstream sequences

To ensure that the discernible non-sporulating phenotype of the *sepF* mutant was caused by the deletion of the *sepF* gene rather than some other genetic mutation during the generation of the knockout mutant, we carried out complementation experiment with different DNA fragments containing the *sepF* gene. If introduction of the complementing DNA fragment into the mutant strain *in trans* restored the wild-type phenotype, we can confirm that the mutant phenotype was caused by the absence of the *sepF* gene. However, we don't have precise information about the positions where transcription of *sepF* is initiated. There are 128 bp between the end of the upstream gene 2080 and the translational start of *sepF*. We decided to create two complementing constructs in the first instance, one construct (named ΔP -*sepF*, as later established) contained the entire *sepF* gene and 128 bp upstream sequences and the other construct (named 2080-*sepF*) that carried the *sepF* gene and ~848 bp upstream sequences that included the promoter-less 2080 gene (Figure 3.23).

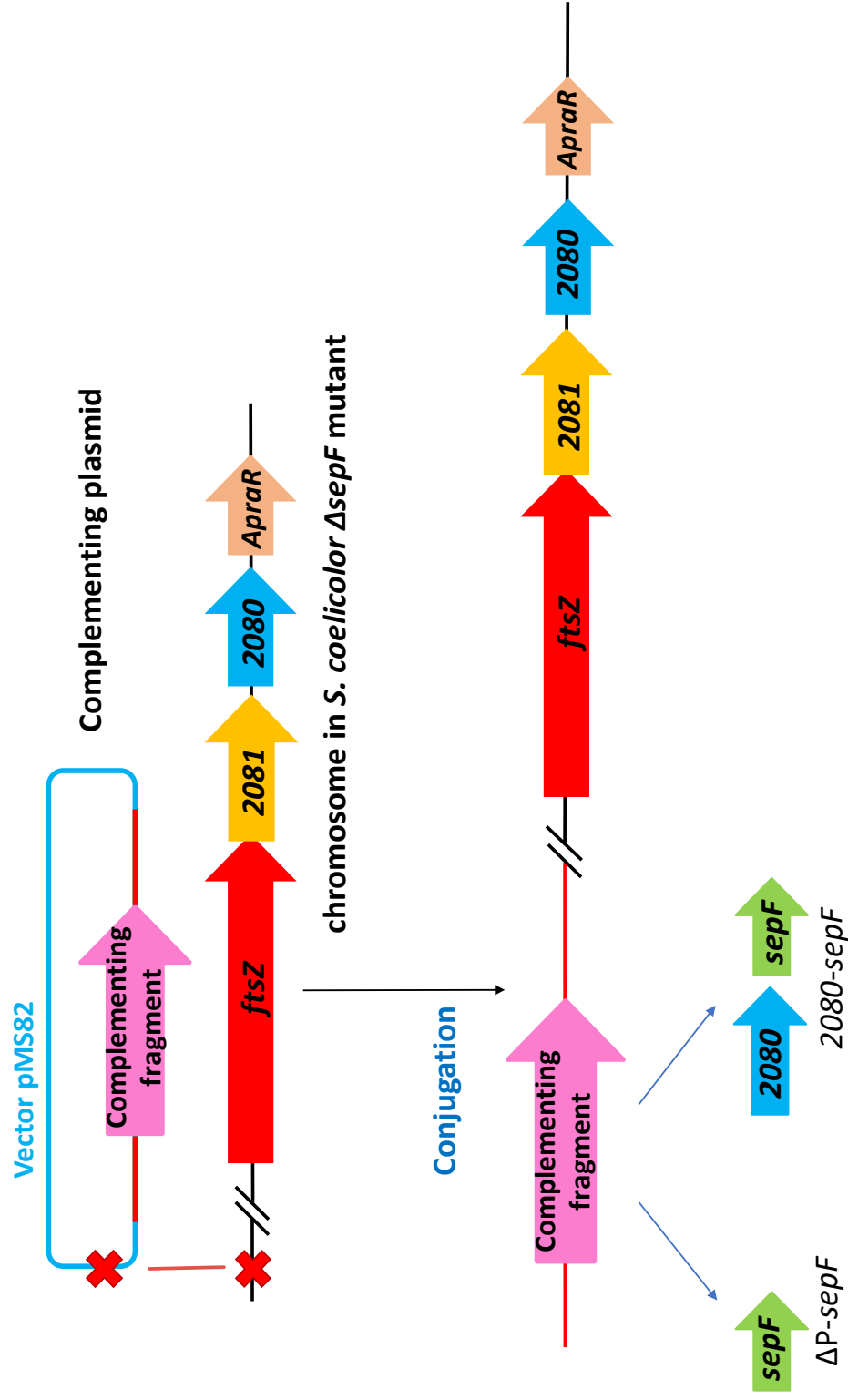


Figure 3.23. Complementation of the *sepF* mutant using two constructs, one containing the *sepF* gene with a short upstream sequence and the other one containing the *sepF* gene and its upstream gene *SCO2080*. These two constructs were cloned into the integrative vector pMS82 and introduced into the *sepF* mutant to test whether the introduction of these constructs into the *sepF* mutant restored the wild-type phenotype.

The plasmid pMS82 integrates at the Φ BT1 attachment site in the *S. coelicolor* chromosome (Gregory *et al.*, 2003), so each chromosome contains a single copy of the plasmid with a hygromycin resistance gene. This allows selection of the presence of this plasmid in the apramycin resistant *sepF* mutant strain.

The primers SepF XbaBgl Prom FRW and SepF 3'END were used to amplify the ΔP -*sepF* (978bp) fragment using cosmid 4A10 as a template. Similarly, primers 2080 Xba Nde FWR and SepF 3' END were used to create the 2080-*sepF* (1643 bp) fragment (Figure 3.24). Then these two complementing fragments were ligated into the *EcoRV* site of pMS82. The ligation mixes for pMS82/ ΔP -*sepF* and pMS82/2080-*sepF* were transformed into *E. coli* DH5 α and grew on media LB (no salt) containing hygromycin. We screened the transformants using colony PCR with primers SepF XbaBgl Prom FRW and SepF 3'END (Figure 3.25). Then the positive colonies were used for large scale plasmid preparation. Sequencing of the cloned fragments was used to confirm the successful generation of the complementation constructs pMS82/ ΔP -*sepF* and pMS82/2080-*sepF*.

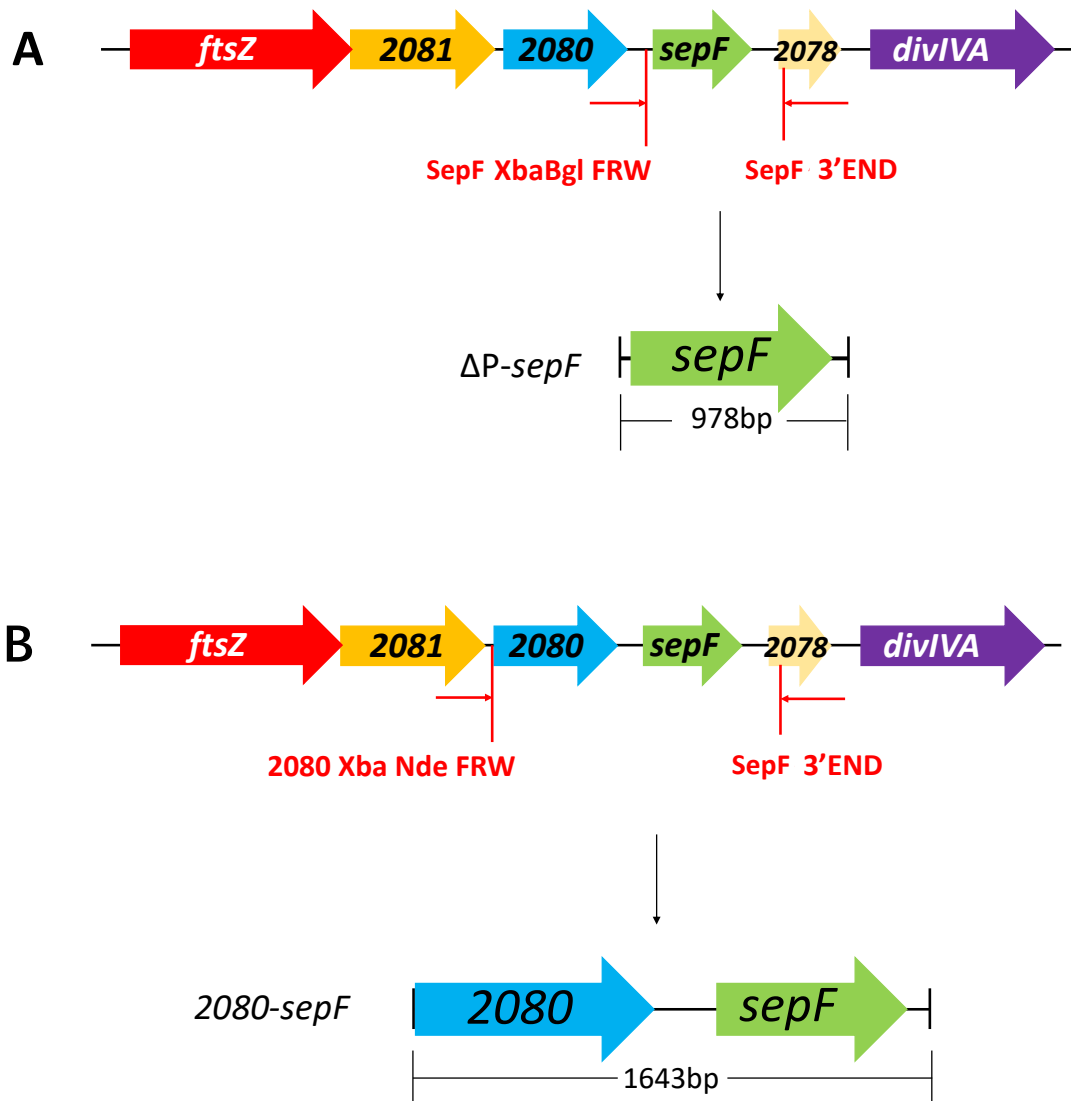


Figure 3.24. Complementation strategy. A. Fragment ΔP-*sepF* (978 bp) containing the *sepF* gene and ~128 bp upstream sequence. **B.** Fragment 2080-*sepF* (1643 bp) containing the *sepF* gene and ~848 bp upstream sequence.

After confirming the successful constructs, we transformed these two constructs into the non-methylating *E. coli* strain ET12567/pUZ8002 and then conjugated them into the *sepF* mutant to create Δ*sepF*/pMS82/ΔP-*sepF* and Δ*sepF*/pMS82/2080-*sepF*. The empty vector pMS82 was also conjugated into the *sepF* mutant in order to generate a control strain, Δ*sepF*/pMS82 to ensure that vector does not affect the complementation. The exconjugant strains were then processed to generate spore preparations.

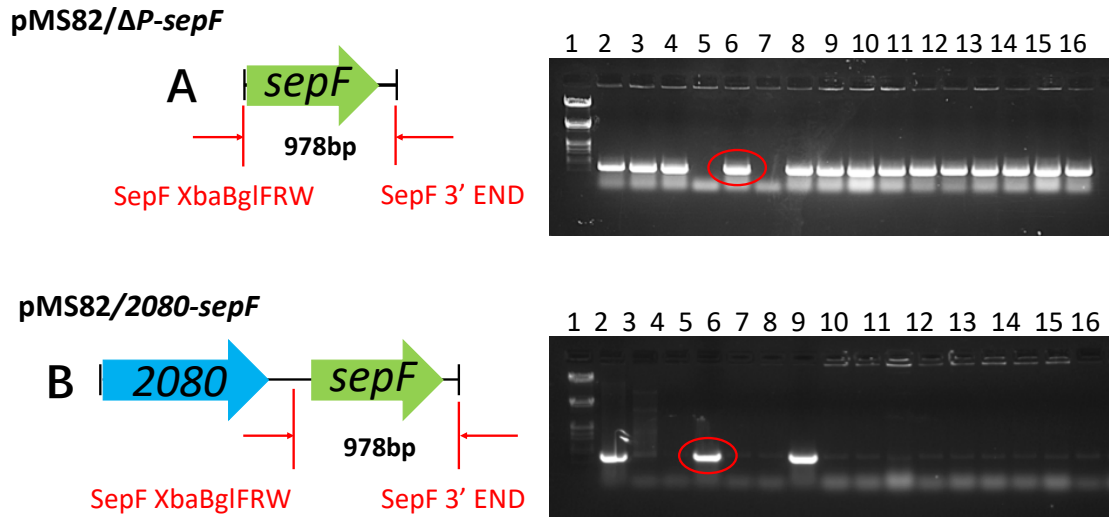


Figure 3.25. Colony PCR for testing the transformants. (A) Testing the putative pMS82/ΔP-sepF constructs using primers indicated (red). Lane 1: λ EcoRI-HindIII ladder; Lane 3-16: each lane represents a PCR product from a single colony. Lane 2: Positive control using the 4A10 cosmid as template. (B) Testing the putative pMS82/2080-sepF constructs using primers indicated (red). Lane1: λ EcoRI-HindIII ladder, Lane 3-16: each lane represents a PCR product from a single colony. Lane 2: Positive control using the 4A10 cosmid as template. The positive colonies that were selected are circled.

To assess whether constructs pMS82/ΔP-sepF and pMS82/2080-sepF complemented the sepF mutant strain we first analysed the phenotype using macroscopic observations (Figure 3.26). The wild-type control M145/pMS82, the mutant control strain ΔsepF/pMS82, together with the complementation test strains, ΔsepF/pMS82/ΔP-sepF and ΔsepF/pMS82/2080-sepF were streaked in a triangle shape of equal size on SFM medium containing hygromycin. These strains were incubated at 30°C and their development was monitored daily. After one day, we detected that all of these strains developed vegetative hyphae presenting a brownish layer on the medium and the mutant control strain ΔsepF/pMS82 showed much slower growth than the other three strains (Figure 3.264 A). After two days, strains began to generate fuzzy white aerial hyphae (Figure 3.26 B). At three days after inoculation of spores, ΔsepF/pMS82/ΔP-sepF and ΔsepF/pMS82/2080-sepF started to produce grey pigments similarly to the wild-type strain M145/pMS82 (Figure 3.26 C). After four days, the control strain, ΔsepF/pMS82 still exhibited white/blue phenotype and lacked the grey pigments associated with mature spores whilst the

other three strains developed grey mature patches (Figure 3.26 D). This suggested that the *sepF* mutant strain was complemented by both constructs.

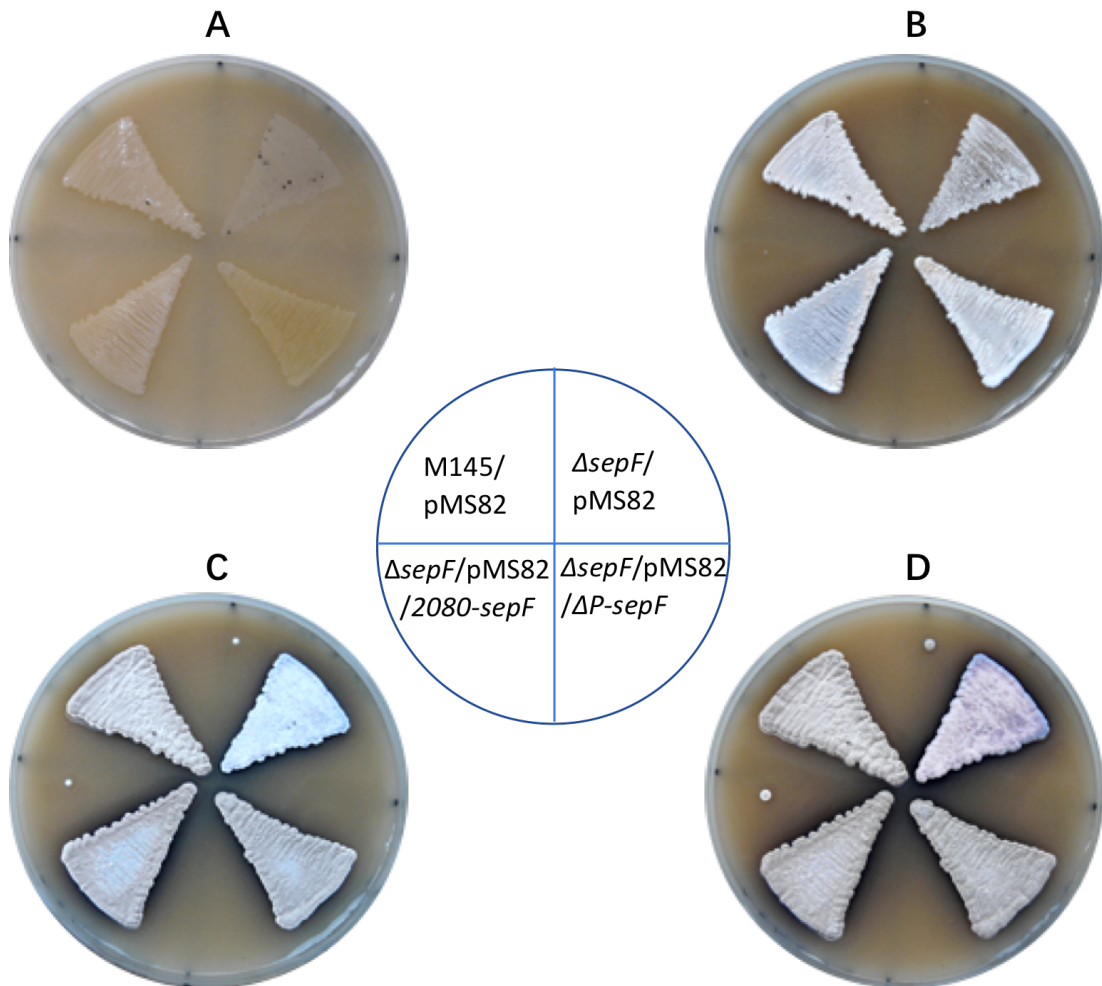


Figure 3.26. Macroscopic analysis of the complementation. The positions of the different strains are shown using the illustration in the middle.

The strains were plated in a triangle patch on SMF medium containing hygromycin. The plates were incubated and monitored at regular time intervals (A) 1 day, (B) 2 days, (C) 3 days and (D) 4 days.

However, to confirm full complementation, further microscopic analysis was needed. We inoculated $\Delta sepF/pMS82/\Delta P-sepF$ and $\Delta sepF/pMS82/2080-sepF$ alongside a coverslip inserted into SFM medium containing hygromycin and hyphae were visualized at 48 hours when the wild-type strain shows regular septation.

Interestingly, in spite of the fact that the macroscopic observations showed grey patches, the aerial hyphae of $\Delta sepF/pMS82/\Delta P-sepF$ failed to produce regular septation (Figure 3.27). Instead, we observed uneven spore compartments with deformed, spiral-shaped septum formation and uneven chromosome distribution. Occasionally a small DNA patch was trapped at the deformed septum (Figure 3.27). This suggested that the construct $pMS82/\Delta P-sepF$ did not complement the $sepF$

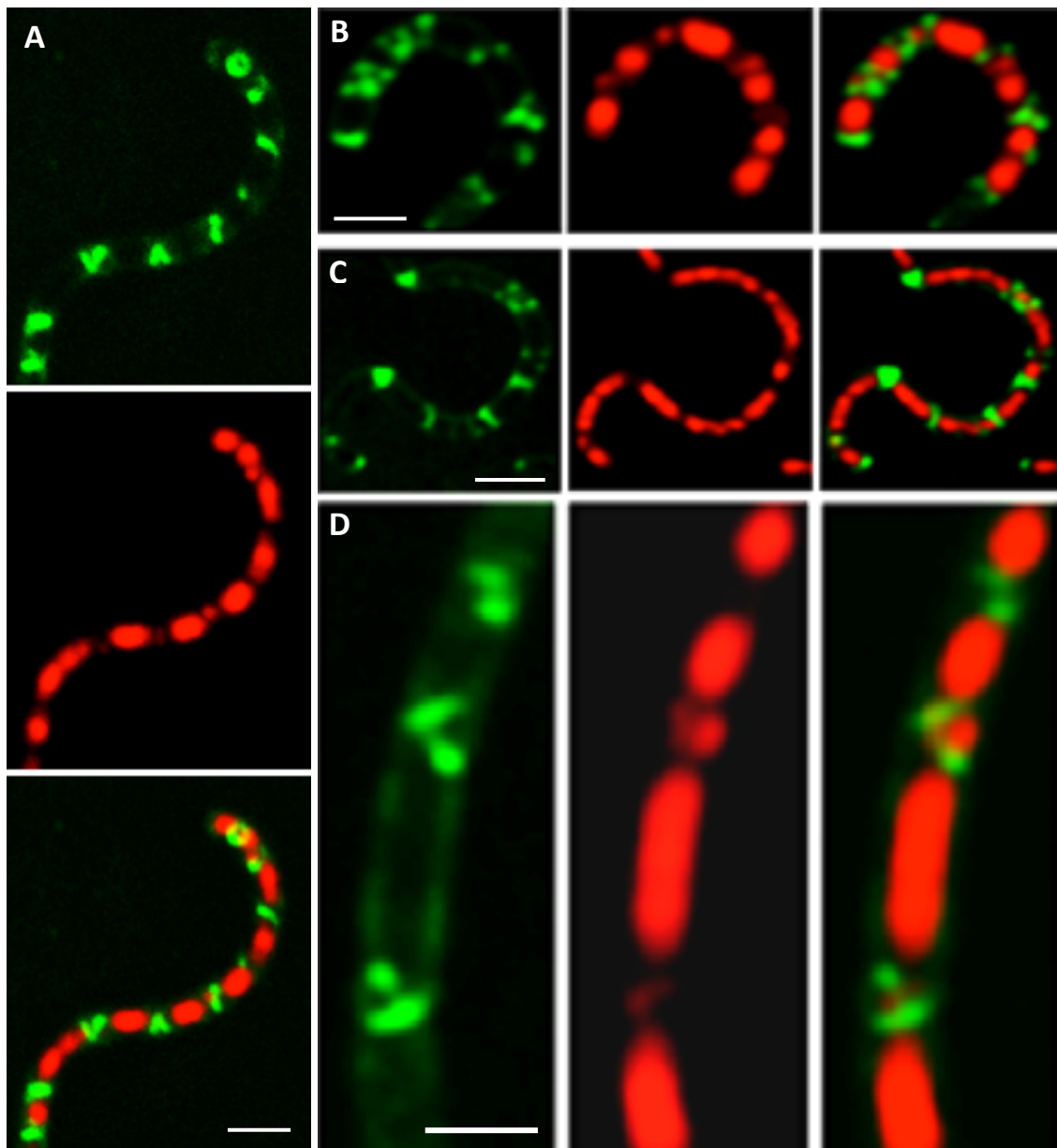


Figure 3.27. Fluorescent microscopy of strain $\Delta sepF/pMS82/\Delta P-sepF$. After 48 hours of growth on SFM medium containing hygromycin the $\Delta sepF/pMS82/\Delta P-sepF$ strain was stained with PI (red-DNA) and WGA-Alexa 488 (green-cell wall). A, B, C, D all show growth in aerial hyphae. All images were generated using confocal microscopy. Size bar represents 1 μm.

mutation. On the other hand, the $\Delta sepF/pMS82/2080-sepF$ strain showed wild-type septation evenly distributed along the aerial hyphae (Figure 3.28). For comparison,

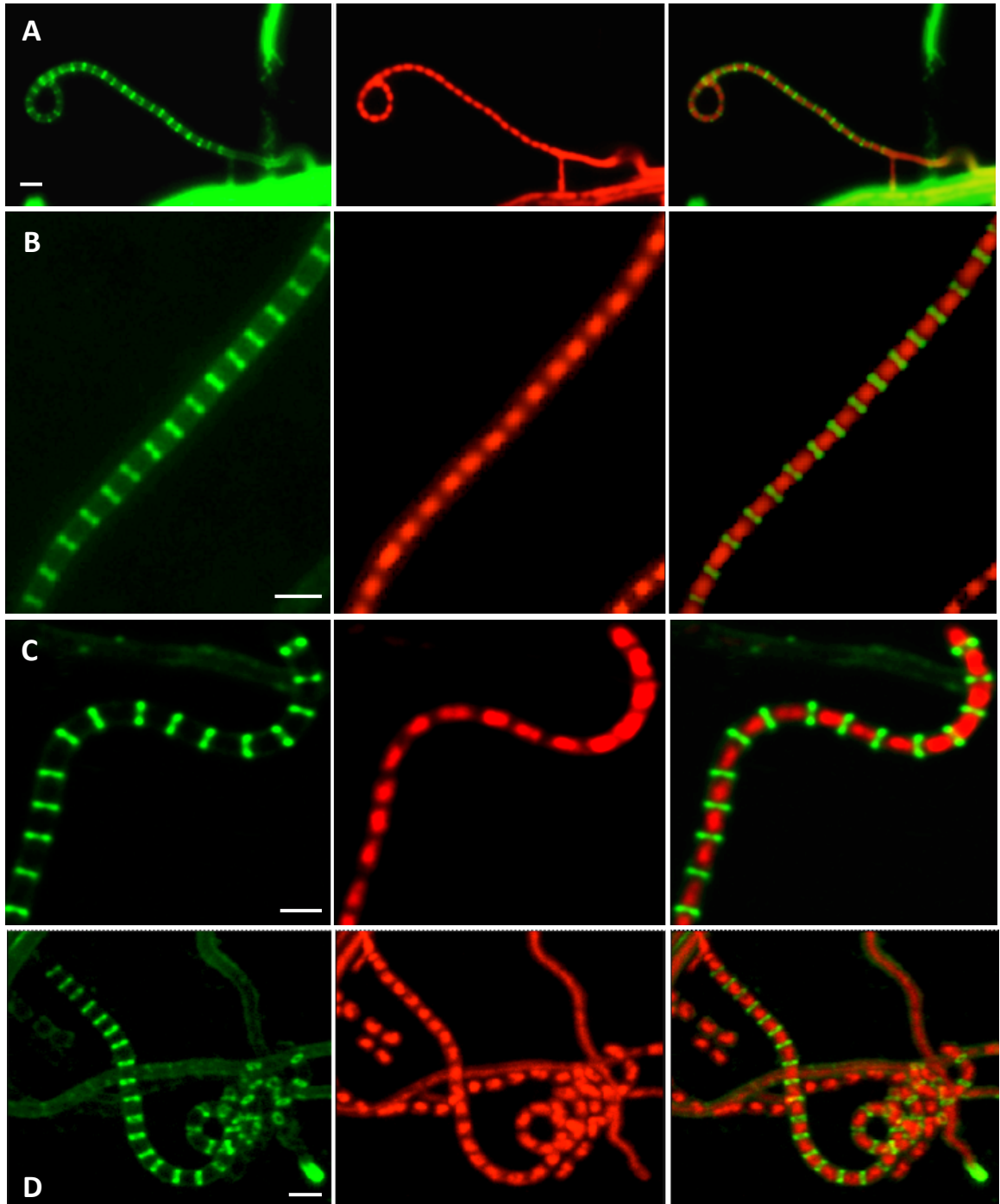


Figure 3.28. Fluorescent microscopy of $\Delta sepF/pMS82/2080-sepF$. After 48 hours of growth on SFM medium containing hygromycin the $\Delta sepF/pMS82/2080-sepF$ strain was stained with PI (red-DNA) and WGA-Alexa 488 (green-cell wall). A, B, C, D all show growth in aerial hyphae. (A) epi-fluorescence microscopy (B-D) confocal microscopy. Size bar represents 1 μ m.

see wild-type sporulation septation in Figure 3.20 D. This confirmed that the pMS82/2080-*sepF* construct fully complemented the *sepF* mutation.

3.5.2 Complementation of the *sepF* mutant using construct P-*sepF*

In previous complementation experiments, the *sepF* mutant was only partially complemented by pMS82/ Δ P-*sepF* but was fully complemented by pMS82/2080-*sepF*, suggesting that the 128 bp sequence upstream of the *sepF* gene was not sufficient for normal SepF expression, but the 848 bp upstream sequence did contain the promoter(s) of *sepF*. However, the pMS82/2080-*sepF* construct contained the full 2080 gene and we wanted to exclude the possibility that the complementation was affected by the presence of the 2080 gene. Therefore, we tried to shorten the upstream sequences. During our efforts, research from Jeong and colleagues (2016) identified transcriptional start points for all *S. coelicolor* genes using RNA seq analysis. This work has identified two transcriptional start points for *sepF*. Interestingly only

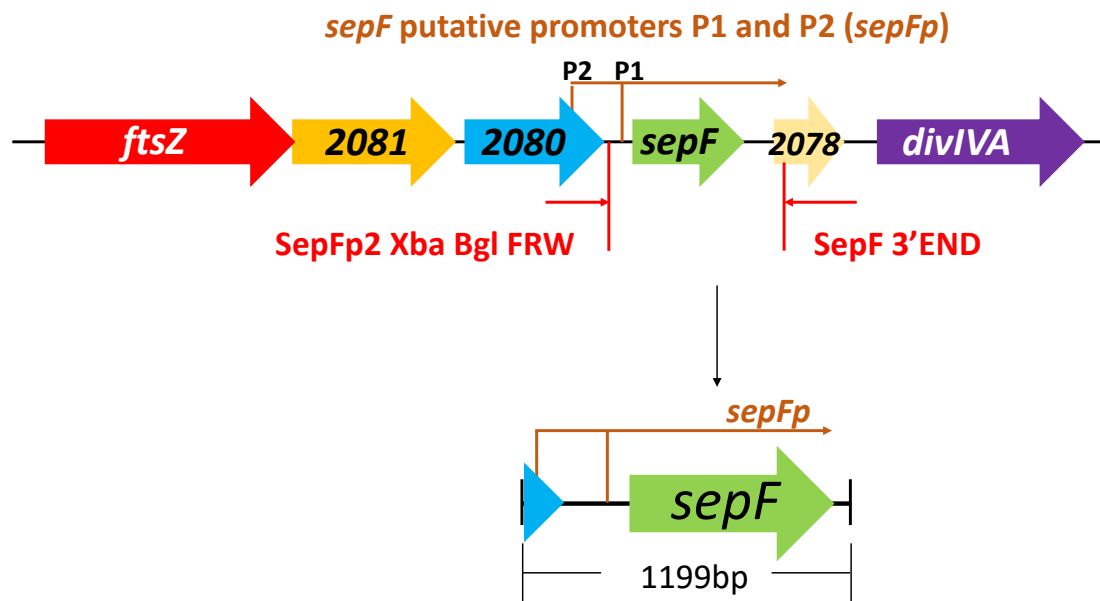


Figure 3.29. Generation of construct P-*sepF* (1199 bp) to complement the *sepF* mutant. This construct contains gene *sepF* and its putative promoters.

one of the transcriptional start point was included in the pMS82/ Δ P-*sepF* construct, which explains why this construct failed to fully complement the *sepF* mutant. Our

final construct carrying P-*sepF* was designed to contain both promoters according to Jeong *et al.* (2016). This fragment was amplified from the 4A10 cosmid using primers SepFp2 XbaI FRW and SepF 3' END by PCR (Figure 3.29). The PCR product was consequently introduced to the EcoRV site of pMS82. Single colonies, which potentially contained the fragment P-*sepF* were tested using colony PCR with primers SepFp2 XbaI FRW and SepF 3' END by PCR (Figure 3.30). One of the positive colonies was used to generate a large plasmid preparation that was confirmed using sequencing.

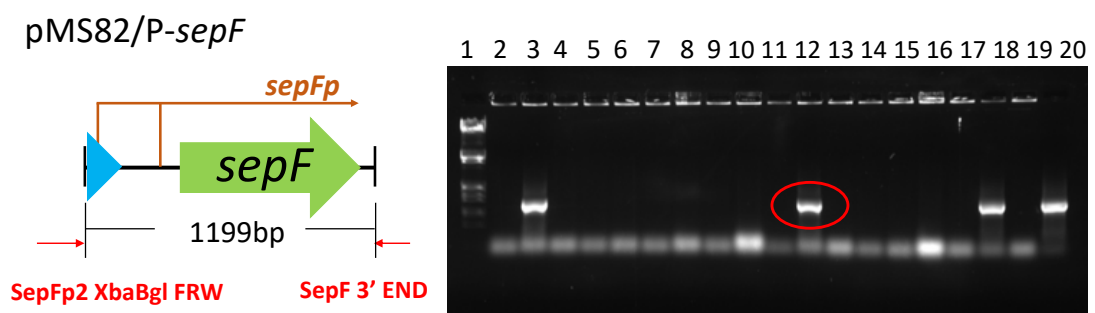


Figure 3.30. Colony PCR for testing the transformants. Testing the putative pMS82/P-*sepF* constructs using primers indicated (red). Lane 1: λ EcoRI-HindIII ladder, Lane 2-19: each lane represent a PCR product from a single colony. Lane 20: Positive control using the 4A10 cosmid as template. The positive colony that was selected is circled.

After transformation of pMS82/P-*sepF* into the *E. coli* strain ET12567/pUZ8002 and conjugation into the *sepF* mutant strain we created the strain Δ *sepF*/pMS82/P-*sepF*. To analyse the macroscopic appearance of the colonies, the Δ *sepF*/pMS82/P-*sepF* strain was compared to the wild-type M145 and the *sepF* mutant strains (Figure 3.31). After 48 and 72 hours of growth, the Δ *sepF*/pMS82/P-*sepF* patch resembled the wild-type patch, developing the characteristic grey surface,

while the *sepF* mutant stayed white. This suggested that the *sepF* mutant was successfully complemented by the pMS82/P-*sepF* construct.

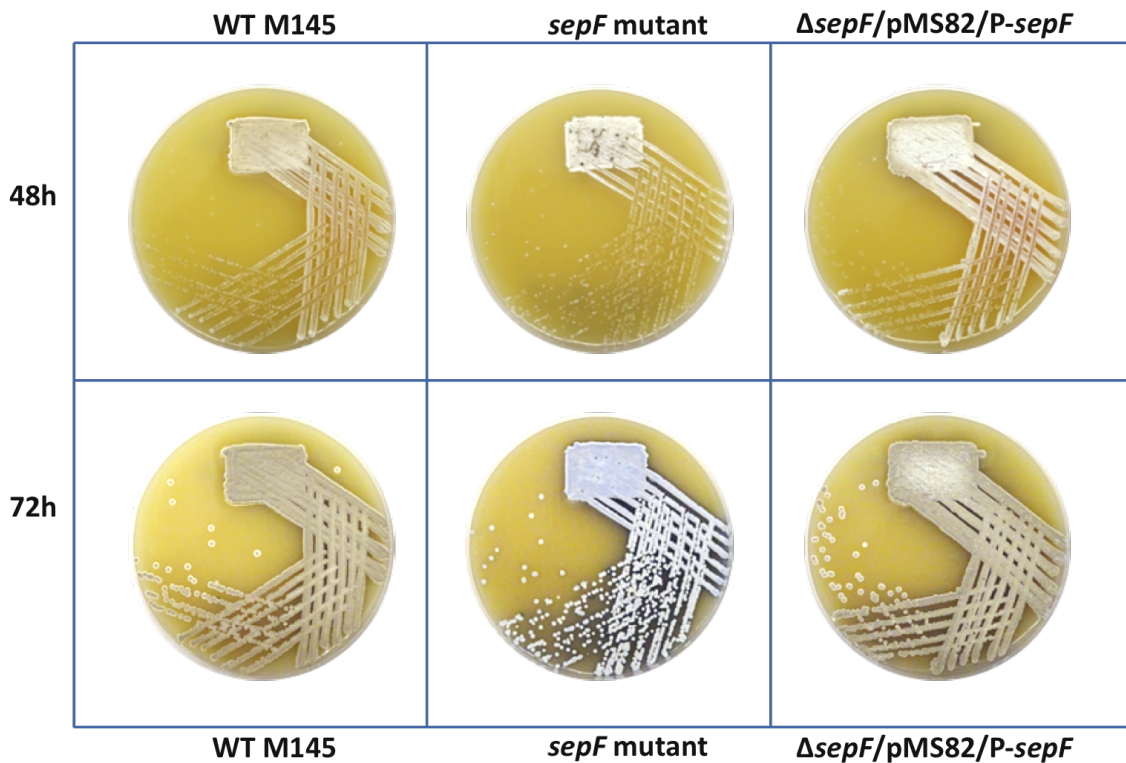


Figure 3.31. Monitoring morphological development for testing complementation. The wild-type strain (left) the *sepF* mutant (middle) and the $\Delta sepF/pMS82/P-sepF$ (right) are grown on SFM medium. The plates were incubated and monitored after 48h and 72h growth.

Microscopy analysis confirmed the full complementation by pMS82/P-*sepF* (Figure 3.32). Regularly spaced septation identical to that of the wild-type strain was observed when development of $\Delta sepF/pMS82/P-sepF$ was monitored. This confirms that the upstream DNA fragment in pMS82/P-*sepF* was sufficient for normal *sepF* expression.

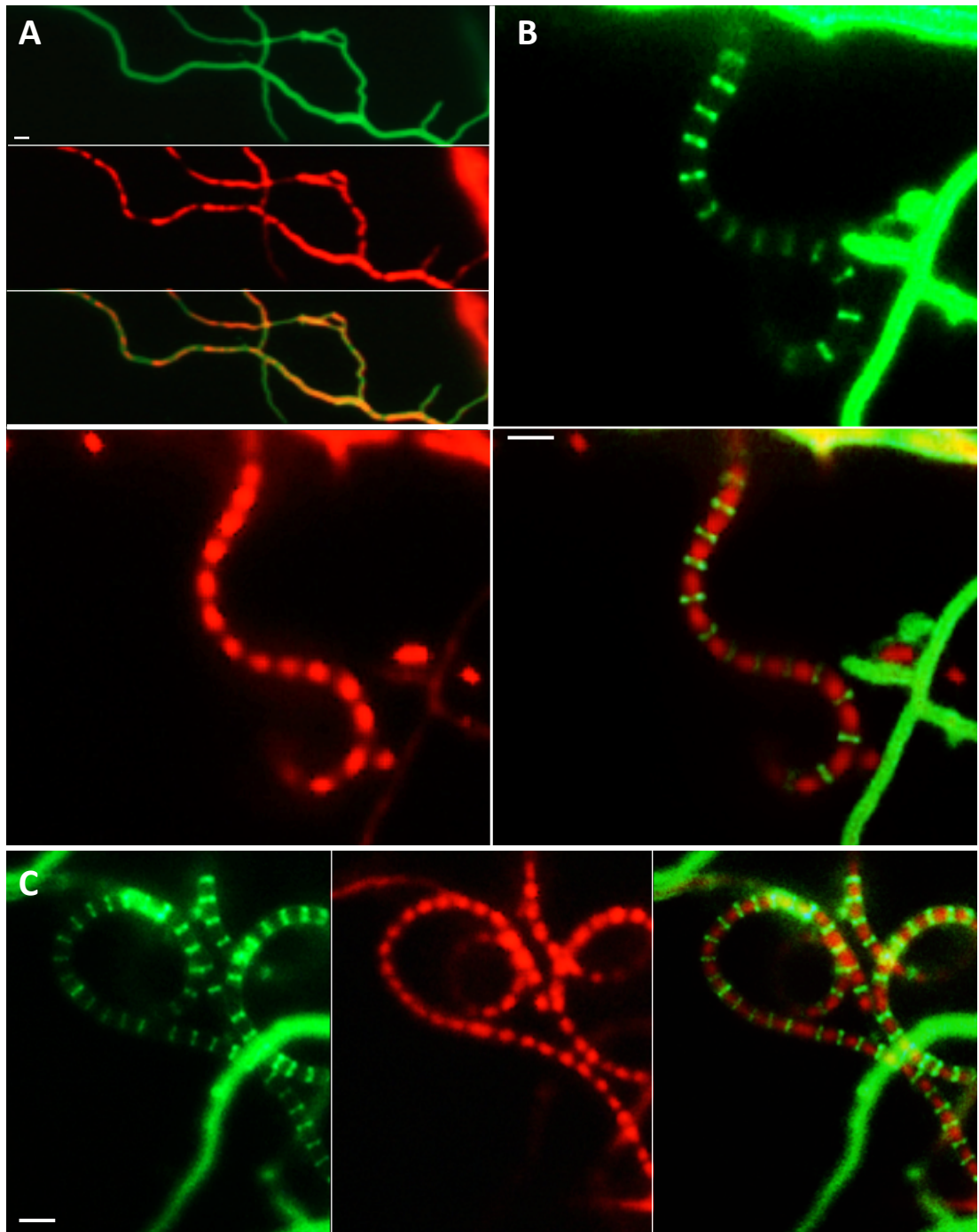


Figure 3.32 Fluorescent microscopy of $\Delta sepF/pMS82/P-sepF$ After 48 hours of growth on SFM medium containing hygromycin the $\Delta sepF/pMS82/P-sepF$ strain was stained with PI (red-DNA) and WGA-Alexa 488 (green-cell wall). (A) shows growth in vegetative hyphae; (B, C) show development in aerial hyphae. All images were generated using epi-fluorescence microscopy. Size bar represents 1 μ m.

3.6 Summary

In this chapter, we begun the characterization of one of the SepF homologues of *S. coelicolor*.

- Bioinformatic searches identified three SepF homologues in *S. coelicolor*, one of which is encoded within the *ftsZ – divIVA* gene cluster. We analysed the gene organisation around the *sepF* genes in *S. coelicolor* and in other bacteria. Some of the neighboring genes and gene organisation were conserved not only amongst the *Actinomycetes* but also in *B. subtilis*.
- Using PCR targeting, we have generated a *sepF* knockout mutant of *S. coelicolor* and confirmed the mutant by analysis of its chromosomal DNA by PCR.
- The *sepF* mutant has a white, non-sporulating phenotype, and this was confirmed by using microscopic analysis. Neither vegetative cross-wall formation nor sporulation septation was detected in the *sepF* mutant, suggesting that SepF was required for septum formation. In *B. subtilis*, the *sepF* mutant is not blocked in septation and only the late stages of septum formation is affected. However, in addition to SepF *B. subtilis* has FtsA and ZipA, while *Streptomyces* lacks these two latter proteins. This might explain why the *sepF* mutant phenotype is more severe in *Streptomyces* and also in *Mycobacterium*, which also lacks FtsA and ZipA.
- To test whether the *sepF* mutant phenotype was indeed due to the absence of SepF, we attempted complementing the knockout mutant using three different constructs. We could fully complement the *sepF* mutant using two of the constructs, whilst the third construct, which contained presumably only one of the promoters of *sepF*, only partially complemented the *sepF* mutant.

Acknowledgements

We are very grateful to Alan Lau and Gamma Cassentari for contribution to the experiments.

Chapter 4 Localisation of SepF protein *in vivo*

Introduction

In *S. coelicolor*, FtsZ is a component of the cytoskeleton for cell division and septum formation. This protein is a bacterial tubulin homologue and is vital for two processes: the occasional cross-wall formation during filamentous growth and synchronous septa formation resulting in the compartmentalisation of aerial hyphae into spores (Jakimowicz and van Wezel, 2012). The crosswall formation in the vegetative hyphae does not lead to cell-cell separation and division. During sporulation the synchronous formation of 50-100 septa is followed by separation of the pre-spore compartments into ovoid spores, which can disperse. We know that FtsZ is involved both in the vegetative cross wall formation and also in sporulation septation. However, it is not known, why the first process fails to lead to cell-cell separation, whilst during sporulation division is completed. It is likely that the difference between these two septation process lies in differences of the proteins that are recruited by FtsZ to the developing septum. FtsZ recruits components of the so called “divisome” that are involved in the synthesis of the developing septum. The divisome components include FtsK, FtsQ/DivIB, FtsL, FtsB/DivIC, FtsW and FtsI (McCormick and Flardh, 2012) but these proteins have not been fully characterised.

A high level of coordination is needed to recruit the FtsZ protein at specific sites on the membrane of the aerial hyphae before FtsZ can polymerise in the presence of GTP into the regularly spaced Z-rings that are often described as FtsZ ladders (Grantcharova *et al.*, 2005). In *Streptomyces* the only protein that has been shown to position FtsZ is the SsgB protein (Willemse *et al.*, 2011), which is shown to positively regulate FtsZ polymerisation. SsgB belongs to an actinomycete-specific protein family (Keijser, *et al.*, 2003) and it has been shown to co-localise with FtsZ *in vivo* (Willemse *et al.*, 2011). In the absence of SsgB, FtsZ fail to form rings, and cells don't initiate

sporulation.

The proteins that stabilise FtsZ filaments in *B. subtilis* include FtsA, ZapA and SepF (Duman *et al.*, 2013). However, *Streptomyces* lacks both FtsA and ZapA, but has SepF, in fact it has three SepF proteins (see Chapter 3). This protein has been found to be conserved across Gram-positive bacteria with *sepF* disruption resulting in cell division impairment (Singh *et al.*, 2008). Electron microscopy has shown that SepF polymerises into rings which bundle FtsZ into structures similar to eukaryotic microtubules at the midpoint of the cells (Gundogdu *et al.*, 2011).

One main contrast to FtsZ in *S. coelicolor* compared to that in rod-shaped bacteria is that the protein is not completely necessary for the bacterium's survival, with a knockout mutation of *ftsZ* not being lethal to the bacterium. An *ftsZ* knockout mutant of *S. coelicolor* develops slower than the wild-type and it does not develop grey colonies indicative of sporulation, instead the *ftsZ* null mutant stays white even after prolonged incubation (McCormick *et al.*, 1994; Celler *et al.*, 2013). The *sepF* mutant generated in Chapter 3 has a similar phenotype to the *ftsZ* mutant. The *sepF* mutant failed to develop dark grey pigments that are associated with sporulation and the surface of the colonies stayed white with some blue colouration, which is the blue actinorhodin antibiotic, although very old samples did develop some elongated spore like structures. The fact that the *sepF* mutant phenotype is similar to the FtsZ phenotype suggests that SepF might have a key role in FtsZ polymerisation to produce the FtsZ-rings. Therefore, we wanted to have *in vivo* data on the cellular localisation of SepF in *S. coelicolor* during differentiation. FtsZ has been localised in *S. coelicolor* using translational fusion to Enhanced Green Fluorescent Protein (EGFP) by introducing an FtsZ-EGFP fusion in addition to the native *ftsZ* gene. Fluorescence microscopy revealed that FtsZ polymerised into rings at regular intervals along the aerial hyphae prior to sporulation. This 'ladder' like organisation was not observed in the vegetative hyphae, however here the protein was found to localise to the sites where vegetative cross-wall was formed (Grantcharova *et al.*, 2005). SepF has only

been localised in *B. subtilis* with the protein accumulating at the sites of cytokinesis, (Hamoen *et al.*, 2006). The suggested model positions SepF to the FtsZ-ring after the initial invagination of the cell membrane (Duman *et al.*, 2013). This would mean that SepF is positioned after FtsZ polymerisation. However, in *S. coelicolor* the *sepF* mutant phenotype is much more severe than that of in *B. subtilis*, where lack of SepF had an effect on the late stages of septum formation. We therefore wanted to monitor SepF localisation in *S. coelicolor* to establish the timing of SepF localisation compared to FtsZ-ring formation. We also wanted to assess SepF localisation together with monitoring the chromosomal DNA, using specific dye the DNA intercalating agent, propidium iodide. This will allow us to test whether SepF localisation precedes chromosome condensation and separation in the sporulating hyphae. *Streptomyces* is thought not to have a nucleoid occlusion system, which would suggest that SepF and FtsZ might localise “over” not separated nucleoid. However, it is conceivable that chromosomes begin their separation, even if they don’t fully complete separation, at the time of FtsZ and SepF localisation. If this was the case, a nucleoid occlusion could exist in *Streptomyces*.

In this chapter we present localisation studies of SepF in *S. coelicolor* using Enhanced Green Fluorescent Protein, an altered version of the Green Fluorescent Protein gene found in the fluorescent Jellyfish *Aequorea victoria* and has been described as an efficient reporter in *Streptomyces* by Sun *et al.* (1999). The REDIRECT[®] protocol described by Gust *et al.* (2002), uses a PCR based approach to knock out gene function in *S. coelicolor*. Our experiment will instead modify this process to fuse EGFP carboxy-terminally to SepF. We will generate SepF-Egfp fusion using three different approaches:

- First, we replaced the wild-type *sepF* gene with the *sepF-egfp* gene in *S. coelicolor* using the modified REDIRECT technology. In the generated strain there is a single copy of *sepF-egfp* gene at the original chromosomal location. To confirm that the

sepF-egfp fusion is fully functional, we assessed the phenotype of this strain to confirm that its development was indistinguishable from the wild-type strain.

- Our second and third approach made use of the *sepF-egfp* fusion generated using the REDIRECT technology. We used PCR to amplify and clone *sepF-egfp* also including upstream sequences of two different lengths, for potential promoter sites, using the pMS82 plasmid that integrates into a specific chromosomal location in the *S. coelicolor* genome. In these approaches we had the wild-type *sepF* gene at its native location and an additional *sepF-egfp* copy at a different (*in trans*) genetic location. To confirm that (a) the *sepF-egfp* fusion was functional and (b) the cloned fragments carried the promoters for *sepF* transcription, we used these constructs to complement the *sepF* null mutant. Full complementation of the *sepF* null mutant using the clones carrying the *sepF-egfp* fusion will indicate that the fusion (a) is fully functional and (b) expresses SepF-Egfp as in its native location.

4.1 Localisation of SepF-EGFP using the knock in construct *sepF-egfp*.

4.1.1 Generation of the knock-in construct in *E. coli*.

To determine the localisation of SepF in *S. coelicolor*, a SepF-EGFP translational fusion was created and expressed at its native location in the chromosome as the only copy of SepF. To express the *egfp* (enhanced green fluorescent protein), we fused it to the 3' end of *sepF* gene. This was conducted through an extended PCR cassette (Figure 4.1) that allows the insertion of the *egfp-Aprar* cassette at the 3'end of the gene via recombination. To allow for selection of generated fusion, the cassette included an apramycin resistance gene (*Aprar*).

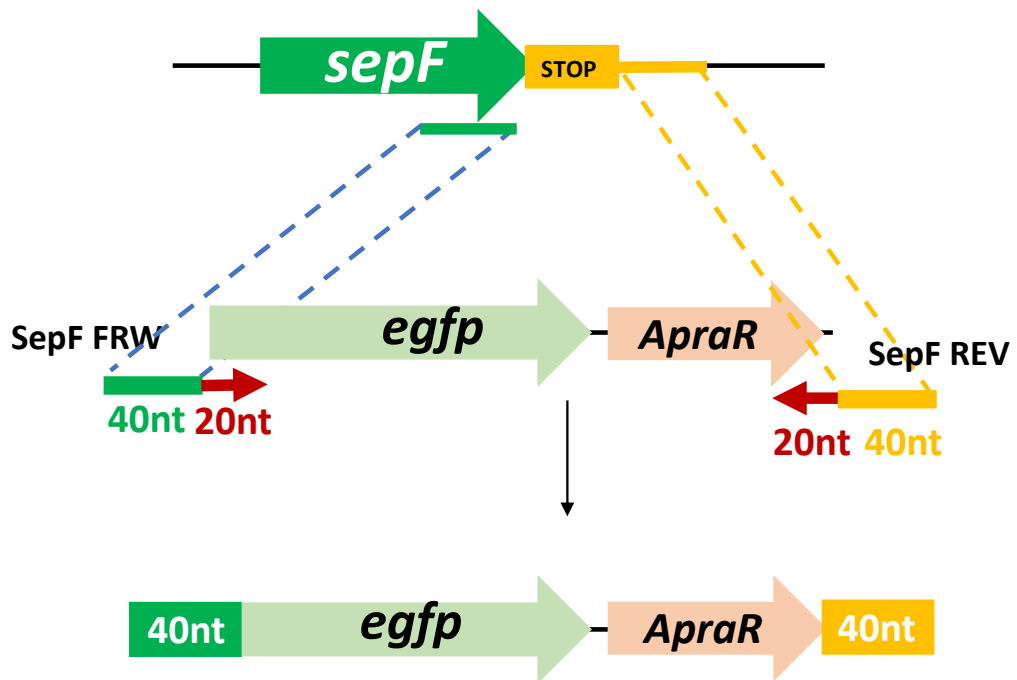


Figure 4.1. Design of the *egfp-Aprar* cassette for delivering successful recombination at the 3' end of the *sepF* gene. Primers SepF FRW and SepF REV containing sequences from both the *sepF* and *egfp-Aprar* cassette, were used to generate an extended cassette.

Extended *egfp-Aprar* cassette was created by PCR using primers SepF FWR and SepF REV, in such a way that the product had 40 bp extensions corresponding to the targeted genomic location. The PCR product was analysed on 0.7% agarose gel (Figure 4.2). The bright band in lane 4 corresponds to the expected 2.2 kbp PCR product corresponding to the extended cassette for targeting the *sepF* gene.

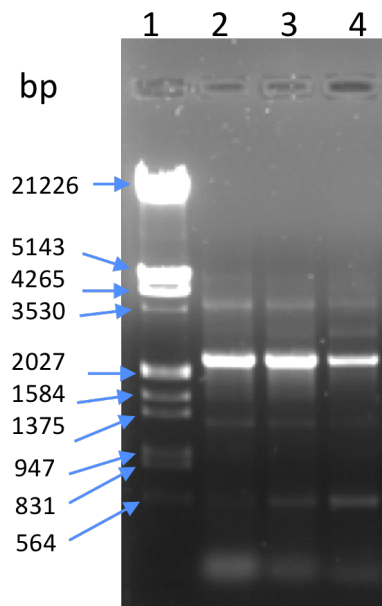


Figure 4.2. Gel electrophoresis of the *sepF* PCR cassette. Lane 1: Lamba DNA digested with *EcoRI* and *HindIII*, sizes are shown in bp. Lane 4: *sepF* specific PCR cassette. Lane 2 and lane 3 are not related to this experiment.

After the PCR product was obtained, we electroporated it into *E. coli* BW25113 cells containing the cosmid 4A10 which contains the region of *S. coelicolor* genome encoding the cell division gene cluster. The recombination between the 40 bp long extensions of the PCR cassette and the same 40 bp regions at the 3' end of the *sepF* gene in the cosmid 4A10 generated the *sepF-egfp* fusion, which was selected for by plating the *E. coli* cells onto LB containing apramycin. The cosmid DNA was extracted of cells from one of these apramycin resistant colonies and then the cosmid was digested using restriction enzymes *EcoRI* and *XbaI* to determine whether the *egfp-*Apra*^R* cassette was correctly inserted to the 3' end of *sepF* gene. Theoretical fragment lengths for the *EcoRI/XbaI* reaction were determined by constructing restriction maps of the 4A10 cosmid and the 4A10/*sepF::sepF-egfp-*Apra*^R* (Figure 4.3).

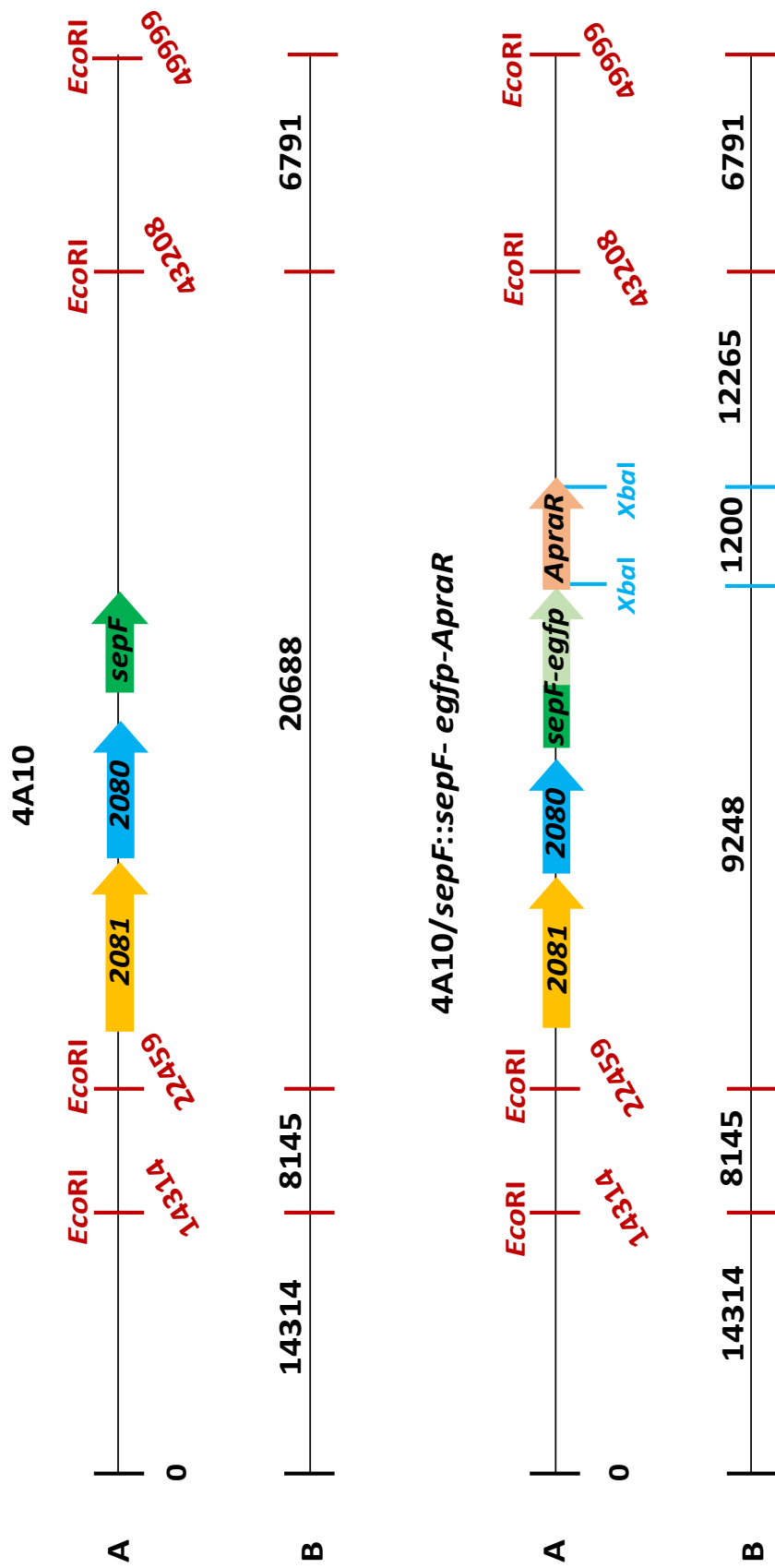


Figure 4.3. Restriction maps of 4A10 cosmid and 4A10/sepF::sepF-egfp-Aprar cosmid. The cosmid drawing is not to scale. EcoRI restriction sites are marked as red dashes, with position (in bp) given and with fragments of the EcoRI/XbaI double digest presented in map B.

The gel image (Figure 4.4) confirms the 4 different fragments for the 4A10 cosmid (lane 2), 20688 bp, 14314 bp, 8145 bp and 6791 bp. The fragments generated from the cosmid 4A10/*sepF::sepF-egfp-ApraR* (lane 4) confirms that three fragments, 14314 bp, 8145 bp and 6791 bp, are unchanged compared to fragments of cosmid 4A10. However, the 20688 bp fragment of cosmid 4A10 is replaced by three different fragments in the cosmid 4A10/*sepF::sepF-egfp-ApraR* (lane 4), namely 12265 bp, 9284 bp and 1200 bp. The expected 12265 bp, 9284 bp fragments are clearly detectable whilst the 1200 bp fragment, although there, is marked by the red arrow to aid detection. The presence of these bands in 4A10/*sepF::egfp-ApraR* suggests that the cassette was successfully inserted to the correct location.

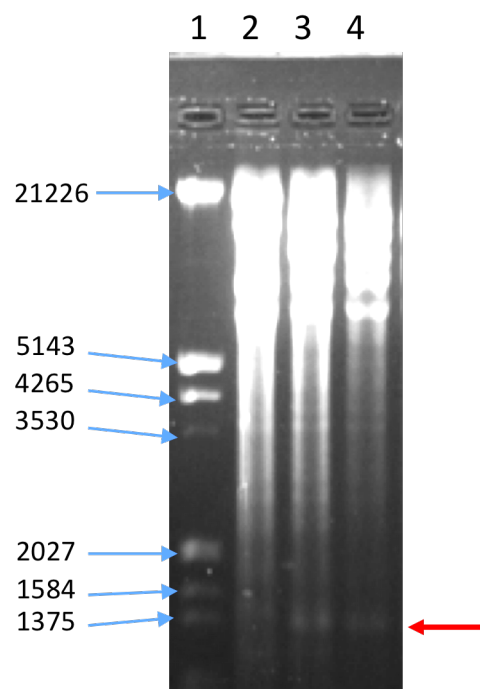


Figure 4.4. Restriction digest using *EcoRI* and *XbaI* enzymes. Cosmid 4A10 (lane 2) and 4A10/*sepF::sepF-egfp-Apra* (lane 4). Ladder (Lambda digested with *EcoRI* and *HindIII*) was loaded into lane 1 to act as a molecular marker, labels are given (bp). Red arrow marks position of 1200 bp bands. Lane numbers were given.

Once the methylation deficient *E. coli* ET12567 had been successfully transformed with cosmid 4A10/*sepF::sepF-egfp-ApraR* using electroporation with the construct, it was used to move the cosmid DNA into *S. coelicolor* M145 using conjugation. Due to the possibility of two different recombination events occurring within the exconjugants, they had to be selected for. Single crossover events would result in the bacterium possessing the *egfp* tagged gene along with another copy of the wild type 4A10 cosmid. These colonies would be resistant to both kanamycin and apramycin. Double crossover events would result in the bacterium possessing only the *Egfp* tagged gene, therefore these colonies would only be resistant to apramycin. Replica plating onto LB containing nalidixic acid + kanamycin and LB containing nalidixic acid + apramycin was used to determine which colonies were single or double crossovers. Nalidixic acid was included in the medium to kill *E. coli* after the conjugation. We have collected spores from both representative single and double crossover strains. Interestingly, the single crossover strains, where in addition to the *sepF-egfp* copy a wild-type *sepF* gene was also present together with a duplication of all other cosmid genes, were very sickly and formed very small colonies. This might be because of gene dosage effect of cell division genes or other genes present on the 4A10 cosmid. The double crossover strains, where the wild-type *sepF* gene was replaced by the *sepF-egfp* allele, looked phenotypically wild-type. This suggested that SepF-Egfp fusion protein was functional and the fusion did not have a polar effect on downstream genes. Due to the poor growth of the single crossovers, only the double crossovers were characterised using microscopy.

4.1.2 Microscopic visualisation of SepF-EGFP in the wild-type strain

The double crossover strain *S. coelicolor* M145/ *sepF::sepF-egfp-ApraR* was used to monitor the localisation pattern of SepF-Egfp throughout the life cycle of *S. coelicolor*. *S. coelicolor* spores were inoculated onto SFM medium in a rectangular patch and microscope coverslips were inserted at a $\sim 70^\circ$ angle to the horizontal plane of this patch. Hyphae were grown at 30°C and then stained using propidium iodide (PI) to allow staining the chromosomes and samples were visualised at regular intervals during the different stages of development. The first sample was collected after 42 hours so that SepF-Egfp localisation could be observed in the vegetative hyphae (Figure 4.5).

During vegetative hyphae, SepF-Egfp presents as discrete irregular foci localising throughout the hyphae. During this stage of development, the chromosomes remain uncondensed and unsegregated as demonstrated by the DNA stain PI. However, while the majority of chromosomes are unsegregated, there are occasional gaps in the chromosomal staining and some irregular staining that might suggest local changes in chromosome organisation within the hyphae. Interestingly, often these gaps or changes in chromosomal staining coincide with the appearance of the SepF-Egfp foci. (Figure 4.5) suggesting that SepF-Egfp localizes to patches devoid of DNA. This raises the question whether SepF is actively involved in organizing the chromosomes or whether SepF localizes to DNA free positions. The latter would mean that DNA organisation might be a positional cue for SepF localisation. As the available cell wall dye, wheat germ agglutinin Alexa-488, emits green fluorescence, it was not possible to establish whether any of the SepF-Egfp foci localise to the positions where vegetative crosswalls were formed.

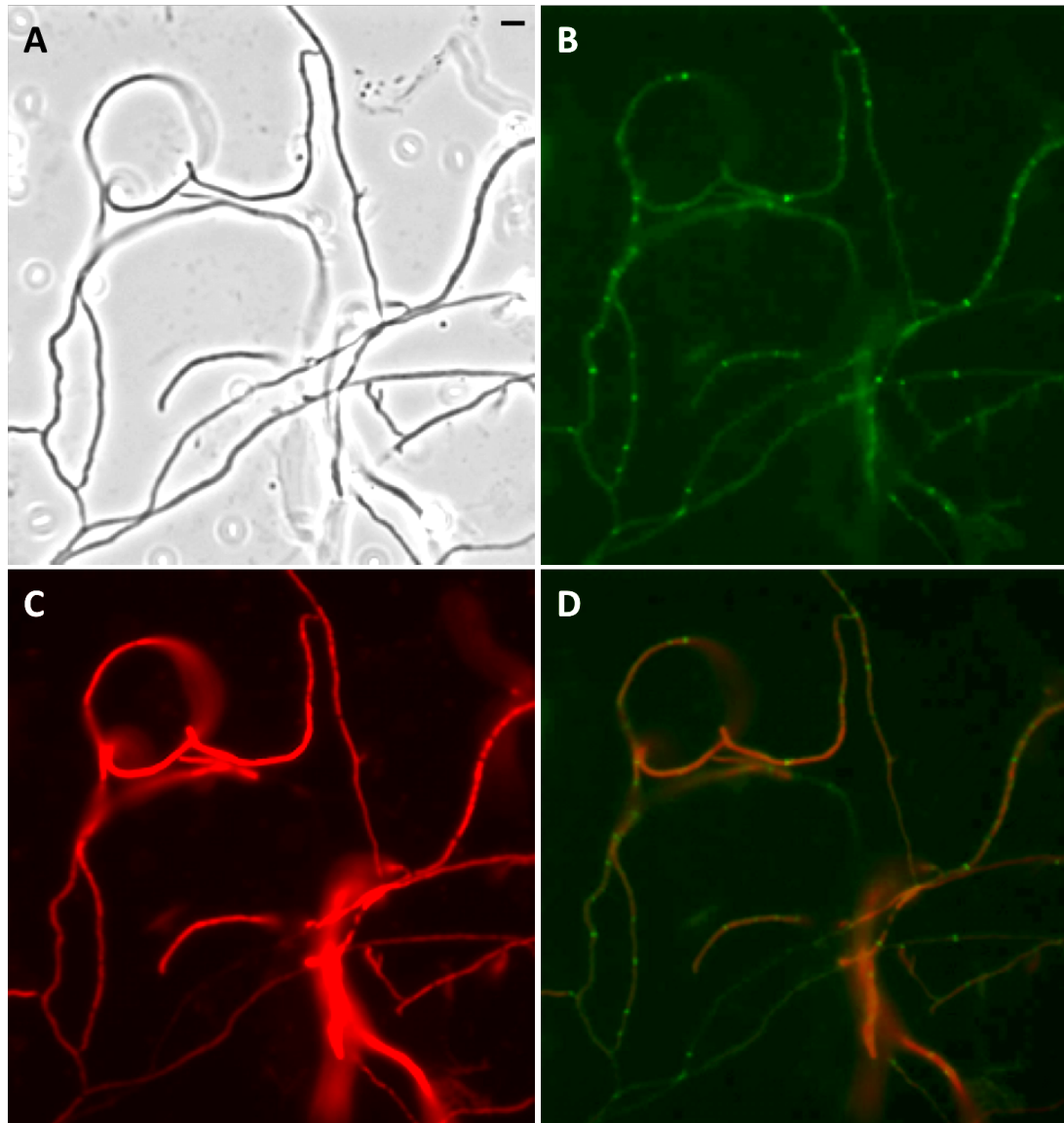


Figure 4.5. Monitoring of SepF-EGFP localisation in vegetative hyphae using epifluorescence microscopy. The M145/ *sepF::sepF-egfp-ApraR* strain was grown for ~42 hours on SFM medium, then were stained using PI for DNA visualisation and viewed using a x100 lens (A) phase contrast image, (B) SepF-Egfp, green (C) DNA, red. (D) Overlaying of the red and green channels. Size bar represents 1 μ m.

The second sets of samples were collected and stained using PI after 46-48 hours to observe SepF localisation in the developing aerial hyphae (Figures 4.6-4.8). The fluorescence images shows that in the early stages of aerial hyphae development, when the chromosomal DNA was still largely uncondensed and septal synthesis had

not yet initiated, as assessed by the phase contrast images, SepF-EGFP begun to form regular foci along the aerial hyphae (Figures 4.6-4.8). Most of the signals are lines perpendicular to the hyphal axis, although there are some tilted patterns, too. Careful comparison of the SepF-Egfp signal and the red DNA staining confirmed the previous finding in the vegetative mycelium that SepF-Egfp was found at places devoid of DNA staining. Whilst the ladder-like regular SepF-Egfp signal is very similar to the FtsZ rings developing in the sporulating aerial hyphae, the resolution of the epi-fluorescence microscopy did not allow us to confirm that the green signal perpendicular to the hyphal axis was indeed a ring viewed from the side.

In order to get higher resolution images of SepF-Egfp localisation, we used confocal microscopy to visualise SepF-Egfp. We prepared samples after 48 hours of growth and stained as before (4.9-4.10)

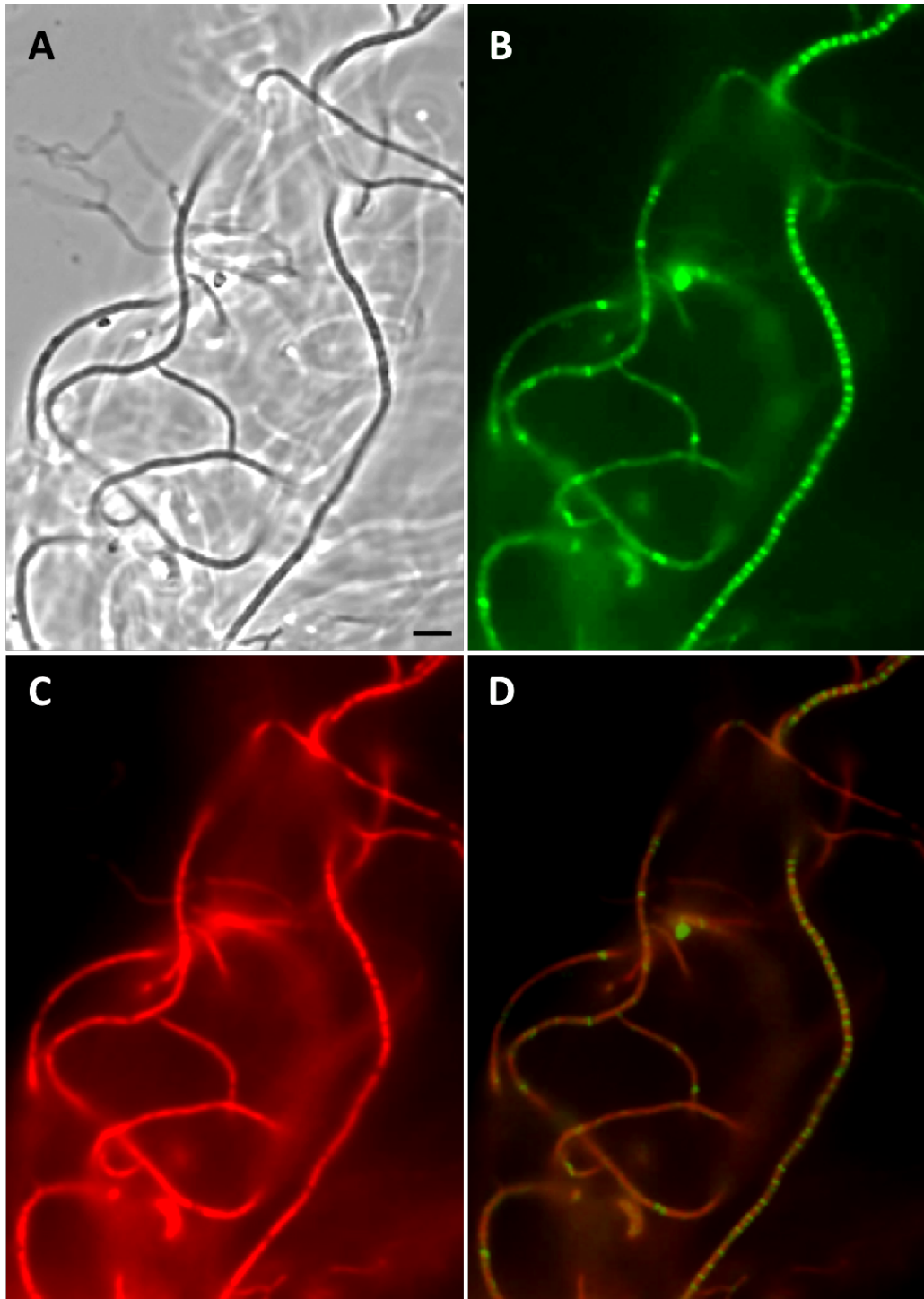


Figure 4.6. Monitoring of SepF-EGFP localisation in early aerial hyphae using epifluorescence microscopy. The M145/ *sepF::sepF-egfp-*ApraR** strain was grown for ~46 hours on SFM medium, then were stained using PI for DNA visualisation and viewed using a x100 lens (A) phase contrast image, (B) SepF-Egfp ,green (C) DNA , red. (D) Overlaying of the red and green channels. Size bar represents 1 μ m.

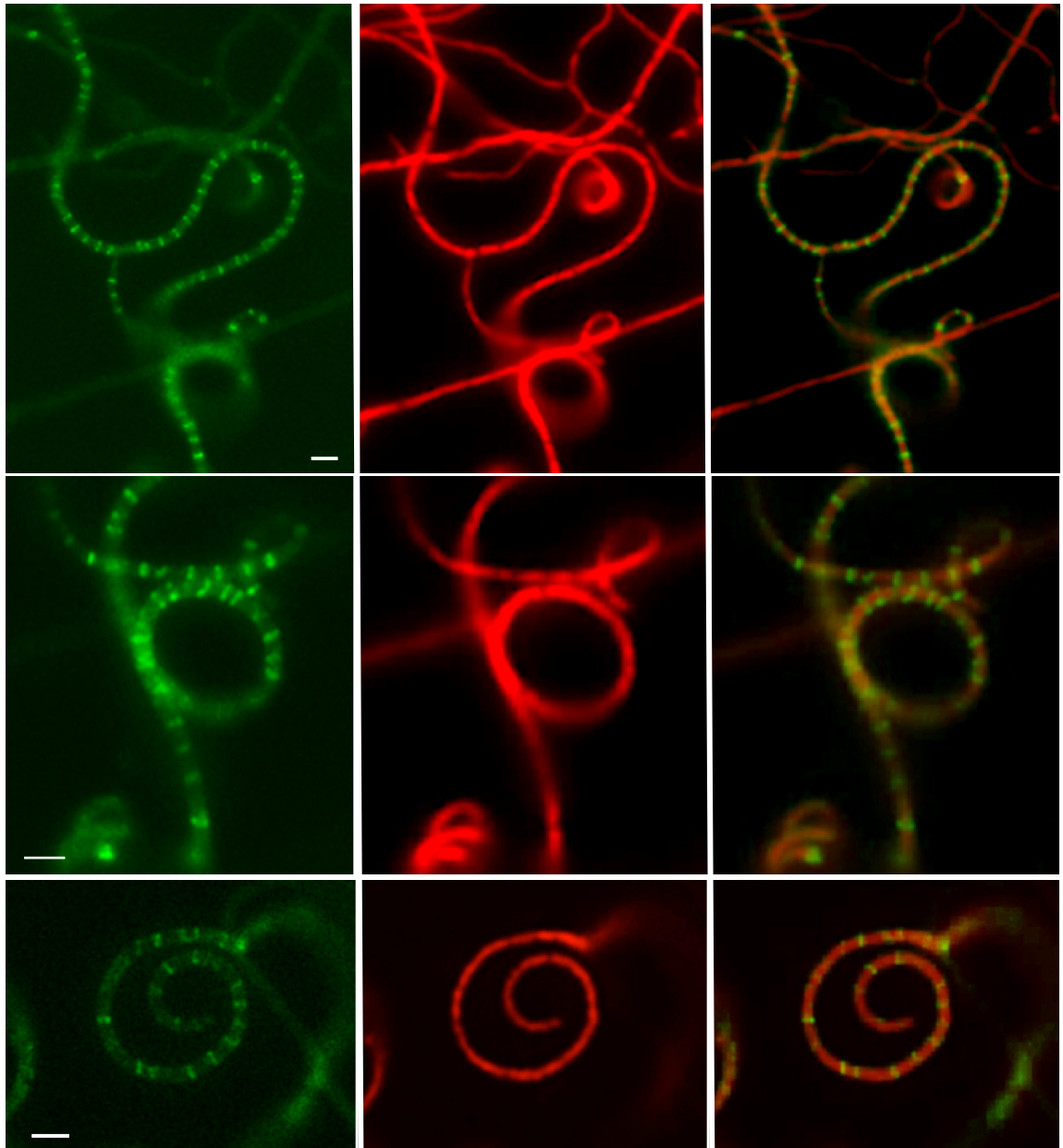


Figure 4.7. Monitoring of SepF-EGFP localisation in early aerial hyphae using epi-fluorescence microscopy. The M145/ *sepF::sepF-egfp-ApraR* strain was grown for ~46 hours on SFM medium, then were stained using PI for DNA visualisation and viewed using a x100 lens. (Left) SepF-Egfp, green (Middle) DNA , red. (Right) Overlaying of the red and green channels. Size bar represents 1 μ m.

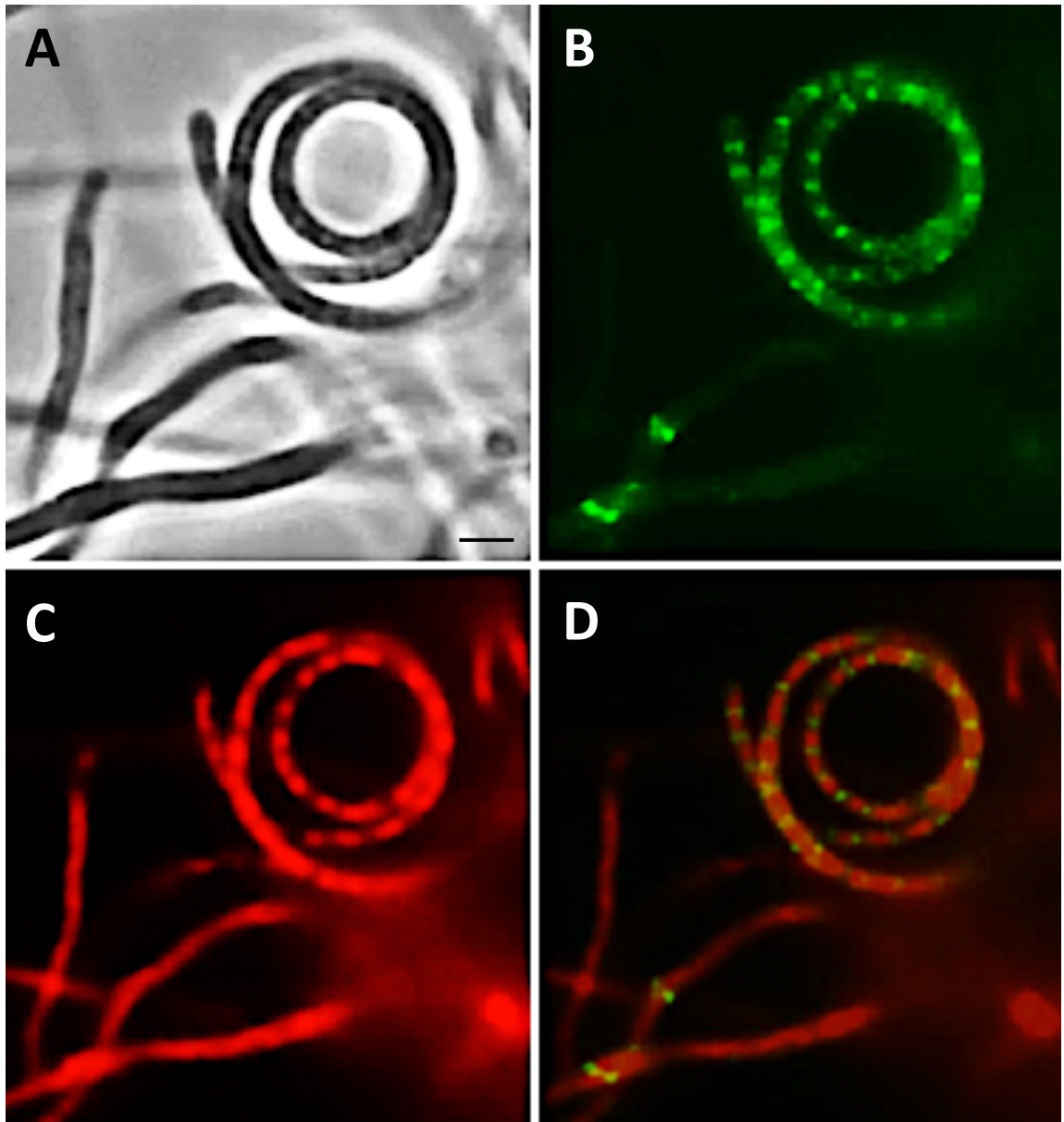


Figure 4.8. Monitoring of SepF-EGFP localisation in early aerial hyphae using epifluorescence microscopy. The M145/ *sepF::sepF-egfp-AprA* strain was grown for ~46 hours on SFM medium, then were stained using PI for DNA visualisation and viewed using a x100 lens (A) phase contrast image, (B) SepF-Egfp, green (C) DNA, red. (D) Overlaying of the red and green channels. Size bar represents 1 μ m.

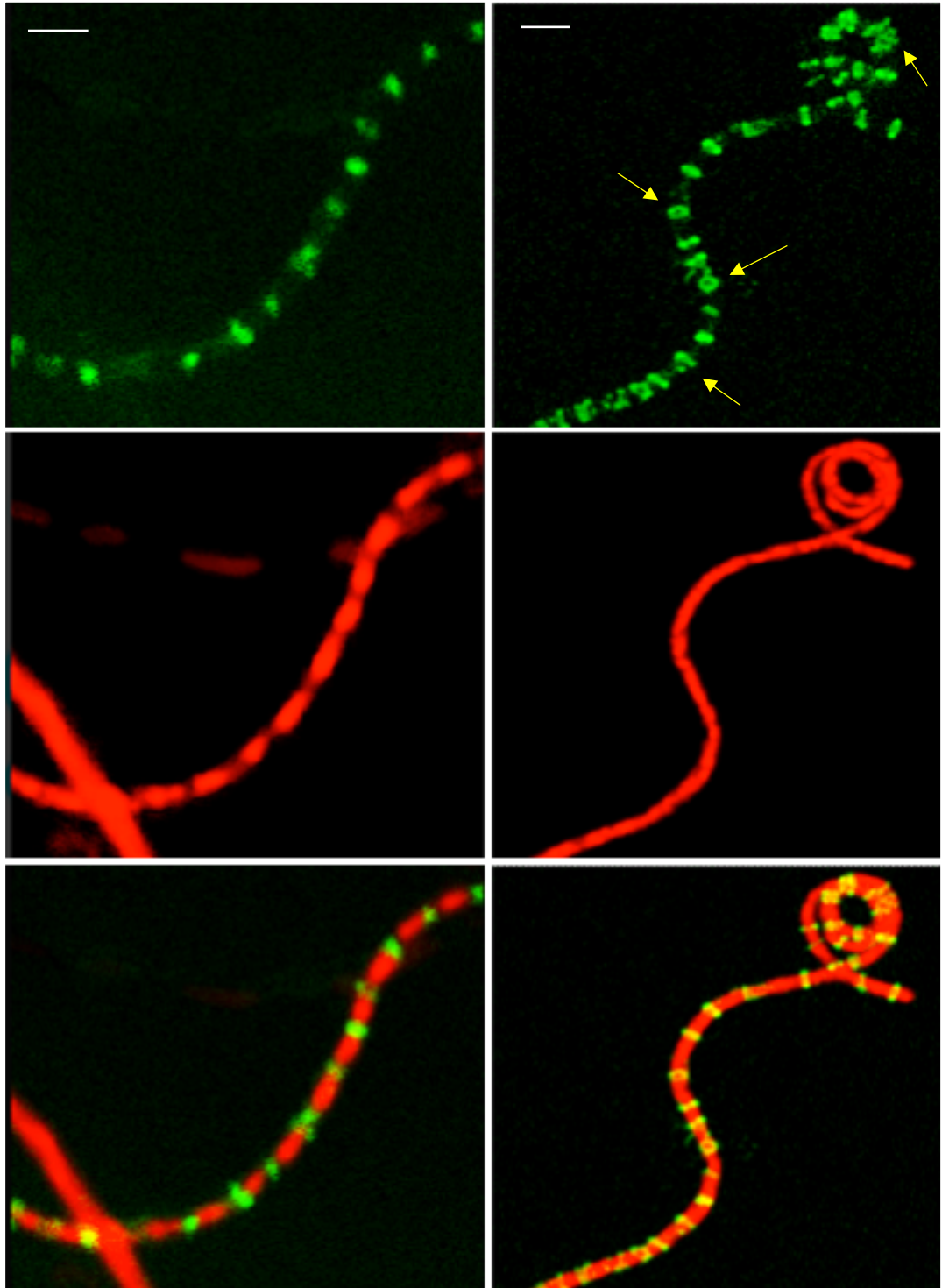


Figure 4.9. Monitoring of SepF-EGFP localisation in early aerial hyphae using confocal microscopy. The M145/ *sepF::sepF-egfp-*ApraR** strain was grown for ~46 hours on SFM medium, then were stained using PI for DNA visualisation and viewed using a x63 lens. (Left) SepF-Egfp, green (Middle) DNA, red. (Right) Overlaying of the red and green channels. Size bar represents 1 μ m. Yellow solid arrows represent SepF-Egfp rings and dashed arrows point at spiral SepF-Egfp patterns.

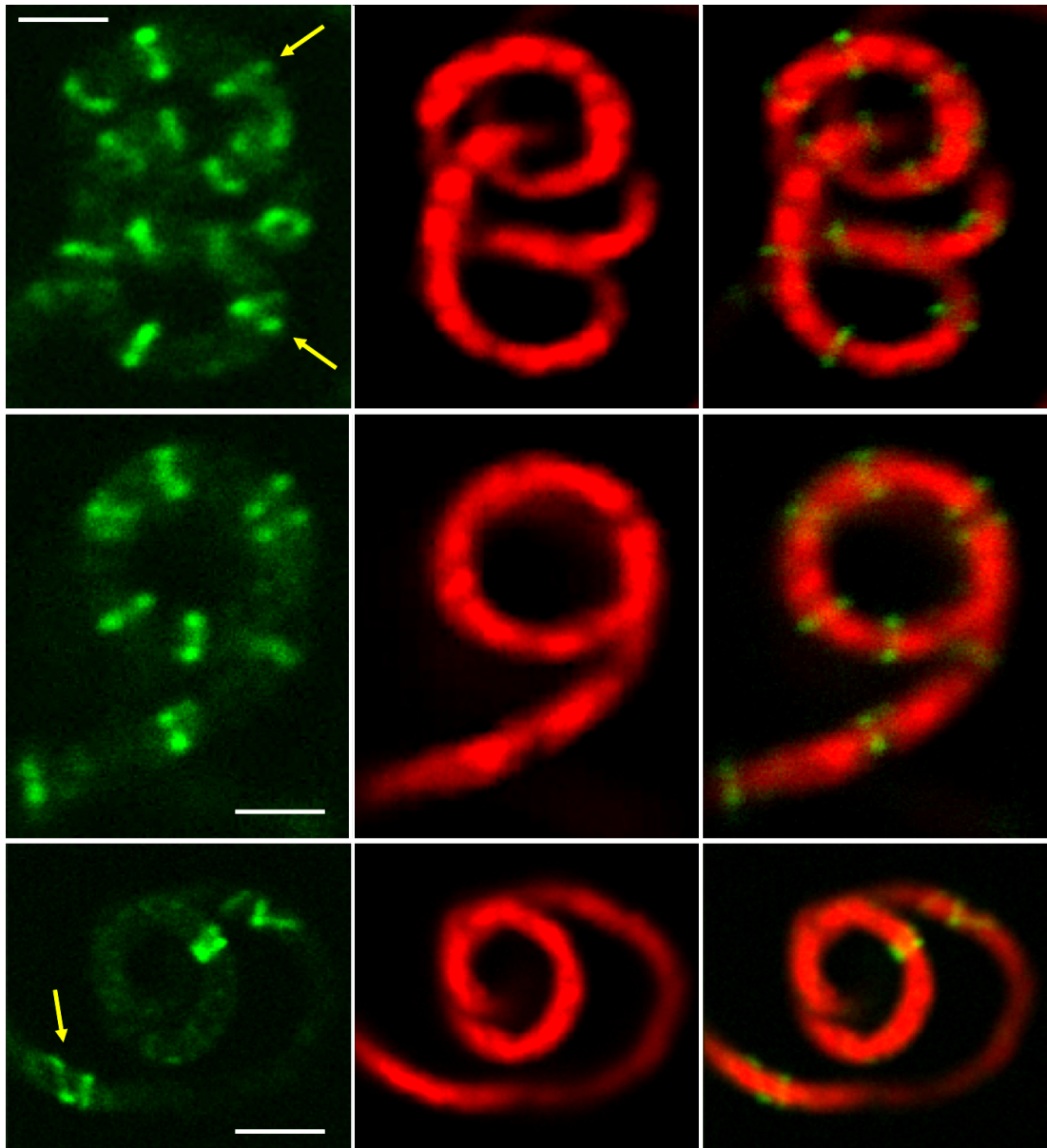


Figure 4.10. Monitoring of SepF-EGFP localisation in early aerial hyphae using confocal microscopy. The M145/ *sepF::sepF-egfp-AprA*R strain was grown for ~46 hours on SFM medium, then were stained using PI for DNA visualisation and viewed using a x63 lens. (Left) SepF-Egfp, green (Middle) DNA , red. (Right) Overlaying of the red and green channels. Size bar represents 1 μ m. Dashed arrows (yellow) point at spiral SepF-Egfp patterns .

In both confocal images (Figures 4.9 and 4.10) we can easily identify SepF-Egfp ring structures, which confirms that SepF, just as FtsZ, does form rings at the time of sporulation in *Streptomyces*. Interestingly, we can also find spiral SepF-Egfp

intermediates, presumably these later coalesce into rings. Spiral intermediates have also been found when monitoring FtsZ (Gundogdu,2011; Krol *et al.*, 2012), suggesting that SepF localisation is very similar to FtsZ localisation.

4.2 SepF-EGFP localisation by introducing *sepF-egfp* in trans

4.2.1 Generation of a *sepF-egfp* clone with a large upstream sequence including the coding region of 2080

In the previous section 4.1, we generated cosmid 4A10/*sepF::sepF-egfp*-Apra where the *sepF* gene was replaced by the *sepF-egfp* fusion. In Chapter 3 we fully complemented the *sepF* null mutant strain using the DNA fragment containing 2080-*sepF* fragment, suggesting that this fragment carried the essentials for expression of *sepF*. Therefore, we first created a plasmid construct carrying the 2080-*sepF-egfp* DNA fragment to further investigate the localisation of SepF-Egfp in the wildtype M145 strain. The fragment 2080*sepF-egfp* was amplified from the cosmid 4A10/*sepF::sepF-egfp*-ApraR using primers 2080 Xba Nde FRW and mCherry Eco REV using PCR (Figure 4.11). The reverse primer, although designated as mCherry Eco REV, does prime on the *egfp* gene, as both *mCherry* and *egfp* have identical nucleotide sequences at their 3' ends. The obtained PCR product 2080-*sepF-egfp* was introduced into the plasmid pMS82, which integrates as a single copy at a single chromosomal location in *S. coelicolor*. Once the construct was created, screened for using colony PCR (Figure 4.12) and confirmed by sequencing, pMS82/2080-*sepF-egfp* was then transformed into the non-methylating *E. coli* strain ET12567/pUZ8002 and conjugated into wild-type M145 strain. In order to test that the 2080-*sepF-egfp* fragment expressed a fully functional SepF-Egfp fusion, pMS82/2080-*sepF-egfp* was also introduced into the *sepF* knockout mutant strain. Exconjugants were selected

using hygromycin and at least two representatives of each strains, M145/pMS82/2080-*sepF-egfp* and Δ *sepF*/pMS82/2080-*sepF-egfp* were then processed to generate spore preparations.

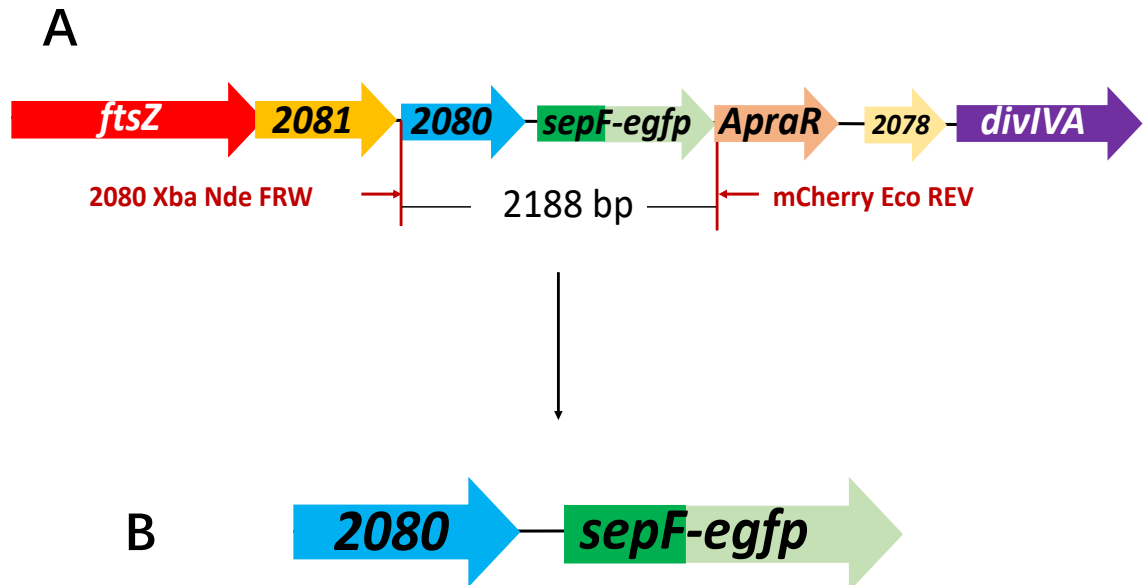


Figure 4.11. Design of the plasmid pMS82/2080-*sepF-egfp*. The fragment 2080-*sepF-egfp* was amplified from the cosmid 4A10/*sepF::sepF-egfp-ApraR*. (A) using primers 2080 Xba Nde FRW and mCherry Eco REV using PCR. The amplified fragment. (B) was introduced into the EcoRV site of plasmid pMS82 plasmid to generate pMS82/2080-*sepF-egfp*.

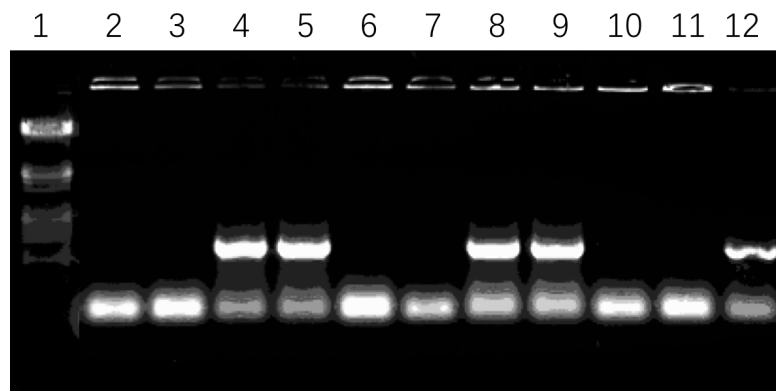


Figure 4.12. Colony PCR for testing the transformants.

Lane 1: λ *EcoRI-HindIII* ladder; lane 2-11: each lane represents a PCR product from a single colony; lane 12: Positive control using the 4A10/*sepF::sepF-egfp-ApraR* cosmid as template.

4.2.2 Complementation of the *sepF* mutant with pMS82/2080-*sepF-egfp*

If the 2080-*sepG-egfp* fragment expresses a fully functional SepF-Egfp, then the strain $\Delta sepF/pMS82/2080sepF-egfp$ should have a wild-type phenotype. To test this, the spores of strains M145/*pMS82/2080-sepF-egfp* and strain $\Delta sepF/pMS82/2080-sepF-egfp$ were streaked onto SFM medium containing hygromycin. Introduction of fragment pMS82/2080*sepF-egfp* into the *sepF* mutant strain restored sporulation and produced colonies indistinguishable from the wild-type (Figure 4.13). We also tested the strain $\Delta sepF/pMS82/2080-sepF-egfp$ using microscopic analysis by staining samples grown on SFM + hygromycin medium for 48 hours using the cell wall stain WGA-Alexa 488. We observed cross-wall development in vegetative hyphae and regular septation in the aerial hyphae of the $\Delta sepF/pMS82/2080-sepF-egfp$ strain very similar to that of the wild-type, which demonstrated that the *sepF* mutant was

fully complemented by the pMS82 construct carrying *2080-sepF-egfp* and that this fragment expressed a fully functional SepF-Egfp (Figure 4.14).



Figure 4.13. Analysis of the macroscopic phenotypes of (A) $\Delta sepF/pMS82/2080-sepF-egfp$ and (B) $M145/pMS82/2080-sepF-egfp$. Stocks were streaked onto SFM medium containing hygromycin and were grown for 4 days at 30°C.

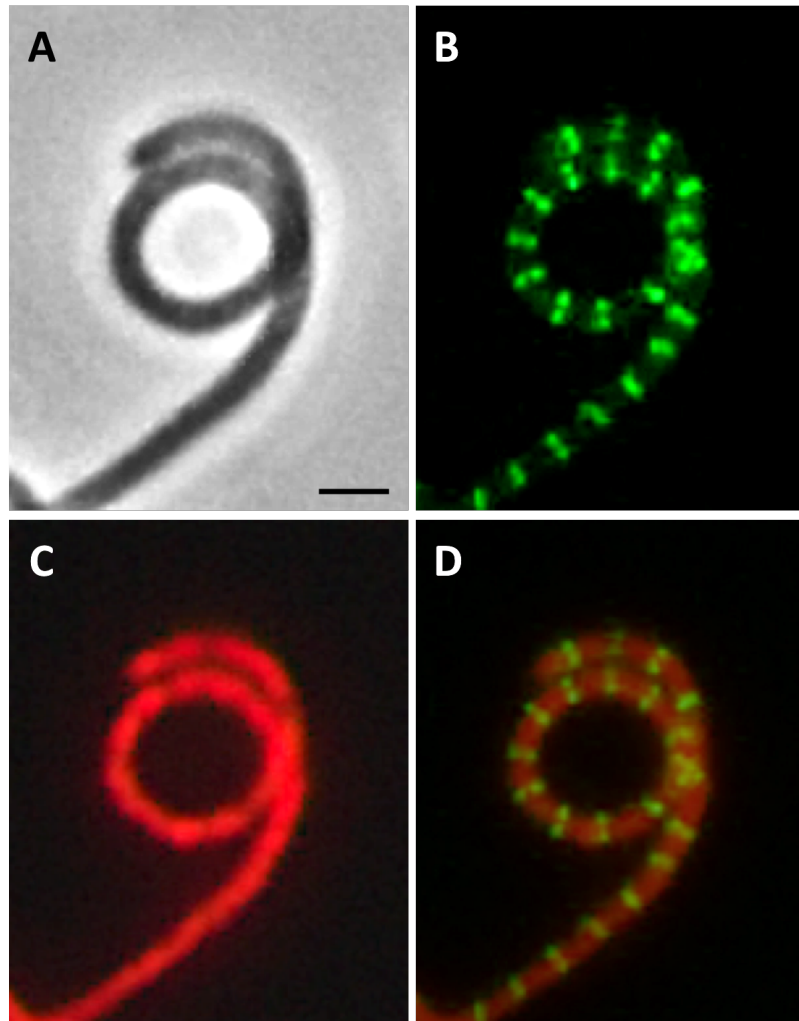


Figure 4.14. The microscopic analysis $\Delta sepF/pMS82/2080-sepF-egfp$ by staining samples. The $\Delta sepF/pMS82/2080-sepF-egfp$ strain was grown for ~ 48 hours on SFM+ hygromycin medium, then were stained using WGA-Alexa 488 for cell wall and PI for DNA visualisation and viewed using a x100 lens (A) phase contrast image; (B) Cell wall, green; (C) DNA , red; (D) Overlaying of the red and green channels. Size bar represents 1 μm .

4.2.3 Monitoring SepF-Egfp using pMS82/2080-sepF-egfp

Epi-fluorescence microscopy was used to investigate SepF-EGFP localization in both M145/pMS82/2080-sepF-egfp and $\Delta sepF/pMS82/2080-sepF-egfp$ strains. Spores were inoculated onto SFM medium containing hygromycin in a rectangular patch and coverslips were inserted at a $\sim 70^\circ$ angle to the horizontal plane of the

medium. Hyphae were then visualized at regular intervals to sample the different stages of development. Samples were collected after 42, 46, 48 and 50 hours growth so that SepF-Egfp localisation could be observed at different stages of cellular development (Figures 4.15-4.20).

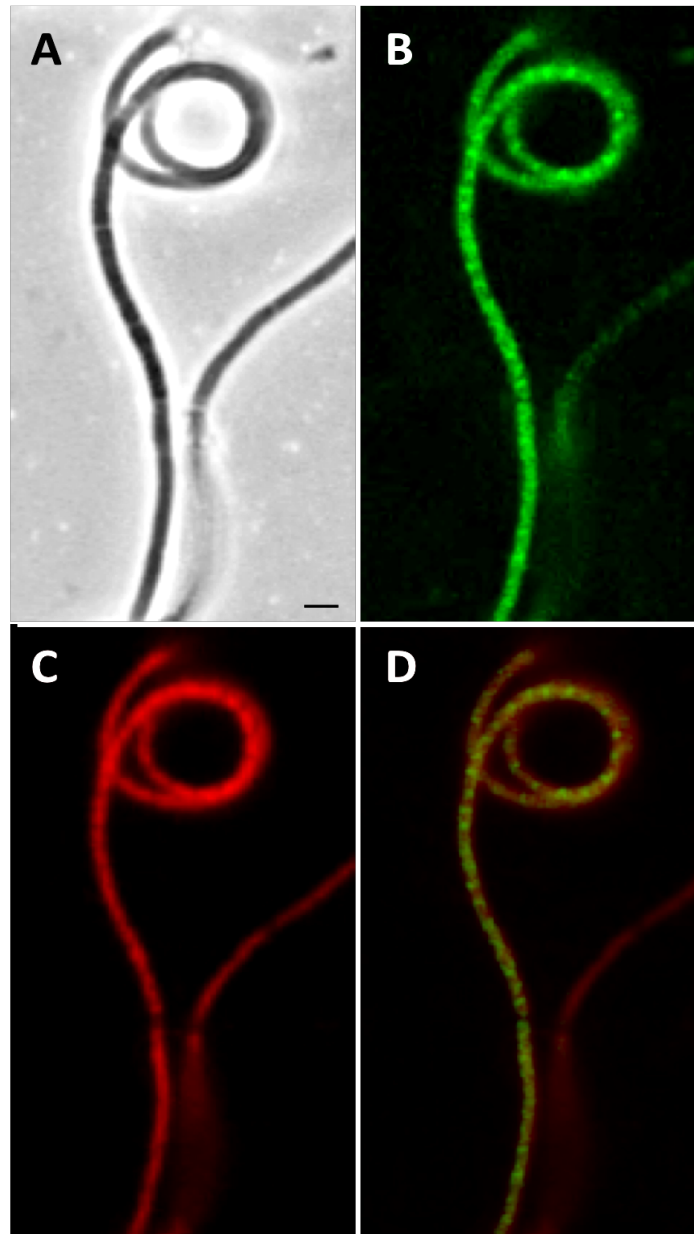


Figure 4.15. Monitoring of SepF-EGFP localisation in a young aerial hyphae of M145/pMS82/2080-*sepF-egfp* using fluorescence microscopy. The strain was grown for ~46 hours on SFM medium containing hygromycin, then was stained using PI for DNA and viewed using fluorescence microscopy (A) Phase contrast image, (B) SepF-Egfp (green), (C) DNA (Red), (D) Overlaying of the red and green channels. Size bar represents 1 μ m.

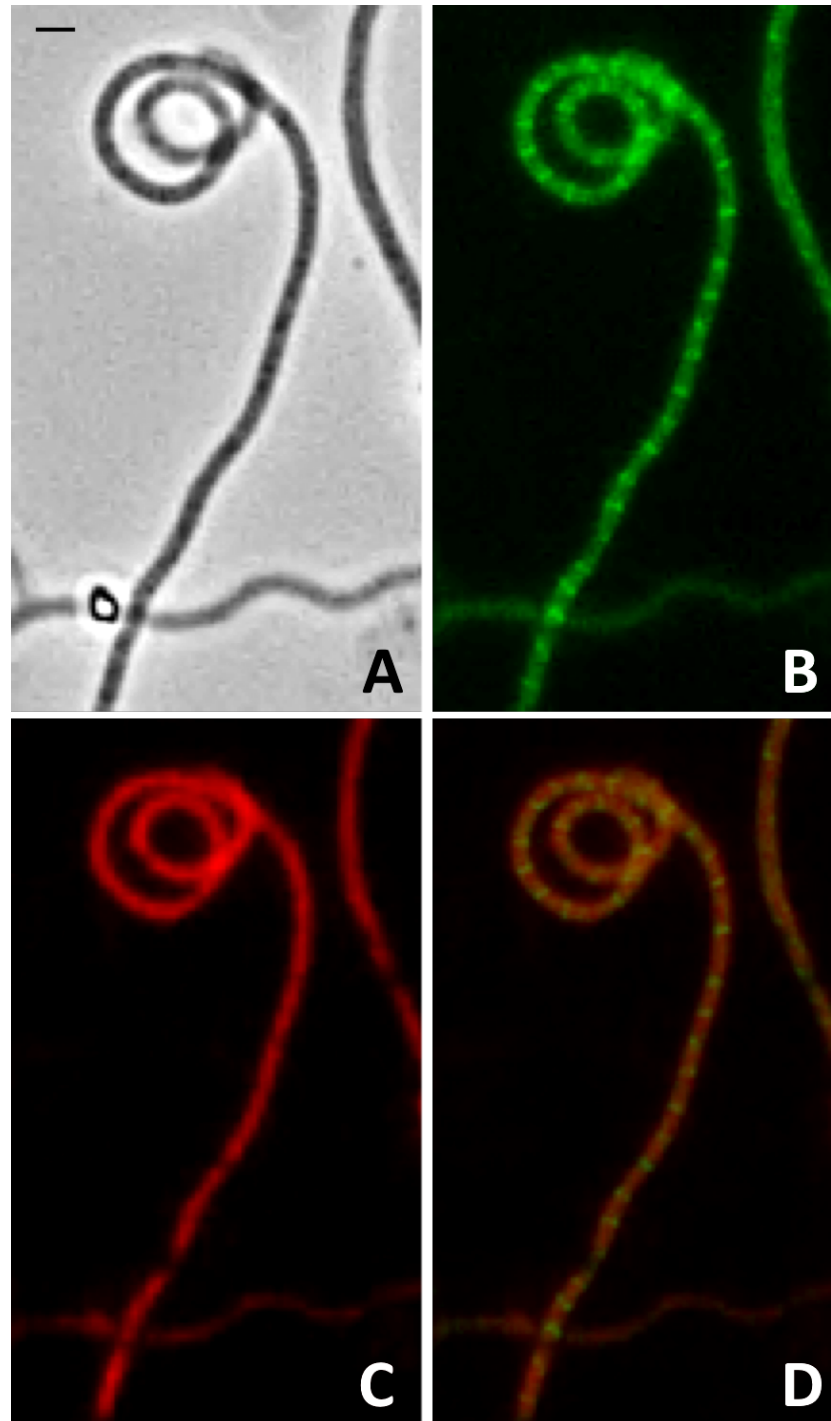


Figure 4.16. Monitoring of SepF-EGFP localisation in a young aerial hyphae of M145/pMS82/2080-*sepF-egfp* using fluorescence microscopy. The strain was grown for ~46 hours on SFM medium containing hygromycin, then was stained using PI for DNA and viewed using fluorescence microscopy (A) Phase contrast image, (B) SepF-Egfp (green), (C) DNA (Red), (D) Overlaying of the red and green channels. Size bar represents 1 μ m.

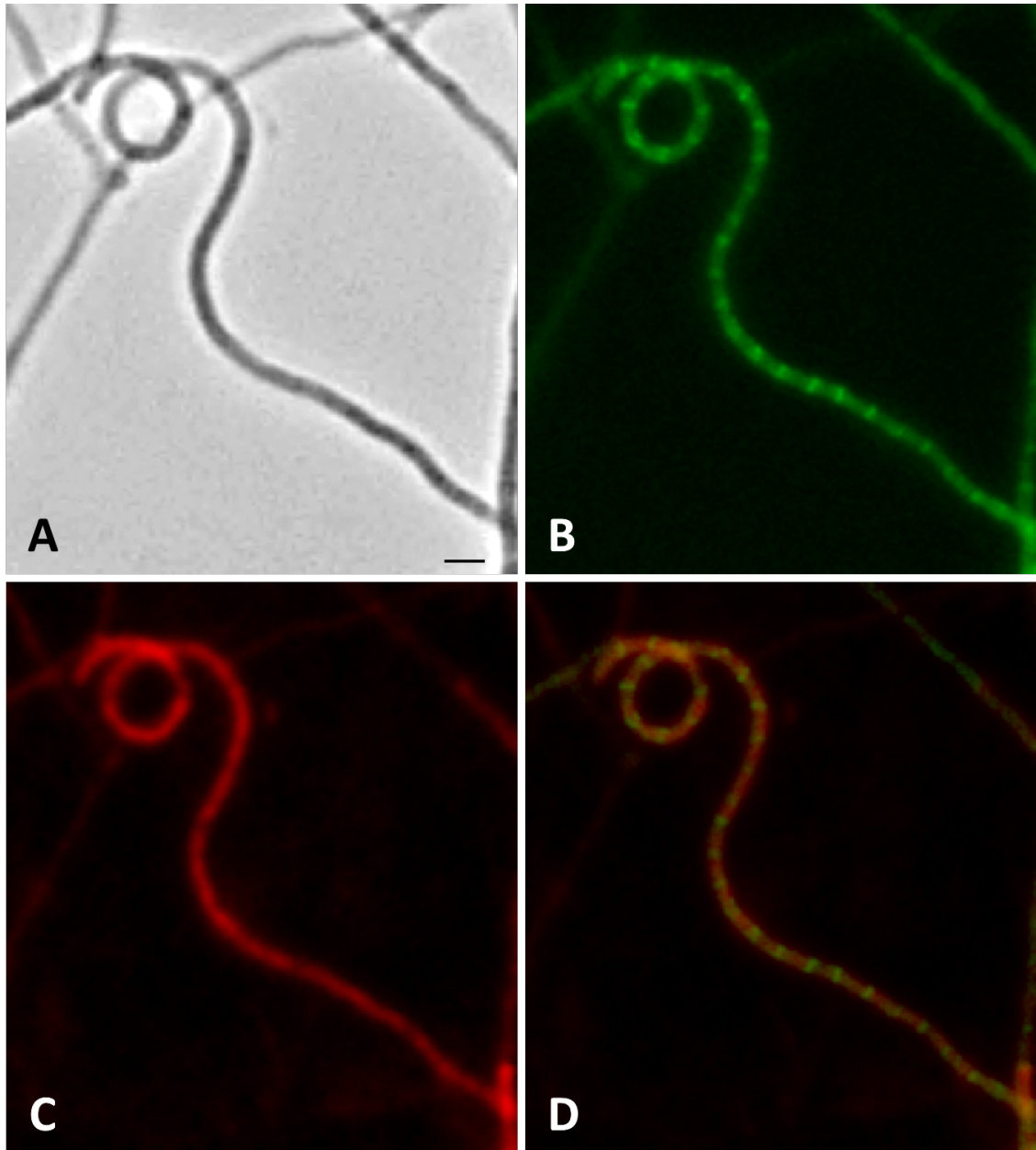


Figure 4.17. Monitoring of SepF-EGFP localisation in a young aerial hyphae of M145/pMS82/2080-*sepF-egfp* using fluorescence microscopy. The strain was grown for ~46 hours on SFM medium containing hygromycin, then was stained using PI for DNA and viewed using fluorescence microscopy. (A) Phase contrast image, (B) SepF-Egfp (green), (C) DNA (Red), (D) Overlaying of the red and green channels. Size bar represents 1 μm .

The SepF-Egfp localisation in strain M145/pMS82/2080-*sepF-egfp* displayed a very similar pattern as in the knockin strain, M145/ *sepF::sepF-egfp-AprA*R. During vegetative growth, SepF-Egfp localised to discrete irregular foci throughout the hyphae. In the early aerial hyphae (Figure 4.15) a strong diffuse green signal accumulated in the part of the aerial hyphae that was to become the spore chain. This suggested that in the sporogenic aerial hyphae SepF expression was upregulated, which first generated the diffuse green signal, which is then followed by the rearrangement of SepF-Egfp into regular rings, although the epi-fluorescent microscopy doesn't allow us to fully visualise the rings. As before in the M145/ *sepF::sepF-egfp-AprA*R strain, in M145/pMS82/2080-*sepF-egfp* the SepF-Egfp "rings" are observed in the nucleoid-free zones in the aerial hyphae (Figure 4.15-4.17). Although at the time of the formation of the SepF-Egfp rings the chromosomes are not fully segregated, the PI staining does show patches of uneven DNA staining that suggests that the chromosomes started their re-organisation prior to sporulation. SepF-Egfp forms regular ring structures well before the chromosomes are fully segregated and the septa begin to form, but we cannot rule out the possibility that SepF localisation is controlled by nucleoid free zones.

In the strain Δ *sepF*/pMS82/2080SepF-EGFP, SepF-EGFP localised in the same manner as in the wild-type strain, suggesting that the fact that SepF-Egfp was expressed at a different chromosomal location in this strain did not affect SepF function (Figure 4.18 – 4.20).

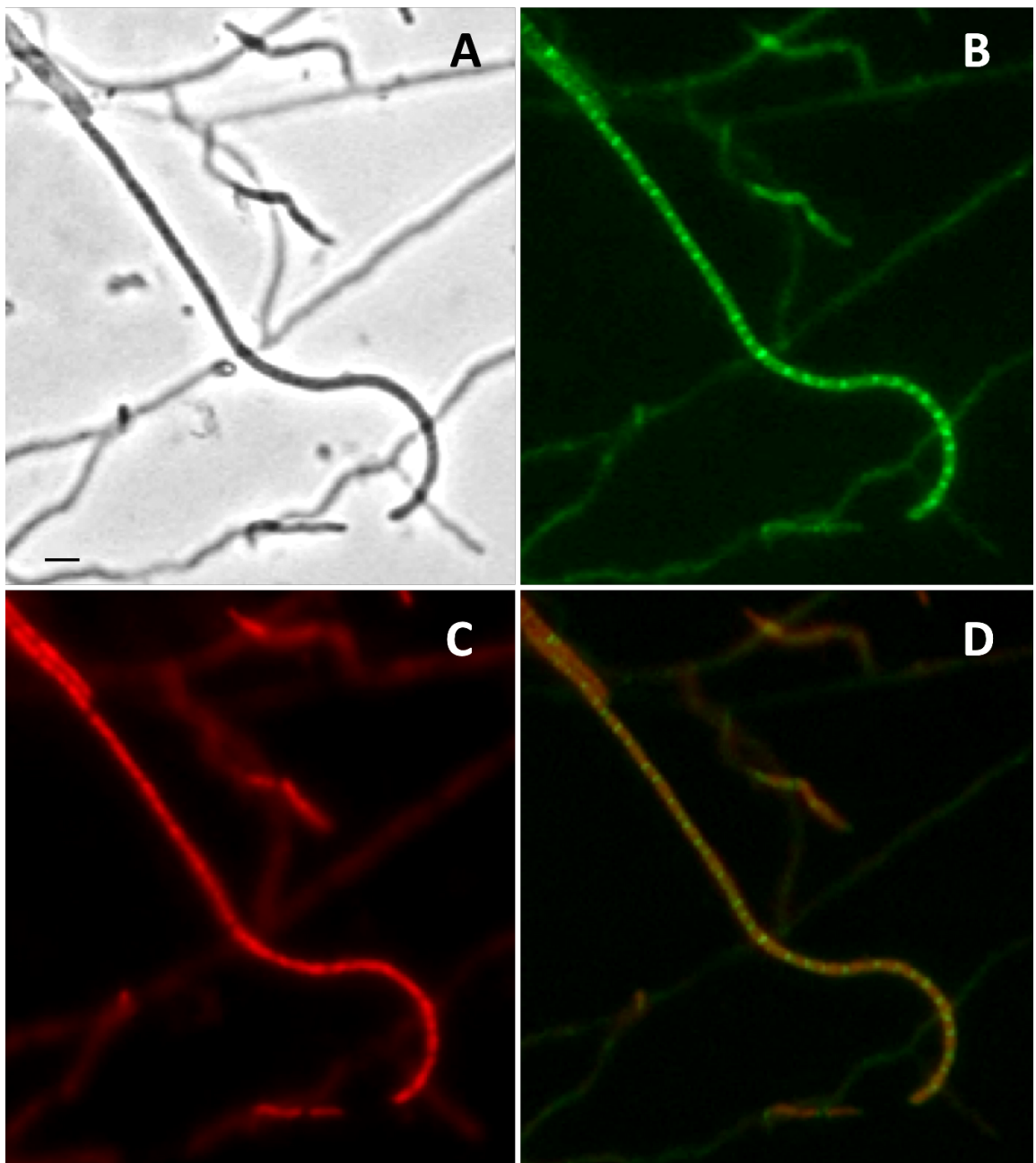


Figure 4.18. Monitoring of SepF-EGFP localisation in a young aerial hyphae of *ΔsepF/pMS82/2080-sepF-egfp* using fluorescence microscopy. The strain was grown for ~46 hours on SFM medium containing hygromycin, then was stained using PI for DNA and viewed using fluorescence microscopy. (A) Phase contrast image, (B) SepF-Egfp (green), (C) DNA (Red), (D) Overlaying of the red and green channels. Size bar represents 1 μm .

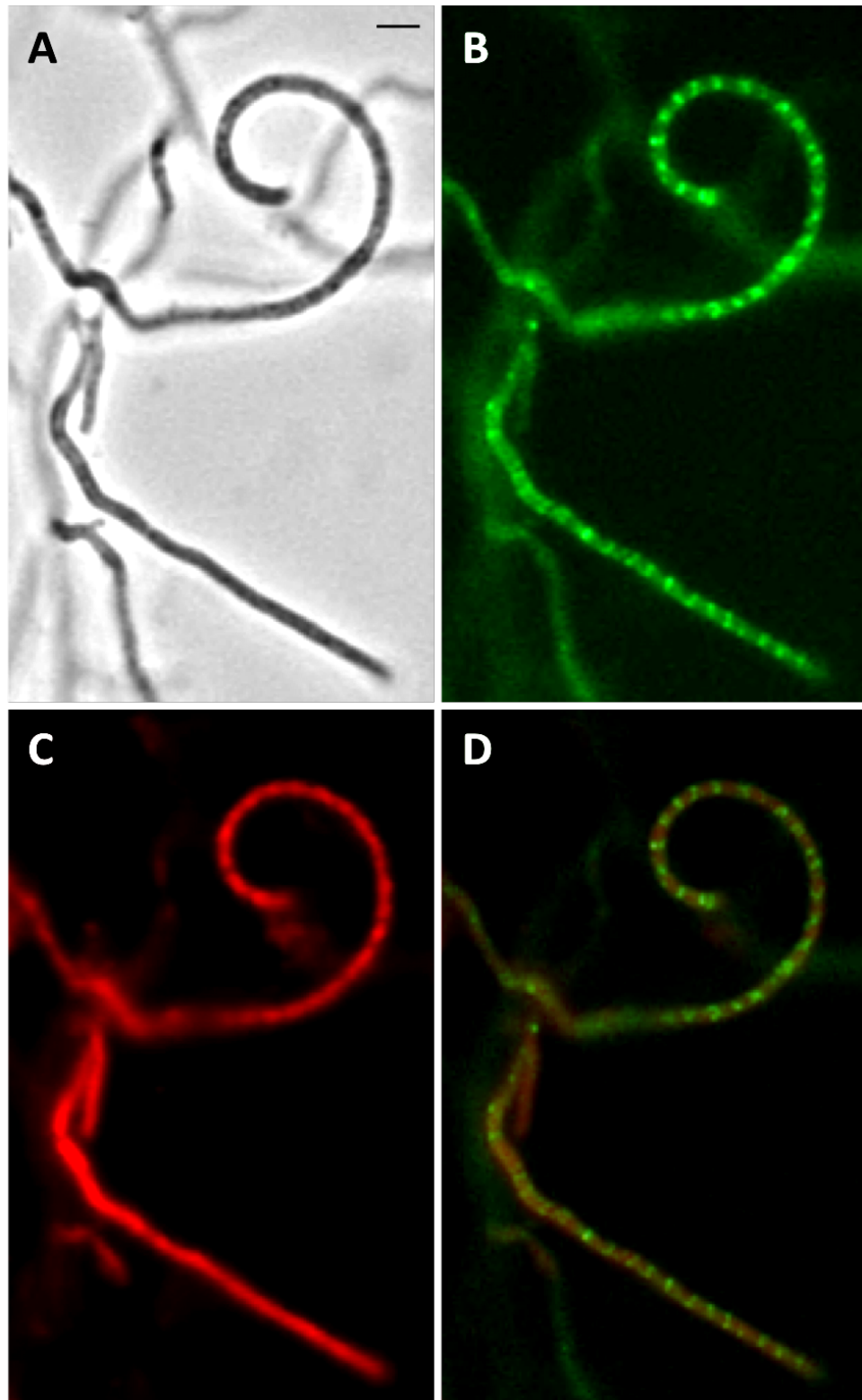


Figure 4.19. Monitoring of SepF-EGFP localisation in a young aerial hyphae of $\Delta sepF$ /pMS82/2080-*sepF-egfp* using fluorescence microscopy. The strain was grown for ~46 hours on SFM medium containing hygromycin, then was stained using PI for DNA and viewed using fluorescence microscopy. (A) Phase contrast image, (B) SepF-Egfp (green), (C) DNA (Red), (D) Overlaying of the red and green channels. Size bar represents 1 μ m.

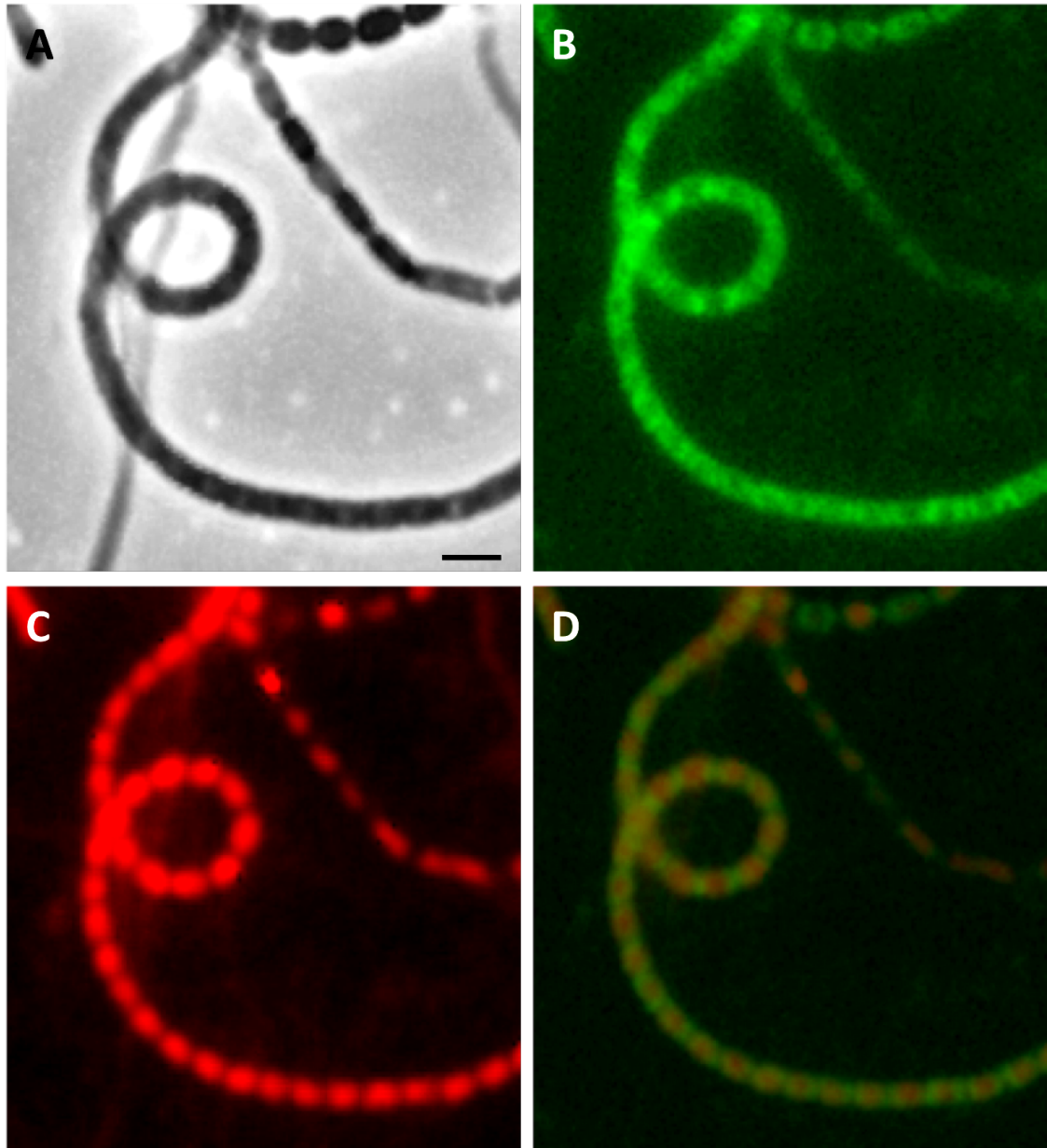


Figure 4.20. Monitoring of SepF-EGFP localisation in a late development stage of aerial hyphae of $\Delta sepF$ /pMS82/2080-*sepF-egfp* using fluorescence microscopy. The strain was grown for ~46 hours on SFM medium containing hygromycin, then was stained using PI for DNA and viewed using fluorescence microscopy. (A) Phase contrast image, (B) SepF-Egfp (green), (C) DNA (Red), (D) Overlaying of the red and green channels. Size bar represents 1 μ m.

4.2.4 Generation of a *sepF-egfp* clone with a shorter upstream sequence

The previous construct used to monitor SepF localisation contained a large DNA fragment upstream of the *sepF* gene to ensure all information needed for *sepF* expression. However, this construct then carried the 2080 gene, although without any of its promoters. We wanted to test whether we could use a shorter upstream sequence for *sepF* expression. We have not carried out any transcriptional mapping to determine the transcriptional start site(s). However, Y. Jeong *et al* (2016) have performed RNA seq to identify the transcriptional start sites for all the genes in *S. coelicolor*. Whilst none of the transcriptional starts were confirmed by independent methods, interestingly, they identified two potential transcriptional starts for *sepF*. In our design, we included both transcriptional starts and their putative promoters using primers sepFp2 XbaBgl FRW and FP Eco REV, to amplify by PCR using the cosmid 4A10/*sepF::sepF-egfp-ApraR* generated in chapter 4.2.1 (Figure 4.21). This fragment contained 343 bp upstream of the *sepF* translational start site. The PCR product was

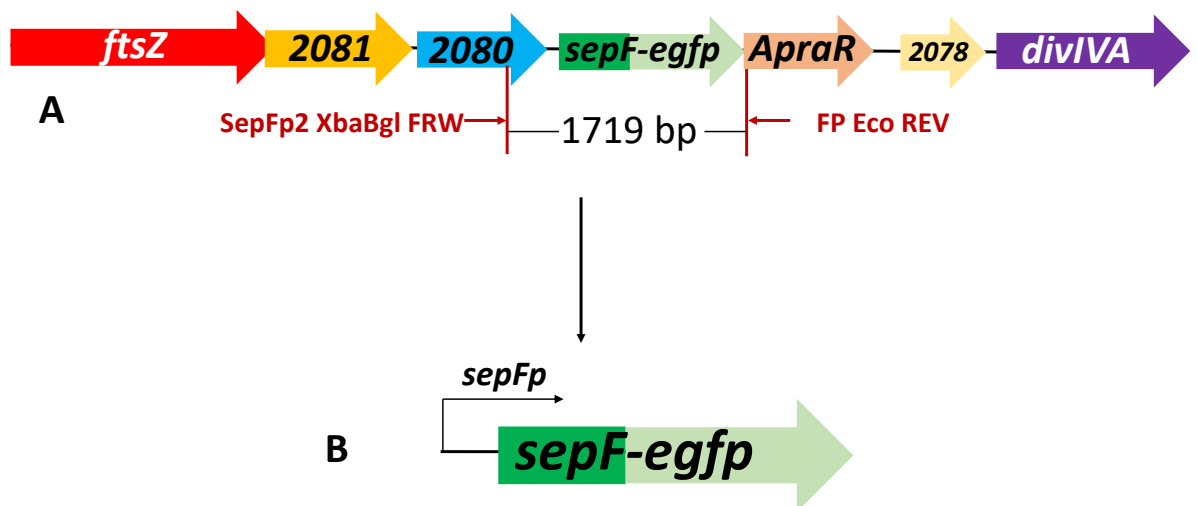


Figure 4.21. Design of the plasmid pMS82/P-*sepF-egfp*. The fragment P-*sepF-egfp* was amplified from the cosmid 4A10/*sepF::sepF-egfp-ApraR*. (A) using primers SepFp2 XbaBgl FRW and FP Eco REV using PCR. The amplified fragment. (B) was introduced into the EcoRV site of plasmid pMS82 plasmid to generate pMS82/P-*sepF-egfp*.

ligated into the *EcoRV* site of vector pMS82 and then transformed into *E. coli* DH5 α strain. Then single colonies, which potentially contain the fragment P-*sepF-egfp* were tested by PCR using the same primers used to generate the fragment (Figure 4.22). After further confirmation by sequencing, we transformed pMS82/P-*sepF-egfp* into the non-methylating *E. coli* strain ET12567/pUZ8002 and conjugated into the wild-type M145 strain and the *sepF* mutant strain to create strains M145/pMS82/P-*sepF-egfp* and Δ *sepF*/pMS82/P-*sepF-egfp*. The exconjugants were used to generate spore stocks.

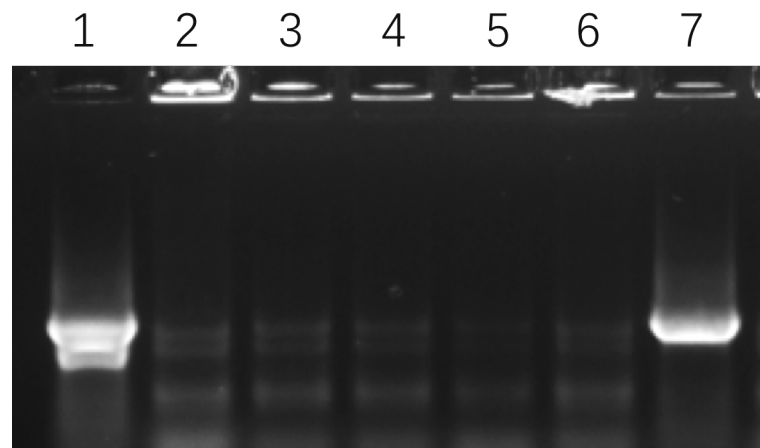


Figure 4.22. Colony PCR for testing the transformants.

Lane 1: Positive control using the 4A10/*sepF*::*sepF-egfp-ApraR* cosmid as template; lane 2-7: each lane represents a PCR product from a single colony. Lane 7 shows the positive colony which contains the pMS82/P-*sepF-egfp* fragment.

To test whether this construct with a shorter upstream sequence fully expressed SepF we tested if this construct could complement the *sepF* knockout mutant. The strain Δ *sepF*/pMS82/P-*sepF-egfp* together with the control strains M145 and Δ *sepF*, both carrying the insert free pMS82 plasmid, were streaked in a triangle patch on plate SFM containing hygromycin. The fragment pMS82/P-*sepF-egfp* was introduced into the *sepF* mutant strain restored sporulation and spore viability (Figure 4.23). We

also stained cells of $\Delta sepF/pMS82/P-sepF-egfp$ using WGA-Alexa 488 and observed cross wall development both in vegetative hyphae and aerial hyphae the same way as in the wild-type strain, which demonstrates that the *sepF* mutant is fully complemented by construct *P-sepF-egfp* (Figure 4.24).

Fluorescence microscopy was used to investigate SepF-EGFP localisation in both wild-type M145 (Figures 4.25 - 4.27) and the *sepF* mutant. The cells were grown alongside a microscope coverslip as before and were grown ~46-48 hours in SFM medium containing hygromycin before stained using PI. Representative samples of M145/*pMS82/P-sepF-egfp* are shown (Figures 4.25 - 4.27), confirming that SepF-Egfp localisation using the *pMS82/P-sepF-egfp* construct was indistinguishable from SepF-Egfp localisation observed using the *pMS82/2080-sepF-egfp* or the knock-in construct *sepF::sepF-egfp-AprR*.

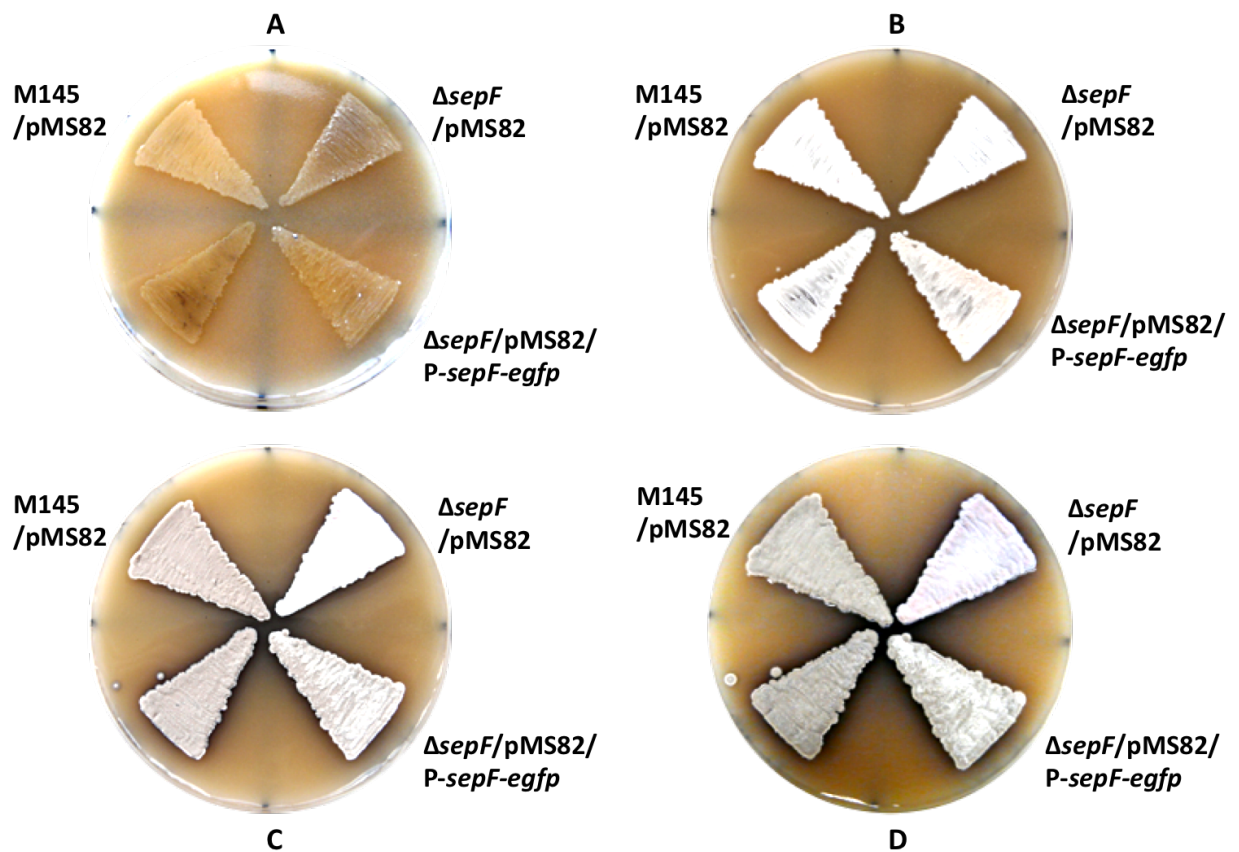


Figure 4.23. Analysis of the macroscopic phenotype of $\Delta sepF/pMS82/P-sepF-egfp$.

The $\Delta sepF/pMS82/P-sepF-egfp$ strain and control strains M145/pMS82 and $\Delta sepF/pMS82$ were streaked in a triangle patch onto SFM medium containing hygromycin. The plate was incubated at 30 °C and monitored at regular time intervals (A) 1 day, (B) 2 days, (c) 3 days and (D) 4 days. The sporulation that indicated by the dark grey spore pigment is restored by pMS82/P-sepF-egfp in strain $\Delta sepF/pMS82/P-sepF-egfp$. The unlabeled strain is not related to this experiment.

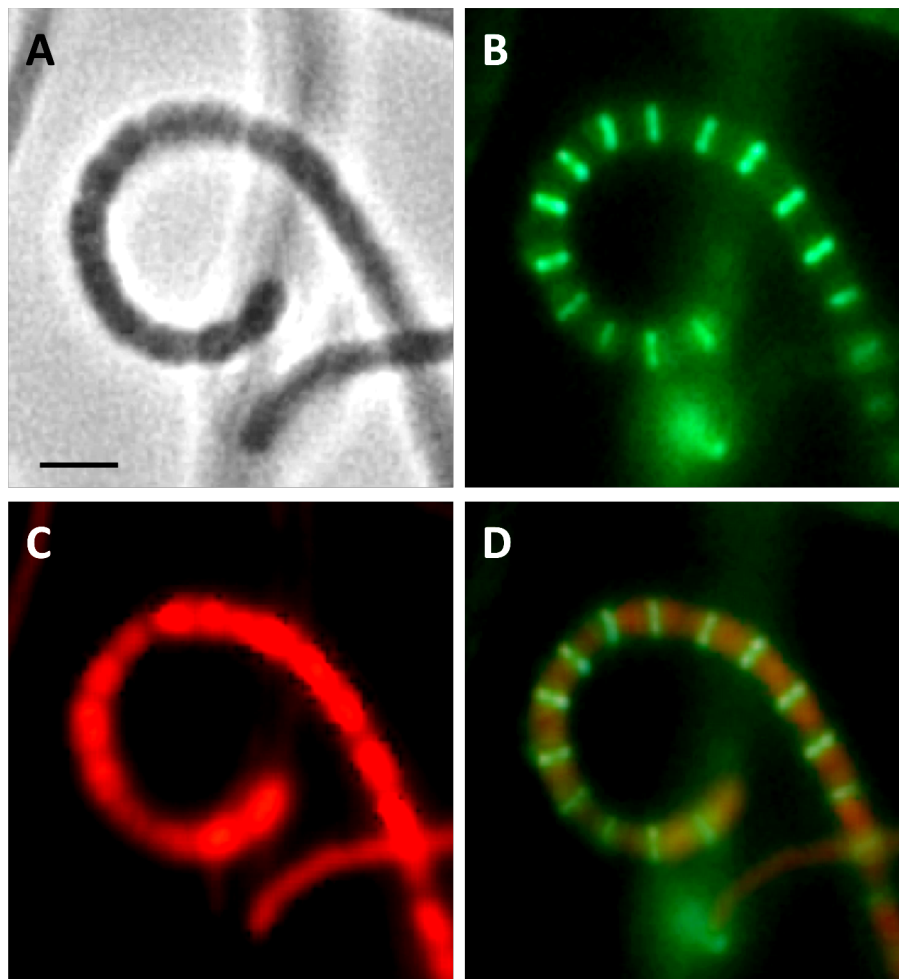


Figure 4.24. The microscopic analysis $\Delta sepF/pMS82/P-sepF-egfp$ by staining samples. The $\Delta sepF/pMS82/P-sepF-egfp$ strain was grown for ~ 48 hours on SFM+ hygromycin medium, then were stained using WGA-Alexa 488 for cell wall and PI for DNA visualisation and viewed using a x100 lens. (A) phase contrast image; (B) Cell wall, green; (C) DNA , red; (D) Overlaying of the red and green channels. Size bar represents 1 μm .

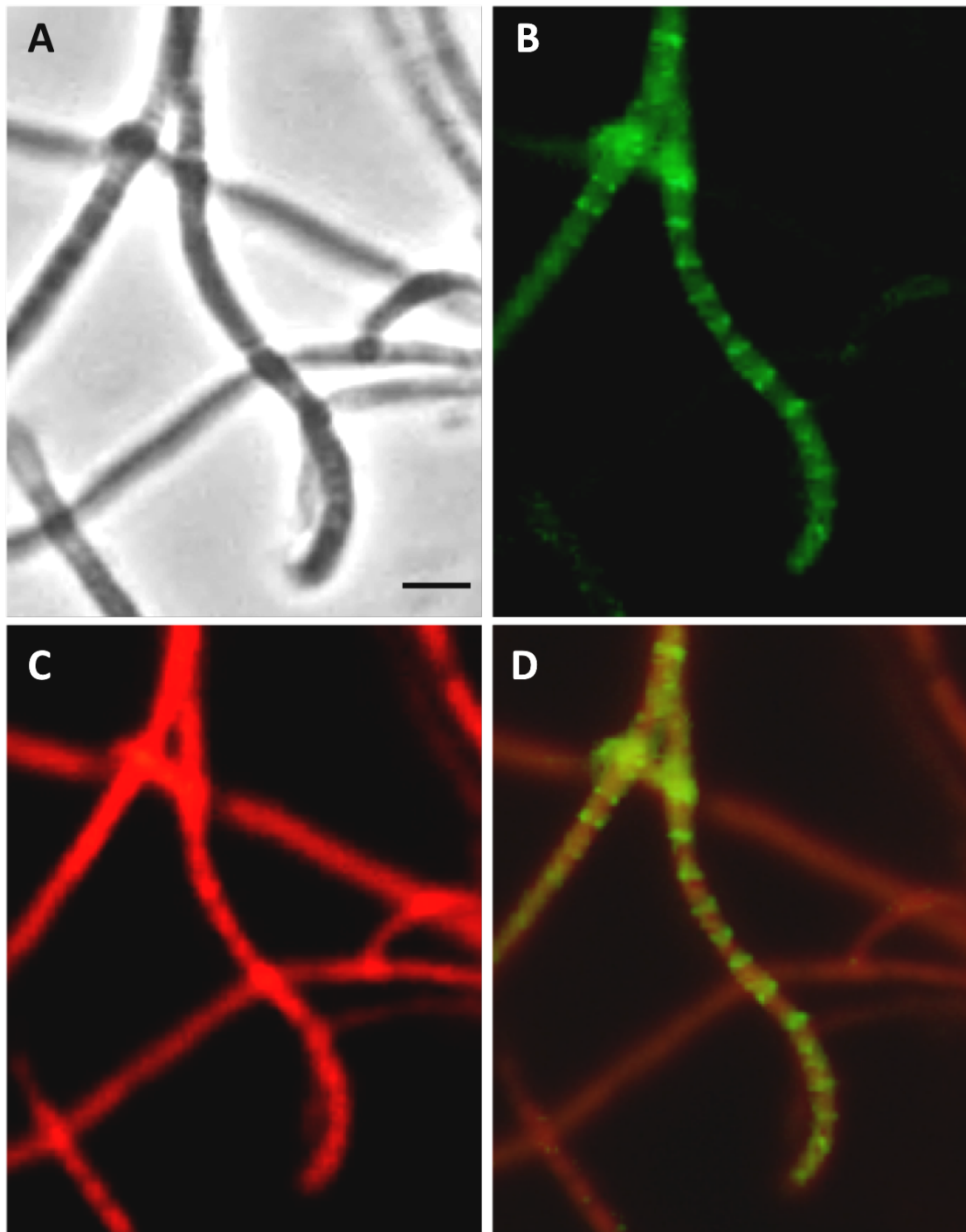


Figure 4.25. Monitoring of SepF-EGFP localisation in a young aerial hyphae of M145/pMS82/P-*sepF-egfp* using fluorescence microscopy. The strain was grown for ~46 hours on SFM medium containing hygromycin, then was stained using PI for DNA and viewed using fluorescence microscopy. (A) Phase contrast image, (B) SepF-Egfp (Green), (C) DNA (Red), (D) Overlaying of the red and green channels. Size bar represents 1 μ m.

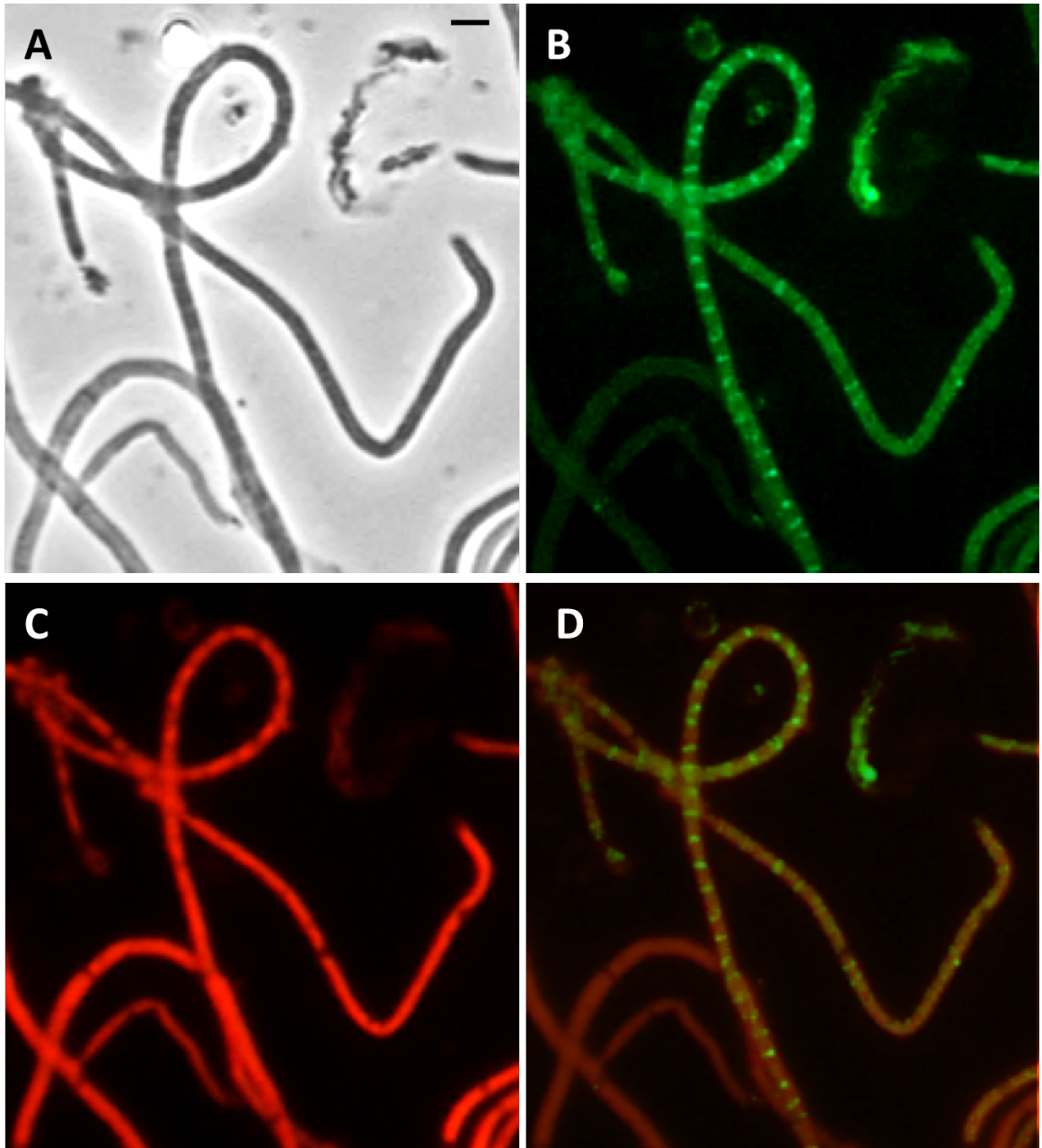


Figure 4.26. Monitoring of SepF-EGFP localisation in a young aerial hyphae of M145/pMS82/P-*sepF-egfp* using fluorescence microscopy. The strain was grown for ~46 hours on SFM medium containing hygromycin, then was stained using PI for DNA and viewed using fluorescence microscopy. (A) Phase contrast image, (B) SepF-Egfp (Green), (C) DNA (Red), (D) Overlaying of the red and green channels. Size bar represents 1 µm.

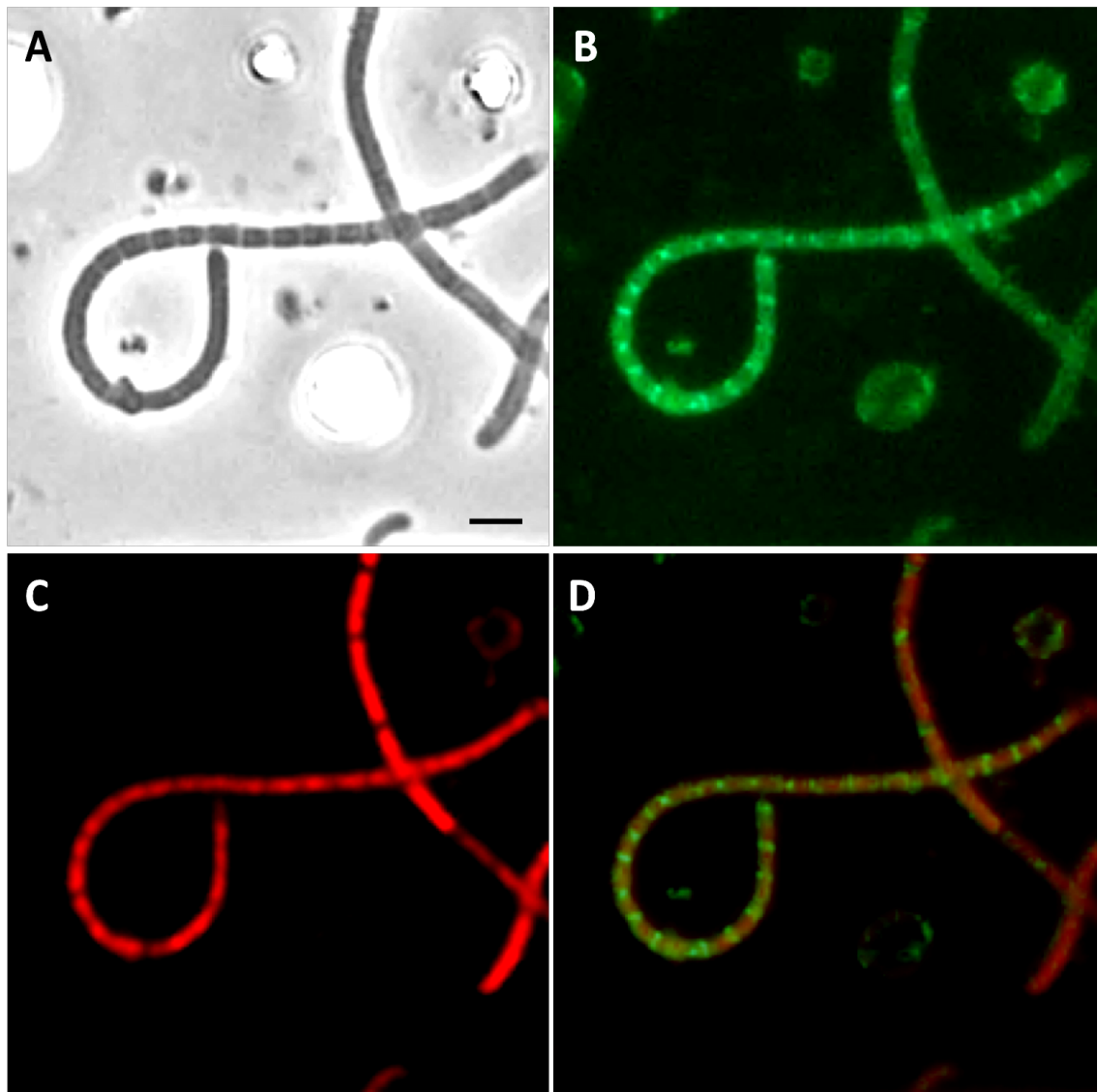


Figure 4.27. Monitoring of SepF-EGFP localisation in a late aerial hyphae of M145/pMS82/P-*sepF-egfp* using fluorescence microscopy. The strain was grown for ~46 hours on SFM medium containing hygromycin, then was stained using PI for DNA and viewed using fluorescence microscopy. (A) Phase contrast image, (B) SepF-Egfp (G), (C) DNA (Red), (D) Overlaying of the red and green channels. Size bar represents 1 μ m.

4.3 Summary

In this chapter we generated SepF-Egfp translational fusions using three different constructs and approaches and monitored fluorescence during *Streptomyces* development.

- The first approach generated *S. coelicolor* M145/ *sepF::sepF-egfp-ApraR*, where the *sepF* gene was replaced by the *sepF-egfp* fusion in the original chromosomal location. The strain M145/ *sepF::sepF-egfp-ApraR* had a wild-type phenotype, which confirmed that the SepF-Egfp fusion in this strain is fully functional.
- The second and third approach introduced the *sepF-egfp* fusion using a plasmid that integrates into a specific chromosomal site in a single copy. Constructs pMS82/2080-*sepF-egfp* and pMS82/P-*sepF-egfp* contained 848 bp and 343 bp DNA upstream of the translational start of *sepF*, respectively. Introduction of both of these constructs into the *sepF* knockout mutant restored the wild-type phenotype. This confirms that SepF-Egfp is functional and expresses at native levels even when using the shortest, 343 bp upstream sequences. This suggests that in the plasmid pMS82/P-*sepF-egfp* contained all that was needed for *sepF* transcription, which was suggested by the RNA Seq data by Young *et al.*, 2016.
- Monitoring SepF-Egfp throughout the developmental cycle of the three different constructs of *S. coelicolor* generated the same localisation patterns. SepF-Egfp localised to positions of possible future cross-wall formation or septation in the vegetative and aerial mycelium, respectively.
- SepF-Egfp formed a ring-like structures that was visualised using confocal microscopy and occasionally spiral-like patterns at the early stages. SepF-Egfp patterns looked like lines perpendicular to the hyphal wall using epi-fluorescence microscopy, or ladders in the aerial hyphae. When fully formed, these ladders had the ~1.2 μm spacing that is characteristic of the distance between sporulation septa.

- The SepF-Egfp ladders in the aerial hyphae formed well before any signs of septation and even chromosome segregation. However, SepF-Egfp signal were visible at places where there was less or no DNA staining, which might suggests that SepF localises to places devoid of DNA.

Acknowledgements

We are very grateful to Benjamin Bone for contribution to the experiments.

Chapter 5 Investigation of the role of *ftsZ* downstream genes, *SCO2080*

Introduction

During bacterial cell division, peptidoglycan synthesis needs to be coordinated with the increase of the cell size, timely genome replication and segregation and septum synthesis followed by cell fission. The prokaryotic cell division scaffold is formed by the tubulin homolog FtsZ (Bi and Lutkenhaus, 1991), which forms a contractile ring (or Z-ring) that mediates the recruitment of the cell division machinery to the mid-cell position (Goehring and Beck, 2005; Adams and Errington, 2009). In unicellular bacteria, cell division results in two identical daughter cells that each contain a single copy of the chromosome.

Cell division in *S. coelicolor* is different from that in the other rod-shape unicellular bacteria such as *E. coli*, *B. subtilis*. It lacks the homologues of MinC and MinE (Marston *et al.*, 1998; Autret and Errington, 2001), the Noc system and Z-ring anchoring proteins such as FtsA and ZipA (Errington *et al.*, 2003; Lowe *et al.*, 2004), it is yet unclear how exactly FtsZ polymers are positioned at regular intervals to produce the distinctive FtsZ-ring ladders during cell division. In the previous chapters we characterized *sepF* located within the *ftsZ-divIVA* gene cluster (Figure 3.6). But several other genes in this cluster of genes, namely *SCO2080*, *SCO2081* and *SCO2078* have not been fully characterized. We assumed that they might play some role in FtsZ-rings positioning during cell division. By analysing this gene cluster (Figure 3.6), *SCO2077* encodes DivIVA, a cytoskeletal protein essential for polar growth and branching (Flardh, 2003), *SCO2078* encodes a small hypothetical membrane protein, *SCO2079* encodes SepF, *SCO2080* encodes a protein that shares a high level of homology with alanine racemase, *SCO2081* encodes a laccase and *SCO2082* encodes FtsZ. The gene cluster containing these genes locates in core region of *S. coelicolor* linear chromosome and were defined as cell division gene cluster (Bentley *et al.*, 2002).

As we have seen in Chapter 3, the gene organisation of this gene cluster is conserved amongst *Streptomyces*, *Mycobacterium* and *Corynebacterium* (Figure 3.10). In *B. subtilis*, the gene organisation is very similar but here there are 7 genes between *ftsZ* and homologues of *SCO2081*, *SCO2080* and *sepF*. Interestingly, *E. coli* does not have a *SepF* homologue, but it does have homologues of *SCO2081* and *SCO2080*, although the genes are not located in the vicinity of the *ftsZ* gene (Figure 5.1). The gene *SCO2080* in *S. coelicolor* and its homologous genes in *M. tuberculosis*, *B. subtilis* and *E. coli* have not been yet fully characterised.

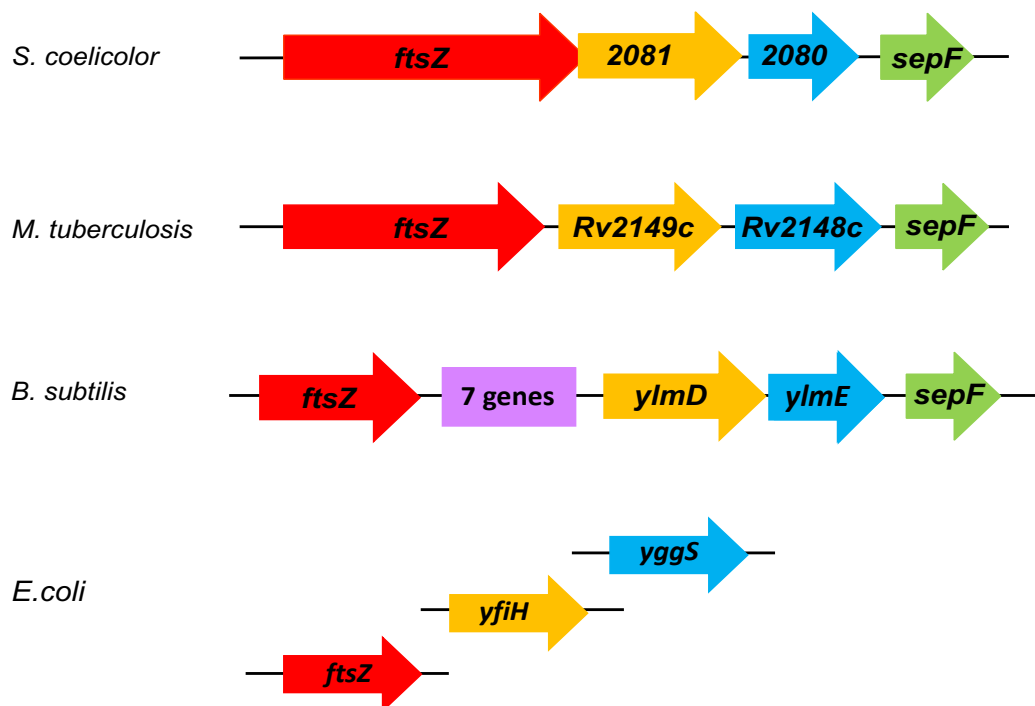


Figure 5.1. Gene organization of *S. coelicolor*, *M. tuberculosis*, *B. subtilis* and *E. coli*. Identical colour represents homologous protein products as identified using BLAST searches and the KEGG database.

SCO2080 lies between *ftsZ* (*SCO2082*) and *sepF* in the *S. coelicolor* genome. *SCO2080* orthologues are wide spread in Gram-positive bacteria, and particularly in firmicutes (*Bacillus*, *Staphylococcus*) and in actinobacteria, but are also occasionally found in Gram-negative bacteria. D-amino acids are generated by racemases and they are important for cell wall synthesis. Recently, it was shown that D-amino acids can also inhibit biofilm formation in *B. subtilis*, where overexpression of *ylmE*, which

encodes a racemase homologous to *SCO2080*, resulted in lack of biofilm formation (Kolodkin-Gal *et al.*, 2010). Mutants of *E. coli* lacking the gene *yggS*, encoding the orthologue of *SCO2080*, had a radical change in their amino acid pool, with enhanced concentrations of the branched chain amino acids valine and leucine, as well as of α -ketoglutarate (Ito *et al.*, 2013). This led to reduced levels of coenzyme A (CoA), which was supported by the full restoration of *yggS* mutants by the CoA precursor pantothenate (Vitamin B5). Interestingly, introduction of *ylmE*, encoding the orthologue of *SCO2080* from *B. subtilis*, also complemented the *yggS* null mutant. These data suggest a role for *SCO2080* in amino acid metabolism. As before, to simplify the designations, we often use gene numbers without the SCO prefix.

In this chapter our aim is to begin the characterization *SCO2080* in *S. coelicolor*.

- Bioinformatic analysis of 2080.
- Generation of a 2080 knockout mutant using the PCR based REDIRECT technology first in *E. coli*. The mutant cosmid was then introduced into *S. coelicolor*, where homologous recombination generated the 2080 knockout mutant.
- Confirmation of the 2080 knockout mutant in *S. coelicolor*.
- Characterisation of the phenotype of the 2080 knockout mutant strain.
- Complementation of the 2080 knockout mutant in *S. coelicolor* using different complementing clones.

5.1 Bioinformatics analysis of 2080, a putative racemase

To investigate the role of protein 2080 encoded by gene 2080 in cell division, the amino acid sequence of protein 2080 was obtained from the StrepDB Streptomyces annotation server (<http://strepdb.streptomyces.org.uk>) and analysed using the software tool SMART (<http://smart.embl-heidelberg.de/>). BLAST searches revealed that the protein encoded by gene 2080 (UniProt Q9S2X1) shared high level of similarity alanine racemases (Alr; E.C. 5.1.1.1) which belong to the Fold Type III of pyridoxal phosphate (PLP) dependent enzymes (Tassoni *et al.*, 2017) and play an

indispensable role in the assembling of the peptidoglycan layer of bacteria cell walls (Im *et al.*, 2011).

The peptidoglycan biosynthetic pathway is a critical process for the generation of the bacterial cell wall. The synthesis of the bacterial cell wall is initiated with uridine diphosphate (UDP)-N-acetylmuramic acid, L-alanine (L-Ala), D-glutamic acid (D-Glu) and meso-diaminopimelic acid to generate UDP-N-acetylmuramyl-L-Ala-D-Glu-meso-diaminopimelate (Shaw *et al.*, 1997; Lovering *et al.*, 2012). D-alanine (D-Ala) is an essential amino acid that can be added onto the growing amino acid chain as a D-Ala dipeptide to generate UDP-N-acetylmuramyl-tripeptide-D-Ala-D-Ala, which is subsequently incorporated into the growing PG peptide chain (Wei *et al.*, 2016). The D-Ala dipeptide is synthesized by two enzymes: Alanine racemase (Alr) and D-Ala ligase. Alr is a unique enzyme responsible for the racemization to convert L-Ala to D-Ala (Wasserman *et al.*, 1984) and D-Ala-D-Ala ligase is involved in generation of the D-Ala dipeptide (Shaw *et al.*, 1997; Cava *et al.*, 2011). The final D-Ala is exchanged for a D-lactic acid (D-Lac) in the case of vancomycin resistance (Vollmer *et al.*, 2008). Specific enzymes catalyze the transamination and racemization of L-amino acids to the D-enantiomer (Radkov and Moe, 2014). One of these enzymes is alanine racemase (Alr), which is essential for growth in most bacteria (Hols *et al.*, 1997; Milligan *et al.*, 2007).

Previous studies have revealed that Alr is essential for the survival of numerous Gram-positive bacteria, such as *B. subtilis* and *M. tuberculosis*. Knockout of the *alr* gene in these bacteria resulted in a strict exogenous D-Ala-dependent growth phenotype (Ferrari *et al.*, 1985; Awasthy *et al.*, 2012; Tassoni *et al.*, 2017). Similar growth arrest and extensive cell lysis were also observed in the *alr* null mutant of Gram-negative bacteria, such as *E. coli* due to deficiency of D-Ala (Wijsman *et al.*, 1972).

First, I compared the protein 2080 with the corresponding proteins from *M. tuberculosis*, *B. subtilis*, and *E. coli*, respectively (Figures 5.2-5.4) using Clustal Omega software. The level of similarity between 2080 of *S. coelicolor* and Rv2184c of *M. tuberculosis* is 42.74% identity, between 2080 of *S. coelicolor* and YImE (Uniprot No: O31727) from *B. subtilis* is 30.22% identity, between 2080 of *S. coelicolor* and YggS (Uniprot No: C3SV52) from *E. coli* is 33.04% identity. I showed the pairwise sequence alignments because when we aligned all four proteins, the level of similarity was low and the pairwise alignments indicate the level of similarities more accurately.

```

SCO2080          -----MTDRKHELAANLAKVEQRITDCAAAGRPRQDVTLIVVTKTYPADDVRILSEL
M. tuRv2148c    MAADLSAYPDRESELTHALAAAMRSRLAAAAEAAGRNVGEIELLPITKFFPATDVAILFRL
                  **: **:  ** :..*:: *. *****  :: *: :** :** ** * . *

SCO2080          GVRHVAENRDQDAAPKAAACS-----DLPLSWHFVQQLQTNKVRVSVGYADVVS
M. tuRv2148c    GCRSVGESREQEASAKMAELNRLAAAELGHSGGVHWHMVGRIQRNKAGSLARWAHTAHS
                  * * *.*.*:*:*: * * . . : **:**:*: * *. *.: :*...:*

SCO2080          VDRARLVTALSKEAVRA-----GREVGCLLQVALDAEEGGRGERGGVPPAGIEELADLV
M. tuRv2148c    VDSSRLVTALDRAVVAALAEHRRGERLRVYVQVSLDG-DGSRGGVDSTTPGAVDRICAQV
                  ** :*****.: . * * *..: :**:* . :*.** ... *...:. *

SCO2080          AGSEGLRLDGLMTVAPLSGEYAGRQQAAFEHLMDLSTRVRRTHPAANMVSAGMSADLEQA
M. tuRv2148c    QESEGLELVGLMGIPPLDWD----PDEAFDRLQSEHNRVRAMFPHAIGLSAGMSNDLEVA
                  ****.* ** : ** . : : **:* . .*** . * * :***** ** *

SCO2080          VAAGATHVRVGTAVLGVRPRLG*
M. tuRv2148c    VKHGSTCVRVGTALLGPRRLRSP
                  * *: * *****:* * .

```

Figure 5.2. Protein sequence alignment of 2080 protein of *S. coelicolor* and Rv2184c (Uniprot No: O53518) from *M. tuberculosis*. (*) indicates positions which have a conserved residue, (:) represents conservation between groups of amino acids with strongly similar properties, and (.) indicates conservation between groups with weakly similar properties. The sequence alignment was generated using Clustal Omega (<https://www.ebi.ac.uk/Tools/msa/clustalo/>).

```

SCO2080          MTRKHELAANLAKVEQRITDACAAAGRPRQDVTLIVVTKTYPADDVRILSELGVRHVAE
B.suYlmE        -----MRVVDNLRHINERINEACNRSGRSSDEVTVIAVTKYVSPERAQEAVDAGITCLGE
                .:. ** ::::**.:** :** ::**.*.*** :. : :* :.*

SCO2080          NRDQDAAPKAAACSDLPLSWHFGQLQTNKVRSVVGYADVQSVDRARLVTALSKEAVRA
B.suYlmE        NRDAELLRKQELM-KGNPEWHFIGLSQSRKAKSVVNSVSYIHSLDRLSLAKEIEK---RA
                *** : * . .***:*.*.*.*.*. . ::**.* *.. :.* **

SCO2080          GREVGCLLQVALDAEEGGRGERGGVPPAGIEELADLVAGSEGLRLDGLMTVAPLSGEYAG
B.suYlmE        EGTVRCFVQVNTSLEPSKHGMK----KEEVIPFIQELSGFEHILVAGLMTMAPLTDDQDQ
                * *:**.* . * . : * : : : : * * : : **:*:**.*.:

SCO2080          RQQAAFEHLMDLST---RVRRTHPAANMVSAGMSADLEQAVAAGATHVRVGTAVLGVRPR
B.suYlmE        -IRSCFRSLRELRDQVQKLNQPNAPCTELSMGMSNDFEIAIEEGATYIRIGSSLVGNETG
                :.*. * :* :.: : : . : * ** *:* * : **:*:*:*:*:* .

SCO2080          LG*-
B.suYlmE        GVQQ

SCO2080          MTRKHELAANLAKVEQRITDACAAAGRPRQDVTLIVVTKTYPADDVRILSELGVRHVAE
EcoliYggS       ----MNDIAHNLAQVRDKISAAATRCGRSPPEITLLAVSKTKPASAIAEAIDAGQRQFGE
                :::* **:*.*.:*: *.: .** ::**.*:* ** . : : * *:..*

SCO2080          NRDQDAAPKAAA---CSDLPLSWHFGQLQTNKVRSVVGYADVQSVDRARLVTALSKEA
EcoliYggS       NYVQEGVDKIRHFQELGVTGLEWHFIGPLQSNKSRLVAEHFDWCHTIDRLRIATRLNDQR
                * *:. * . *.*.* * **:* * . : * ::**.* :.* *..:

SCO2080          VRAGREVGCLLQVALDAEEGGRGERGGVPPAGIEELADLVAGSEGLRLDGLMTVAPLSGE
EcoliYggS       PAELPPLNVLIQINISD----ENSKSGIQLAELDELAAVAELPRLRLRGLMAIPAPESE
                . : *:* :. . . . : * : : ** * ** * ** * : . *

SCO2080          YAGRQQAAFEHLMDLSTRVRRTHPAANMVSAGMSADLEQAVAAGATHVRVGTAVLGVRPR
EcoliYggS       YVRQFEVARQMAV-AFAGLKTRYPHIDTSLGMSDDMEAAIAAGSTMVRIGTAIFGARDY
                *. : :.* : : : : * : : * ** *:* * : **:*:* * **:*:**.*

SCO2080          LG*
EcoliYggS       SKK

```

Figure 5.3. Protein sequence alignment of 2080 protein of *S. coelicolor* and YlmE (Uniprot No: O31727) from *B. subtilis* (top) and YggS (Uniprot No: C3SV52) from *E. coli*. (*) indicates positions which have a conserved residue, (:) represents conservation between groups of amino acids with strongly similar properties, and (.) indicates conservation between groups with weakly similar properties. The sequence alignment was generated using Clustal Omega (<https://www.ebi.ac.uk/Tools/msa/clustalo/>).

By using SMART searches, we identified 5 possible Alr proteins in *S. coelicolor* (encoded by gene 1609, 2080, 3903, 4757 and 6438), 4 Alr proteins in *M. tuberculosis*, 3 Alrs in *B. subtilis* and 4 Alrs in *E. coli*. Tassoni (2017) generated the *alr* (SCO4757) null mutant by deletion of gene SCO4757 in *S. coelicolor*. The *alr* mutant strain was dependent on D-Ala for its growth, which suggests that SCO4757 is the main alanine racemase that is essential for cell wall synthesis. The 2080 protein shares only 25.23% identity with SCO4757, Alr (Figure 5.4). We considered that the protein encoded by 2080 could also be involved in cell wall synthesis in *S. coelicolor* at a specific stage during development. We hypothesized that there might be a separate enzyme generating D-amino acids at septum formation that would be independent on the

```

SCO2080      MTD---RK-----H--E---LAANLAKVEQRITDACAAGRPRQDVTLIVVTKTYP
SCO4745      MSETTARRDADAVLRARAEIDLALANRANVRALRERA-----PGAALMAVVKADAYG
              *::  *:           :  * ** :  :::*           *  :  :*  :::*

SCO2080      ADDVRI---LSELGVRHVAENRDQDAAPKAAACSDL-----PLSWHFV--GQLQTNKVRS
SCO4745      HGAIPCARAAVAAGATWLGTATPQEALALRAAEPGLPDDVRIMCWLWTPGGPWREA-VEA
              .  :           *.  :.  *:*  **  .*           :.*  :.  *  :  *.:

SCO2080      VVGADVVQSVDRARLVTALSKEAVRAGREVGCLLQVALDAEEGGRGERGGVPPAGIEEL
SCO4745      ---RLDV--SVSAMW----AMEEVTGAARAAGVPARVQLKAD-TGLGRGGCQPQADWERL
              **  ** .           :*.  *.  .*  :*  *.*:  *  *  *  *  *  *.*

SCO2080      ADLVAGSEGLRLDGLMTVAPLSGEYAGRQQAAFEHLMDLSTRVRRTHPAANMVSAGMSAD
SCO4745      VG---AALRAEEEGLLRVTGLWSHFACADEPGHPSIAAQLTRFREMAY--AEQRGLRPE
              ..  .:  .  :** : *  *  :.*  :.  .  :  **.*  .  * :  :

SCO2080      LEQ-----AVAAGATHVRVGTAVLGVRPRL--G*-----
SCO4745      VRHIANS PATLTL PD AHFDLVRPGIAMYGVS PSPEIGTPAD FGLRPVMTLAASLALVKQV
              :.:           *  ** * * : ** *  *

SCO2080      -----
SCO4745      PGGHGVS YGHHTTPGETTLGLVPLGYADGI PRHASSSGPVLVDGKWRTVAGRIAMDQFV

SCO2080      -----
SCO4745      VDLGGDRPEPGAEAVLFGPGDRGEPTAEDWAQAAGTIAYEIVTRIGSRVPRVYVNE*

```

Figure 5.4. Sequence alignment of proteins encoded by the SCO2080 and SCO4745 (*alr*) from *S. coelicolor*. (*) indicates positions which have a conserved residue, (:) represents conservation between groups of amino acids with strongly similar properties, and (.) indicates conservation between groups with weakly similar properties. The sequence alignment was generated using Clustal Omega (<https://www.ebi.ac.uk/Tools/msa/clustalo/>).

main Alr, which would be essential for growth and perhaps localized at the hyphal tips. We already referred to *ylmE* of *B. subtilis* that was shown to be involved in the generation of the D-amino acid pool in *B. subtilis*, which in turn, affected biofilm formation (Kolodkin-Gal *et al.*, 2010).

5.2 Generation of the 2080 knockout mutant

After the bioinformatic analysis, we studied the role of gene 2080 in cell division of *S. coelicolor* by creating a knockout mutant using the REDIRECT© PCR-

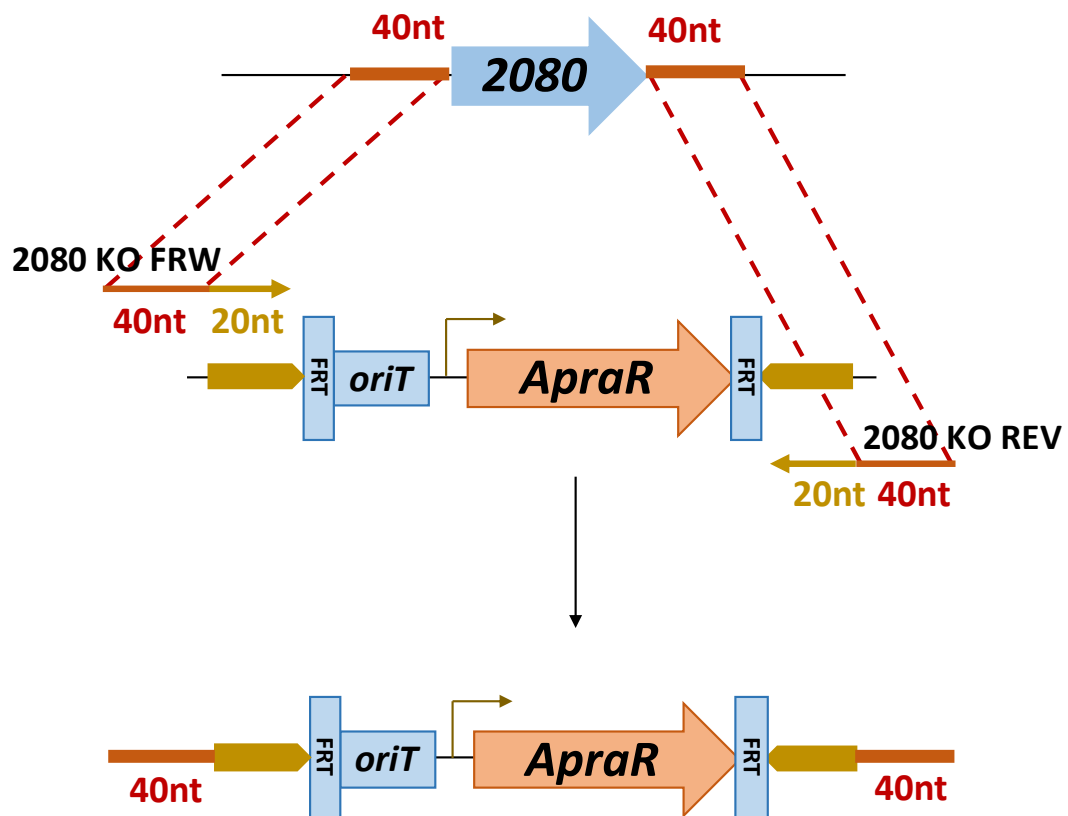


Figure 5.5. PCR amplification of the apramycin resistance cassette from PIJ773 for gene 2080 knockout using primers 2080 KO FRW and 2080 KO REV. The apramycin resistance cassette contained an *oriT* site, an apramycin resistance gene, and FLP recognition targets (FRT) required to excise the resistance marker. Primers were used containing DNA complementary to the DNA sequences (20 nt) of the template and DNA complementary to sequences flanking the region of DNA we wanted to replace (40 nt). PCR was used to create the disruption cassettes with appropriate combinations of primers (Gust, *et al.*, 2002).

targeting system (Gust *et al.*, 2003). As in Chapter 3, to generate a *2080* gene knockout mutant (Figure 5.5), an apramycin resistance cassette containing 40 bp flanking regions that are homologous to the flanking regions of target gene can be used to disrupt the target gene. As before, cosmid 4A10 containing *S. coelicolor* chromosomal DNA inserted into supercos-1 was used to be targeted with the apramycin resistance disruption cassette (Figure 5.6).

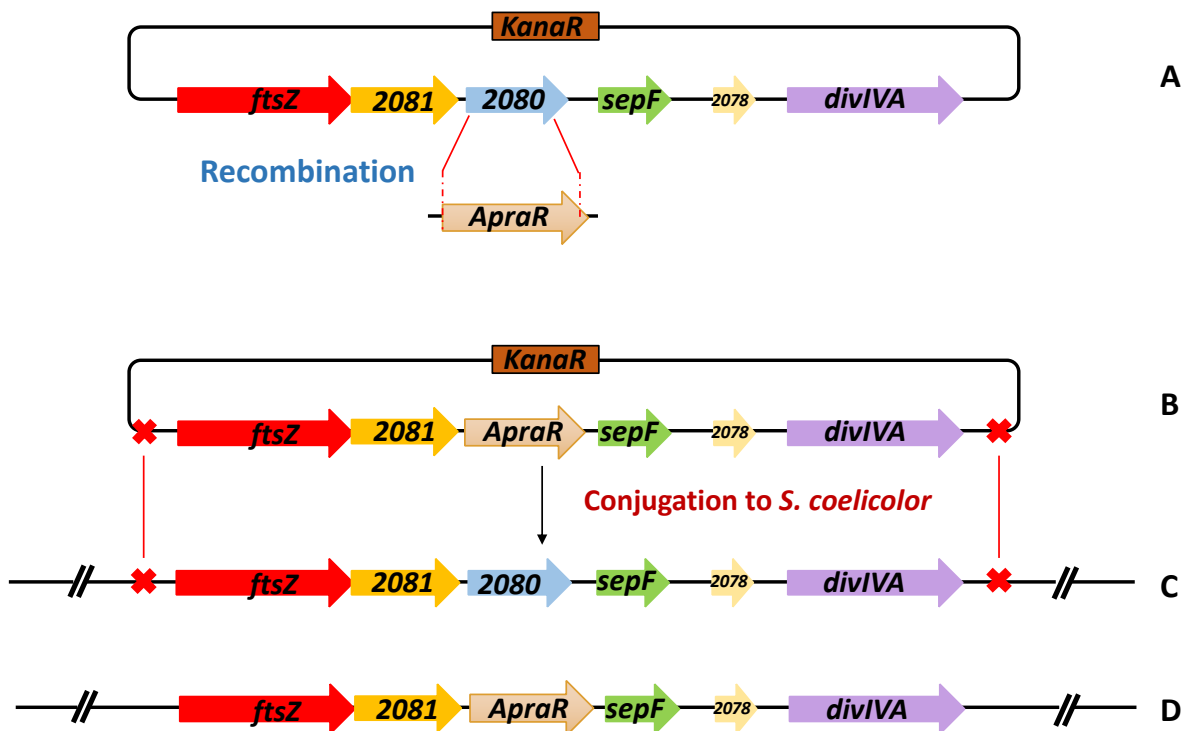


Figure 5.6. Knockout design for the generation of the *2080* null mutant in *S. coelicolor*. In a cosmid containing *2080* and its flanking genes, the *2080* gene was replaced with an apramycin resistance cassette (*ApraR*) (A). Then the resulting cosmid (B) was conjugated into *S. coelicolor* (C). The apramycin resistance cassette replaced the *2080* gene in *S. coelicolor* chromosome (D) after a double crossover event (B-D).

The apramycin resistant cassette (~1.3 kb) from plasmid pIJ773 was PCR amplified to generate the cassette for the knockout of *2080* using primers 2080 KO FRW and 2080 KO REV (Figure 5.5). The PCR resulting product of apramycin cassettes produced for the knockout of *2080* was desalted using a self-made mini gel filtration column and analysed on a 0.7% agarose gel (Figure 5.7) which confirmed that PCR reactions resulted in correct amplification of the expected ~ 1.3 kb apramycin

cassette.

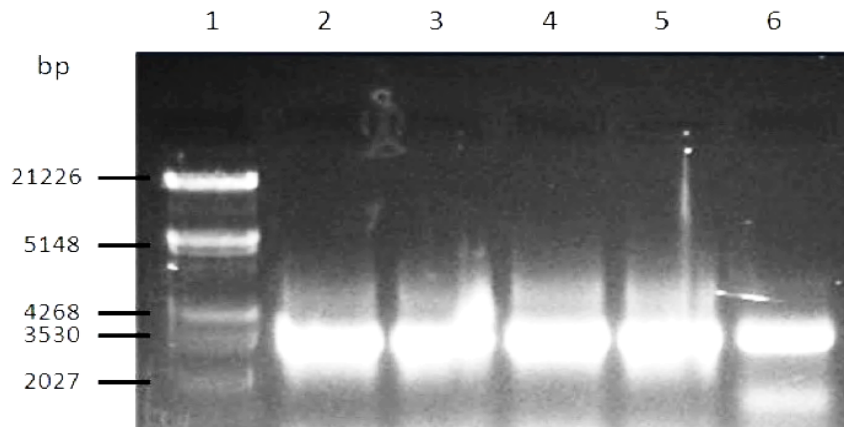


Figure 5.7. Amplification of the apramycin disruption cassette using primers 2080 KO FRW and 2080 KO REV. Gel analysis of the PCR amplification of the apramycin disruption cassette for the targeted knockout of 2080 (lane 6). Lane 1: lambda DNA cut with *EcoRI* and *HindIII* as a molecular weight marker (sizes are shown in bp). Lanes 2, 3, 4 and 5 are not relevant here.

Then this apramycin resistance disruption cassette was electroporated into the *E. coli* strain BW25113 carrying the *S. coelicolor* cosmid 4A10. The addition of L-arabinose to the media growing the BW25113 cells induces the expression of the recombinase enzyme which initiates a homologous recombination event between the flanking regions of the apramycin resistance cassette and the reciprocal sequence flanking the gene 2080. The plasmid pIJ790 contains a temperature sensitive origin of replication which results in its loss when the BW strain is grown at temperatures higher than 30°C. Therefore, after the disruption cassette was transformed into the BW25113, cells containing the 4A10 cosmid obtained from the transformation were plated onto LB containing apramycin, to select for cells that underwent successful recombination events, and grown at 37°C to induce the loss of pIJ790. We picked single BW transformants and then extracted their cosmid DNA.

To test whether the 2080 gene was successfully replaced with the apramycin cassette from cosmid 4A10, we conducted a restriction digest of the extracted cosmid DNA using *EcoRI* and *XbaI*. An “in-silico” restriction digest map was generated (Figure

5.8) using ARTEMIS (Rutherford *et al.*, 2000) highlighting the fragment sizes (Table 5.1). The restriction digest of the extracted cosmids were run on a 0.7% agarose gel (Figure 5.9). The 4A10 cosmid digest generated four fragments between 5-20 kb which corresponded to the sizes determined by the restriction map. According to the restriction maps the 20 kb fragment should be absent in the knockout gene cluster whilst the 6.7 kb, 8.0 kb and 14.0 kb fragments should remain uniform. The apramycin cassette introduced three new restriction sites causing the replacement of the 20 kb fragment to with four new fragments, three of which were visible on the gel. A 1.3 kb fragment, representing the apramycin cassette, the 7.0 kb and the 13.0 kb fragments are all seen in the knockout sample confirming the knockout cosmid.

Table 5.1. The expected fragments that are generated by restriction digest using endonucleases *EcoRI* and *XbaI* of the wild-type 4A10 cosmid and 4A10/2080::*ApraR* cosmid. Shaded fragments represent those that remain the same in both cosmid digests.

4A10	4A10/2080:: <i>ApraR</i>
20714	-
14318	14318
-	13072
8145	8145
-	7000
6792	6792
-	1288
-	34

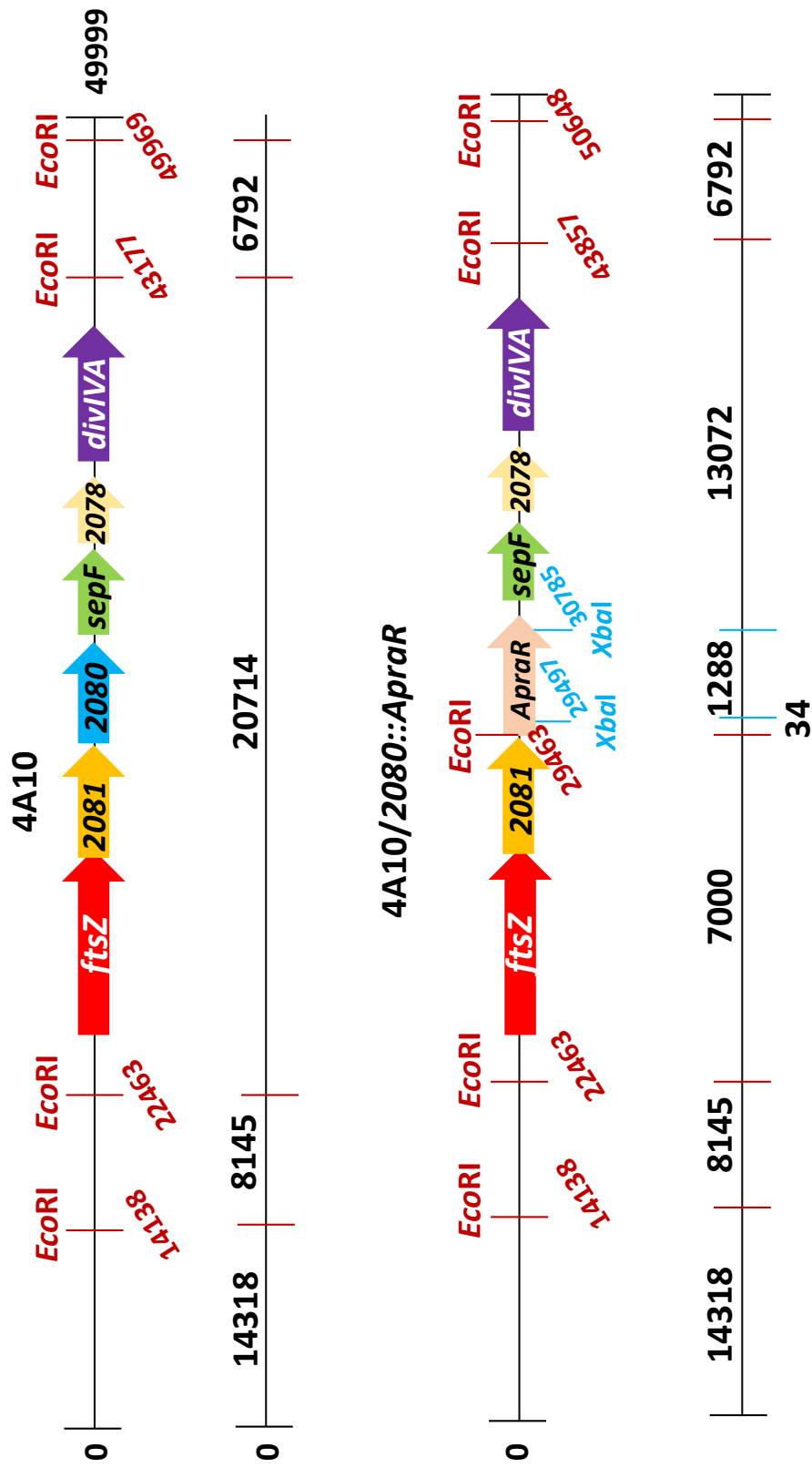


Figure 5.8. The gene map of the 4A10 cosmid and the 4A10/2080::ApraR cosmid highlighting the position of *EcoRI* and *XbaI* restriction enzyme cleavage sites and the subsequent fragment sizes generated by a restriction digest (bold red). The tilted numbers represent the location of the restriction sites using the cosmid numbering. The horizontal numbers represent the size of each restriction fragments (bp).

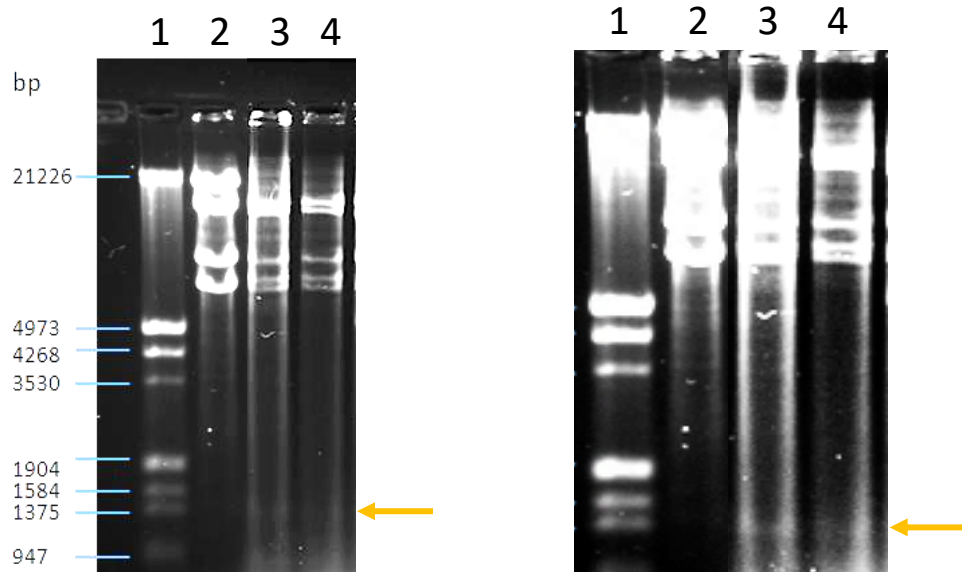


Figure 5.9. Confirmation of the mutant *4A10/2080::ApraR* cosmid using restriction digest with *EcoRI* and *XbaI*. The restriction digest of the extracted cosmids were run on a 0.7% agarose. The wild-type *4A10* cosmid (lane 2) and two *4A10/2080::ApraR* cosmids (lane 3 and 4) were digested with *EcoRI* and *XbaI* and the digests were analysed on a 0.7% agarose gel. Lambda DNA cut with *EcoRI* and *HindIII* was used as a molecular weight marker (Lane 1), sizes shown in bp. The 1.3 kb fragment carrying the apramycin resistance cassette is shown by the orange arrow. The gel images represent the same gels. The bands with an arrow are too weak to be visible, so I over exposed the gel image on the right to detect these bands.

After confirmation, the cosmid *4A10/2080::ApraR* was transformed into the methylation-deficient *E. coli* strain ET12567/pUZ8002 which can overcome the methyl-specific restriction endonuclease system to allow conjugation of cosmid/plasmid containing *oriT* into *S. coelicolor* by the action of non-transmissible pUZ8002 (MacNeil *et al.*, 1992). Then we conjugated the ET cells carrying the modified cosmid without gene *2080* into *S. coelicolor* wildtype stain M145. After conjugation, we selected the colonies that had successfully carried the modified cosmid by overlaying the conjugation plates with both apramycin that the cosmid *4A10/2080::ApraR* was resistant to and nalidixic acid to kill *E. coli* cells. However, the selection using apramycin was not able to differentiate between the desired double crossover event and single crossover event. In order to distinguish two events, we used replica plating to detect double crossover mutants by selection for apramycin

resistant, kanamycin sensitive colonies, which can identify the double crossover event. Mutant colonies identified as double crossover were then streaked and stocks were generated by growing the strains on the surface of cellophane discs and collecting all hyphal fragments into a storage medium. These stocks were stored at -20°C for further analysis.

5.3 Confirmation of the *2080* mutant

To confirm whether the gene *2080* was successfully knocked out from chromosome of *S. coelicolor*, the chromosome extracts of the *2080* mutant and wild-type were tested by PCR using primers. We used two external flanking primers of *2080* gene, one (2080 BglProm FRW) located within its upstream gene *2081* and the other (2080 3' END) located in the downstream gene *sepF* (Figure 5.10 A). With these two primers, a PCR product will be generated from both M145 wild-type and the *2080* mutant chromosome extract. The size of apramycin disruption cassette (~1.3kb) is larger than size of *2080* (720 bp), therefore the PCR product generated from the *2080* mutant chromosome (1878 bp) will be larger than the PCR product generated from the wildtype chromosome (1240 bp) (Table 5.2). In addition, we performed another test to confirm *2080* gene knockout in the chromosome. The chromosomal DNA extracts of the *2080* mutant and wild-type M145 were PCR tested using two different pairs of primers. The primers Apra 5' FRW and Apra 3' REV, which are situated in apramycin resistant cassette, were used to cooperate with primer 2080 Bgl Prom FRW and primer 2080 3' END to test the presence of the apramycin resistance disruption cassette in the *2080* mutant. The primer 2080 Bgl Prom FRW is located outside the apramycin resistant cassette and primer Apra 3' REV is located inside the apramycin cassette (Figure 5.10 B). These two primers only can generate PCR products in the presence of apramycin resistant cassette at the correct location, therefore only the *2080* mutant containing apramycin resistance cassette can provide the PCR resulting products while M145 will not show PCR resulting products. In the same way, primer Apra 5' FRW is located inside the apramycin resistant

cassette and primer 2080 3' END is situated outside the apramycin cassette (Figure 5.10 B), which will generate PCR products only in the 2080 mutant chromosome

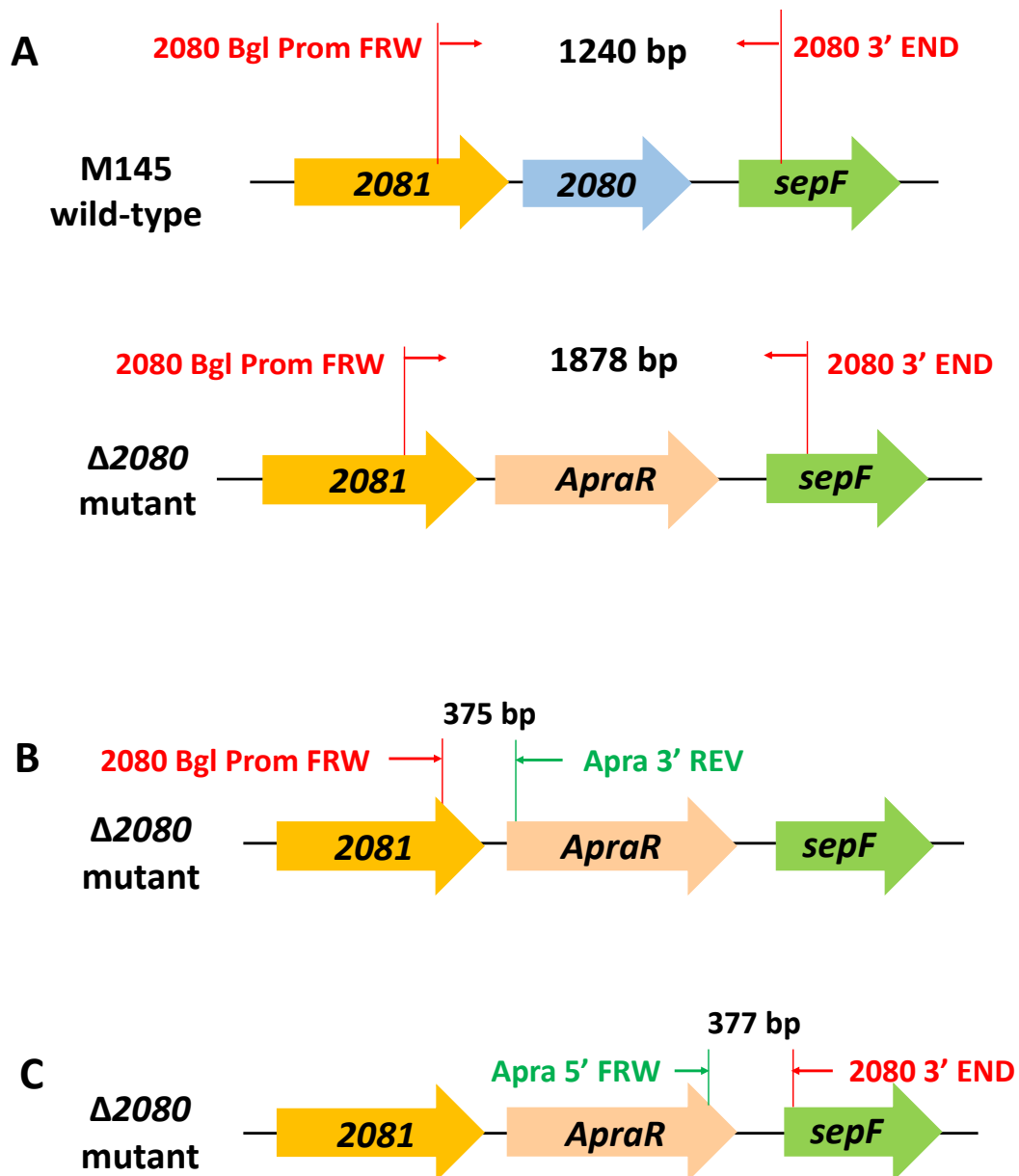


Figure 5.10. PCR design for the confirmation of the 2080 knockout mutant. (A) The primers 2080 Bgl Prom FRW and 2080 3' END generate PCR products of different sizes depending on the template DNA. (B) The primers 2080 Bgl Prom FRW and Apra 3' REV will generate a PCR product only in the 2080 mutant. (C) The primers Apra 5' FRW and 2080 3' END will generate a PCR product only in the 2080 mutant.

extract. The expected size of fragments generated by the different primer pairs are shown in table 5.2.

Table 5.2. The expected sizes of PCR fragments using selected oligo pairs in the wild-type strain and the *2080* mutant strain.

Oligos	Size in wild-type	Size in Δ sepF mutant
2080 Bgl Prom FRW 2080 3'END	1240 bp	1878 bp
2080 Bgl Prom FRW Apra 3'REV	-	375 bp
Apra 5' FRW 2080 3' END	-	377 bp

The PCR products were run on a 0.7% agarose gel and then analysed (Figure 5.11). Using the external primers, 2080 BglProm FRW and 2080 3' END both wild-type and the *2080* mutant DNA generated PCR products at their expected sizes of 1240 bp and 1878 bp, respectively (Figure 5.11 A). There was no fragment of 1240 bp when the mutant DNA was tested, which confirms that in the generated the *2080* mutant the *2080* gene was fully replaced by the apramycin resistance cassette. When one of the primers was priming in the apramycin resistance cassette, only the *2080* mutant DNA generated a PCR product of around 375 bp (Figure 5.11 B). All these confirmed that the *2080* knockout mutant was successfully generated.

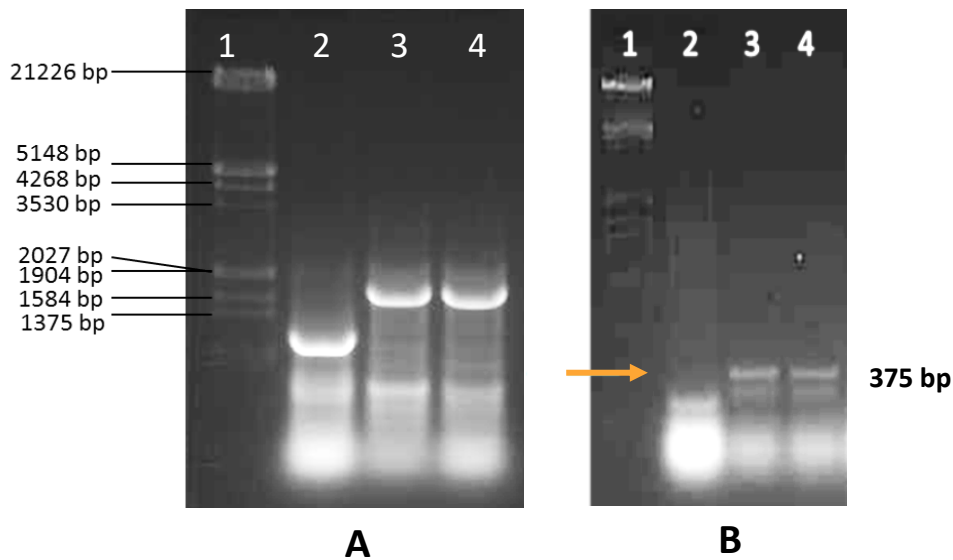


Figure 5.11. Confirmation of the *2080* knockout mutant. Chromosomal DNA generated from the selected strains was used as a template in PCR reactions.

- A.** Lane 1: Lambda DNA digested with *EcoRI* and *HindIII*, sizes shown in bp. Lane 2: wild-type M145 chromosome. Lane 3 and lane 4: *2080* mutant chromosome. M145 wild-type and *2080* mutant chromosome extracts were PCR tested using primers 2080 BglProm FRW and 2080 3' END.
- B.** Lane 1: the λ *EcoRI-HindIII* ladder. Lane 2: wild-type M145 chromosome. Lane 3 and lane 4: The *2080* mutant chromosome. Lane3: 2080 BglProm FRW and Apra 3' REV; Lane 4: Apra 5' FRW and 2080 3' END. M145 wild-type and the *2080* mutant chromosome extracts were PCR tested using two primer pairs. The ~ 375 bp fragment is marked by the orange arrow.

5.4 Analysis of the phenotype of the *2080* mutant.

5.4.1 Macroscopic observations of the *2080* mutant.

To determine the phenotype of the *2080* mutant strain, it was plated onto SFM medium along with the wild-type control M145 and the *sepF* mutant generated in Chapter 3. The plates were grown at 30°C and observed daily (Figure 5.12). After one day, the development of the wild-type strain was ahead of both the *2080* and *sepF* mutant strains (Figure 5.12 A). However, we inoculated the wild-type strain from

spore stocks whilst the *2080* and *sepF* mutants were inoculated from “hyphae” stocks as mutants cannot produce spores. We could not make sure that we have inoculated the same amount of “cells”. Therefore, any observation related to delayed growth might just be the result of the different inoculation. After two days, the colonies developed the fuzzy and white morphology which indicated the growth of aerial hyphae (Figure 5.12 B). After three to four days, the *2080* mutant strain and wild-type M145 strain showed clear differences in development. The wild-type M145 strain presented the classic grey pigment associated with spore maturation. In the same time, the *2080* mutant strain showed white morphology suggesting that the

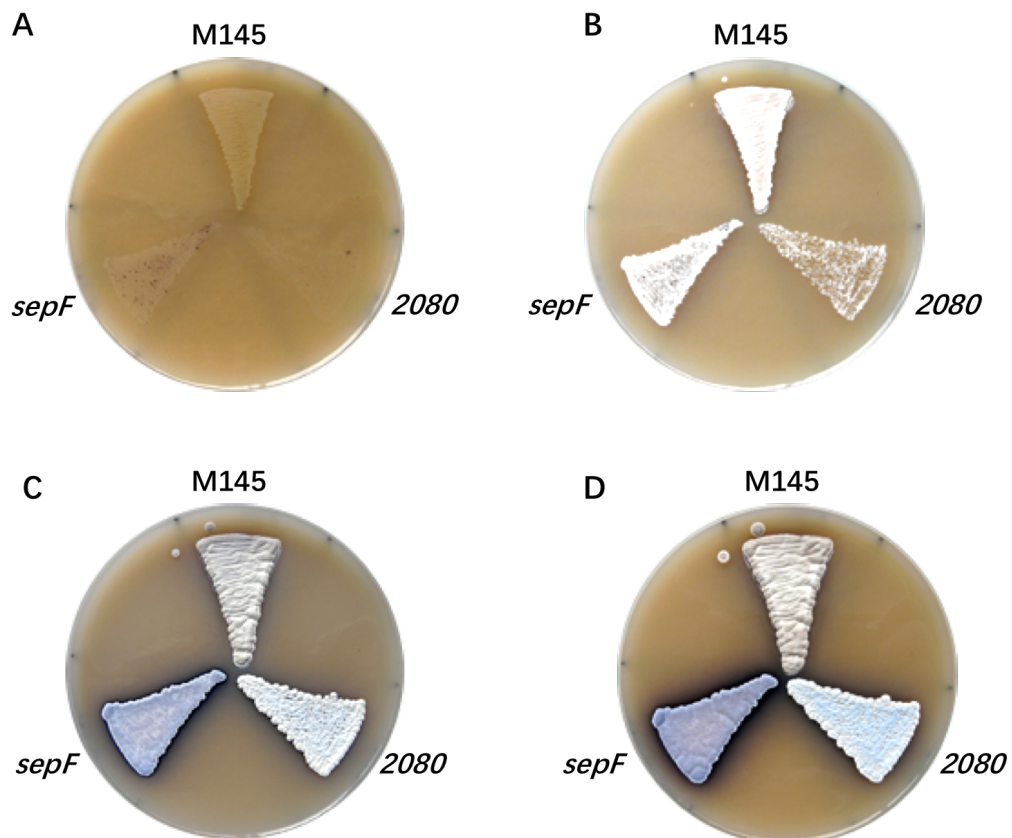


Figure 5.12. Macroscopic analysis of the *2080* mutant strain.

Wild-type M145, the *2080* and *sepF* mutant strains were plated in a triangle patch on a plate using SMF medium. The plate was incubated and monitored at regular time intervals (A) 1 day, (B) 2 days, (C) 3 days and (D) 4 days. The wild-type strain developed faster than *2080* mutant and produced grey pigment associated with spore maturation. While the *2080* mutant failed to become grey suggesting that it failed to sporulate. The *sepF* mutant was also included for comparison.

colonies have not yet produced spores (Figure 5.12 C and D). Interestingly, the *2080* mutant differed from the *sepF* mutant as the latter produced the blue pigment that showed in the aerial surface, whilst the *2080* mutant stayed white.

5.4.2 Microscopic analysis of the *2080* mutant.

After observation of the macroscopic phenotype of the wild-type M145 strain and the *2080* mutant, the microscopic phenotype of these strains was also investigated using epi-fluorescence microscopy where wild-type M145 strain acted as a control. These two strains were inoculated into patches onto SFM media with coverslips at an $\sim 70^\circ$ angle and were incubated at 30°C . In order to monitor different stages of the growth during cell division in *S. coelicolor*, we stained the cells using wheat germ agglutinin (WGA) Alexa Flour[®] 488 and propidium iodide (PI) for cell wall and chromosome visualisation, respectively.

The vegetative hyphae of the *2080* mutant was very similar to that of the wild-type strain (Figure 5.13). Vegetative crosswalls developed in both strains. However,

Vegetative hyphae

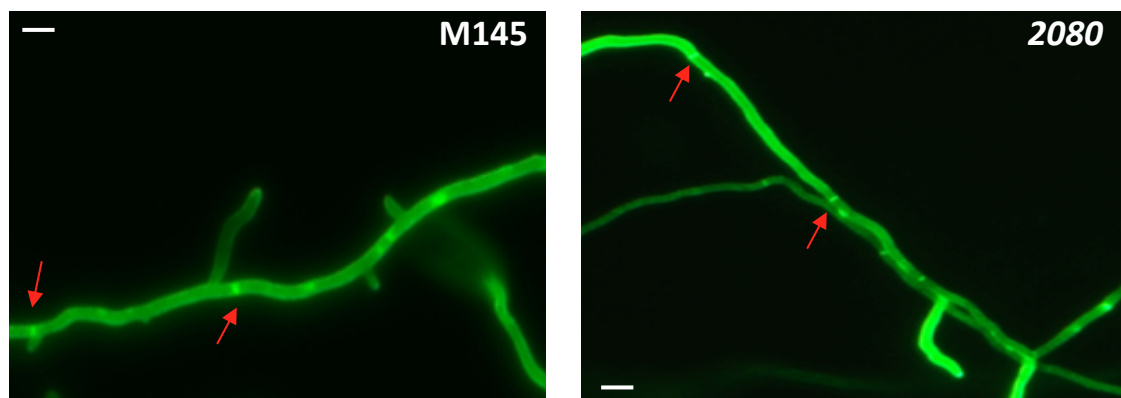


Figure 5.13. Epi-fluorescence microscopy of the vegetative hyphae of the wild-type M145 (left) and *2080* mutant strain (right). Spores of the wild-type strain M145 and *2080* mutant strain were plated on SFM medium and incubated at 30°C before staining with WGA-Alexa 488 (green-cell wall). Vegetative cross-walls are marked by the red arrows. Size bar represents $1\mu\text{m}$.

the aerial development of the *2080* mutant was very different from the wild-type as it failed to develop any spores (Figure 5.14). We firstly detected smooth and curly aerial hyphae of the *2080* mutant with even DNA staining and very little sign of chromosomes being organized into packages. Later samples showed more clear chromosome organisation and segregation but still no septation could be detected (Figure 5.14). Unlike in the wild-type strain where we detected evenly placed septa flanked with well segregated individual chromosomes, for reference see Figure 3.20 (Chapter 3.4.2), the *2080* mutant lacked any regular septation. However, the chromosomes of the *2080* mutant segregated and condensed into small packages very similarly to the DNA segregation and condensation during sporulation in the wild-type strain, suggesting that only septation but not chromosome segregation was affected in the *2080* mutant. This was very similar to what we observed when we characterized the *sepF* mutant phenotype in Chapter 3.

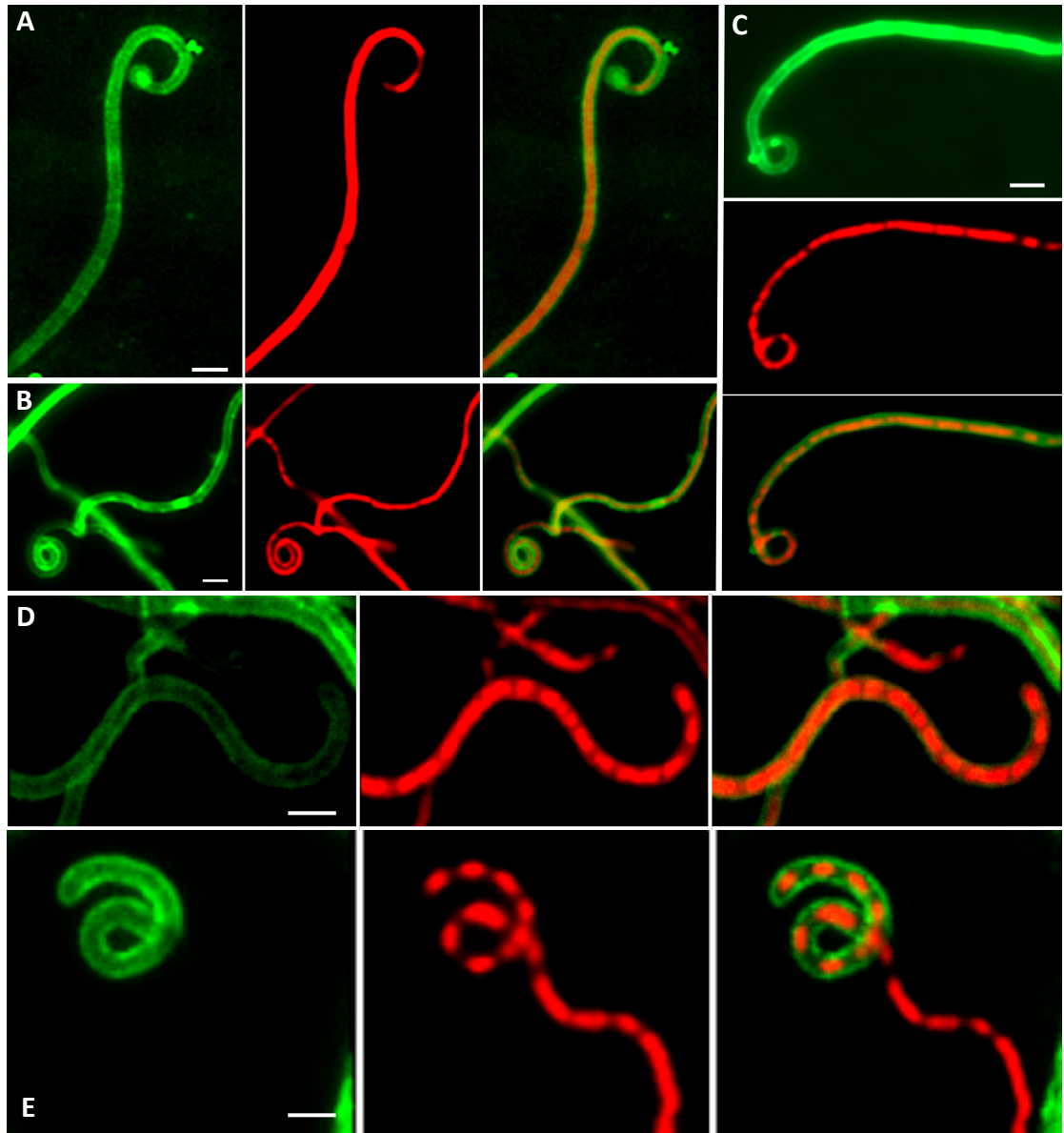


Figure 5.14. Fluorescence microscopy showing the developmental of the *2080* mutant strain. The *2080* mutant strain was plated onto SFM medium and incubated at 30°C before staining with PI (red-DNA) and WGA-Alexa 488 (green-cell wall). Size bar represents 1 μ m. (A-C) Growth of the aerial hyphae with coiling tips; (D-E) The chromosomes begun to condense and segregate but no septa were placed separating individual chromosomes. (A-C, E) epi-fluorescence microscopy; (D) confocal microscopy.

5.5 Complementation attempts of the *2080* mutant

To confirm that the observed non-sporulation phenotype of the *2080* mutant is the result of the absence of *2080*, we attempted to complement the mutant by introducing a single copy of a complementing construct containing gene *2080* (Figure 5.15). If the wild-type phenotype is restored but the constructs, then we could conclude that the mutant phenotype was a true reflection of the effects of *2080* deletion in *S. coelicolor*.

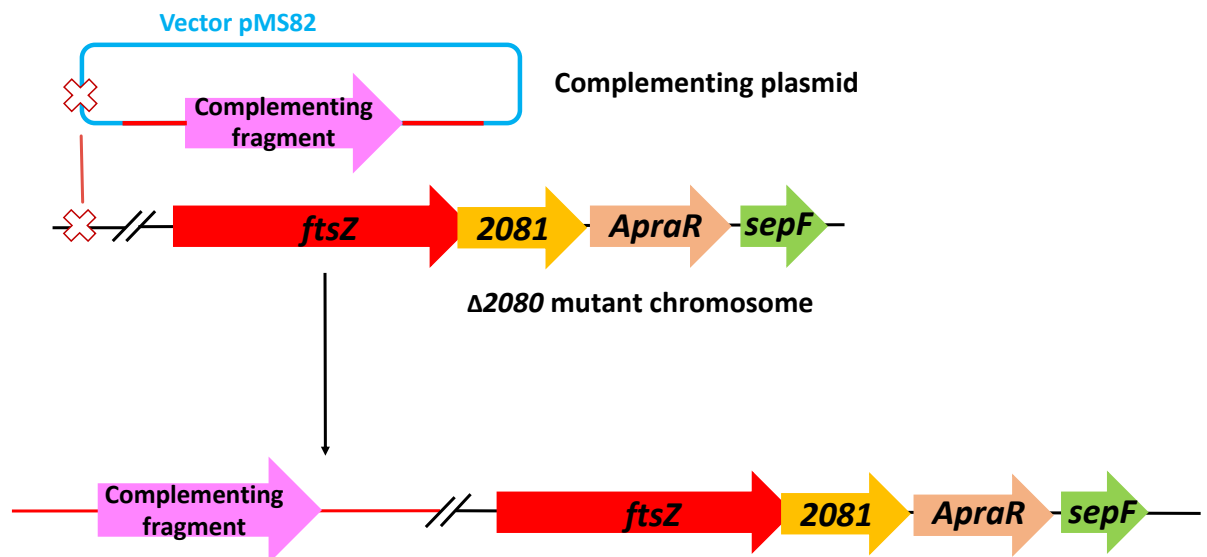


Figure 5.15. Strategy for the complementation of the *2080* mutant. Different complementing fragments were cloned and introduced into the *2080* mutant to test whether wild-type phenotype could be restored in the mutant strain.

5.5.1 Complementation experiments of the *2080* mutant using constructs containing the *2080* gene

There are only 6 bp that separate the genes *2080* and *2081* (Figure 5.16). In addition, at the time of performing the complementation experiments, we did not have any information about transcriptional start sites for *2080* transcription. We hypothesized that there might be a putative promoter (here designated as P_{2080})

somewhere at the end of the upstream gene *2081*. Moreover, gene *2080* lies downstream of *ftsZ* in the *S. coelicolor* genome. Because of the high gene density, we had to consider that there might be transcription reading through from the *ftsZ* gene. It has been shown that *ftsZ* is transcribed from three promoters located upstream of the *ftsZ* gene, one constitutive, one transcribed during vegetative growth and one transcribed during sporulation (here designated as P_{ftsZ} ; Flardh, *et al.*, 2000).

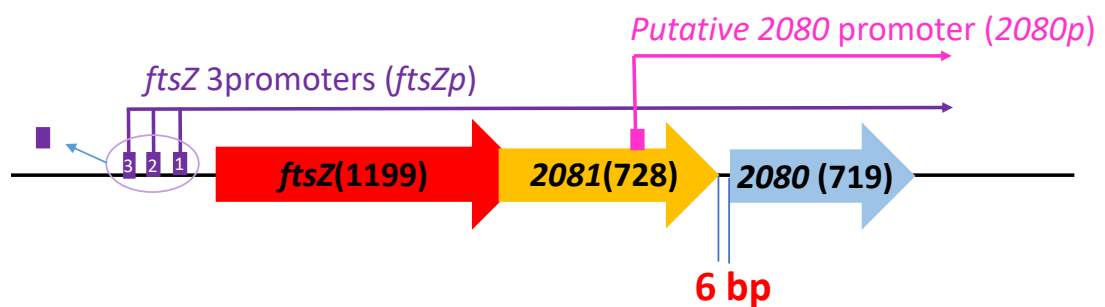


Figure 5.16. The gene operon in *S. coelicolor* containing *ftsZ*, *2081* and *2080*. Three known promoters upstream of *ftsZ* are shown (*ftsZp*) along with *2080* promoter *2080p*. The complementation constructs had to be designed under consideration of both the *ftsZ* and *2080* promoters (Flardh, *et al.*, 2000).

We designed three constructs, which included different possible promoters including the putative promoter(s) of gene *2080* and/or the three *ftsZ* promoters, P_{ftsZ} and assumed *2080* promoter, P_{2080} (Figure 5.16 and 5.17). For delivering the three different complementing constructs into *S. coelicolor* we used the plasmid pMS82, a vector that can integrate at the Φ BT1 attachment site in *S. coelicolor* leading each chromosome to contain a single copy of the plasmid (Gregory *et al.*, 2003). This vector also contains the hygromycin resistance gene, which allows for selection in the apramycin resistant *S. coelicolor* mutant strain.

The three complementing constructs all carry entire *2080* sequence but with different upstream sequences (Figure 5.17). The first construct (referred as P_{2080} -*2080*) consists purely of the *2080* gene and its putative promoter P_{2080} which was assumed at the end of *2801* (Figure 5.17 A). This Construct 1 can be directly amplified from the 4A10 cosmid using PCR and appropriate primers without any further genetic

manipulation. The second construct, construct 2 (referred as P_{ftsZ} -2080) contains gene 2080 and three *ftsZ* promoters P_{ftsZ} . This construct can be generated using PCR once the *ftsZ* and 2081 genes are knocked out, first by replacing them with the apramycin resistance disruption cassette, and then removing the apramycin resistance cassette using the Flip recombinase. The third construct, construct 3 (referred as $P_{ftsZ+2080}$ -2080) carries the three *ftsZ* promoters P_{ftsZ} , the putative promoter P_{2080} and the 2080 gene (Figure 5.17 C). To generate this construct we

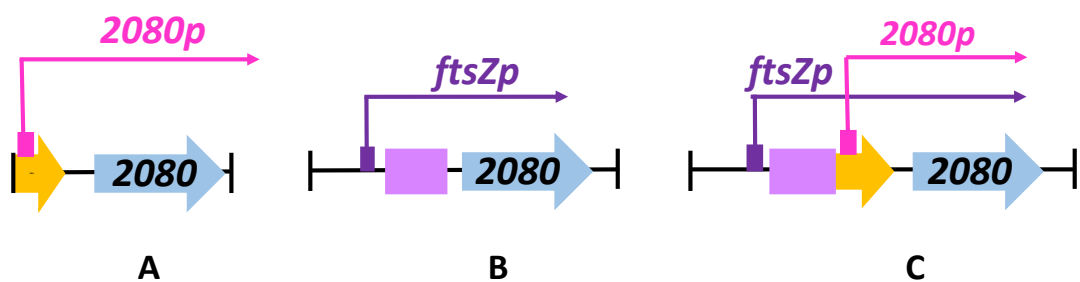


Figure 5.17. Complementation strategy. (A) Construct 1: P_{2080} -2080 containing 2080 gene and its putative promoter. (B) Construct 2: P_{ftsZ} -2080 containing 2080 gene and 3 *ftsZ* promoters. (C) Construct 3: $P_{ftsZ+2080}$ -2080 containing 2080 gene, 3 *ftsZ* promoters and 2080 putative promoter. The purple box represents a scar which is left by removing the apramycin resistant mark gene.

needed to replace the *ftsZ* gene and large part of the 2081 gene with the apramycin resistance cassette and then remove this cassette using Flip recombinase. This mutant cosmid then could be used in a PCR reaction to amplify the final construct.

To generate construct 1, PCR amplification using primers 2080 Bgl Prom FRW and 2080 3' END and the 4A10 cosmid as a template (Figure 5.18). This PCR product

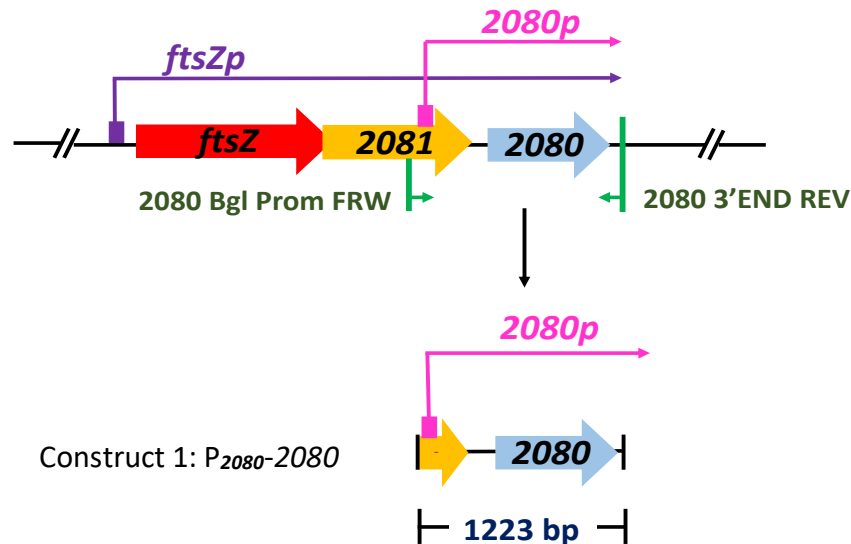
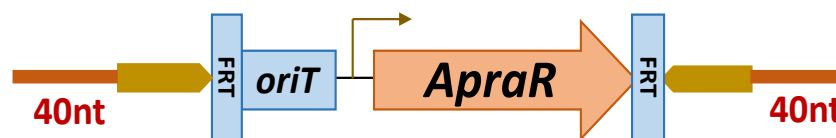


Figure 5.18. Generation of Construct 1, P₂₀₈₀-2080 (1223bp). The construct 1 was directly amplified from the 4A10 cosmid using primers 2080 Bgl Prom FRW and 2080 3' END.

included 258 bp upstream of the 2080 gene.

To create the next two constructs P_{ftsZ}-2080 and P_{ftsZ+2080}-2080 we needed to replace DNA fragments of the 4A10 cosmid using the PCR targeting we used before



Construct	Direction	Oligos
Construct 2	Forward	FtsZ KO FRW
	Reverse	2081 KO REV
Construct 3	Forward	FtsZ KO FRW
	Reverse	2081 KO2 Apra REV

Figure 5.19. Primers used for the generation of the apramycin resistance cassette.

for knockout generation. Firstly, an apramycin resistance cassette containing *oriT* and FLP recognition targets (FRT) was amplified using appropriate primers (Figure 5.19), which contain DNA complementary sequences flanked the cassette and DNA complementary sequences flanked the genes which need to be knocked out. The presence of the FRT sites allow us later to remove the apramycin resistance gene using the Flip recombinase that will excise the DNA fragment between the FRT sites (Figure 5.19). The PCR cassette of 1.3 kb was analysed in Figure 5.20.

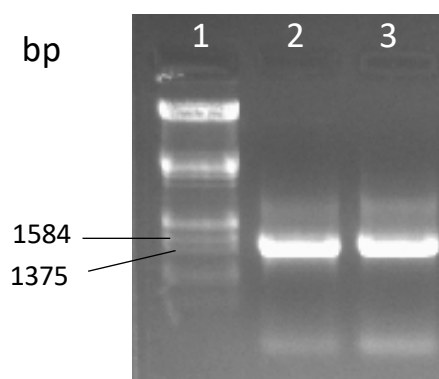


Figure 5.20. Amplification of the apramycin disruption cassette.

Lane 1: lambda *EcoRI HindIII* ladder; lane 2: Amplification of apramycin disruption cassette using primers *FtsZ KO FRW* and *2081 KO REV* for constructs 2; lane 3: Amplification of apramycin disruption cassette using primers *FtsZ KO FRW* and *2081 KO2 Apra REV* for constructs 3.

We electroporated the apramycin resistance disruption cassette into *E. coli* BW25113 cells containing cosmid 4A10 and selected for transformants resistant to apramycin. In order to confirm whether the target genes were successfully replaced, the restriction enzymes *EcoRI/XbaI* and *HindIII/XbaI* were used to digest the obtained cosmids. The *XbaI* restriction enzymes site is absent in cosmid 4A10 but exists in the apramycin resistance cassette. Therefore, the *XbaI* restriction enzyme can be used to confirm whether the target genes are successfully replaced with apramycin disruption cassette after recombination. An “in-silico” restriction digest map was generated (Figure 5.21) using ARTEMIS (Rutherford *et al.* 2000) highlighting the

different fragment sizes (Table 5.2 A). At this step, these two cosmids were referred as 4A10/*ftsZ-2081::ApraR2* and 4A10/*ftsZ-2081::ApraR3*.

The digestion using *EcoRI* and *XbaI* can distinguish between the 4A10 cosmid and the 4A10/*ftsZ-2081::ApraR2* or the 4A10/*ftsZ-2081::ApraR3* cosmids. But from these sizes of PCR resulting products, it is hard to distinguish cosmids between 4A10/*ftsZ-2081::ApraR2* and 4A10/*ftsZ-2081::ApraR3*. Therefore, we decided to use restriction enzymes *HindIII* and *XbaI* to digest these two constructs. The expected size of fragments was shown in Figure 5.21 and table 5.2 B.

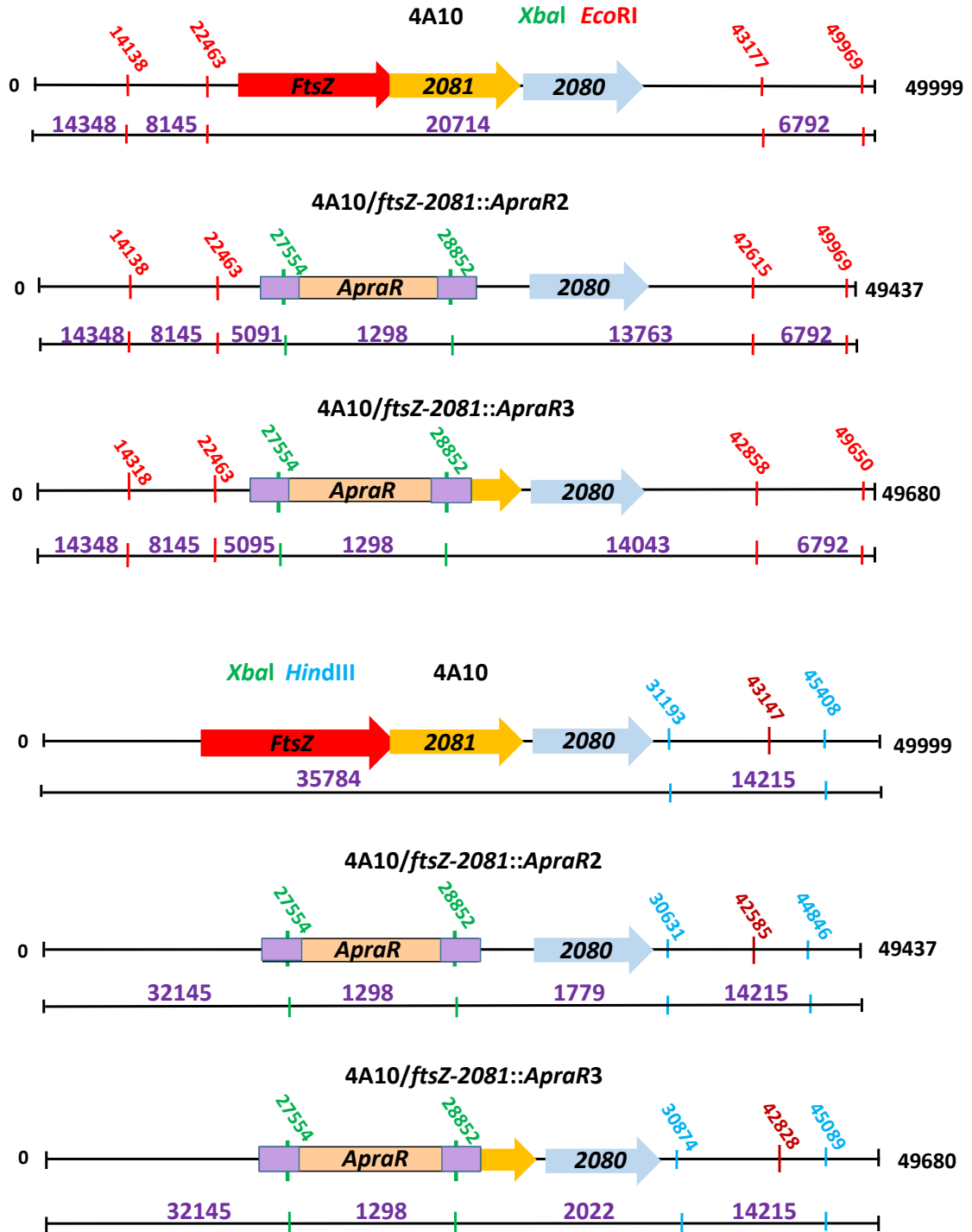


Figure 5.21. Restriction maps of 4A10 cosmid, 4A10/*ftsZ*-2081::*ApraR2* and 4A10/*ftsZ*-2081::*ApraR3*. The cosmid drawing is not to scale. The restriction sites are marked as red dashes for *EcoRI*, blue dashes for *XbaI* and green dashes for *HindIII*, with positions (in bp) given in the maps. 4A10 has no *XbaI* sites.

4A10/*ftsZ*-2081::*ApraR2* and 4A10/*ftsZ*-2081::*ApraR3* have *XbaI* sites because of the introduction of the apramycin resistance cassette.

Table 5.2. Expected fragment sizes after digestion of the apramycin marked knockout cosmids with (A) *EcoRI/XbaI* and (B) *HindIII/XbaI*. 4A10 cosmid digested with same enzymes is used as a control.

A <i>XbaI</i> and <i>EcoRI</i>			B <i>XbaI</i> and <i>HindIII</i>		
4A10	4A10/ <i>ftsZ</i> - 2081:: <i>ApraR2</i>	4A10/ <i>ftsZ</i> - 2081:: <i>ApraR3</i>	4A10	4A10/ <i>ftsZ</i> - 2081:: <i>ApraR2</i>	4A10/ <i>ftsZ</i> - 2081:: <i>ApraR3</i>
20714	-	-	35784	-	-
14348	14348	14348	-	32145	32145
-	-	14006	14215	14215	14215
-	13763	-	-	-	-
8145	8145	8145	-	-	-
6792	6792	6792	-	-	2022
-	5091	5091	-	1779	-
-	1298	1298	-	1298	1298

The expected sizes of digested cosmids were analysed using gel electrophoresis (Figure 5.22). After digestion using *EcoRI* and *XbaI*, the ~20kb fragment of the 4A10 cosmid was replaced by three fragments in the mutant cosmids, 13.7-14.0 kb, 5.1 kb and 1.3 kb fragments all detectable (Figure 5.22). The agarose gel was not able to separate the 13.7-14.0 kb and the 14.4 kb fragments, but the absence of the 20 kb fragment and the appearance of the 5.1 kb and 1.3 kb fragments in the mutant cosmids did confirm that the mutant cosmids were successfully generated. The digestion using *HindIII* and *XbaI* allowed the distinction between 4A10/*ftsZ*-2081::*ApraR2* and 4A10/*ftsZ*-2081::*ApraR3*. The 1779 bp fragment generated from 4A10/*ftsZ*-2081::*ApraR2* (Lane 5) and the 2022 bp fragment generated from 4A10/*ftsZ*-2081::*ApraR3* (lane 6) confirmed the difference between these two constructs (Figure 5.22).

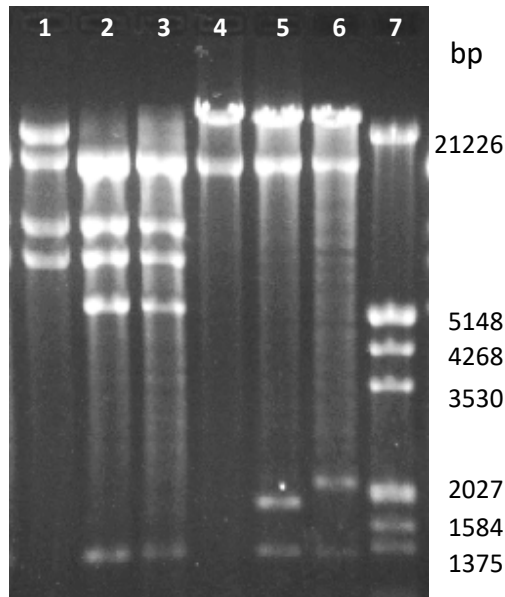


Figure 5.22. Gel analysis of the knockout cosmids *4A10/ftsZ-2081::ApraR2* and *4A10/ftsZ-2081::ApraR3*.

Lane 7: lambda DNA digested using *EcoRI* and *HindIII*, sizes shown in bp. Lanes 1 and 4: *4A10* cosmid; Lanes 2 and 5: *4A10/ftsZ-2081::ApraR2*; lanes 3 and 6: *4A10/ftsZ-2081::ApraR3*. Lanes 1-3: digestion using *EcoRI* and *XbaI*, lanes 4-6: digestion using *HindIII* and *XbaI*.

After confirmation of the construct *4A10/ftsZ-2081::ApraR2* and *4A10/ftsZ-2081::ApraR3*, we removed the apramycin resistant cassette from these two constructs by FLP-recombinase in *E. coli*, leaving an 81 bp scar where the resistance cassette was, to generate the unmarked constructs. It is necessary to remove the apramycin cassette because it may interfere the transcription of the *2080* gene. To remove the resistance cassette, we moved the mutant cosmids into *E. coli* DH5 α /BT340 cells, which contain the temperature sensitive FLP recombination plasmid encoding a FLP-recombinase (FLP). The FLP recognises FRT (FLP recognition targets) sites surrounding the apramycin resistance gene (Figure 5.19). FLP is expressed by growing the cells at 42°C which lead to the loss of the temperature sensitive plasmid. After “flipping” and an 81 bp scar sequence will be left in the constructs. After the incubation at 42°C the single colonies were tested for the loss of the apramycin resistance gene by streaking onto LB plates containing either

apramycin or kanamycin. The successful flipped cosmids were apramycin sensitive and kanamycin resistant.

The flipped cosmids were confirmed by using both *EcoRI/XbaI* and *HindIII/XbaI* restriction enzymes. The restriction map was generated and shown in Figure 5.23. The expected size of the fragments are shown in table 5.3. After removal of the apramycin resistance cassette, the cosmids 4A10/*ftsZ-2081::ApraR2* and 4A10/*ftsZ-2081::ApraR3* were named as 4A10/*ftsZ-2081::Scar2* and 4A10/*ftsZ-2081::Scar3*. The restriction digests were analysed on an agarose gel. As the predicted (Figure 5.23), after flipping the apramycin resistance cassette, the 1.3 kb fragments in the knockout cosmids were absent (Figure 5.24).

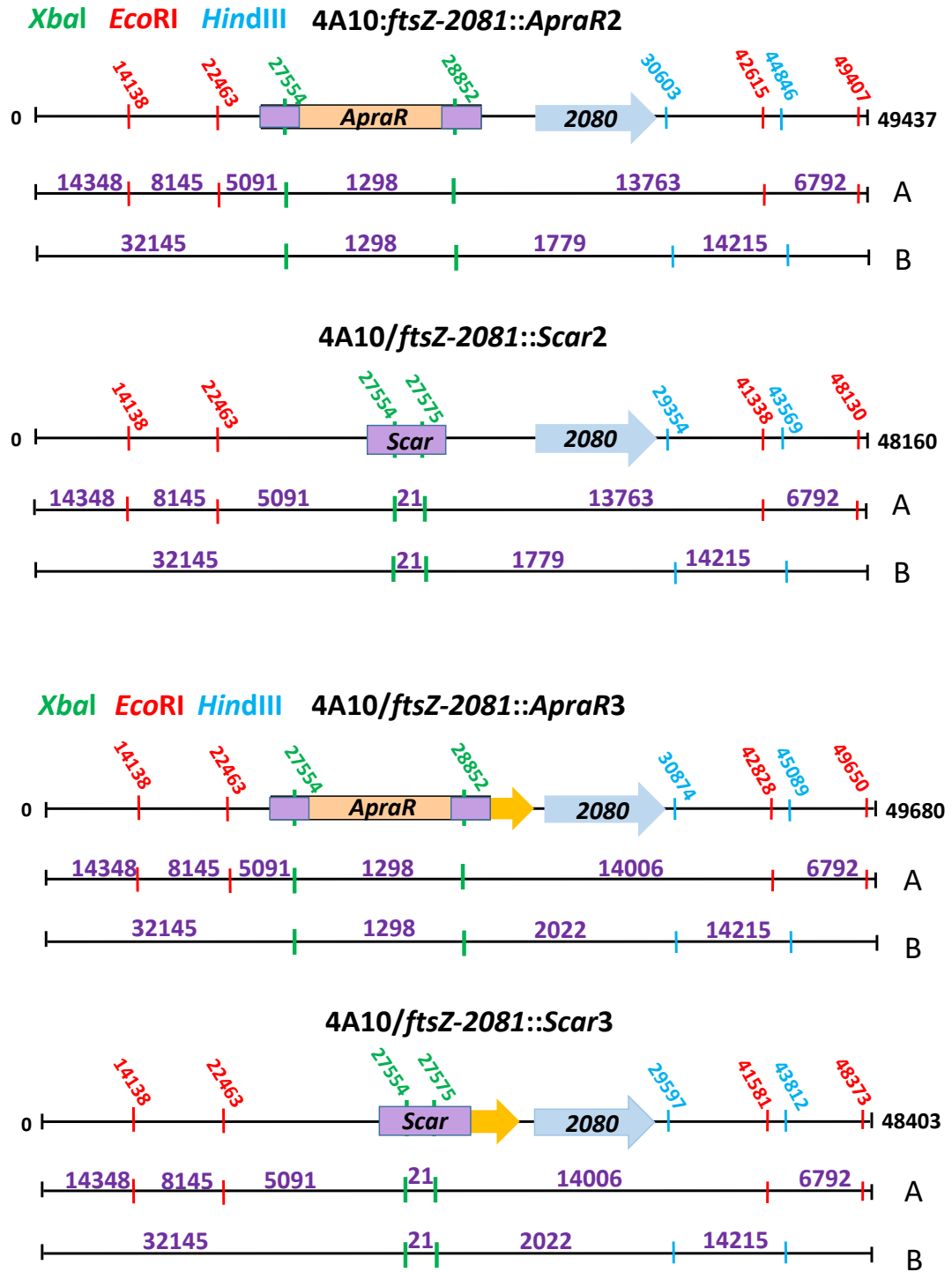


Figure 5.23. Comparison of the restriction maps of the knockout 4A10 cosmids and the flipped cosmids. The cosmid drawing is not to scale. (A) map with *Eco*RI/*Xba*I; (B) map with *Hind*III/*Xba*I. Restriction enzyme sites are shown as coloured lines: *Eco*RI in red, *Xba*I in green, *Hind*III in blue.

Table 5.3. The expected fragment sizes after restriction digestion of the knockout cosmids 4A10/*ftsZ-2081::ApraR2* and 4A10/*ftsZ-2081::ApraR3* and the flipped knockout cosmids 4A10/*ftsZ-2081::Scar2* and 4A10/*ftsZ-2081::Scar3* with *EcoRI* /*XbaI* (top) and *HindIII*/*XbaI* (bottom).

XbaI* and *EcoRI

4A10	4A10/ <i>ftsZ-2081::ApraR2</i>	4A10/ <i>ftsZ-2081::ApraR3</i>	4A10/ <i>ftsZ-2081::Scar2</i>	4A10/ <i>ftsZ-2081::Scar3</i>
20714	-	-		
14348	14348	14348	14348	14348
-	-	14006	-	14006
-	13763	-	13763	-
8145	8145	8145	8145	8145
6792	6792	6792	6792	6792
-	5091	5091	5091	5091
-	1298	1298	-	-
-	-	-	21	21

XbaI* and *HindIII

4A10	4A10/ <i>ftsZ-2081::ApraR2</i>	4A10/ <i>ftsZ-2081::ApraR3</i>	4A10/ <i>ftsZ-2081::Scar2</i>	4A10/ <i>ftsZ-2081::Scar3</i>
35784	-	-	-	-
-	32145	32145	32145	32145
14215	14215	14215	14215	14215
-	-	-	-	-
-	-	2022	-	2022
-	1779	-	1779	-
-	-	-	21	21

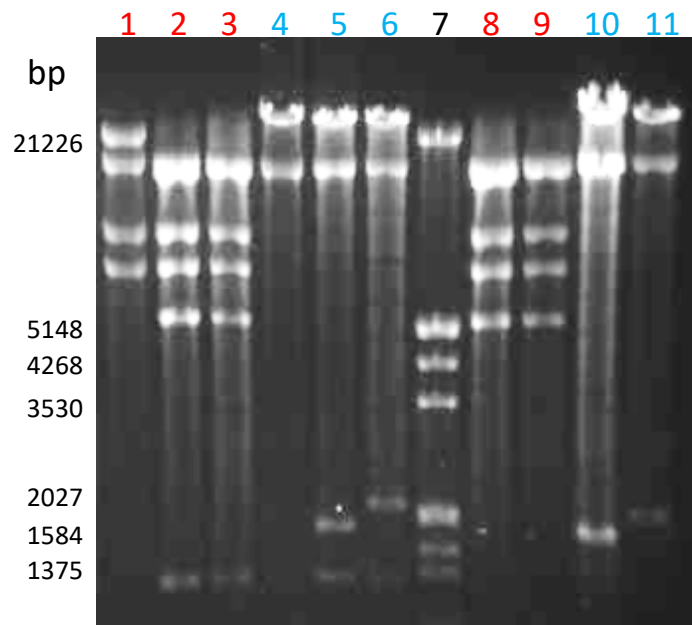


Figure 5.24. Gel analysis the of flipped knockout cosmids 4A10/*ftsZ-2081::Scar2* and 4A10/*ftsZ-2081::Scar3*.

Lane 7: lambda DNA digested with *EcoRI* and *HindIII* ladder; Lanes 1 and 4: 4A10 cosmid; lanes 2 and 5: 4A10/*ftsZ-2081:ApraR2*; lanes 3 and 6: 4A10/*ftsZ-2081::ApraR3*; lanes 8 and 10: 4A10/*ftsZ-2081::Scar2*; lanes 9 and 11: 4A10/*ftsZ-2081::Scar3*.

Lanes 1, 2, 3, 8, 9: digestion with *EcoRI* and *XbaI*, lanes 4, 5, 6, 9, 10: digestion with *HindIII* and *XbaI*.

After the knockout cosmids were flipped successfully, the complementing clones were generated by PCR amplification using primers FtsZ Bgl Prom FRW and 2080 3' END and the introduction of the PCR product into first the pGEM Easy cloning vector (Figure 5.25), which encodes the gene *lacZ* allowing blue and white screening.

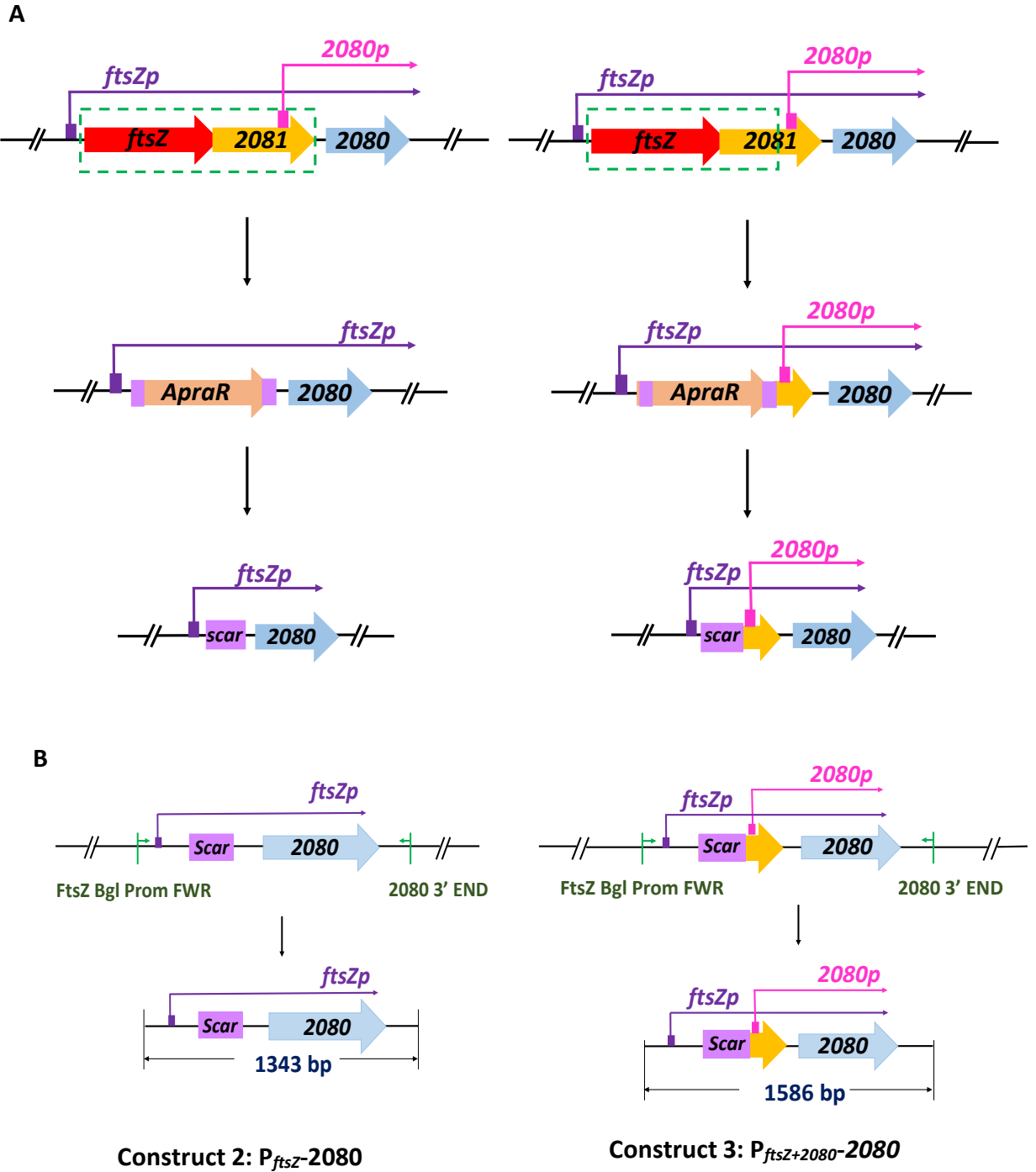


Figure 5.25. The final design of construct 2 and construct 3. A: knockout of *ftsZ*-2081 genes. B: PCR amplification using the knock-out cosmids with primers FtsZ Bgl Prom FRW and 2080 3'END to generate construct 2 and 3.

A small-scale plasmid preparation was made from two white single colonies and then the plasmids were digested using *EcoRI*, which flanks the cloned inserts and analysed on an agarose gel (Figure 5.26).

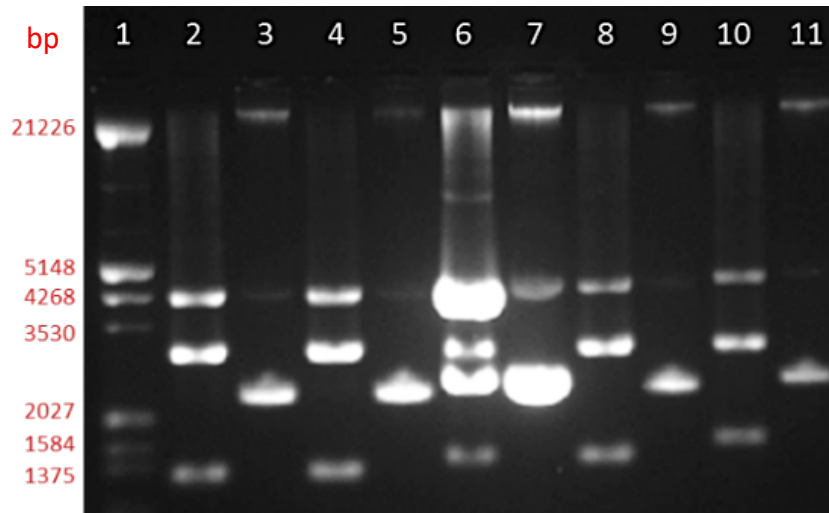


Figure 5.26. Gel analysis of *EcoRI* digested plasmid constructs. Lane 1: lambda DNA digested with *EcoRI/HindIII*. Lanes 2-5: two putative construct 1 plasmids; lanes 6-9: two putative construct 2 plasmids; lanes 10-11: one putative construct 3 plasmid. Lanes 2-11: even numbers contain the plasmids digested with *EcoRI*, odd numbers contain the non-digested plasmids.

In gel image, the smallest fragments (lane 2,4,6,8 and 10) are the cloned inserts at the expected sizes: 1223 bp, 1343 bp, and 1586 bp for construct 1, 2 and 3. The pGEM vector (3015 bp) is the middle fragment, whilst the top fragments indicate that the plasmids were only partially digested (Figure 5.26). The pGEM clones were sequenced and their inserts were moved into the plasmid pMS82. The transformants following the cloning onto pMS82 were grid streaked on LB (no salt) containing hygromycin. To identify the correct clones, colony PCR was carried out using primers 2080 XbaI Nde FRW and 2080 Nde REV (Figure 5.27).

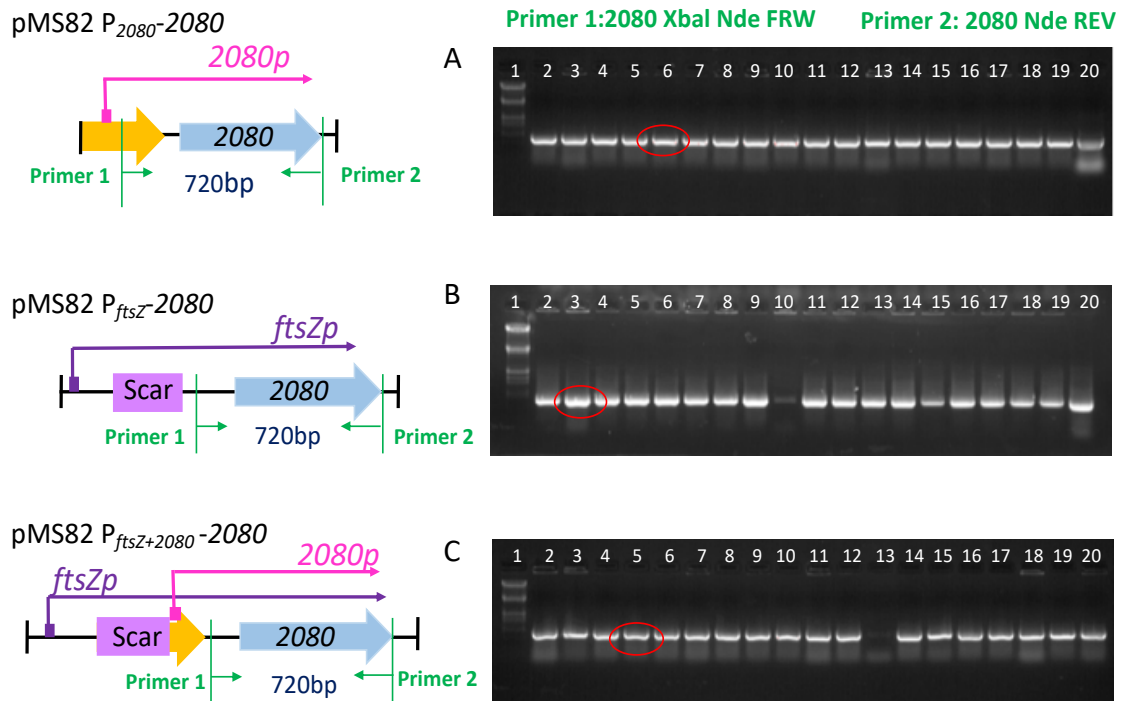


Figure 5.27. Colony PCR identify successful integration of the correct inserts into pMS82 plasmid.

(A) Lane 1: λ *EcoRI-HindIII* ladder, Lane 2-19: each lane represents a single transformant for pMS82 P_{2080} -2080, Lane 20: positive control. **(B)** Lane 1: λ *EcoRI-HindIII* ladder, Lane 2-19: each lane represents a single transformant for pMS82 P_{ftsZ} -2080, Lane 20: positive control. **(C)** Lane 1: λ *EcoRI-HindIII* ladder, Lane 2-20: each lane represents a single transformant for pMS82 $P_{ftsZ+2080}$ -2080.

Primer 1 is 2080 XbaI Nde FRW and primer 2 is 2080 Nde REV. Red circle represents constructs that were further used.

The colony PCR suggested that most colonies contained relevant inserts (Figure 5.27). One representative was picked from each set and large-scale plasmid preparations were generated. The extracted plasmids were then moved into *E. coli* strain ET12567/pUZ8002 by electroporation and then conjugated into the *2080* mutant using nalidixic acid and hygromycin for selection. In addition, the vector pMS82 was also conjugated into the *2080* mutant and the wild-type M145 strains to test that complementation was due to the presence of the complementing fragments and not the plasmid pMS82 alone. We picked the grown healthy single colonies and grew them on media SFM containing hygromycin to generate stocks. To test for

complementation, these strains were plated on SFM medium containing hygromycin and incubated at 30°C monitoring their macroscopic phenotype daily (Figure 5.28). Surprisingly after four days growth, the strains $\Delta 2080/pMS82/P_{2080-2080}$,



Figure 5.28. The macroscopic analysis of the complementation assays. Strains $\Delta 2080/pMS82/P_{2080-2080}$, $\Delta 2080/pMS82/P_{ftsZ-2080}$ and $\Delta 2080/pMS82/P_{2080+ftsZ-2080}$ and the control strains, the wild-type M145/pMS82 and $\Delta 2080/pMS82$ were streaked onto SFM medium containing hygromycin and were viewed after 4 days at 30°C.

$\Delta 2080/pMS82/P_{ftsZ-2080}$ and $\Delta 2080/pMS82/P_{2080+ftsZ-2080}$ all stayed white just as the control strain $\Delta 2080/pMS82$. The strain M145/pMS82 control strain developed the dark grey colour that is characteristic of the mature, sporulating colonies. This result indicated that none of the designed DNA fragments complemented the mutant phenotype of the *2080* knockout strain, which was unexpected. One possible explanation for the failure in complementation was that transcription of *2080* did not

originate from the 3 *ftsZ* promoters but initiated from a promoter that was more upstream than we assumed. This we could have tested by cloning a new fragment with a larger upstream sequence. The other possibility was that the *2080* mutant had a polar effect on the expression of the downstream gene *sepF*. This was quite possible, taking into consideration the fact that the *2080* and *sepF* mutant phenotypes were very similar. At the time of attempting complementation of the *2080* mutant, the paper of Young *et al.*, 2016 was not published. However, in the light of the transcriptional starts identified by Young *et al.*, 2016, it is clear that by deleting the *2080* gene completely, we also removed one of the *sepF* promoters and might have affected the expression even from the second *sepF* promoter. Even without knowing about the positions of the *sepF* promoters, we did consider the possibility that the *2080* mutant was in fact a *2080-sepF* double mutant, or at least a *2080* knockout with an altered, highly reduced *sepF* expression. So next, we tested whether we could complement the *2080* mutant with a clone expressing *sepF*.

5.5.2 Complementation experiments of the *2080* mutant using constructs containing the *sepF* gene.

To attempt complementation of the *2080* mutant, we used three constructs created already in Chapter 3.5. Construct ΔP -*sepF* (978 bp) contains the entire *sepF* gene with 128 bp upstream sequences, which potentially contain one of the *sepF* promoters. Construct P-*sepF* (1199 bp) contains entire *sepF* gene and both of its putative promoters. This construct did fully complement the *sepF* knockout mutant. Construct *2080-sepF* (1643 bp) contains entire gene *sepF* together with its upstream gene *2080* (Figure 5.29).

In chapter 3.5, we have introduced these fragments into pMS82, generating pMS82/ ΔP -*sepF*, pMS82/P-*sepF* and pMS82/*2080-sepF*. These constructs were introduced to the *2080* mutant to create the strains $\Delta 2080$ /pMS82/ ΔP -*sepF*, $\Delta 2080$ /pMS82/P-*sepF* and $\Delta 2080$ /pMS82/*2080-sepF*. Stocks of these strains were generated and stored.

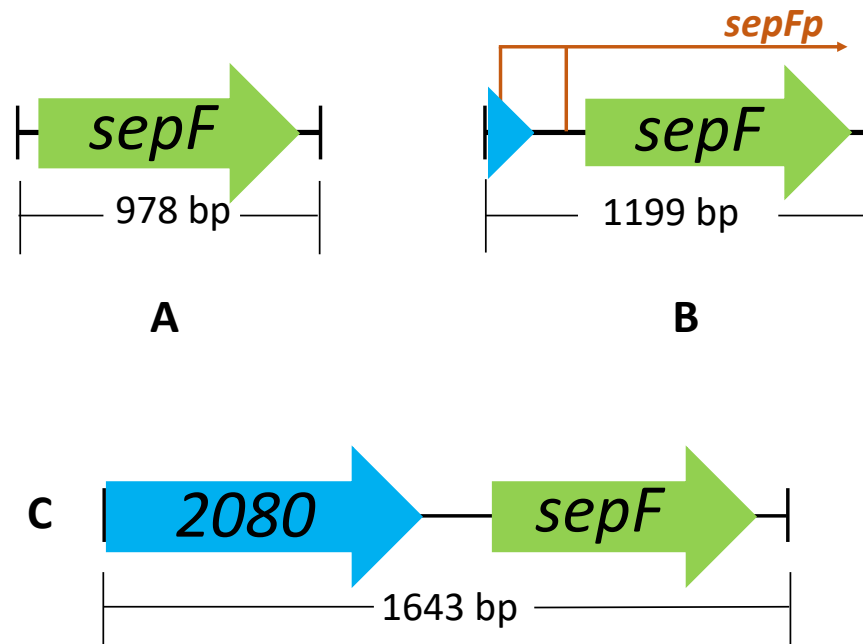


Figure 5.29. The complementation strategy.

A: Construct ΔP -*sepF* (978 bp) containing the *sepF* gene and ~128 bp upstream sequence. **B:** Construct P-*sepF* (1199 bp) contains entire sequencing of gene *sepF* and its putative promoter present. **C:** Construct 2080-*sepF* (1643 bp) containing the *sepF* gene and ~848 bp upstream sequence.

We firstly tested the $\Delta 2080$ /pMS82/ ΔP -*sepF*, $\Delta 2080$ /pMS82/2080-*sepF* strains together with the control strains, M145/pMS82 and $\Delta 2080$ /pMS82 on SFM containing hygromycin (Figure 5.30 A and B). After one and two days the 2080 knockout mutant grew slower than all the other strains. After 3-4 days incubation at 30°C three of the strains produced the dark grey pigment suggestive of sporulation, and only the control 2080 mutant strain stayed white (Figure 5.30 C and D). This suggested that the 2080 mutant might have been successfully complemented by these two complementation constructs containing gene *sepF*. However, we have seen before with the *sepF* mutant, that macroscopic observation of grey pigment formation does not necessarily mean full complementation and fully restored sporulation.

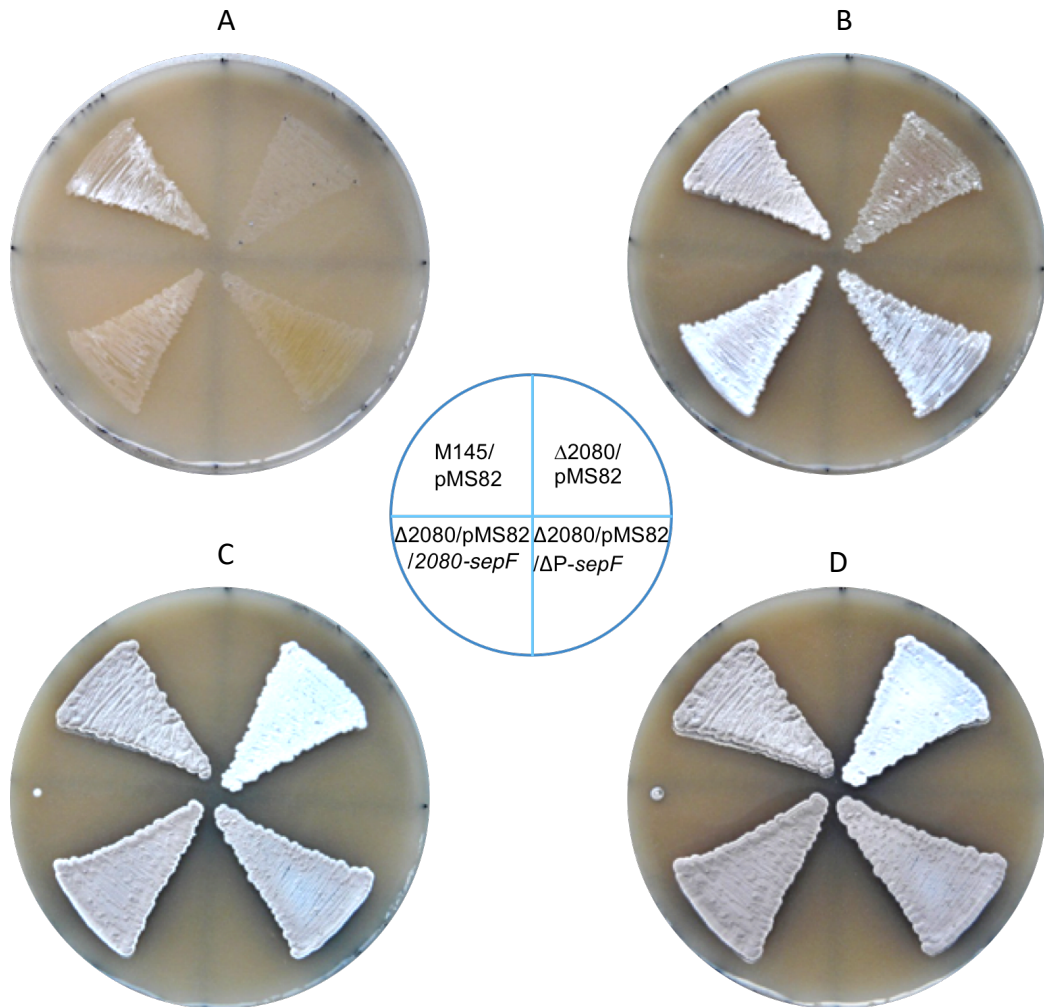


Figure 5.30. Macroscopic analysis of the complementation strains. The positions of the different strains are shown using the illustration in the middle. The strains were plated in a triangle patch on SMF medium containing hygromycin. The plates were incubated and monitored at regular time intervals (A) 1 day, (B) 2 days, (C) 3 days and (D) 4 days.

The third construct was tested in a separate experiment by monitoring the development of Δ 2080/pMS82/P-*sepF* on SFM containing hygromycin together with the control strains, wild-type M145 and the 2080 mutant on SFM medium (Figure 5.31). As we have generated spore preparations from both the wild-type M145 and Δ 2080/pMS82/P-*sepF* strains, we could inoculate the same number of spores when generating the patches, which allowed direct comparisons of the development of these two patches. Interestingly, after 2 days (48h), the development of the wild-type

was ahead of the $\Delta 2080/pMS82/P-sepF$ strain, while the growth of the *2080* mutant was further delayed (Figure 5.31). Three days (72h) after inoculation, the $\Delta 2080/pMS82/P-sepF$ appeared very similar to the wild-type strain, showing the dark grey pigmentation, suggesting that the *2080* mutant was complemented with a construct that contained only the *sepF* gene (Figure 5.31).

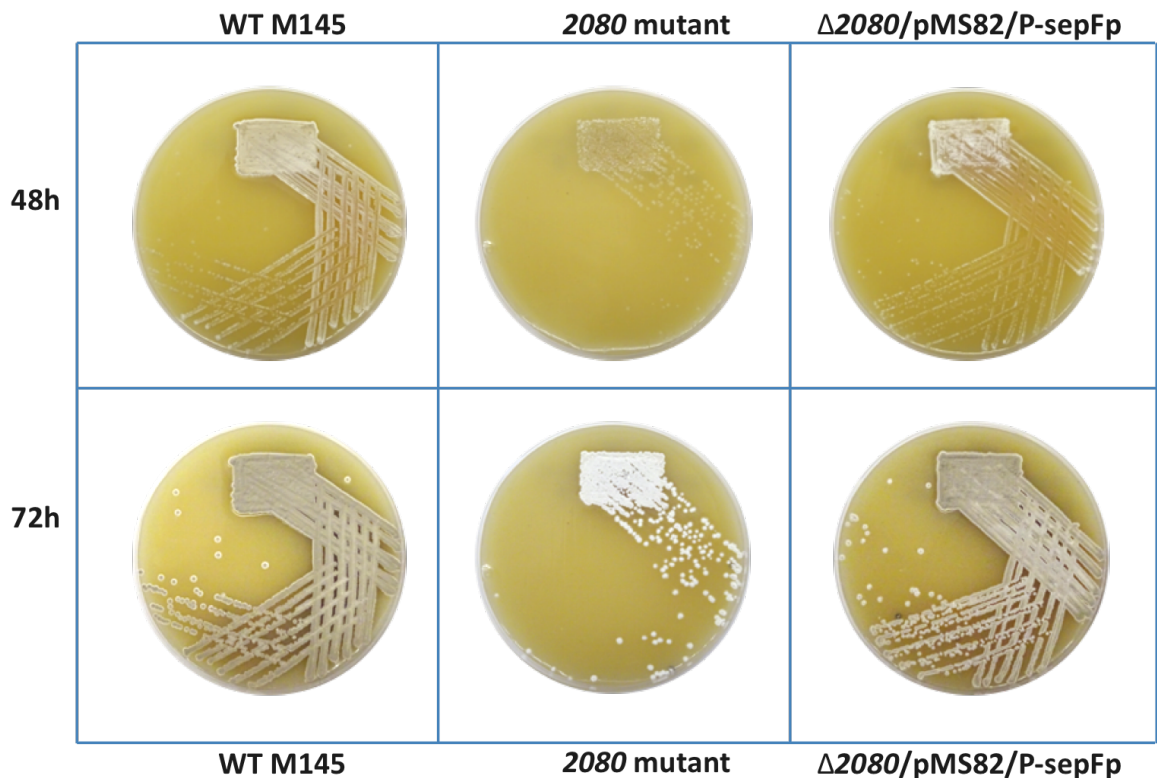


Figure 5.31. Monitoring morphological development for testing complementation of the *2080* mutant. The wild-type strain (left) the *2080* mutant (middle) and the $\Delta 2080/pMS82/P-sepF$ (right) are grown on SFM medium. The plates were incubated and monitored after 48h and 72h growth.

To confirm that the grey pigment formation reflected full complementation using all three constructs, we also monitored aerial hyphae development in the three strains $\Delta 2080/pMS82/\Delta P-sepF$, $\Delta 2080/pMS82/2080-sepF$ and $\Delta 2080/pMS82/P-sepF$ using fluorescence microscopy. First, we monitored development of the $\Delta 2080/pMS82/\Delta P-sepF$ strain (Figure 5.32). Compared to the *2080* mutant phenotype (Figure 5.14), the $\Delta 2080/pMS82/\Delta P-sepF$ strain showed some sporulation septation, which was consistent with grey colonies (Figure 5.30) on SFM medium.

However, this was not a full complementation as we detected very uneven septation and the septa often were not fully completed. The chromosomes were arranged around these incomplete septa with the possibility that septation could also guillotine some of the chromosomes. The fact that a construct containing only the *sepF* gene partially complemented the *2080* mutant suggested that the knockout mutation indeed had a polar effect on the downstream gene, *sepF*.

When the $\Delta 2080/pMS82/P-sepF$ strain was monitored, we observed regular septation and chromosome segregation very similar to that of the wild-type (Figure 5.33). This construct contains the *sepF* gene with its promoters sufficient for full complementation of the *sepF* knockout mutant, which suggests that the severe developmental, non-sporulating phenotype of the *2080* mutant was mainly caused by the absence of *sepF* expression in this mutant. Interestingly, the development of this strain was somewhat delayed compared to that of the wild-type strain (Figure 5.31) and there are perhaps some irregularities during septum formation of the $\Delta 2080/pMS82/P-sepF$ strain (Figure 5.33), which might account for the “true” *2080* knockout phenotype. If so, further confirmation of this is needed by generating statistical analysis of septum placement and confocal microscopy.

The third strain generated, $\Delta 2080/pMS82/2080-sepF$, which carried both the *2080* and the *sepF* genes, showed full complementation where the sporulation septation was very regular generating identical compartments with a single chromosome in each compartment (Figure 5.34) which was identical to the developing spore chains of the wild-type strain (Figure 3.20).

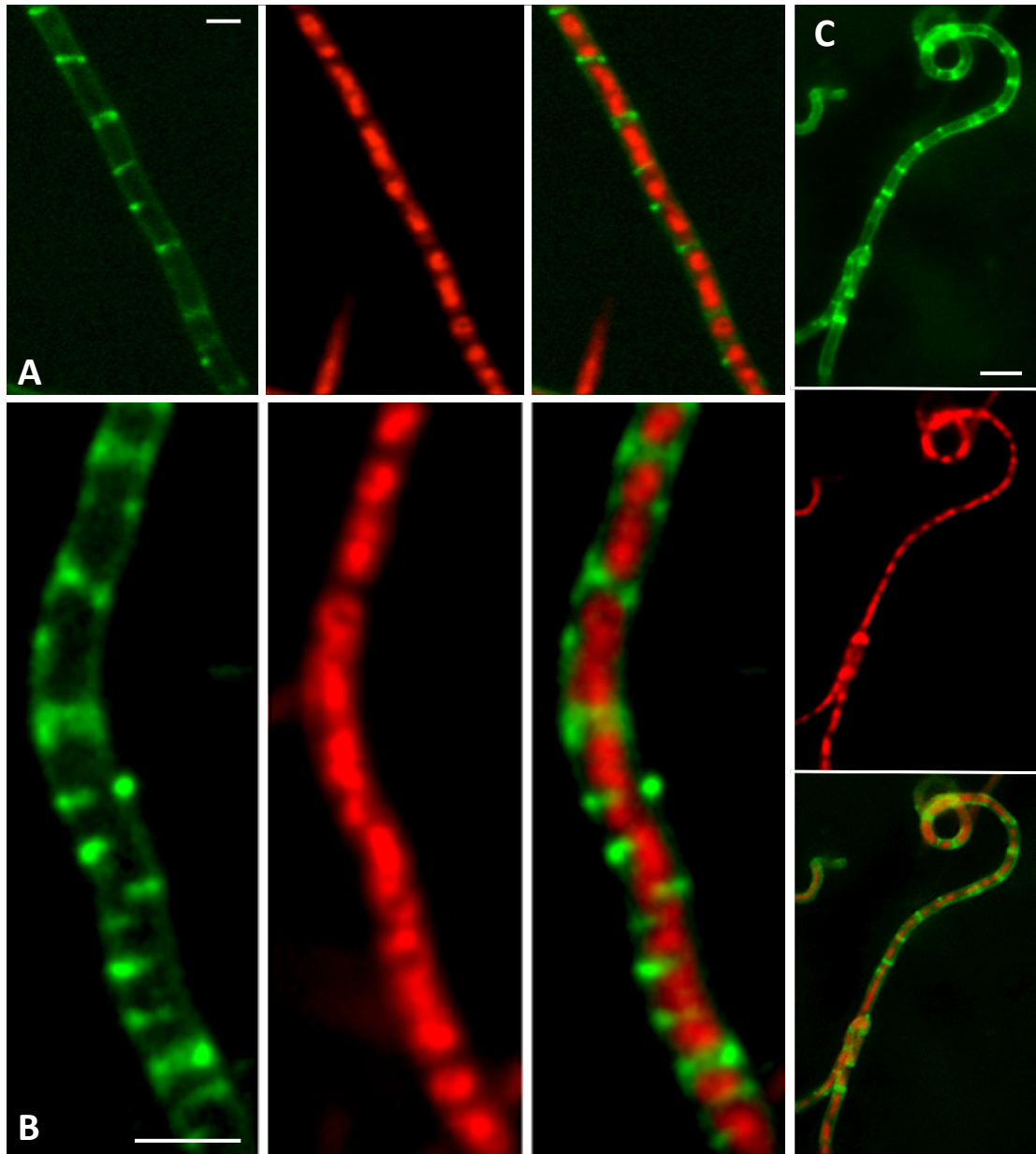


Figure 5.32. Fluorescence microscopy of $\Delta 2080/pMS82/\Delta P-sepF$ after 48 hours of growth on SFM medium containing hygromycin. The $\Delta 2080/pMS82/\Delta P-sepF$ strain was stained with PI (red-DNA) and WGA-Alexa 488 (green-cell wall). (A-B) confocal microscopy (C) epi-fluorescence microscopy. Size bar represents $1\mu m$.

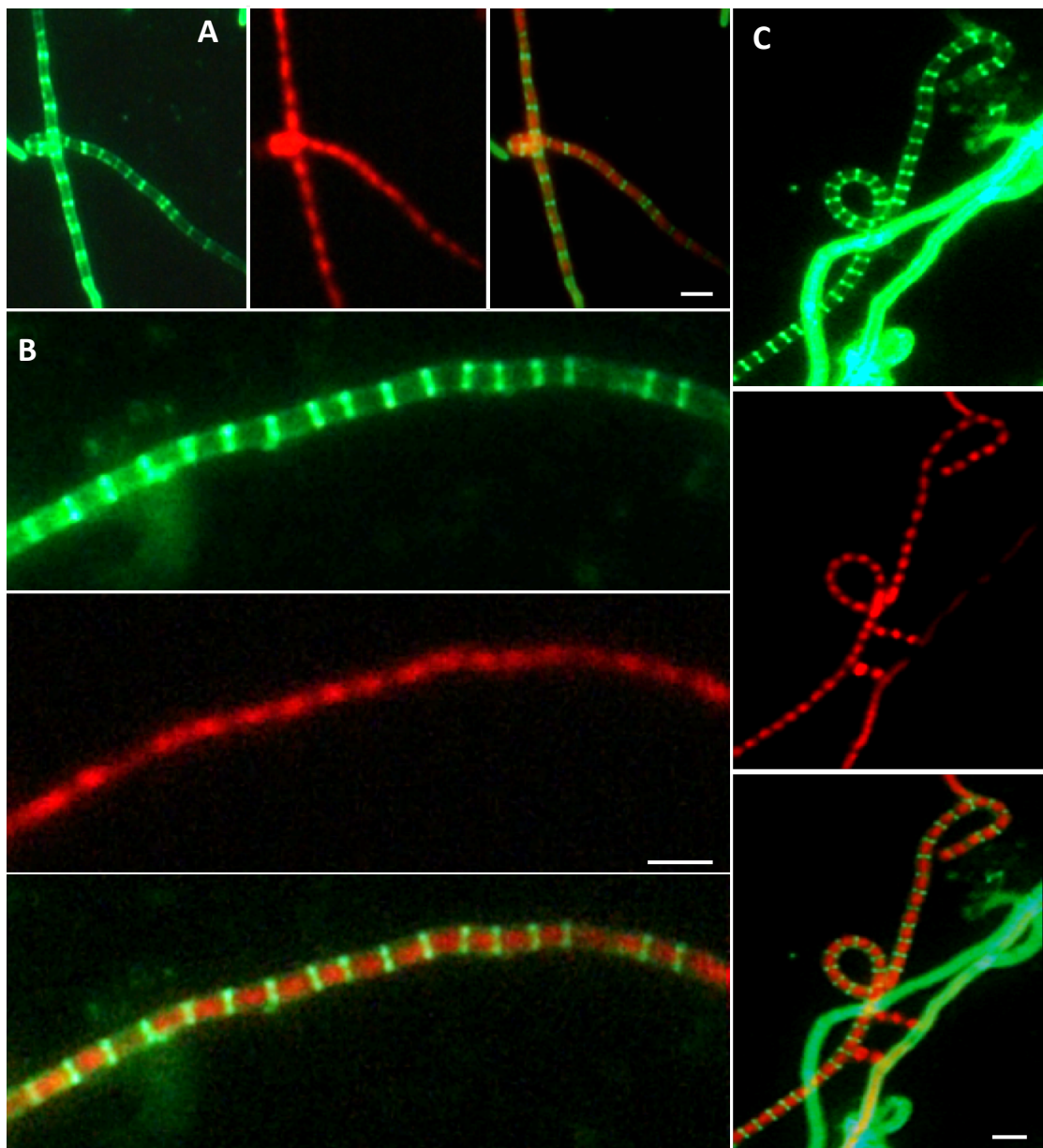


Figure 5.33. Fluorescence microscopy of $\Delta 2080/pMS82/P-sepF$ after 48 hours of growth on SFM medium containing hygromycin. The $\Delta 2080/pMS82/P-sepF$ strain was stained with PI (red-DNA) and WGA-Alexa 488 (green-cell wall). All images were generated using epi-fluorescence microscopy. Size bar represents 1 μm .

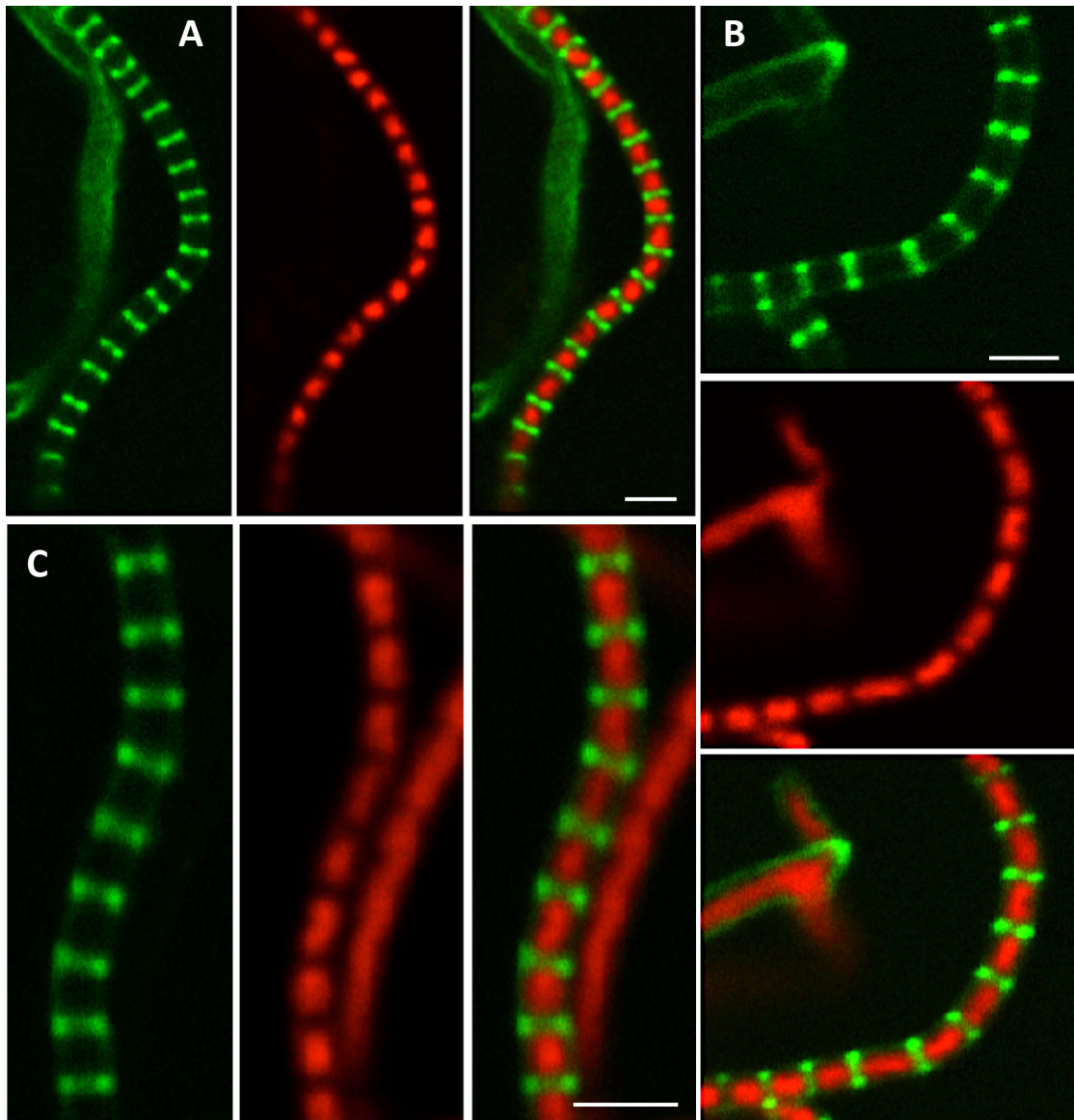


Figure 5.34. Fluorescence microscopy of $\Delta 2080/pMS82/2080-sepF$ after 48 hours of growth on SFM medium containing hygromycin. The $\Delta 2080/pMS82/2080-sepF$ strain was stained with PI (red-DNA) and WGA-Alexa 488 (green-cell wall). All images were generated using confocal microscopy. Size bar represents 1 μ m.

5.6 Summary

In this chapter we focused on the characterization of the *2080* gene. Although homologues of *2080* were found wide-spread amongst bacteria, including *B. subtilis* and *E. coli*, we do not fully understand the role of this protein.

- Bioinformatic analysis suggested that *2080* is homologous to alanine racemases, so it might have a function producing D-amino acids in the cell. This was supported by studies of *ylmE* in *B. subtilis*, where this gene was shown to contribute to the bacterium's D-amino acid pool and was affecting biofilm formation.
- We generated a gene knockout mutant in *S. coelicolor* using the REDIRECT technology and we confirmed the mutants generated by PCR tests using chromosomal DNA preparations made from the mutant strains.
- We characterized the mutant phenotype that was not identical but very similar to that of the *sepF* mutant, failing to develop sporulation septation.
- We have attempted to complement the *2080* mutant using constructs that carried the *2080* gene and different promoter combinations, however, not of our constructs complemented the white, non-sporulating phenotype of the *2080* mutant.
- We hypothesized that the lack of complementation using the *2080* gene constructs was because in the *2080* knockout not only the *2080* gene was absent but also the *sepF* gene was not (fully) expressed.
- We then attempted to complement the *2080* mutant using constructs carrying the *sepF* gene either alone or together with the *2080* gene. Interestingly, the clone that carried the *sepF* gene with all upstream fragments required for full complementation of the *sepF* knockout mutant, did complement the *2080* mutant, suggesting that the non-sporulating phenotype of the *2080* mutant was due to lack of SepF in this mutant. It is conceivable, that the $\Delta 2080/pMS82/P-sepF$ strain has a subtle delay in development and have slight irregularities during septation, which might just be the "true" *2080* mutant phenotype. If so, lack of the putative racemase and consequently reduced D-amino acid pool could have delayed sporulation in the *2080* mutant, but this needs to be confirmed by testing

the D-amino acid content of the *2080* mutant. It will also be important to localise the 2080 protein in *S. coelicolor* to test whether its localisation sheds any light on its possible function.

- Full complementation was confirmed when a DNA fragment carrying both *2080* and *sepF* genes were used.

Acknowledgements

We are very grateful to Alan Lau and Neal Greenway for contribution to the experiments.

Chapter 6 Brief characterisation of the *2081* gene

Introduction

Cell division within bacteria is a complex and not completely understood process. Most bacteria use binary fission, where the division septum forms at the mid-point of the rod-shaped cell (Wu and Errington, 2012). Within rod-shaped bacteria cell division is controlled by a macromolecular complex known as a divisome and bacterial cytoskeletal proteins (Adams and Errington, 2009). Positioning of the septum at the mid-point of the cell maximises the collective fitness of the progeny, with neither cell possessing incomplete genomes which could arise if this did not occur. For this positioning, cell division has to be highly regulated. The key cytoskeletal protein that begins the assembly of the divisome is FtsZ. Protofilaments of FtsZ are formed through polymerisation of the FtsZ subunits in the presence of GTP, before forming a Z-ring at the mid-point of the cell. This ring acts as a scaffold for recruiting other downstream components of the divisome, with mutations in this ring structure resulting in abnormal septa formation (Addinall and Lutkenhaus, 1996; Adams and Errington, 2009). GTP binding allows for polymerisation of FtsZ to occur, with the intrinsic GTPase activity of FtsZ resulting in constant remodelling of the Z-ring (Stricker *et al.* 2002; Jindal and Panda, 2013).

Cell division in *Streptomyces* is more complex and still not fully understood. Some genes in the division and cell wall (dcw) cluster remain uncharacterized. One notable example is the gene *2081* which is located immediately downstream of *ftsZ* and slightly overlapped with *ftsZ* that the start codon of *2081* overlaps with the stop codon of *ftsZ*. In the *Streptomyces* genomes analysed, *ftsZ*, *2081* and *2080* most likely form an operon, with overlapping start and stop codons between *ftsZ* and *2081* and only 6 bp spacing between *2081* and *2080* (Świątek *et al.*, 2013; Świątek, 2012). The gene *2081* is less studied in *Streptomyces* but its location suggest that it may play a role in cell division.

In this brief chapter, we focus on the generation and initial characterisation of a 2081 knockout mutant.

6.1 Bioinformatics study of gene 2081

To investigate the role of the 2081 protein in cell division, the amino acid sequence was obtained from the StrepDB *Streptomyces* annotation server (<http://strepdb.streptomyces.org.uk>) and analysed using SMART (<http://smart.embl-heidelberg.de/>) software. The BLAST results revealed that the protein 2081 (UniProt: P45497) was identified as a Cu-oxidase which is able to oxidise their substrate by accepting electrons at a mononuclear copper center and transferring them to a trinuclear copper center (Vashchenko *et al.*, 2013). Multi-copper oxidases have been studied in terms of their structure and sequence, some of which have lost the ability to bind copper. The 2081 protein is located downstream of FtsZ a gene organisation that is well conserved amongst the Actinobacteria (Figure 5.1, Chapter 5). In *B. subtilis*, the 2081 homologue, YlmD is encoded 7 genes downstream of *ftsZ*, but it is clustered with genes encoding the 2080 and SepF homologues. In *E. coli*, the 2081 homologue, YfiH is not located in the vicinity of either the *ftsZ* or 2080 genes (Figure 5.1, Chapter 5). Comparisons of 2081 from *S. coelicolor* and its *M. tuberculosis* homologue (Figure 6.1) revealed 49.79 % identity. Whilst, the similarity between the *Streptomyces* and *Bacillus* proteins is somewhat lower, 30.17 % identity (Figure 6.2) and also lower when compared to the *E. coli* homologue, YfiH, with 38.89 % identity (Figure 6.3).

```

SCO2081          -----VIGQRDT--V-NGAHFGFTDRWGGVSAVPYEELNLGGAVGDDPGAVTANRELA
M.tuRv2149c     LLASTRHIARGDTGNVSVRIIRRVTTTRAGGVSAPPFDTFNLGDHVGDDPAAVAANRARLA
                  *.: ** *      :   * * ***** *.: :***. *****.*:*** *
SCO2081          KSLGVDPARVVWMNQVHGADVAVVDAPWGDRPVPRVDAVVTAERGLALAVLTADCVPVLL
M.tuRv2149c     AAIGLPGNRVVWMNQVHGDRVELVDQPRNT-ALDDTDGLVTATPRLALAVVTADCVPVLM
                  :*: ***** * :** * .   : .*:*** *****:*****:
SCO2081          ADPVSGVAAAAHAGRPGLVAGVVPAAVRAMAELGADPARIVARTGPAVCGRCYEVPEEMR
M.tuRv2149c     ADARAGIAAAVHAGRAGAQRGVVVRALVMSLGAQVRDISALLGPAVSGRNYEVPAAAMA
                  ** :*:***.*** *   *** *:. . * .***:   * * *****.* ** *
SCO2081          AEVAAVEPAAYAETGWCTPALDVSAGVHAQLERLGVHDRAQSPVCTRESADHFSYRRDRT
M.tuRv2149c     DEVEAALPGSRTTTAACTPGVDLRAGIACQLRDLGVESIDVDPRCTVADPTLFSHRRDAP
                  ** * . *: : * . ***.:*: **: .** .***. . * ** .   **:***
SCO2081          TGRLAGYVWLD*
M.tuRv2149c     TGRFASLVWME-
                  ***:* . **: :

```

Figure 6.1. Protein sequence alignment of 2081 from *S. coelicolor* and its homologue, Rv2149 (Uniprot No.: P9WKD5) from *M. tuberculosis*. (*) indicates positions which have a conserved residue, (:) represents conservation between groups of amino acids with strongly similar properties, and (.) indicates conservation between groups with weakly similar properties. The sequence alignment was generated using Clustal Omega (<https://www.ebi.ac.uk/Tools/msa/clustalo/>).

```

SCO2081      -----VIGQRDTVNGAHFGFTDRWGGVSAVPYEELNLGGAVGDDPG
B.suYlmD    MNTYHPFSLTTPSTLMIQDWAQTNQNNKEVIAGFTTKNGGVSQKPFESLNTGLHVHDKDA
              .:. : . *** : **** *:*.** * * * . .

SCO2081      AVTANRELAAKSLGVDPARVVWMNQVHGADVAVVDAPW---G----DRPVPRVDAVVTAE
B.suYlmD    DVVKNREYIADMFNTDLQSWVFADQTHDNRVQKVTQRDRGKRGAREYHTALKATDGIYTNE
              *. *** * . :..* * : :*. * * * . : .*: * *

SCO2081      RGLALAVLTADCVPVLLADPVSQVAAAAHAGRPGLVAGVVPAAVRAM-AELGADPARIVA
B.suYlmD    KNVFLALCFADCVPPLFFYDPVKSLVGVVAHAGWKGTQKQIGREMVKQWTEKEGSNPSDIYA
              :.: **: *****: : *..:..***** * * : * : * : * : * *

SCO2081      RTGPAVCGRCYEVPEEMRAEVAAVEPAAYAET---GWGTPALDVSAGVHAQLE--RLGVH
B.suYlmD    VIGPSISGACYTVDDRVMDAVRALPVSADLAANQTAKAQYQLDLKELNRLILMDSGLASE
              **: :.* ** * :.: * * : :* : . . **: . : * * . .

SCO2081      DRAQSPVCTRESADHFS-YRRD-RTTGRLAGYVWLD*-
B.suYlmD    QISVSGLCSEPSLFYSHRRDQKGTGRMMSFIGMKEA
              : : * :**... . * :*** .***: .: : .

```

Figure 6.2. Protein sequence alignment of 2081 from *S. coelicolor* and its homologue, YlmD (Uniprot No.: O31726) from *B. subtilis*. (*) indicates positions which have a conserved residue, (:) represents conservation between groups of amino acids with strongly similar properties, and (.) indicates conservation between groups with weakly similar properties. The sequence alignment was generated using Clustal Omega (<https://www.ebi.ac.uk/Tools/msa/clustalo/>).

```

SCO2081      ----VIGQRDTVNGAHFGFTDRWGGVSAVPYEELNLGGAVGDDPGAVTANRELAAKSLGV
E.coliYfiH   MSKLIVPQWPQPKGVAACSSTRIGGVSLPPYDSLNLGAHCGDNPDHVEENRKRL-FAAGN
              :: *      :*.      : * **** **:_.****. **:*. * **:      : *

SCO2081      DPARVVWMNQVHGADVAVVD-APWGDRPVPRVDAVVTAERGLALAVLTADCVPLLADPV
E.coliYfiH   LPSKPVWLEQVHGKDVCLKLTGEPYA---SKRADASYSNTPGTVCVAVMTADCLPVLFCNRA
              *:: **:**** ** :   *:.      *.** :   * . **:****:****:.. .

SCO2081      SGVAAAAHAGRPGLVAGVVPAAVRAMAE LGADPARI VARTGPAVCGRCYEVPEEMRAEVA
E.coliYfiH   GTEVAAAHAHAGWRGLCAGVLEETVSCF---ADNPENILAWLGP AIGPRAF EVGGEVREAFM
              . .***** ** **: :* .: . :* .:* * **: *_.** **: * .

SCO2081      AVEPAAYA---ETGWGTPALDVSAGVHAQLERLGVHDRAQSPVCT-RESADHFSYRRDRT
E.coliYfiH   AVDAKASAAFIQHGDK-YLADIYQLARQLANVGVEQIFGGDRCTY TENE TFFSYRRDKT
              **: * * : *      *: .: :* .:***: . ** *_.*****:*

SCO2081      TGRLAGYVWLD*
E.coliYfiH   TGRMASFIWLI-
              ***:*.::**

```

Figure 6.3. Protein sequence alignment of the 2081 from *S. coelicolor* and its homologue, YfiH (Uniprot No.: P33644) from *E. coli*. (*) indicates positions which have a conserved residue, (:) represents conservation between groups of amino acids with strongly similar properties, and (.) indicates conservation between groups with weakly similar properties. The sequence alignment was generated using Clustal Omega (<https://www.ebi.ac.uk/Tools/msa/clustalo/>).

6.2 Generation of knockout 2081 mutant

We created 2081 gene knockout mutant using the REDIRECT© PCR-targeting system as before for the *sepF* and 2080 gene knockout (Chaper 3 and 5). To generate a 2081 gene knockout mutant, an extended apramycin resistance cassette containing 40 bp flanking regions that are homologous to the flanking regions of target gene was used to disrupt the target gene (Figure 3.11 from chapter 3). We amplified a apramycin resistance disruption cassette from pIJ733 using primers 2081 KO2 FRW and 2081 KO2 REV by PCR (Figure 6.4). The PCR product was run on 0.7% agarose gel for analysis. The size of PCR product is around 1.3 kb which corresponded to the expected size (Figure 6.5).

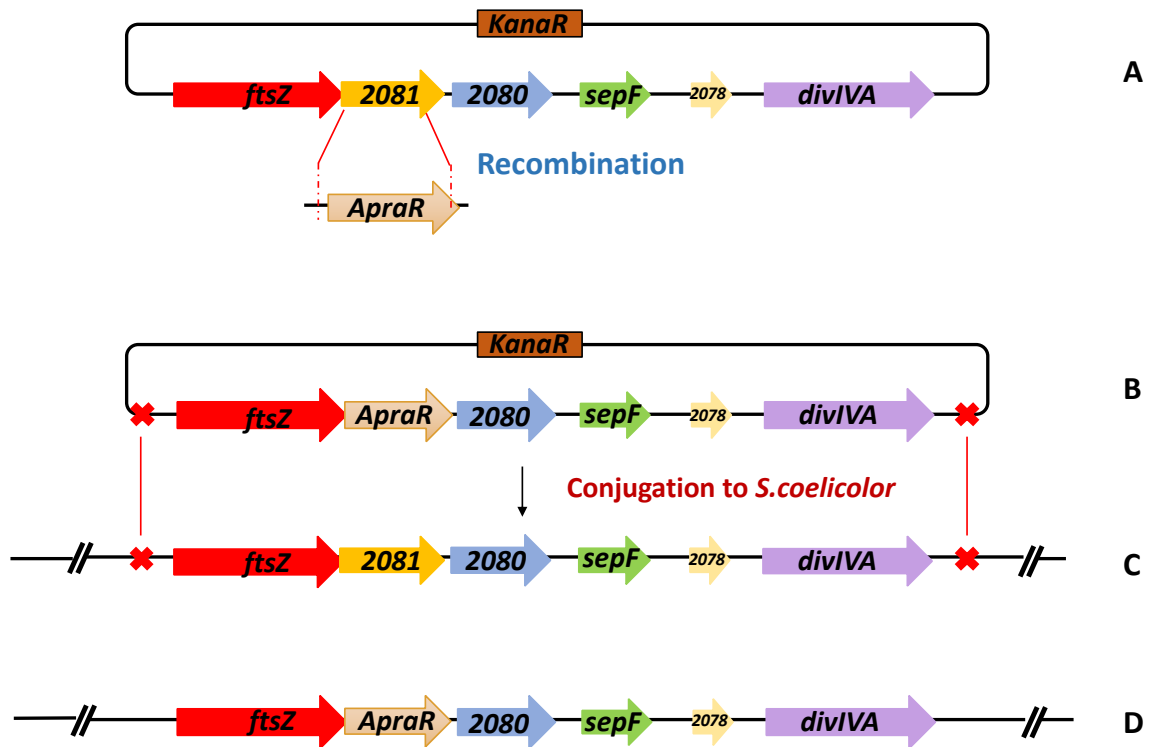


Figure 6.4. Knock out design for the generation of the 2081 null mutant in *S. coelicolor*. In a cosmid containing 2081 and its flanking genes, the 2081 gene was replaced with an apramycin resistance cassette (ApraR) (A). Then the resulting cosmid (B) was conjugated into *S. coelicolor* (C). The apramycin resistance cassette replaced the 2080 gene in *S. coelicolor* chromosome (D) after a double crossover event (B-D).

This apramycin disruption cassette was transformed into *E. coli* BW25113 cells carrying the *S. coelicolor* cosmid 4A10 by electroporation. The addition of L-arabinose to the media growing the BW25113 cells causes expression of the recombinase enzyme which initiates a homologous recombination event between the flanking regions of the apramycin resistance cassette and the reciprocal sequence flanking the gene 2081. Therefore, after the disruption cassette was transformed into the BW25113, cells containing the 4A10 cosmid obtained from the transformation were plated onto LB containing apramycin, to select for cells that underwent successful

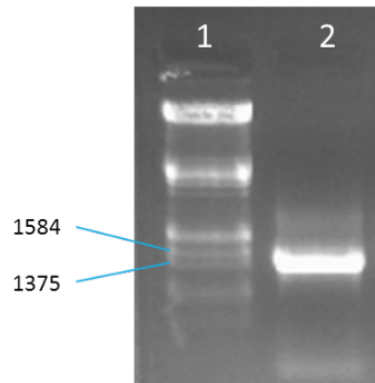


Figure 6.5. Amplification of apramycin disruption cassette using primers 2081 KO2 FRW and 2081 KO2 REV of gene 2081.

Gel analysis of the PCR amplification for the targeted knockout of 2081 (lane 2) using lambda DNA cut with *EcoRI* and *HindIII* as a molecular weight marker (lane 1). Sizes shown in bp. For lane 2, 2081 KO2 FRW and 2081 KO2 REV primers were used.

recombination events and grown at 37 °C to induce the loss of pIJ790. We picked the single BW transformants and then extracted the cosmid DNA from the cultured single colony using large scale cosmid extraction to obtain the cosmid DNA that had been disrupted.

To test whether the gene 2081 has been successfully replaced with apramycin resistant disruption cassette, as before, we used restriction enzymes *EcoRI/XbaI* to digest the extracted plasmid. An “in-silico” restriction digest map was generated (Figure 6.6) illustrating the fragment sizes (Table 6.1). The restriction digest of the extracted cosmids were run on a 0.7% agarose gel. Results of gel analysis shown in Figure 6.2.4 suggest that the apramycin cassette has been successfully replaced the target fragment by gene recombination. The ~20kb fragment in the 4A10 cosmid was replaced by three fragments of 14.0 kb, 6.3 kb and 1.3 kb fragments. Unfortunately, the 14.0 kb and 6.3 kb fragments of the mutant cosmid run close to the 14.3 kb and 6.7 kb fragments that are unchanged between the original 4A10 and the mutant cosmids. However, we can clearly confirm that the 20 kb fragment was absent in the mutant cosmids, and the ~14.0 kb and 6.3 kb fragments looked more intense,

suggesting the presence of two similarly sized fragments. The diagnostic 1.3 kb fragment was detectable in the mutant cosmid (Figure 6.7).

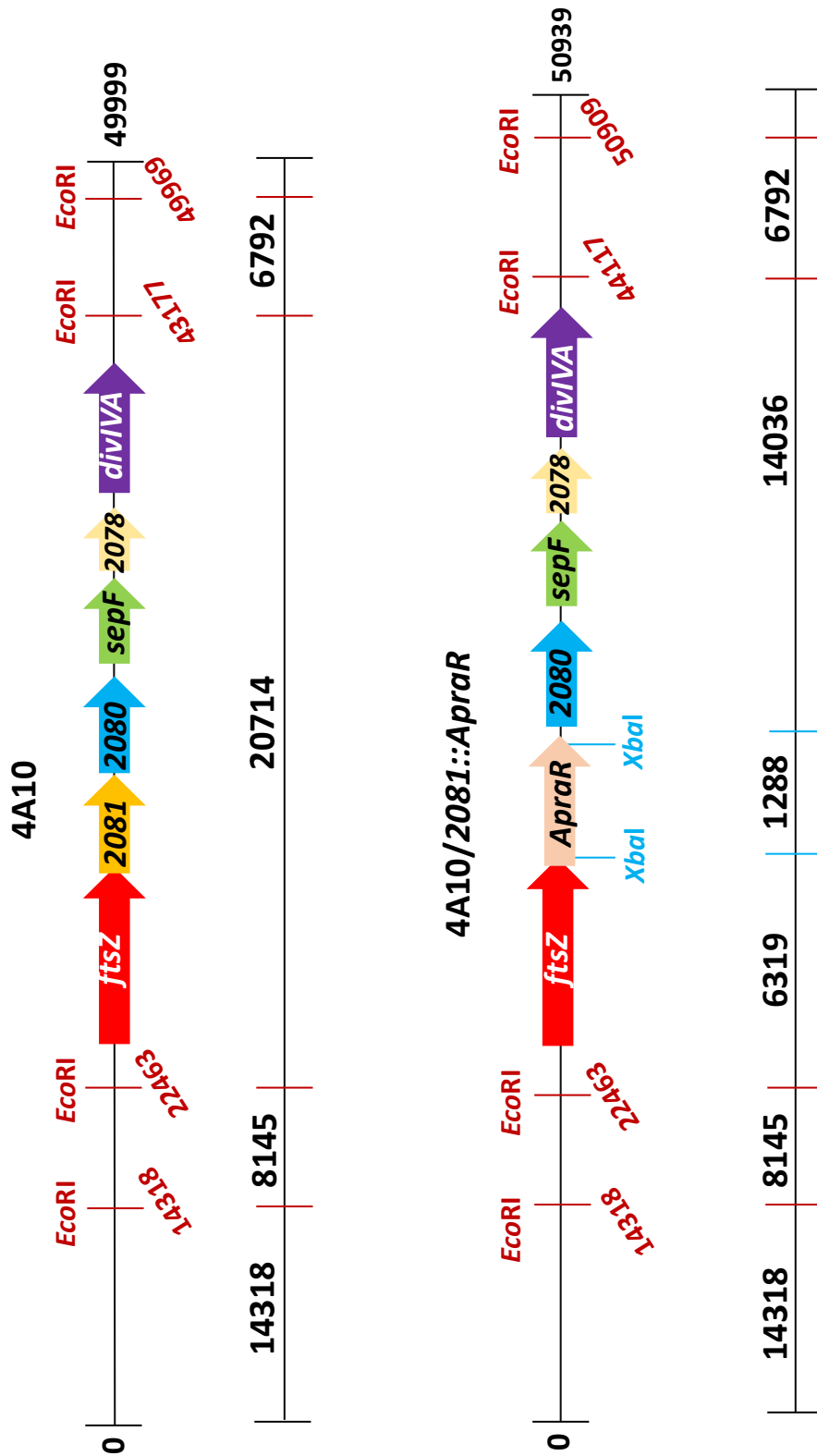


Figure 6.6. The gene map of the 4A10 cosmid and the 4A10/2081::ApraR cosmid highlighting the position of *EcoRI* and *XbaI* restriction enzyme cleavage sites and the subsequent fragment sizes generated by a restriction digest (bold red). The tilted numbers represent the location of the restriction sites using the cosmid numbering. The horizontal numbers represent the size of each restriction fragments (bp).

Table 6.1. The expected fragments that are generated by restriction digest using endonucleases *EcoRI* and *XbaI* of the wild-type 4A10 cosmid and 4A10/2081::*ApraR* cosmid. Shaded fragments represent those that remain the same in both cosmid digests.

4A10	4A10/2081:: <i>ApraR</i>
20714	-
14348	14348
-	14036
8145	8145
6792	6792
-	6319
-	1288

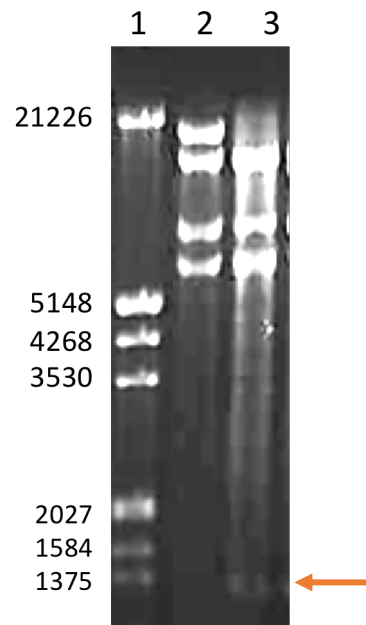


Figure 6.7. Confirmation of the mutant 4A10/2081::*ApraR* cosmid using restriction digest with *EcoRI* and *XbaI*. The restriction digest of the extracted cosmids were run on a 0.7% agarose. The wild-type 4A10 cosmid (lane 2) and 4A10/2081::*ApraR* cosmids (lane 3) were digested with *EcoRI* and *XbaI* and the digests were analysed on a 0.7% agarose gel. Lambda DNA cut with *EcoRI* and *HindIII* was used as a molecular weight marker (Lane 1), sizes shown in bp. The 1.3 kb fragment carrying the apramycin resistance cassette is shown by the orange arrow.

After confirmation of the cosmid 4A10/2081::*ApraR*, it was transformed into methylation-deficient *E.coli* strain ET12567/pUZ8002 and then conjugated into the wildtype *S. coelicolor* strain M145. Selection of exconjugants containing the apramycin cassette was achieved by overlaying plates using apramycin and nalidixic acid. To distinguish colonies that had undergone a double crossover event and thus contain a single copy of the gene cluster without the *2081* gene, we used replica plating to identify colonies that were sensitive to kanamycin but resistant to apramycin. The selected colonies identified as double crossover were streaked on SFM medium and spores of the *2081* mutant was collected for making stock for future analysis.

6.3 Confirmation of *2081* mutant strain

To confirm that the gene *2081* was successfully knocked out from the chromosome of *S. coelicolor*, chromosomal DNA was obtained from the *2081* mutant and was PCR tested using different primer pairs. We firstly used two external flanking primers of *2081* gene, one (FtsZ XbaNde FRW) located within the upstream gene *ftsZ* and the other (2080 Nde REV) situated in the downstream gene *2080*, to PCR test the extracted chromosomes of wild-type and $\Delta 2081$ mutant. With these two primers, PCR products were expected from both M145 wild-type and *2081* mutant but with different sizes. The size of apramycin disruption cassette (~1.3 kb) is larger than size of *2081* (729 bp), therefore the PCR product generated from the *2081* mutant chromosome (3303 bp) will be larger than the PCR product generated from the wild-type chromosome (2649 bp) (Figure 6.8). In addition, we used another two primers, one located in *ftsZ* gene and the other one situated in apramycin cassette, to further test the presence of apramycin resistant cassette in mutant strain. These primers will produce PCR products in *2081* mutant strain but not in wild-type, with expected sizes shown in table 6.2. All the expected PCR products were confirmed when the PCR

products were analysed on an agarose gel (Figure 6.9), confirming that the *2081* mutant was successfully generated.

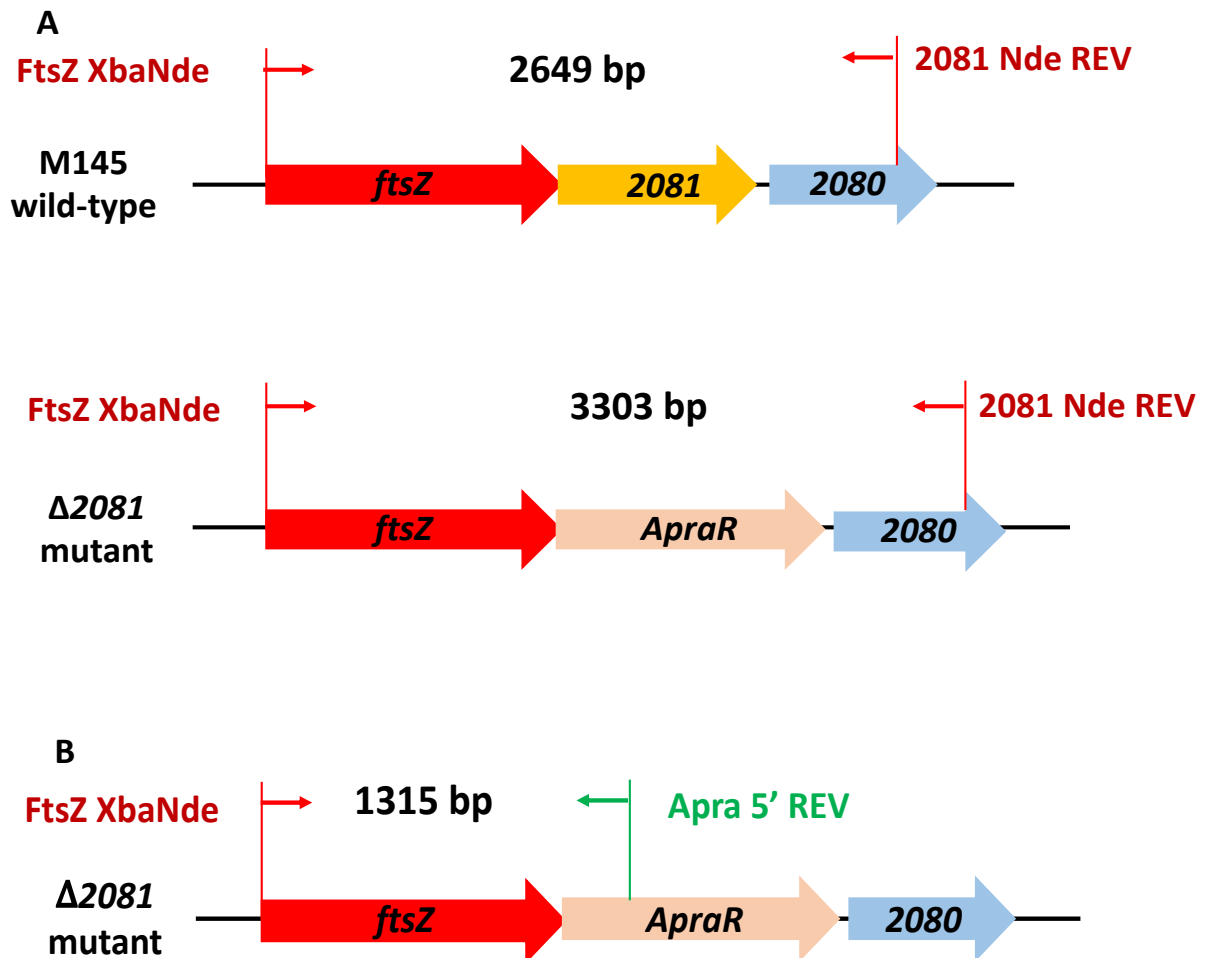


Figure 6.8. Experimental design for the confirmation of the *2081* mutant using PCR.

(A) The primers FtsZ XbaNde FRW and 2081 Nde REV were used to generate PCR products to test whether the *2081* gene was successfully replaced with the apramycin resistant disruption cassette in the chromosome of *S. coelicolor*. The expected sizes of PCR products showed difference in wild-type strain M145 and *2081* mutant strain due to the replacement of apramycin resistant cassette (*ApraR* cassette). (B) The primers FtsZ XbaNde FRW and *Apra* 5' REV will generate a PCR product only in the *2081* mutant.

Table 6.2. The expected size of PCR products using wild-type and the *2080* mutant chromosomal DNA as templates.

Oligos	Size in wild-type	Size in $\Delta 2081$ mutant
FtsZ XbaNde 2080NdeREV	2649 bp	3303 bp
FtsZ XbaNde Apra 5'REV	-	1315 bp

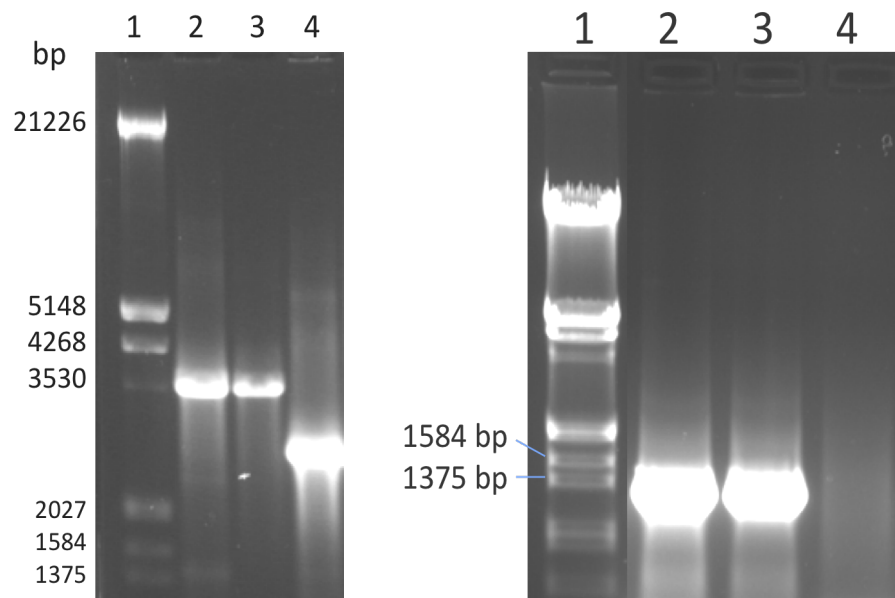


Figure 6.9. The gel analysis of the PCR products generated using chromosomal DNA of M145 wild-type and the *2081* mutant strains for confirmation of the *2081* mutant.

- A. Chromosome extracts from M145 wild-type and the *2081* mutant were PCR tested using primers FtsZ XbaNde FRW and 2080 Nde REV. Lane 1, the λ EcoRI-HindIII ladder, sizes shown in bp. Lane 2 and 3, two independent *2081* mutants. Lane 4, M145 wild-type.
- B. Chromosome extracts from M145 wild-type and the *2081* mutant were PCR tested using FtsZ XbaNde FRW and Apra 5' REV. Lane 1, λ EcoRI-HindIII ladder, sizes shown in bp. Lane 2 and 3, two independent *2081* mutants. Lane 4, M145 wild-type.

6.4 Characterisation of the *2081* mutant phenotype

6.4.1 Macroscopic analysis of the *2081* mutant

After we generated the mutant, the spores of wildtype and the *2081* mutant strains were grown on SFM medium at 30°C and observed daily to determine the phenotype. The fact that we generated a spore stock from the *2081* mutant suggested that the mutant phenotype is not as severe as that of the *sepF* mutant for example, where the white colonies prompted us to store hyphal fragments collected from cells grown on the surface of cellophane disks for storage. We monitored the



Figure 6.10. Macroscopic phenotype analysis of *2081* mutant strain.

Wild-type M145 and *2081* mutant strains were grown on SMF medium for 3 days. The plates were incubated and monitored at regular time intervals. It was observed that *2081* mutant produced the grey pigment associated with spore maturation, and its appearance was very similar to the wild-type strain M145.

phenotypes daily but we did not observe any major difference when the wild-type strain was compared to the *2081* mutant (Figure 6.10). After three days (72hrs), the

2081 mutant strain and wild-type M145 strain had very similar appearance which presented classic grey pigment associated with mature spores.

However, in some of the previous complementation experiments we found that the grey appearance of a bacterial lawn can be misleading, and it is wrong to assume no effect on sporulation. In fact, the $\Delta 2080/pMS82/\Delta P-sepF$ strain was grey when grown on SFM medium but its sporulation septation was severely affected (Chapter 5, Figure 5.5.2.4). To test whether the grey phenotype of the *2081* mutant reflected normal sporulation septation, we used fluorescence microscopy together with staining the cell walls (WGA-Alexa 488) and the cellular DNA (PI) analysing samples taken at different stages during development.

6.4.2 Microscopic analysis of *2081* mutant

We inoculated spores of the *2081* mutant onto SFM in rectangular patches and inserted coverslips at a 70° angle to the horizontal plane of the media. The hyphae were then visualized, using WGA-Alexa 488 for cell wall stain and PI for chromosomes, at regular intervals to follow the different stages of development.

When the first sample was collected and stained after 42 hours of growth, we observed that vegetative hyphae of the *2081* mutant developed hyphae as network of branching mycelium where the chromosome is dispersed throughout the hyphae (Figure 6.11 A), which remained same performance as wild-type. After 48 hours of growth, after aerial hyphae have formed, we could detect the somewhat curled hyphae starting to undergo the sporulation septation where single chromosomes were divided into compartments with condensed nucleoids, separated by sporulation septa. Although many of the sporulation septa was placed at regular

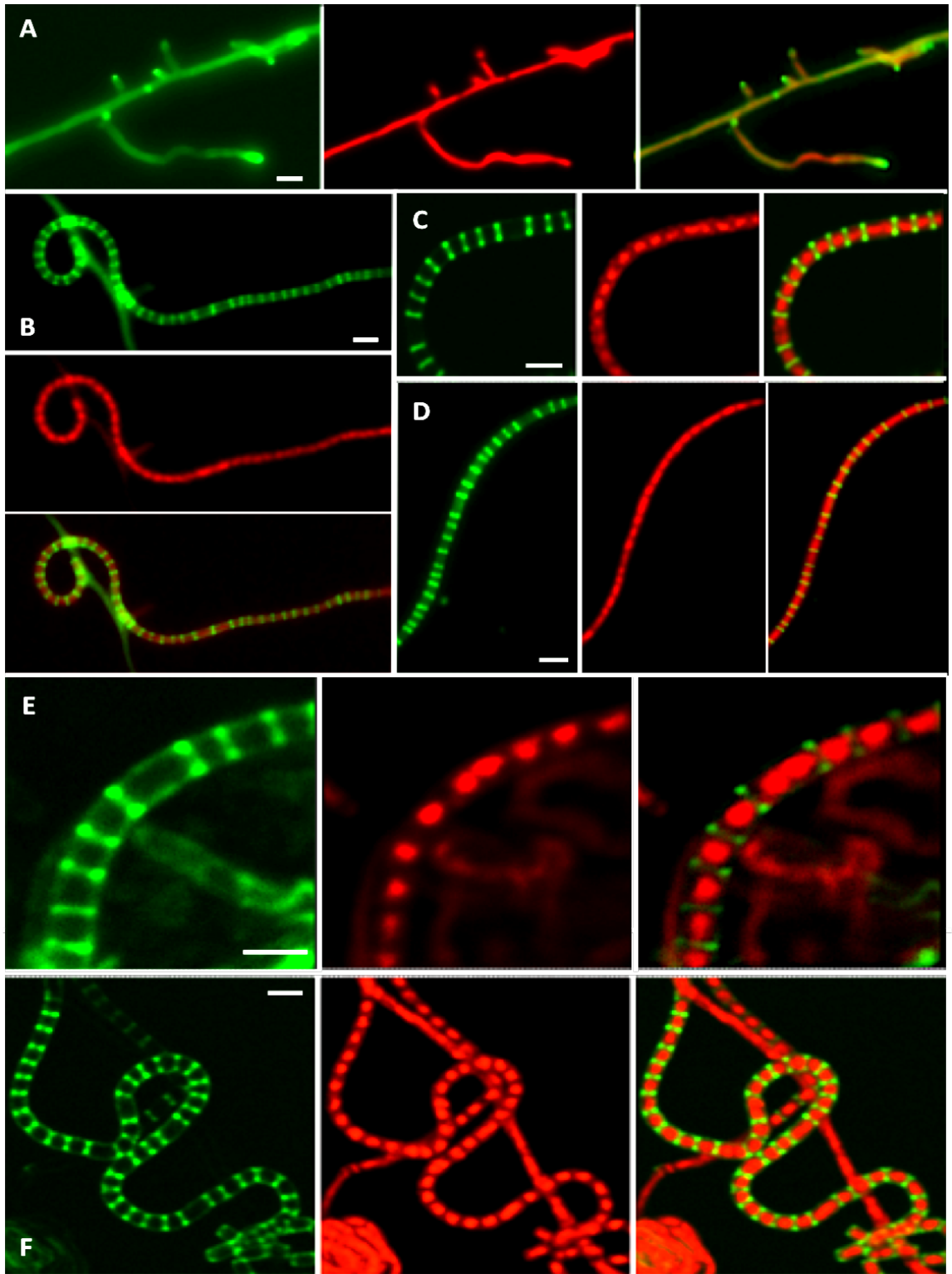


Figure 6.11. Fluorescence microscopy of the *2081* mutant strain.

Spores of the *2081* mutant strain were plated onto SFM medium and incubated at 30°C before staining with PI (red-DNA) and WGA-Alexa 488 (green-cell wall). (A) The vegetative hyphae, (B-F) septum development in the aerial hyphae. Size bar represents 1 μ m. A, B and D were generated using epi-fluorescence microscopy, C, E and F were generated using confocal microscopy.

into mature spores. We found septa laid down at uneven intervals throughout the aerial hyphae which often created compartments containing two chromosomes. This observation suggests that the *2081* mutant might have a subtle mutant phenotype that is different from the wild-type strain M145 (Figure 6.11 and 6.12).

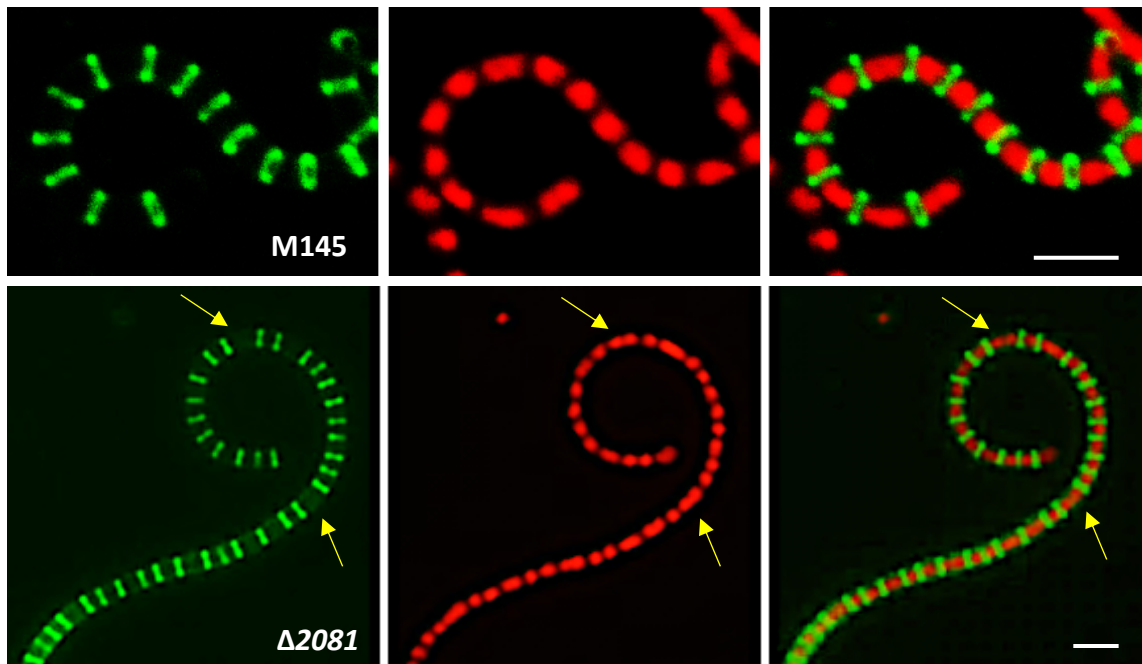


Figure 6.12. Sporulation septation in the wild-type M145 (top) and the *2081* mutant (bottom). Cell wall (green) stained with WGA-Alexa 488 (left) and DNA (red) stained with PI (middle) are shown, together with the overlaid image (right). Images were generated using confocal microscopy.

6.4.3 Quantitative analysis of septum placement in the *2081* mutant

To quantify the irregularity of septum placement observed in the *2081* mutant, we measured the distance between septa in both the *2081* mutant and wild-type M145 strains and compared the results. Images were analysed using the Zeiss Axiovision software which has a measurement tool, with data collated in excel and histograms generated. The frequency bar chart for the *2081* mutant strain was plotted against the wild-type strain to demonstrate the differences in septum placement in the *2081* mutant strain compared to that of the wild-type strain M145 (Figure 6.13).

The *2081* mutant strain had a larger range of distances between neighboring septa with some smaller and some larger than the average 1.09 μm . Interestingly, the median of both the wild-type and the *2081* mutant were around 1.1 μm , which is the average distance between two septa. The standard error is low, so we have confidence in the data (Figure 6.13). However, the *2081* mutant shows bimodal distribution, suggesting that the septa are either placed regularly or, in some cases, the septum is placed with around 1.8 μm distance, representing compartments with two chromosomes (Figure 6.12). Although this phenotype of the *2081* mutant is subtle, it is significant and confirmed that 2081 protein did effect septum formation in *S. coelicolor*.

<i>M145</i>		<i>2081</i>	
Mean	1.121725	Mean	1.162497
Standard Error	0.007687	Standard Error	0.007914
Median	1.1	Median	1.09
Mode	1.15	Mode	1.03
Standard Deviation	0.178472	Standard Deviation	0.307924
Sample Variance	0.031852	Sample Variance	0.094817
Range	1.61	Range	2.23
Minimum	0.76	Minimum	0.63
Maximum	2.37	Maximum	2.86
Count	539	Count	1514
Largest(1)	2.37	Largest(1)	2.86
Smallest(1)	0.76	Smallest(1)	0.63
Confidence Level(95.0%)	0.015101	Confidence Level(95.0%)	0.015523

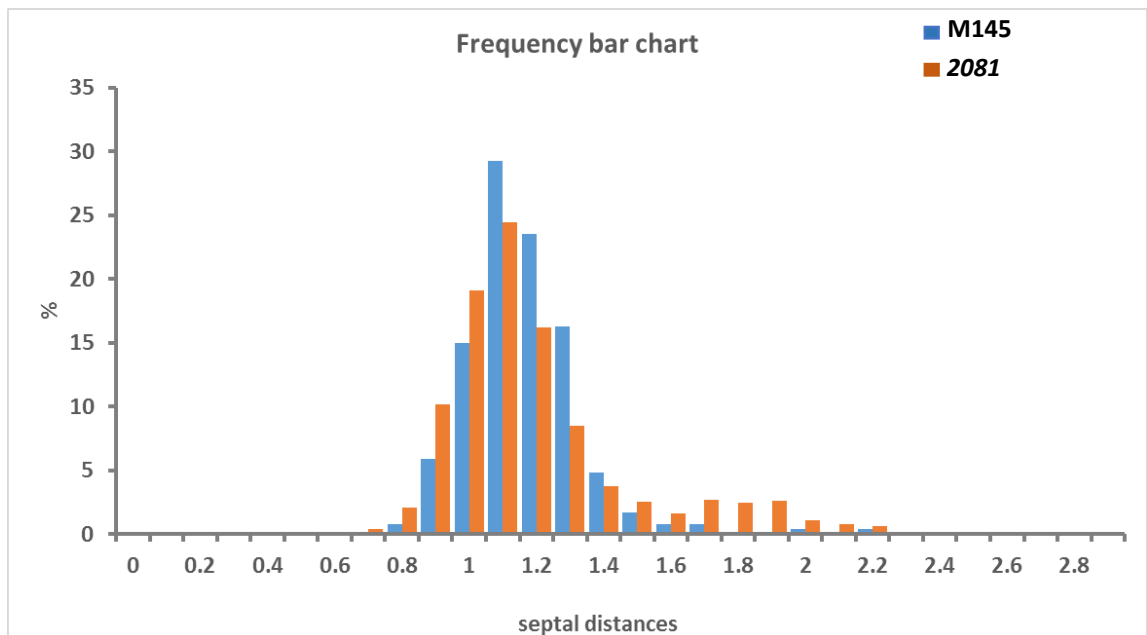


Figure 6.13. The statistical analysis of 2081 mutant strain. Top: General statistics of the septal distances measured. Bottom: Frequency bar chart is shown, the wild-type M145 is blue and the 2081 mutant is orange. 539 distances were measured for the wild-type strain and 1514 for the 2081 mutant strain. The unit of septal distances is μm .

6.5 Summary

The gene *2081* lies immediately downstream of, and most likely in operon with, *ftsZ*, which plays key role in cell division. Homologues of *2081* are found in many bacteria but their role is largely unknown.

- In this chapter we generated the *2081* gene knockout mutant using the PCR targeting.
- We have confirmed the generated mutant by performing a series of PCR reactions using chromosomal DNA extracted from the putative mutant strains.
- We characterized the mutant phenotype using fluorescence microscopy and found that this mutant produced unevenly spaced septa with ~10% of the compartments were larger, likely containing two chromosomes. This suggests that *2081* has a role in septum placement in *S. coelicolor*.
- We measured the distances between septa in the *2081* mutant, with wild-type strain M145 as a control. The statistical analysis showed that the *2081* mutant strain had a larger range of septal distances with a bimodal characteristics, with some compartments containing two chromosomes, hence some of the longer septal distances.
- We did not have time to confirm the mutant phenotype by complementing the knockout mutant.

Acknowledgements

We are very grateful to Alan Lau for contribution to the experiments.

Chapter 7 General Discussion

Streptomyces have a complex life cycle. Firstly, unlike in uni-genomic bacteria, where cell growth and cell division are essentially interlinked, in *Streptomyces* cellular growth can take place in the absence of cell division. The two phases, cellular growth and fully completed cell division are separated both in time and space. Cell division in *Streptomyces* differs from cell division in most bacteria, mainly because of its mycelial life style. There are two different types of cell division in *Streptomyces*: cytokinesis and cell fission are only fully completed during sporulation of the aerial hyphae, while in the vegetative hyphae, cell division is suspended at the formation of cross-walls, a stage, which is not followed by cell-cell separation (McCormick and Flardh, 2012; Claessen *et al.*, 2014; Kelemen, 2017). Secondly, the regulation of cell division is also very unique. In most model bacteria, such *E. coli* and *B. subtilis*, cell division and septum formation is dependent on FtsZ polymerization into the so called Z-ring. FtsZ polymerization at the mid-point of the cells is primarily negatively controlled, preventing division septum formation at places near the poles (Min system) or avoiding damage to the nucleoid (NO system) (Huang *et al.*, 2013). Whereby the septum is formed only at the middle of the cell and safely out of the way when the DNA is duplicated. This immediately highlights a major difference in *Streptomyces*, as the long hyphae of do not have a clear mid-cell position. In addition, the positive regulators, such as ZipA, FtsA and SepF, can actively promote the stabilisation of the Z-ring and its anchor to the cell membrane, which are necessary to complete division (Pichoff and Lutkenhaus, 2002; Willemsse *et al.*, 2011). However *Streptomyces* lacks the Min and NO systems and it does not have ZipA or FtsA, therefore *Streptomyces* possesses only SepF, amongst the proteins that control FtsZ organisation in other bacteria. It is not clear how septum placement is governed properly in time and space in the long and multi-nucleoid hyphae of *Streptomyces* during sporulation. Therefore we investigated three genes which potentially play indispensable role in cell division.

There were several major questions we attempted to address. What are the specific proteins that control the positioning of the septum formation temporally and spatially in aerial hyphae? And how do they avoid the damage to the chromosomes during synchronous multiple cell division in multi-nucleoid hyphae? One interesting place to start our investigation is the *dcw* cluster which contains genes related to cell wall synthesis and cell division. The function of several genes between *ftsZ* (*SCO2082*) and *divIVA* (*SCO2077*) have not been well characterised, despite the fact they are downstream of *ftsZ* in many Gram-positive bacteria, including *Streptomyces*. All four genes located in this region are gene *SCO2081*, *SCO2080*, *SCO2079* (*sepF*) and *SCO2078*. In this study we mainly focus on the first three genes due to special role of SepF which was previously shown to tether the Z-ring to the membrane in *B. subtilis* and promote FtsZ protofilament formation (Hamoen *et al.*, 2006; Ishikawa *et al.*, 2006).

Therefore, in this study we set out to begin the characterization of these genes in *Streptomyces* to better understand their role in the interplay with FtsZ and its polymerisation during sporulation. First, we created the knockout mutant strains of these genes and explored their mutant phenotypes.

SepF, required for septation in *S. coelicolor*

SepF is a protein involved in septum development and was first identified by Hamoen *et al* (2005) and Ishikawa *et al* (2006). SepF was found to be essential for the completion of cell division in *B. subtilis*, but not for the initiation of septation. SepF has also been discovered to interact with both the cell membrane and the C-terminal end of FtsZ and is in fact responsible for the correct localization and ring formation of FtsZ (Duman, 2013). This protein is conserved among Gram-positive bacteria but it is not essential for viability in *B. subtilis*. However, in *B. subtilis* SepF is not the only protein that can sequester FtsZ to the membrane, FtsA and ZipA also play a role in membrane anchoring FtsZ. In contrast, *Streptomyces* lacks FtsA and ZipA but its

chromosome encodes three SepF homologues, SepF1, SepF2 and SepF3. SepF2 encoded by gene *SCO2079* shares the highest identity with SepF of *B. subtilis*. In addition, *sepF2* (*SCO2079*) is located in the cell division gene cluster containing the essential cell division gene *ftsZ*. This might suggest that the role of SepF2 potentially is more linked to the role of FtsZ assembly during cell division. Therefore we focused on SepF2, using the designation of SepF in this study.

We generated a *sepF* knockout mutant strain by replacement of *sepF* gene with an apramycin resistant cassette using PCR-directed mutagenesis (Gust *et al.*, 2002) to characterise its role in cell division in *S. coelicolor*. The *sepF* mutant strain showed a severe developmental mutant phenotype. When the wild-type strain presented classic grey pigment associated with mature spores, the *sepF* mutant produced white colonies with blue colony surface on solid media, which suggests that septation in mutant is blocked in sporulation stage. Microscopic analysis of the *sepF* mutant strain revealed that the deletion of the *sepF* gene resulted in severe defect in generation of septa, which is consistent with the white colonies of its macroscopic phenotype. In wild-type strain M145, we followed the formation of the vegetative septa in vegetative hyphae and the regularly placed sporulation septa in the aerial hyphae generating a ladder-like structure. The *sepF* mutant fail to develop any septation during both vegetative and aerial growth. However, the absence of the septa did not affect chromosome segregation. The chromosomes in the aerial hyphae of the *sepF* mutant still underwent some segregation albeit without generating fully segregated single chromosomes.

To confirm that the noticeable non-sporulating phenotype of the *sepF* mutant is caused by deletion of gene *sepF*, we carried out complementation experiments with different constructs containing the *sepF* gene. We generated three different constructs and introduced them into the *sepF* mutant to monitor their development. Firstly, the construct ΔP -*sepF* only contained *sepF* and a very short upstream sequence, potentially containing only one of the promoters of *sepF* (Jeong *et al.*, 2016) was induced into the *sepF* mutant strain generating $\Delta sepF/pMS82/\Delta P$ -*sepF*. This strain produced grey pigments, which was identical to the wild-type strain. However,

microscopic analysis confirmed that $\Delta sepF/pMS82/\Delta P-sepF$ did not look like the wild-type, as we observed deformed septa placed at uneven positions. Some septa were spiral shaped and enclosed either quite small or large patches of chromosomes, which suggests this construct did not contain a DNA fragment that fully expressed SepF. The second construct *2080-sepF* that contained the *sepF* gene and its upstream gene *2080* confirmed this. When we induced this construct into the *sepF* mutant strain we found that the wild-type phenotype was fully restored in mutant strain both macroscopically and microscopically. In this strain, $\Delta sepF/pMS82/2080-sepF$ we can see the regular septa laid down in the aerial hyphae between two evenly segregated chromosomes. However, we were not sure of the location of the *sepF* promoters until Jeong (2016) provided some large scale data on *Streptomyces* promoters. Our last construct, *P-sepF* contained the *sepF* gene and its putative promoters, and was introduced into the *sepF* mutant strain generating $\Delta sepF/pMS82/P-sepF$. This strain presented the same phenotype as that of the wild-type strain which produced grey pigment and regular septation during sporulation.

As the mutant generated was fully confirmed, we can state that the *sepF* mutant failed to generate septa in general, which suggests that SepF has a key role in septation in *Streptomyces*. In *B. subtilis*, the *sepF* mutant was not affected in the early stages of septation and only the septum closure was defective in the *sepF* mutant (Hamoen *et al.*, 2006). But *B. subtilis* possesses FtsA and ZipA that are anchoring FtsZ to the membrane during the early stages of septum formation. It seems, that lack of FtsA and ZipA in *Streptomyces*, and in the other *Actinomycetes*, such as *M. tuberculosis*, SepF has a major role in FtsZ positioning. It is not clear whether there is any structural difference in the SepF proteins from the *Actinomycetes* themselves that supports this major role. It is also intriguing that *Streptomyces* has 3 SepF proteins, and it will be important to characterise the role of the other two SepF proteins and whether they are also involved in cell division.

SepF localisation to the future septum sites

After the characterisation of the *sepF* mutant strain, we turned to the analysis of SepF localisation to explore how it aids FtsZ polymerisation in *S. coelicolor* during sporulation. In *B. subtilis*, SepF oligomerises to form large rings that bundle FtsZ protofilaments into tubular structures similar to microtubules (Gündoğdu *et al.*, 2011). It is possible that *S. coelicolor* FtsZ protofilaments are bundled via a similar mechanism. In order to establish that, future work is needed to overexpress and purify both SepF and FtsZ from *E. coli* and perform *in vitro* assays using the purified proteins.

SepF has been localised in *B. subtilis* with the protein accumulating at the sites of cytokinesis, (Hamoen *et al.*, 2006). The suggested model positions SepF to the FtsZ ring after the initial invagination of the cell membrane (Duman *et al.*, 2013), which suggests that SepF is positioned after FtsZ polymerisation. SepF localization was monitored also in *M. tuberculosis* (Gola *et al.*, 2015) and in the cyanobacterium, *Synechocystis* (Marbouty *et al.*, 2009), in both cases SepF localised to the developing septum.

We generated SepF-Egfp translational fusions using three different constructs and approaches and monitored fluorescence during *Streptomyces* development. The first approach generated *S. coelicolor* M145/*sepF::sepF-egfp-ApraR*, where the *sepF* gene was replaced by the *sepF-egfp* fusion in the original chromosomal location. The strain M145/*sepF::sepF-egfp-ApraR* had a wild-type phenotype, which confirmed that the SepF-Egfp fusion in this strain is fully functional. The second and third approach introduced the *sepF-egfp* fusion using a plasmid that integrated into a specific chromosomal site in a single copy. Constructs pMS82/2080-*sepF-egfp* and pMS82/P-*sepF-egfp* contained 848 bp and 343 bp DNA upstream of the translational start of *sepF*, respectively. Introduction of both of these constructs into the *sepF* knockout mutant restored the wild-type phenotype. This confirms that SepF-Egfp is functional and expresses at native levels even when using the shortest, 343 bp

upstream sequences. This suggests that in the plasmid pMS82/*sepFp2-egfp* contained all that was needed for *sepF* transcription, which was suggested by the RNA Seq data by Young *et al.*, 2016. Monitoring SepF-Egfp throughout the developmental cycle of the three different constructs of *S. coelicolor* generated the same localisation patterns. SepF-Egfp localised to positions of possible future cross-wall formation or septation in the vegetative and aerial mycelium, respectively. SepF-Egfp formed ring-like structures that were visualised using confocal microscopy and occasionally spiral-like patterns were observed at the early stages. SepF-Egfp patterns looked like lines perpendicular to the hyphal wall using epi-fluorescence microscopy, or ladders in the aerial hyphae. When fully formed, these ladders had the ~1.2 μm spacing that is characteristic of the distance between sporulation septa. The SepF-Egfp ladders in the aerial hyphae formed well before any signs of septation and even chromosome segregation. However, SepF-Egfp signal were visible at places where there was less or no DNA staining, which might suggests that SepF localises to places devoid of DNA.

We assume that SepF and FtsZ interacts in *Streptomyces*, as this was shown in *B. subtilis* and *M. tuberculosis* (Hamoen *et al.*, 2006; Gupta *et al.*, 2009; Gola *et al.*, 2015) and our bioinformatics analysis revealed that the residues in SepF that are involved in making contact with FtsZ are conserved and are present in the *Streptomyces* SepFs (Figure 3.1.3). What we cannot state at this stage is exactly what the order of appearance is of FtsZ and SepF, and whether any of them is dependent on the other. For this, we need to localise FtsZ in the *sepF* mutant and SepF in the *ftsZ* mutant. We have tried to monitor FtsZ-Egfp in the *sepF* mutant and we could not detect any FtsZ-Egfp rings, instead, some green foci could be seen in the aerial hyphae that did not develop into rings. This suggest that SepF is required for FtsZ polymerization at the correct location. We could not test the reciprocal experiment, which is to monitor SepF-Egfp in the *ftsZ* mutant as we do not have an *ftsZ* knockout in the lab. The current model based on studies in *B. subtilis*, is that SepF accumulates at initial invagination of the cell membrane (Duman *et al.*, 2013), which is a late event. It is conceivable that in *Streptomyces*, and maybe also amongst other *Actinomycetes*, SepF is required for FtsZ ring formation and acts much earlier than in *B. subtilis*. To

test this we, could use membrane stains and check whether SepF-Egfp localises at membrane invagination sites. What we definitely can say is that SepF-Egfp localised at positions where there was a lack of DNA staining. This might suggest that either SepF is involved in chromosome organisation leading to full chromosome segregation later, or that SepF localises to nucleoid free zones.

2080, an role in cell wall/ septum synthesis?

Most of the genes in the *dcw* cluster for proteins involved in cell division and cell-wall biosynthesis have been studied extensively and their functions have been well characterized. Little is known of the genes *SCO2080* that lie immediately downstream of *ftsZ* (*SCO2082*) on the *S. coelicolor* genome. *SCO2080* is wide spread in Gram-positive bacteria, and particularly in firmicutes (*Bacillus*, *Staphylococcus*) and in actinobacteria, but are also occasionally found in Gram-negative bacteria.

The gene *SCO2080* was previously implicated in the production of D-amino acids for cell-wall synthesis (Kolodkin-Gal *et al.*, 2010). During bacterial cell division, peptidoglycan synthesis needs to be coordinated with the increase of the cell size, timely genome replication, segregation and septum synthesis followed by cell fission. Mutants of *E. coli* lacking the *yggS*, the orthologue of *SCO2080*, had a radical change in the amino acid pool, with enhanced concentrations of the branched chain amino acids valine and leucine, as well as of α -ketoglutarate (Ito *et al.*, 2013). This most likely led to reduced levels of coenzyme A (CoA), which was supported by the full restoration of *yggS* mutants by the CoA precursor pantothenate (Vitamin B5). These suggest a role for *SCO2080* in amino acid metabolism.

We generated a *2080* knockout mutant strain by replacement of *2080* gene with an apramycin resistant cassette using PCR-directed mutagenesis (Gust *et al.*, 2002) to characterise its role in cell division in *S. coelicolor*. In this work, the *2080* mutant strain produced white colonies, which suggested that the mutant was blocked in sporulation septation. Monitoring microscopically the *2080* mutant strain indicated

that the absence of gene *2080* resulted in a phenotype that was very similar to that of the *sepF* mutant, apart from the fact that this mutant did produce some vegetative septa and it did not have a blue aerial surface when grown on solid SFM medium.

However, when we attempted to complement this *2080* mutant using a range of constructs carrying the *2080* gene, we did not get any complementation. This raised the possibility that the deletion of the *2080* gene in this mutant caused a polar effect on its downstream gene *sepF*.

Therefore, we used the three constructs which we previously used for the complementation of the *sepF* mutant strain. Confirming that the *2080* mutant indeed had a polar effect on the gene *sepF*, all three constructs restored the grey pigment production when introduced into the *2080* mutant strain. However, microscopic analysis revealed that the construct ΔP -*sepF* containing only one of the *sepF* promoters, only partially complemented the *2080* mutant. In the strain $\Delta 2080/pMS82/\Delta P$ -*sepF*, we detected many half closed septa and irregularly segregated chromosomes. The second construct containing *sepF* and its putative promoters (Jeong *et al.*, 2016) restored regular septum formation when introduced to the *2080* mutant, although we observed some delay in development in this $\Delta 2080/pMS82/P$ -*sepF* strain, together with some signs that the septation was not as regular as that in the wild-type. However, to confirm this, we need to provide statistical analysis of the septal distances in this strain. The third construct, which contain both the *2080* and *sepF* genes, fully restored the wild-type phenotype with regular septation and even septal distances.

What is then the role of *2080* in septation in *Streptomyces*? We cannot answer this question, yet. But after the confirmation of the phenotype of the $\Delta 2080/pMS82/P$ -*sepF* strain, together with the generation of a new knockout strain for *2080*, where the two promoters of *sepF* are not affected, we will be able to answer this question. More studies are also needed to address whether the *2080* protein is an amino acid racemase and if so, how the generation of D-amino acids affect septation.

Can 2081 protein affect the efficiency of septum synthesis?

It is well known that the tubulin-like protein FtsZ is essential for septation process. There are still some genes in the Streptomyces division and cell wall (dcw) cluster that remain uncharacterized. One notable example is the gene SCO2081 which locates adjacently downstream of *ftsZ* and is slightly overlaps with *ftsZ*. In all Streptomyces genomes analysed, *ftsZ*, *2081* and *2080* most likely form an operon, with translational coupling between *ftsZ* and *2081* (overlapping start and stop codons), suggesting the gene 2081 may play a prominent role in cell division (Świątek *et al.*, 2013; Świątek, 2012). By bioinformatics studies, 2081 was identified as a Cu-oxidase which is able to oxidise their substrate by accepting electrons at a mononuclear copper center and transferring them to a trinuclear copper center (Vashchenko *et al.*, 2013).

We generated the 2081 knockout mutant strain by replacement of 2080 gene with an apramycin resistant cassette in *S. coelicolor*. This mutant did not show an obvious mutant phenotype, as it produced grey pigment in a similar manner to the wild-type strain. However, microscopic analysis of the 2081 mutant strain revealed that there is a subtle but significant difference between septal distances in the 2081 mutant and the wild-type strain. To understand the irregularity of septum placement observed in 2081 mutant, we measured the distances between septa in both 2081 mutant and wild-type M145 and compared the results. From this analysis, the 2081 mutant generated bimodal distribution of septal distances, suggesting that this mutant occasionally failed to generate a septum, producing the occasional “double-sized” compartments with more than one nucleoid. This phenotype was so subtle after the initial observation that we did not create a complementing clone. However, as we now have a tool (septal distance measurements), the mutant phenotype will need to be confirmed by complementation. This again will need some consideration, to generate a construct that will fully express 2081.

The protein 2081 will also need to be characterised to answer the question whether and how a copper oxidase can influence the efficiency of cell division. It will be also interesting to test whether FtsZ interacts with either 2080 or 2081, or whether 2080 and 2081 interacts with each other or with SepF. These interactions can be tested using the bacterial two hybrid assays initially and further confirmed by biochemical assays.

- Abeles, A. L., Friedman, S. A., and Austin, S. J. (1985). Partition of unit-copy miniplasmids to daughter cells. *J Mol Biol* 185, 261-272.
- Adams, D.W., Errington, J. (2009). Bacterial cell division: assembly, maintenance and disassembly of the Z ring. *Nat Rev Microbiol* 7, 642–653.
- Adams, D.W., Wu L.J., Errington, J. (2015). Nucleoid occlusion protein Noc recruits DNA to the bacterial cell membrane. *EMBO J* 34, 491–501.
- Addinall, S.G., Lutkenhaus J. (1996). FtsZ-spirals and -arcs determine the shape of the invaginating septa in some mutants of *Escherichia coli*. *Mol Microbiol* 22, 231–237.
- Aldridge, B.B., Fernandez-Suarez, M., Heller, D., Ambravaneswaran, V., Irimia, D., Toner, M., and Fortune, S.M. (2012). Asymmetry and aging of mycobacterial cells lead to variable growth and antibiotic susceptibility. *Science* 335, 100-104.
- Allan, I., and Pearce, J.H. (1983). Differential amino acid utilization by *Chlamydia psittaci* (strain guinea pig inclusion conjunctivitis) and its regulatory effect on chlamydial growth. *J Gen Microbiol* 129, 1991-2000.
- Aussel, L., Barre, F.X., Aroyo, M., Stasiak, A., Stasiak, A.Z., and Sherratt, D. (2002). FtsK is a DNA motor protein that activates chromosome dimer resolution by switching the catalytic state of the XerC and XerD recombinases. *Cell* 108, 195-205.
- Awasthy, D., Bharath, S., Subbulakshmi, V. (2012). Alanine racemase mutants of *Mycobacterium tuberculosis* require D-alanine for growth and are defect. *Microbiology*, 158, 319–327.
- Bagchi, S., Tomenius, H., Belova, L.M., and Ausmees, N. (2008). Intermediate filament-like proteins in bacteria and a cytoskeletal function in *Streptomyces*. *Mol Microbiol* 70, 1037-1050.
- Barák, I., and Wilkinson, A.J. (2007). Division site recognition in *Escherichia coli* and *Bacillus subtilis*. *FEMS Microbiol Rev* 31: 311–326.
- Beall, B., Lutkenhaus, J. (1992). Impaired cell division and sporulation of a *Bacillus subtilis* strain with the *ftsA* gene deleted. *J Bacteriol* 174, 2398–2403.
- Beall, B., Lowe, M., Lutkenhaus J. (1988). Cloning and characterization of *Bacillus subtilis* homologs of *Escherichia coli* cell division genes *ftsZ* and *ftsA*. *J Bacteriol* 170, 4855–4864.
- Bentley, S.D., Chater, K.F., Cerdeno-Tarraga, A.M., Challis, G.L., Thomson, N.R., James, K.D., Harris, D.E., Quail, M.A., Kieser, H., Harper, D., *et al.* (2002). Complete genome

sequence of the model actinomycete *Streptomyces coelicolor* A3(2). *Nature* 417, 141-147.

Bernhardt, T.G., and de Boer, P.A. (2003). The *Escherichia coli* amidase AmiC is a periplasmic septal ring component exported via the twin-arginine transport pathway. *Molecular microbiology* 48, 1171-1182.

Bernhardt, T.G., de Boer, P.A. (2005). SlmA, a nucleoid-associated, FtsZ binding protein required for blocking septal ring assembly over Chromosomes in *E. coli*. *Mol Cell* 18, 555–564.

Bi, E.F., Lutkenhaus, J. (1991). FtsZ ring structure associated with division in *Escherichia coli*. *Nature* 354,161–164.

Bibb, M. J. (2005). Regulation of secondary metabolism in streptomycetes. *Curr Opin Microbiol* 8, 208- 215.

Bigot, S., Corre, J., Louarn, J.M., Cornet, F., and Barre, F.X. (2004). FtsK activities in Xer recombination, DNA mobilization and cell division involve overlapping and separate domains of the protein. *Mol Microbiol* 54, 876-886.

Bramhill, D., Kornberg, A. (1988). Duplex opening by dnaA protein at novel sequences in initiation of replication at the origin of the *E. coli* chromosome. *Cell* 52,743–755.

Brown, P.J., de Pedro, M.A., Kysela, D.T., Van der Henst, C., Kim, J., De Bolle, X., Fuqua, C., and Brun, Y.V. (2012). Polar growth in the Alphaproteobacterial order Rhizobiales. *Proc Natl Acad Sci U S A* 109, 1697-1701.

Buddelmeijer, N., and Beckwith, J. (2004). A complex of the *Escherichia coli* cell division proteins FtsL, FtsB and FtsQ forms independently of its localization to the septal region. *Mol Microbiol* 52, 1315-1327.

Bush, M.J., Bibb, M.J., Chandra, G., Findlay, K.C., Buttner, M.J. (2013). Genes required for aerial growth, cell division, and chromosome segregation are targets of WhiA before sporulation in *Streptomyces venezuelae*. *MBio* 4, e00684–e00613

Bush, M.J., Tschowri, N., Schlimpert, S., Flardh, K., Buttner, M.J. (2015). c-di-GMP signalling and the regulation of developmental transitions in *streptomycetes*. *Nat Rev Microbiol* 13,749–760..

Bush, M.J., Chandra, G., Bibb, M.J., Findlay, K.C., Buttner, M.J. (2016). Genome-wide ChIP-seq analysis shows that WhiB is a transcription factor that co-controls its regulon with WhiA to initiate developmental cell division in *Streptomyces*. *MBio* 7, e00523–e00516

- Cabeen, M.T., and Jacobs-Wagner, C. (2005). Bacterial cell shape. *Nat Rev Microbiol* 3, 601-610
- Cabre, E.J., Monterroso, B., Alfonso, C., Sanchez-Gorostiaga, A., Reija, B., Jimenez, M., Vicente, M., Zorrilla, S., and Rivas, G. (2015). The Nucleoid Occlusion SImA Protein Accelerates the Disassembly of the FtsZ Protein Polymers without Affecting Their GTPase Activity. *PLoS One* 10, e0126434.
- Cameron, T.A., Zupan, J.R., and Zambryski, P.C. (2015). The essential features and modes of bacterial polar growth. *Trends Microbiol* 23, 347-353.
- Carballido-Lopez, R., and Errington, J. (2003). A dynamic bacterial cytoskeleton. *Trends Cell Biol* 13, 577-583.
- Carballido-Lopez, R., Formstone, A., Li, Y., Ehrlich, S.D., Noirot, P., and Errington, J. (2006). Actin homolog MreBH governs cell morphogenesis by localization of the cell wall hydrolase LytE. *Dev Cell* 11, 399-409.
- Cha, J.H., and Stewart, G.C. (1997). The divIVA minicell locus of *Bacillus subtilis*. *J Bacteriol* 179, 1671-1683.
- Chater, K.F. (1993). Genetics of differentiation in *Streptomyces*. *Annu Rev Microbiol* 47, 685-713.
- Chen, Y., Bjornson, K., Redick, S.D., Erickson, H.P. (2005). A rapid fluorescence assay for FtsZ assembly indicates cooperative assembly with a dimer nucleus. *Biophys J* 88, 505-514.
- Chen, Y, Erickson, H.P. (2005). Rapid in vitro assembly dynamics and subunit turnover of FtsZ demonstrated by fluorescence resonance energy transfer. *J Biol Chem* 280, 22549-22554..
- Chen, Y., Erickson, H.P. (2009). FtsZ filament dynamics at steady state: subunit exchange with and without nucleotide hydrolysis. *Biochemistry* 48, 6664-6673.
- Cho, H., Mcmanus, H.R., Dove, S.L., Bernhardt, T.G. (2011). Nucleoid occlusion factor SImA is a DNA-activated FtsZ polymerization antagonist. *Proc Natl Acad Sci U S A* 108, 3773-3778.
- Claessen, D., Rozen, D. E., Kuipers, O. P., Sogaard-Andersen, L. and van Wezel, G. P. (2014). Bacterial solutions to multicellularity: a tale of biofilms, filaments and fruiting bodies. *Nat Rev Micro- biol* 12, 115-124.
- Dai, K., Xu, Y., Lutkenhaus, J. (1993). Cloning and characterization of ftsN, an essential cell division gene in *Escherichia coli* isolated as a multicopy suppressor of ftsA12(Ts).

J Bacteriol 175, 3790–3797.

Dajkovic, A., Mukherjee, A., Lutkenhaus, J. (2008). Investigation of regulation of FtsZ assembly by SulA and development of a model for FtsZ polymerization. J Bacteriol 190, 2513–2526.

Dalton, K.A., Thibessard, A., Hunter, J.I., and Kelemen, G.H. (2007). A novel compartment, the 'subapical stem' of the aerial hyphae, is the location of a sigN-dependent, developmentally distinct transcription in *Streptomyces coelicolor*. Mol Microbiol 64, 719-737.

Daniel, R.A., and Errington, J. (2003). Control of cell morphogenesis in bacteria: two distinct ways to make a rod-shaped cell. Cell 113, 767-776.

Datsenko, K.A., and Wanner, B.L. (2000). One-step inactivation of chromosomal genes in Escherichia coli K-12 using PCR products. Proc Natl Acad Sci U S A 97, 6640-6645.

Davis, M.A., Martin, K.A., and Austin, S.J. (1992). Biochemical activities of the parA partition protein of the P1 plasmid. Mol Microbiol 6, 1141-1147

De Boer, P.A. (2010). Advances in understanding E. coli cell fission. Curr Opin Microbiol 13, 730–737.

De Boer, P.A., Crossley, R.E., Rothfield, L. (1989). A division inhibitor and a topological specificity factor coded for by the minicell locus determine proper placement of the division septum in *E. coli*. Cell 56, 641–649.

De Boer, P.A., Crossley, R., Rothfield, L. (1992). The essential bacterial cell-division protein FtsZ is a GTPase. Nature 359, 254–256.

Dedrick, R. M., Wildschutte, H. and McCormick, J. R. (2009). Genetic interactions of smc, ftsK, and parB genes in *Streptomyces coelicolor* and their developmental genome segregation phenotypes. J Bacteriol 191, 320-332.

Defeu Soufo, H.J., and Graumann, P.L. (2006). Dynamic localization and interaction with other *Bacillus subtilis* actin-like proteins are important for the function of MreB. Mol Microbiol 62, 1340-1356.

Ditkowski, B., Holmes, N., Rydzak, J., Donczew, M., Bezulska, M., Ginda, K., Kedzierski, P., Zakrzewska-Czerwinska, J., Kelemen, G.H., and Jakimowicz, D. (2013). Dynamic interplay of ParA with the polarity protein, Scy, coordinates the growth with chromosome segregation in *Streptomyces coelicolor*. Open Biol 3, 130006.

Doi, M., Wachi, M., Ishino, F., Tomioka, S., Ito, M., Sakagami, Y., Suzuki, A., and

Matsuhashi, M. (1988). Determinations of the DNA sequence of the mreB gene and of the gene products of the mre region that function in formation of the rod shape of *Escherichia coli* cells. *J Bacteriol* *170*, 4619-4624.

Dominguez-Cuevas, P., Porcelli, I., Daniel, R.A., and Errington, J. (2013). Differentiated roles for MreB-actin isologues and autolytic enzymes in *Bacillus subtilis* morphogenesis. *Mol Microbiol* *89*, 1084-1098.

Dominguez-Escobar, J., Chastanet, A., Crevenna, A.H., Fromion, V., Wedlich-Soldner, R., and Carballido-Lopez, R. (2011). Processive movement of MreB-associated cell wall biosynthetic complexes in bacteria. *Science* *333*, 225-228.

Donachie, W.D., Begg, K.J., Lutkenhaus, J.F., Salmond, G.P., Martinez-Salas, E., Vincente, M. (1979). Role of the *ftsA* gene product in control of *Escherichia coli* cell division. *J Bacteriol* *140*, 388–394.

Donachie, W.D. (1993). The cell cycle of *Escherichia coli*. *Annu Rev Microbiol* *47*, 199-230.

Du, S., Lutkenhaus, J. (2014). SlmA antagonism of FtsZ assembly employs a two pronged mechanism like MinCD. *PLoS Genet* *10*, e1004460.

Duman, R. *et al.* (2013). Structural and genetic analyses reveal the protein SepF as a new membrane anchor for the Z ring. *PNAS* *110* (48), E4601-E4610.

Ebersbach, G., and Gerdes, K. (2001). The double par locus of virulence factor pB171: DNA segregation is correlated with oscillation of ParA. *Proc Natl Acad Sci U S A* *98*, 15078-15083.

Egan, A.J., Biboy, J., van't Veer, I., Breukink, E., Vollmer, W. (2015). Activities and regulation of peptidoglycan synthases. *Philos Trans R Soc Lond Ser B Biol Sci* *370*.

Erickson, H.P. (2007). Evolution of the cytoskeleton. *Bioessays* *29*, 668–677.

Erickson, H.P. *et al.* (1996). Bacterial cell division protein FtsZ assembles into protofilament sheets and minirings, structural homologs of tubulin polymers. *Proc Natl Acad Sci U S A* *93*, 519–523.

Errington, J. (2003). Regulation of endospore formation in *Bacillus subtilis*. *Nat Rev Microbiol* *1*, 117–126.

Errington, J. (2015). Bacterial morphogenesis and the enigmatic MreB helix. *Nat Rev Microbiol* *13*, 241-248.

Erzberger, J.P., Mott, M.L., Berger, J.M. (2006). Structural basis for ATP-dependent

DnaA assembly and replication-origin remodeling. *Nat Struct Mol Biol* 13, 676–683.

Eswaramoorthy, P., Erb, M.L., Gregory, J.A., Silverman, J., Pogliano, K., Pogliano, J., Ramamurthi, K.S. (2011). Cellular architecture mediates DivIVA ultrastructure and regulates min activity in *Bacillus subtilis*. *MBio* 2.

Flardh, K. (2003a). Essential role of DivIVA in polar growth and morphogenesis in *Streptomyces coelicolor* A3(2). *Mol Microbiol* 49, 1523-1536.

Flardh, K. (2003b). Growth polarity and cell division in *Streptomyces*. *Curr Opin Microbiol* 6, 564-571.

Flardh, K., and Buttner, M.J. (2009). *Streptomyces* morphogenetics: dissecting differentiation in a filamentous bacterium. *Nat Rev Microbiol* 7, 36-49.

Flardh, K., Leibovitz, E., Buttner, M.J., and Chater, K.F. (2000). Generation of a non-sporulating strain of *Streptomyces coelicolor* A3(2) by the manipulation of a developmentally controlled *ftsZ* promoter. *Mol Microbiol* 38, 737-749.

Flardh, K., Richards, D.M., Hempel, A.M., Howard, M., and Buttner, M.J. (2012). Regulation of apical growth and hyphal branching in *Streptomyces*. *Curr Opin Microbiol* 15, 737-743.

Ferrari, E., Henner, D.J., Yang, M.Y. (1985). Isolation of an alanine racemase gene from *Bacillus subtilis* and its use for plasmid maintenance in *B. subtilis*. *Biotechnology* 3(11), 1003–1007.

Fuchino, K., Bagchi, S., Cantlay, S., Sandblad, L., Wu, D., Bergman, J., Kamali-Moghaddam, M., Flardh, K., and Ausmees, N. (2013). Dynamic gradients of an intermediate filament-like cytoskeleton are recruited by a polarity landmark during apical growth. *Proc Natl Acad Sci U S A* 110, E1889-1897.

Fuller, R. S., Funnell, B. E. and Kornberg, A. (1984). The DnaA protein complex with the *E. coli* chromosomal replication origin (*oriC*) and other DNA sites. *Cell* 38, 889-900.

Fuchino, K., Flardh, K., Dyson, P., and Ausmees, N. (2017). Cell-Biological Studies of Osmotic Shock Response in *Streptomyces* spp. *J Bacteriol* 199.

Fu, G., Huang, T., Buss, J., Coltharp, C., Hensel, Z., Xiao, J. (2010). In vivo structure of the *E. coli* FtsZ-ring revealed by photoactivated localization microscopy (PALM). *PLoS ONE* 5, e12682.

Fu, X., Shih, Y.L., Zhang, Y., Rothfield, L.I. (2001). The MinE ring required for proper placement of the division site is a mobile structure that changes its cellular location

during the *Escherichia coli* division cycle. Proc Natl Acad Sci U S A 98, 980–985.

Garner, E.C., Bernard, R., Wang, W., Zhuang, X., Rudner, D.Z., and Mitchison, T. (2011). Coupled, circumferential motions of the cell wall synthesis machinery and MreB filaments in *B. subtilis*. Science 333, 222–225.

Geissler, B., Elraheb, D., Margolin, W. (2003). A gain-of-function mutation in ftsA bypasses the requirement for the essential cell division gene zipA in *Escherichia coli*. Proc Natl Acad Sci U S A 100, 4197–4202.

Gerding, M.A., Liu, B., Bendezu, F.O., Hale, C.A., Bernhardt, T.G., De Boer, P.A. (2009). Self-enhanced accumulation of FtsN at division sites and roles for other proteins with a SPOR domain (DamX, DedD, and RlpA) in *Escherichia coli* cell constriction. J Bacteriol 191, 7383–7401.

Gueiros-Filho, F.J., Losick, R. (2002). A widely conserved bacterial cell division protein that promotes assembly of the tubulin-like protein FtsZ. Genes Dev 16, 2544–2556.

Gundogdu, M.E., Kawai, Y., Pavlendova, N., Ogasawara, N., Errington, J., Scheffers, D.J., and Hamoen, L.W. (2011). Large ring polymers align FtsZ polymers for normal septum formation. EMBO J 30, 617–626.

Goehring, N.W., Beckwith, J. (2005). Diverse paths to midcell: assembly of the bacterial cell division machinery. Curr Biol 15, 514–526..

Goffin, C., and Ghuysen, J.M. (1998). Multimodular penicillin-binding proteins: an enigmatic family of orthologs and paralogs. Microbiol Mol Biol Rev 62, 1079–1093

Gola, S., Munder, T., Casonato, S., Manganelli, R., Vicente, M. (2015). The essential role of SepF in mycobacterial division. Mol Microbiol 97(3), 560–76.

Goley, E.D. *et al.* (2011). Assembly of the caulobacter cell division machine. Mol Microbiol 80, 1680–1698.

Grantcharova, N., Lustig, U., and Flardh, K. (2005). Dynamics of FtsZ assembly during sporulation in *Streptomyces coelicolor* A3(2). J Bacteriol 187, 3227–3237.

Gupta, S., Banerjee, S.K., Chatterjee, A., Sharma, A.K., Kundu, M., Basu, J. (2015). Essential protein SepF of mycobacteria interacts with FtsZ and MurG to regulate cell growth and division. Microbiology 161, 1627–1638.

Gust, B., Challis, G.L., Fowler, K., Kieser, T., and Chater, K.F. (2003). PCR-targeted *Streptomyces* gene replacement identifies a protein domain needed for biosynthesis of the sesquiterpene soil odor geosmin. Proc Natl Acad Sci U S A 100, 1541–1546.

Haeusser, D.P., and Margolin, W. (2016). Splitsville: structural and functional insights into the dynamic bacterial Z ring. *Nat Rev Microbiol* 14, 305-319.

Hajduk, I.V., Rodrigues, C.D., and Harry, E.J. (2016). Connecting the dots of the bacterial cell cycle: Coordinating chromosome replication and segregation with cell division. *Semin Cell Dev Biol* 53, 2-9.

Hamoen, L.W., Meile, J.C., de Jong, W., Noirot, P., and Errington, J. (2006). SepF, a novel FtsZ-interacting protein required for a late step in cell division. *Mol Microbiol* 59, 989–999.

Hanahan, D. (1983). Studies on transformation of *Escherichia coli* with plasmids. *J Mol Biol* 166, 557-580.

Hale, C.A., de Boer, P.A.J. (1997). Direct binding of FtsZ to ZipA, an essential component of the septal ring structure that mediates cell division in *E. coli*. *Cell* 88, 175–185.

Hale, C.A., de Boer, P.A. (1999). Recruitment of ZipA to the septal ring of *Escherichia coli* is dependent on FtsZ and independent of FtsA. *J Bacteriol* 181, 167–176.

Hale, C.A., Meinhardt, H., De Boer, PA (2001). Dynamic localization cycle of the cell division regulator MinE in *Escherichia coli*. *EMBO J* 20, 1563–1572.

Hamoen, L.W., Meile, J.C., De Jong, W., Noirot, P., Errington, J. (2006). SepF, a novel FtsZ-interacting protein required for a late step in cell division. *Mol Microbiol* 59, 989–999.

Harry, E.J., Monahan, L., Thompson, L. (2006), Bacterial cell division: the mechanism and its precision. *Int Rev Cytol* 253, 27–94.

Hempel, A.M., Cantlay, S., Molle, V., Wang, S.B., Naldrett, M.J., Parker, J.L., Richards, D.M., Jung, Y.G., Buttner, M.J., and Flardh, K. (2012). The Ser/Thr protein kinase AfsK regulates polar growth and hyphal branching in the filamentous bacteria *Streptomyces*. *Proc Natl Acad Sci U S A* 109, E2371-2379.

Hempel, A.M., Wang, S.B., Letek, M., Gil, J.A., and Flardh, K. (2008). Assemblies of DivIVA mark sites for hyphal branching and can establish new zones of cell wall growth in *Streptomyces coelicolor*. *J Bacteriol* 190, 7579-7583.

Holmes, N.A., Walshaw, J., Leggett, R.M., Thibessard, A., Dalton, K.A., Gillespie, M.D., Hemmings, A.M., Gust, B., and Kelemen, G.H. (2013). Coiled-coil protein Scy is a key component of a multiprotein assembly controlling polarized growth in *Streptomyces*. *Proc Natl Acad Sci U S A* 110, E397-406.

Hopwood, D.A., Bibb, M., Chater, K., Bruton, C.J., Kieser, H., Lydiate, D.J., Smith, C.P., Ward, J.M., and Schrempf, H. (1985). Genetic Manipulation of *Streptomyces*. A Laboratory Manual. John Innes Foundation, Norwich.

Hopwood, D.A. (2007). Therapeutic treasures from the deep. *Nat Chem Biol* 3, 457–458.

Hu, Z., Gogol, E.P., Lutkenhaus, J. (2002). Dynamic assembly of MinD on phospholipid vesicles regulated by ATP and MinE. *Proc Natl Acad Sci U S A* 99, 6761–6766.

Hu, Z., Lutkenhaus, J. (2001). Topological regulation of cell division in *E. coli* spatiotemporal oscillation of MinD requires stimulation of its ATPase by MinE and phospholipid. *Mol Cell* 7, 1337–1343.

Hu, Z., Lutkenhaus, J. (2003). A conserved sequence at the C-terminus of MinD is required for binding to the membrane and targeting MinC to the septum. *Mol Microbiol* 47, 345–355.

Hu, Z., Mukherjee, A., Pichoff, S., Lutkenhaus, J. (1999). The MinC component of the division site selection system in *Escherichia coli* interacts with FtsZ to prevent polymerization. *Proc Natl Acad Sci U S A* 96, 14819–14824.

Hu, Z., Saez, C., Lutkenhaus, J. (2003). Recruitment of MinC, an inhibitor of Z-ring formation, to the membrane in *Escherichia coli*: role of MinD and MinE. *J Bacteriol* 185, 196–203.

Huang, K.H., Durand-Heredia, J., Janakiraman, A. (2013). FtsZ ring stability: of bundles, tubules, crosslinks, and curves. *J Bacteriol* 195, 1859–1868.

Ishikawa, S, Kawai, Y., Hiramatsu, K., Kuwano, M., Ogasawara, N. (2006). A new FtsZ-interacting protein, YlmF, complements the activity of FtsA during progression of cell division in *Bacillus subtilis*. *Mol Microbiol* 60, 1364–1380.

Jacob, F., and Brenner, S. (1963). On the regulation of DNA synthesis in bacteria: the hypothesis of the replicon. *C R Hebd Seances Acad Sci* 256, 298-300.

Jakimowicz, D., Gust, B., Zakrzewska-Czerwinska, J., and Chater, K.F. (2005). Developmental-stage-specific assembly of ParB complexes in *Streptomyces coelicolor* hyphae. *J Bacteriol* 187, 3572-3580.

Jakimowicz, D., Chater, K. and Zakrzewska-Czerwińska, J. (2002). The ParB protein of *Streptomyces coelicolor* A3(2) recognizes a cluster of parS sequences within the origin-proximal region of the linear chromosome. *Mol Microbiol* 45, 1365-1377.

Jakimowicz, D., Gust, B., Zakrzewska-Czerwińska, J. and Chater, K. F. (2005)

Developmental-stage-specific assembly of ParB complexes in *Streptomyces coelicolor* hyphae. *J Bacteriol* 187: 3572-3580.

Jakimowicz, D., Majka, J., Messer, W., Speck, C., Fernandez, M., Cruz Martin, M., Sanchez, J., Schauwecker, F., Keller, U., Schrempf, H. and Zakrzewska-Czerwińska, J. (1998). Structural elements of the *Streptomyces* oriC region and their interactions with the DnaA protein. *Microbiology* 144, 1281-1290.

Jakimowicz, D., van Wezel, G.P. (2012). Cell division and DNA segregation in *Streptomyces*: how to build a septum in the middle of nowhere? *Mol Microbiol* 85, 393-404.

Jones, L.J., Carballido-Lopez, R., and Errington, J. (2001). Control of cell shape in bacteria: helical, actin-like filaments in *Bacillus subtilis*. *Cell* 104, 913-922.

Jyothikumar, V., Tilley, E.J., Wali, R., and Herron, P.R. (2008). Time-lapse microscopy of *Streptomyces coelicolor* growth and sporulation. *Appl Environ Microbiol* 74, 6774-6781.

Kaguni, J. M. (2006). DnaA: controlling the initiation of bacterial DNA replication and more. *Annu Rev Microbiol* 60, 351-375.

Kang, C.M., Nyayapathy, S., Lee, J.Y., Suh, J.W., and Husson, R.N. (2008). Wag31, a homologue of the cell division protein DivIVA, regulates growth, morphology and polar cell wall synthesis in mycobacteria. *Microbiology* 154, 725-735.

Karimova, G., Dautin, N., Ladant, D. (2005). Interaction network among *Escherichia coli* membraneproteins involved in cell division as revealed by bacterial two-hybrid analysis. *J Bacteriol* 187,2233-2243.

Karimova, G., Ullmann, A., and Ladant, D. (2000). A bacterial two-hybrid system that exploits a cAMP signaling cascade in *Escherichia coli*. *Methods Enzymol* 328, 59-73.

Karoui, M.E., Errington, J. (2001). Isolation and characterization of topological specificity mutants of minD in *Bacillus subtilis*. *Mol Microbiol* 42,1211-1221.

Katayama, T., Ozaki, S., Keyamura, K., Fujimitsu, K. (2010). Regulation of the replication cycle: conserved and diverse regulatory systems for DnaA and oriC. *Nat Rev Microbiol* 8, 163-170.

Katis, VL, Wake, RG, Harry, E.J. (2000). Septal localization of the membrane-bound division proteins of *Bacillus subtilis* DivIB and DivIC is codependent only at high temperatures and requires FtsZ. *J Bacteriol* 182, 3607-3611.

Kawai, Y., Asai, K., and Errington, J. (2009). Partial functional redundancy of MreB

isoforms, MreB, Mbl and MreBH, in cell morphogenesis of *Bacillus subtilis*. Mol Microbiol 73, 719-731.

Kawai, Y., Ogasawara, N. (2006). *Bacillus subtilis* EzrA and FtsL synergistically regulate FtsZ ring dynamics during cell division. Microbiology 152, 1129–1141.

Keijsers, B.J., Noens, E.E., Kraal, B., Koerten, H.K., van Wezel, G.P. (2003). The *Streptomyces coelicolor* ssgB gene is required for early stages of sporulation. FEMS Microbiol Lett 225, 59–67.

Kelemen, G.H. (2017). Intermediate filaments supporting cell shape and growth in bacteria. Subcell Biochem 84, 161-211.

Kelemen, G.H., and Buttner, M.J. (1998). Initiation of aerial mycelium formation in *Streptomyces*. Curr Opin Microbiol 1, 656-662.

Kelemen, G.H., Brian, P., Flardh, K., Chamberlin, L., Chater, K.F., and Buttner, M.J. (1998). Developmental regulation of transcription of whiE, a locus specifying the polyketide spore pigment in *Streptomyces coelicolor* A3 (2). J Bacteriol 180, 2515-2521.

Kieser, T., Bibb, M., Buttner, M.J., Chater, K., and Hopwood, D.A. (2000). Practical *Streptomyces* Genetics. The John Innes Foundation.

Koonin, E.V. (1993). A superfamily of ATPases with diverse functions containing either classical or deviant ATP-binding motif. J Mol Biol 229, 1165-1174.

Krol, E., van Kessel, S. P., van Bezouwen, L. S., Kumar, N., Boekema, E. J., Scheffers, D. J. (2012). *Bacillus subtilis* SepF binds to the C-terminus of FtsZ. PLoS ONE 7, e43293.

Kruse, T., Bork-Jensen, J., and Gerdes, K. (2005). The morphogenetic MreBCD proteins of *Escherichia coli* form an essential membrane-bound complex. Mol Microbiol 55, 78-89.

Kwak, J., Dharmatilake, A.J., Jiang, H., and Kendrick, K.E. (2001). Differential regulation of ftsZ transcription during septation of *Streptomyces griseus*. J Bacteriol 183, 5092-5101.

Lackner, L.L., Raskin, D.M., de Boer, P.A.J. (2003). ATP-dependent interactions between *Escherichia coli* Min proteins and the phospholipid membrane in vitro. J Bacteriol 185, 735–749.

Leonard, A. C. and Grimwade, J. E. (2010). Regulating DnaA complex assembly: it is time to fill the gaps. Curr Opin Microbiol 13, 766-772.

- Leonard, T.A., Butler, P.J., and Lowe, J. (2005). Bacterial chromosome segregation: structure and DNA binding of the Soj dimer- a conserved biological switch. *EMBO J* *24*, 270-282.
- Letek, M., Ordonez, E., Vaquera, J., Margolin, W., Flardh, K., Mateos, L.M., and Gil, J.A. (2008). DivIVA is required for polar growth in the MreB-lacking rod-shaped actinomycete *Corynebacterium glutamicum*. *J Bacteriol* *190*, 3283-3292.
- Levin, P.A., Losick, R. (1994). Characterization of a cell division gene from *Bacillus subtilis* that is required for vegetative and sporulation septum formation. *J Bacteriol* *176*, 1451–1459.
- Levin, PA, Margolis, P.S., Setlow, P., Losick, R., Sun, D. (1992). Identification of *Bacillus subtilis* genes for septum placement and shape determination. *J Bacteriol* *174*, 6717–6728.
- Lin, Y.S., Kieser, H.M., Hopwood, D.A., and Chen, C.W. (1993). The chromosomal DNA of *Streptomyces lividans* 66 is linear. *Mol Microbiol* *10*, 923-933.
- Livny, J., Yamaichi, Y., and Waldor, M.K. (2007). Distribution of centromere-like *parS* sites in bacteria: insights from comparative genomics. *J Bacteriol* *189*, 8693-8703.
- Lowe, J., Amos, L.A. (1998). Crystal structure of the bacterial cell-division protein FtsZ. *Nature* *391*, 203–206.
- Lovering, A.L., Safadi, S.S., Strynadka, N.C. (2012). Structural perspective of peptidoglycan biosynthesis and assembly. *Annu Rev Biochem* *81*, 451–478.
- Lutkenhaus, J., Addinall, S.G. (1997). Bacterial cell division and the Z ring. *Annu Rev Biochem* *66*, 93–116.
- Lutkenhaus, J. (2007). Assembly dynamics of the bacterial MinCDE system and spatial regulation of the Z ring. *Annu Rev Biochem* *76*, 539–562.
- Lutkenhaus, J. (2012). The ParA/MinD family puts things in their place. *Trends Microbiol* *20*, 411-418.
- Lutkenhaus, J., Du, S., (2017). Assembly and activation of the *Escherichia coli* divisome. *Molecular Microbiology* *105*(2), 177–187.
- Ma, X., Margolin, W. (1999). Genetic and functional analyses of the conserved C-terminal core domain of *Escherichia coli* FtsZ. *J Bacteriol* *181*, 7531–7544.

MacNeil, D.J., Gewain, K.M., Ruby, C.L., Dezeny, G., Gibbons, P.H., and MacNeil, T. (1992). Analysis of *Streptomyces avermitilis* genes required for avermectin biosynthesis utilizing a novel integration vector. *Gene* 111, 61-68.

Makarova, K.S., Yutin, N., Bell, S.D., and Koonin, E.V. (2010). Evolution of diverse cell division and vesicle formation systems in Archaea. *Nat Rev Microbiol* 8, 731–741.

Majka, J., Zakrzewska-Czerwińska, J. and Messer, W. (2001). Sequence recognition, cooperative interaction, and dimerization of the initiator protein DnaA of *Streptomyces*. *J Biol Chem* 276, 6243- 6252

Marbouty, M., Saguez, C., Cassier-Chauvat, C., and Chauvat, F. (2009). Characterization of the FtsZ-interacting septal proteins SepF and Ftn6 in the spherical-celled cyanobacterium *Synechocystis* strain PCC6803. *J Bacteriol* 191, 6178–6185.

Marston, A.L., and Errington, J. (1999). Selection of the midcell division site in *Bacillus subtilis* through MinD-dependent polar localization and activation of MinC. *Mol Microbiol* 33, 84-96.

Marston, A.L., Thomaidis, H.B., Edwards, D.H., Sharpe, M.E., and Errington, J. (1998). Polar localization of the MinD protein of *Bacillus subtilis* and its role in selection of the mid-cell division site. *Genes Dev* 12, 3419-3430.

Margolin, W. (2000). Organelle division: Self-assembling GTPase caught in the middle. *Curr Biol* 10, R328-330.

Margolin, W. (2001). Bacterial cell division: a moving MinE sweeper boggles the MinD. *Curr Biol* 11, R395-398.

Margolin, W. (2005). FtsZ and the division of prokaryotic cells and organelles. *Nat Rev Mol Cell Biol* 6(11), 862–871.

Mazza, P., Noens, E. E., Schirner, K., Grantcharova, N., Mommaas, A. M., Koerten, H. K., Muth, G., Flårdh, K., van Wezel, G. P. and Wohlleben, W. (2006). MreB of *Streptomyces coelicolor* is not essential for vegetative growth but is required for the integrity of aerial hyphae and spores. *Mol Microbiol* 60, 838-852.

McCormick, J.R., Flardh, K. (2012), Signals and regulators that govern *Streptomyces* development. *FEMS Microbiol Rev* 36, 206–231.

McCormick, J.R., Su, E.P., Driks, A., and Losick, R. (1994). Growth and viability of *Streptomyces coelicolor* mutant for the cell division gene *ftsZ*. *Mol Microbiol* 14, 243-254.

Meinhardt, H., de Boer, P.A.J. (2001). Pattern formation in *Escherichia coli*: a model for the pole-to-pole oscillations of Min proteins and the localization of the division site. *PNAS* 98, 14202–14207.

Meniche, X., Otten, R., Siegrist, M.S., Baer, C.E., Murphy, K.C., Bertozzi, C.R., and Sassetti, C.M. (2014). Subpolar addition of new cell wall is directed by DivIVA in mycobacteria. *Proc Natl Acad Sci U S A* 111, E3243-3251.

McCormick, J.R., Su, E.P., Driks, A., and Losick, R. (1994). Growth and viability of *Streptomyces coelicolor* mutant for the cell division gene *ftsZ*. *Mol Microbiol* 14, 243-254.

Michie, K.A., Monahan, L.G., Beech, P.L., Harry, E.J. (2006). Trapping of a spiral-like intermediate of the bacterial cytokinetic protein FtsZ. *J Bacteriol* 188, 1680–1690.

Mingorance, J., Tadros, M., Vicente, M., Gonzalez, J.M., Rivas, G., Velez, M. (2005). Visualization of single *Escherichia coli* FtsZ filament dynamics with atomic force microscopy. *J Biol Chem* 280, 20909–20914.

Miyagishima, S.Y., Wolk, C.P., and Osteryoung, K.W. (2005). Identification of cyanobacterial cell division genes by comparative and mutational analyses. *Mol Microbiol*. 56, 126–143.

Mohammadi, T., Van Dam, V., Sijbrandi, R., Vernet, T., Zapun, A., Bouhss, A., Diepeveen-De, Bruin M., Nguyen-Disteche, M., de Kruijff, B., Breukink, E. (2011). Identification of FtsW as a transporter of lipid-linked cell wall precursors across the membrane. *EMBO J* 30, 1425–1432.

Mori, H., Mori, Y., Ichinose, C., Niki, H., Ogura, T., Kato, A., and Hiraga, S. (1989). Purification and characterization of SopA and SopB proteins essential for F plasmid partitioning. *J Biol Chem* 264, 15535-15541.

Mukherjee, A., Lutkenhaus, J. (1998). Dynamic assembly of FtsZ regulated by GTP hydrolysis. *EMBO J* 17, 462–469.

Mukherjee, P., Sureka, K., Datta, P., Hossain, T., Barik, S., Das, K.P., Kundu, M., and Basu, J. (2009). Novel role of Wag31 in protection of mycobacteria under oxidative stress. *Mol Microbiol* 73, 103-119.

Muller, P., Ewers, C., Bertsche, U., Anstett, M., Kallis, T., Breukink, E., Fraipont, C., Terrak, M., Nguyen-Disteche, M., Vollmer, W. (2007). The essential cell division protein FtsN interacts with the murein (peptidoglycan) synthase PBP1B in *Escherichia coli*. *J Biol Chem* 282,36394–36402.

- Murray, H., and Errington, J. (2008). Dynamic control of the DNA replication initiation protein DnaA by Soj/ParA. *Cell* *135*, 74-84.
- Nanninga, N. (1998). Morphogenesis of *Escherichia coli*. *Microbiol Mol Biol Rev* *62*, 110-129.
- Nguyen, L., Scherr, N., Gatfield, J., Walburger, A., Pieters, J., and Thompson, C.J. (2007). Antigen 84, an effector of pleiomorphism in *Mycobacterium smegmatis*. *J Bacteriol* *189*, 7896-7910.
- Noens, E.E., Mersinias, V., Traag, B.A., Smith, C.P., Koerten, H.K., van Wezel, G.P. (2005). SsgA-like proteins determine the fate of peptidoglycan during sporulation of *Streptomyces coelicolor*. *Mol Microbiol* *58*, 929-944.
- Nogales, E., Downing, K.H., Amos, L.A., Lowe, J. (1998). Tubulin and FtsZ form a distinct family of GTPases. *Nat Struct Biol* *5*, 451-458.
- Ohashi, T., Hale, C.A., de Boer, P.A., and Erickson, H.P. (2002). Structural evidence that the P/Q domain of ZipA is an unstructured, flexible tether between the membrane and the C-terminal FtsZ-binding domain. *J Bacteriol* *184*, 4313-4315.
- Oliva, M.A., Halbedel, S., Freund, S.M., Dutow, P., Leonard, T.A., Veprintsev, D.B., Hamoen, L.W., and Lowe, J. (2010). Features critical for membrane binding revealed by DivIVA crystal structure. *EMBO J* *29*, 1988-2001.
- Olshausen, P.V., Defeu Soufo, H.J., Wicker, K., Heintzmann, R., Graumann, P.L., and Rohrbach, A. (2013). Superresolution imaging of dynamic MreB filaments in *B. subtilis*--a multiple-motor-driven transport? *Biophys J* *105*, 1171-1181.
- Osawa, M., Anderson, D.E., Erickson, H.P. (2008). Reconstitution of contractile FtsZ rings in liposomes. *Science* *320*: 792-794.
- Park, K.T., Wu, W., Battaile, K.P., Lovell, S., Holyoak, T., Lutkenhaus, J. (2011). The Min oscillator uses MinD-dependent conformational changes in MinE to spatially regulate cytokinesis. *Cell* *146*, 396-407.
- Park, K.T., Wu, W., Lovell, S., Lutkenhaus, J. (2012). Mechanism of the asymmetric activation of the MinD ATPase by MinE. *Mol Microbiol* *85*, 271-281.
- Patrick, J.E., and Kearns, D.B. (2008). MinJ (YvjD) is a topological determinant of cell division in *Bacillus subtilis*. *Mol Microbiol* *70*, 1166-1179.
- Pichoff, S., Lutkenhaus, J. (2002). Unique and overlapping roles for ZipA and FtsA in septal ring assembly in *Escherichia coli*. *EMBO J* *21*, 685-693.

Pichoff, S., Lutkenhaus, J. (2005). Tethering the Z ring to the membrane through a conserved membrane targeting sequence in FtsA. *Mol Microbiol* 55, 1722–1734.

Pichoff, S., Shen, B., Sullivan, B., Lutkenhaus, J. (2012). FtsA mutants impaired for self-interaction bypass ZipA suggesting a model in which FtsA's self-interaction competes with its ability to recruit downstream division proteins. *Mol Microbiol* 83, 151–167.

Ramamurthi, K.S., Losick, R. (2009). Negative membrane curvature as a cue for subcellular localization of a bacterial protein. *Proc Natl Acad Sci U S A* 106, 13541–13545.

Ramos, A., Honrubia, M.P., Valbuena, N., Vaquera, J., Mateos, L.M., and Gil, J.A. (2003). Involvement of DivIVA in the morphology of the rod-shaped actinomycete *Brevibacterium lactofermentum*. *Microbiology* 149, 3531-3542.

Raskin, D.M., de Boer, P.A. (1999). Rapid pole-to-pole oscillation of a protein required for directing division to the middle of *Escherichia coli*. *Proc Natl Acad Sci U S A* 96, 4971–4976.

Raychaudhuri, D. (1999). ZipA is a MAP-Tau homolog and is essential for structural integrity of the cytokinetic FtsZ ring during bacterial cell division. *EMBO J* 18, 2372–2383.

Raychaudhuri, D., Park, J.T. (1992). *Escherichia coli* cell-division gene ftsZ encodes a novel GTP-binding protein. *Nature* 359, 251–254.

Redenbach, M., Kieser, H.M., Denapaite, D., Eichner, A., Cullum, J., Kinashi, H., and Hopwood, D.A. (1996). A set of ordered cosmids and a detailed genetic and physical map for the 8 Mb *Streptomyces coelicolor* A3(2) chromosome. *Mol Microbiol* 21, 77-96.

Reimold, C., Defeu, Soufo, H.J., Dempwolff, F., and Graumann, P.L. (2013). Motion of variable-length MreB filaments at the bacterial cell membrane influences cell morphology. *Mol Biol Cell* 24, 2340-2349.

Richards, D.M., Hempel, A.M., Flardh, K., Buttner, M.J., and Howard, M. (2012). Mechanistic basis of branch-site selection in filamentous bacteria. *PLoS Comput Biol* 8, e1002423.

Rutherford, K., Parkhill, J., Crook, J., Hornsnell, T., Rice, P., Rajandream, M. and Barrell, B. (2000). Artemis: sequence visualisation and annotation, *Bioinformatics* (Oxford, England), 16 (10), 944-945 .

Saalbach, G., Hempel, A.M., Vigouroux, M., Flardh, K., Buttner, M.J., and Naldrett, M.J. (2013). Determination of phosphorylation sites in the DivIVA cytoskeletal protein of

- Streptomyces coelicolor* by targeted LC-MS/MS. *J Proteome Res* 12, 4187-4192.
- Salje, J., van den Ent, F., de Boer, P., and Lowe, J. (2011). Direct membrane binding by bacterial actin MreB. *Mol Cell* 43, 478-487.
- Schwedock, J., McCormick, J.R., Angert, E.R., Nodwell, J.R., and Losick, R. (1997). Assembly of the cell division protein FtsZ into ladder-like structures in the aerial hyphae of *Streptomyces coelicolor*. *Mol Microbiol* 25, 847-858.
- Sharp, M.D., and Pogliano, K. (2003). The membrane domain of SpoIIIE is required for membrane fusion during *Bacillus subtilis* sporulation. *J Bacteriol* 185, 2005-2008.
- Shaw, J.P., Petsko, G.A., Ringe, D. (1997). Determination of the structure of alanine racemase from *Bacillus stearothermophilus* at 1.9-Å resolution. *Biochemistry* 36(6), 1329-1342.
- Shih, Y.L., Le, T., Rothfield, L. (2003). Division site selection in *Escherichia coli* involves dynamic redistribution of Min proteins within coiled structures that extend between the two cell poles. *Proc Natl Acad Sci U S A* 100, 7865-7870.
- Singh, J.K., Makde, R.D., Kumar, V., Panda, D. (2008). SepF increases the assembly and bundling of FtsZ polymers and stabilizes FtsZ protofilaments by binding along its length. *Biol Chem* 283(45), 31116-24.
- Storts, D.R., Aparicio, O.M., Schoemaker, J.M., and Markovitz, A. (1989). Overproduction and identification of the ftsQ gene product, an essential cell division protein in *Escherichia coli* K-12. *J Bacteriol* 171, 4290-4297.
- Sieger, B., Schubert, K., Donovan, C., and Bramkamp, M. (2013). The lipid II flippase RodA determines morphology and growth in *Corynebacterium glutamicum*. *Mol Microbiol* 90, 966-982.
- Sievers, J., Raether, B., Perego, M., Errington, J. (2002). Characterization of the parB-like yyaA gene of *Bacillus subtilis*. *J Bacteriol* 184, 1102-1111.
- Stricker, J., Maddox, P., Salmon, E.D., Erickson, H.P. (2002). Rapid assembly dynamics of the *Escherichia coli* FtsZ-ring demonstrated by fluorescence recovery after photobleaching. *Proc Natl Acad Sci U S A* 99, 3171-3175.
- Studier, F.W., and Moffatt, B.A. (1986). Use of bacteriophage T7 RNA polymerase to direct selective high-level expression of cloned genes. *J Mol Biol* 189, 113-130.
- Swilius, M.T., Chen, S., Jane Ding, H., Li, Z., Briegel, A., Pilhofer, M., Tocheva, E.I., Lybarger, S.R., Johnson, T.L., Sandkvist, M., *et al.* (2011). Long helical filaments are not seen encircling cells in electron cryotomograms of rod-shaped bacteria. *Biochem*

Biophys Res Commun 407, 650-655.

Szeto, T.H., Rowland, S.L., Rothfield, L.I., King, G.F. (2002). Membrane localization of MinD is mediated by a C-terminal motif that is conserved across eubacteria, archaea, and chloroplasts. Proc Natl Acad Sci U S A 99, 15693–15698.

Szwedziak, P., Wang, Q., Freund, S.M., Lowe, J. (2012). FtsA forms actin-like protofilaments. EMBO J 31, 2249–2260.

Tamames, J, González-Moreno, M., Mingorance, J., Valencia, A., Vicente, M. (2001). Bringing gene order into bacterial shape. Trends Genet 17, 124–126.

Tonthat, N.K., Arold, S.T., Pickering, B.F., Van Dyke, M.W., Liang, S., Lu, Y., Beuria, T.K., Margolin, W., Schumacher, M.A. (2011). Molecular mechanism by which the nucleoid occlusion factor, SlmA, keeps cytokinesis in check. EMBO J 30, 154–164.

Tonthat, N.K., Milam, S.L., Chinnam, N., Whitfill, T., Margolin, W., Schumacher, M.A. (2013). SlmA forms a higher-order structure on DNA that inhibits cytokinetic Z-ring formation over the nucleoid. Proc Natl Acad Sci U S A 110, 10586–10591.

Touzain, F., Petit, M.A., Schbath, S., and El Karoui, M. (2011). DNA motifs that sculpt the bacterial chromosome. Nat Rev Microbiol 9, 15-26.

Traag, B.A., van Wezel, G.P. (2008). The SsgA-like proteins in actinomycetes: small proteins up to a big task. Antonie Van Leeuwenhoek 94, 85–97.

Ursinus, A., Van Den Ent, F., Brechtel, S., De Pedro, M, Holtje, J.V., Lowe, J., Vollmer, W. (2004). Murein (peptidoglycan) binding property of the essential cell division protein FtsN from *Escherichia coli*. J Bacteriol 186, 6728–6737.

van den Ent, F., Amos, L., and Lowe, J. (2001a). Bacterial ancestry of actin and tubulin. Curr Opin Microbiol 4, 634-638.

van den Ent, F., Amos, L.A., and Lowe, J. (2001b). Prokaryotic origin of the actin cytoskeleton. Nature 413, 39-44.

Van Den Ent, F., Löwe, J. (2000). Crystal structure of the cell division protein FtsA from *Thermotoga maritima*. EMBO J 19, 5300–5307.

van den Ent, F., Izore, T., Bharat, T.A., Johnson, C.M., and Lowe, J. (2014). Bacterial actin MreB forms antiparallel double filaments. Elife 3, e02634.

van den Ent, F., Vinkenvleugel, T.M., Ind, A., West, P., Veprintsev, D., Nanninga, N., den Blaauwen, T., and Lowe, J. (2008). Structural and mutational analysis of the cell division protein FtsQ. Molecular microbiology 68, 110-123.

van Teeffelen, S., Wang, S., Furchtgott, L., Huang, K.C., Wingreen, N.S., Shaevitz, J.W., and Gitai, Z. (2011). The bacterial actin MreB rotates, and rotation depends on cell-wall assembly. *Proc Natl Acad Sci U S A* *108*, 15822-15827.

van Wezel, G.P., van der Meulen, J., Kawamoto, S., Luiten, R.G., Koerten, H.K., and Kraal, B. (2000). *ssgA* is essential for sporulation of *Streptomyces coelicolor* A3(2) and affects hyphal development by stimulating septum formation. *J Bacteriol* *182*, 5653-5662.

van Wezel, G. P. and McDowall, K. J. (2011) The regulation of the secondary metabolism of *Streptomyces*: new links and experimental advances. *Nat Prod Rep* *28*, 1311-1333.

Varley, A.W., and Stewart, G.C. (1992). The *divIVB* region of the *Bacillus subtilis* chromosome encodes homologs of *Escherichia coli* septum placement (*minCD*) and cell shape (*mreBCD*) determinants. *J Bacteriol* *174*, 6729-6742.

Vaughan, S. *et al.* (2004). Molecular evolution of FtsZ protein sequences encoded within the genomes of archaea, bacteria, and eukaryota. *J Mol Evol* *58*(1), 19–29.

Vicente, M., Rico, A.I. (2006) The order of the ring: assembly of *Escherichia coli* cell division components. *Mol Microbiol* *61*, 5–8.

Viollier, P.H., Thanbichler, M., McGrath, P.T., West, L., Meewan, M., McAdams, H.H., and Shapiro, L. (2004). Rapid and sequential movement of individual chromosomal loci to specific subcellular locations during bacterial DNA replication. *Proc Natl Acad Sci U S A* *101*, 9257-9262.

Wachi, M., Doi, M., Tamaki, S., Park, W., Nakajima-Iijima, S., and Matsushashi, M. (1987). Mutant isolation and molecular cloning of *mre* genes, which determine cell shape, sensitivity to mecillinam, and amount of penicillin-binding proteins in *Escherichia coli*. *J Bacteriol* *169*, 4935-4940.

Walshaw, J., Gillespie, M.D., and Kelemen, G.H. (2010). A novel coiled-coil repeat variant in a class of bacterial cytoskeletal proteins. *J Struct Biol* *170*, 202-215.

Walter, S., Wellmann, E., and Schrempf, H. (1998). The cell wall-anchored *Streptomyces reticuli* avicel-binding protein (AbpS) and its gene. *J Bacteriol* *180*, 1647-1654.

Wang, Y., Jones, B.D., Brun, Y.V. (2001). A set of *ftsZ* mutants blocked at different stages of cell division in *Caulobacter*. *Mol Microbiol* *40*(2), 347–360.

Watanabe, E., Inamoto, S., Lee, M.H., Kim, S.U., Oguwa, T., Mori, H., Hiraga, S.,

- Yamasaki, M., and Nagai, K. (1989). Purification and characterization of the *sopB* gene product which is responsible for stable maintenance of mini-F plasmid. *Mol Gen Genet* 218, 431-436.
- Wasserman, S.A., Daub, E., Grisafi, P. (1984). Catabolic alanine racemase from *Salmonella typhimurium*: DNA sequence enzyme purification and characterization. *Biochemistry* 23(22), 5182–5187.
- Weiss, D.S. (2004). Bacterial cell division and the septal ring. *Mol Microbiol* 54, 588-597.
- Wijsman, H.J. (1972). The characterization of an alanine racemase mutant of *Escherichia coli*. *Genet Res* 20(3), 269–277.
- Willemse, J. *et al.* (2011). Positive control of cell division: FtsZ is recruited by SsgB during sporulation of *Streptomyces*. *Genes Dev* 25, 89–99.
- Wolański, M., Jakimowicz, D. and Zakrzewska-Czerwińska, J. (2014). Fifty years after the replicon hypothesis: cell-specific master regulators as new players in chromosome replication control. *J Bacteriol* 196, 2901-2911.
- Wolański, M., Wali, R., Tilley, E., Jakimowicz, D., Zakrzewska-Czerwinska, J. and Herron, P. (2011b) Replisome trafficking in growing vegetative hyphae of *Streptomyces coelicolor* A3(2). *J Bacteriol* 193, 1273-1275.
- Woldringh, C.L., Mulder, E., Valkenburg, J.A., Wientjes, F.B., Zaritsky, A., Nanninga, N. (1990). Role of the nucleoid in the toporegulation of division. *Res Microbiol* 141, 39–49.
- Wu, L.J., Errington, J. (2003). RacA and the Soj-Spo0J system combine to effect polar chromosome segregation in sporulating *Bacillus subtilis*. *Mol Microbiol* 49, 1463–1475.
- Wu, L.J., Errington, J. (2004). Coordination of cell division and chromosome segregation by a nucleoid occlusion protein in *Bacillus subtilis*. *Cell* 117, 915–925.
- Wu, L.J., Errington, J. (2012). Nucleoid occlusion and bacterial cell division. *Nat Rev Microbiol*, 10, 8–12.
- Wu, L.J., Ishikawa, S., Kawai, Y., Oshima, T., Ogasawara, N., Errington, J. (2009) Noc protein binds to specific DNA sequences to coordinate cell division with chromosome segregation. *EMBO J* 28, 1940–1952.
- Wu, W., Park, K.T., Holyoak, T., Lutkenhaus, J. (2011) Determination of the structure of the MinD- ATP complex reveals the orientation of MinD on the membrane and the

relative location of the binding sites for MinE and MinC. *Mol Microbiol* 79, 1515–1528.

Yu, X.C., Margolin, W. (1999) FtsZ ring clusters in min and partition mutants: role of both the Min system and the nucleoid in regulating FtsZ ring localization. *Mol Microbiol* 32, 315–326.

Zakrzewska-Czerwińska, J., Jakimowicz, D., Zawilak-Pawlik, A. and Messer, W. (2007). Regulation of the initiation of chromosomal replication in bacteria. *FEMS Microbiol Rev* 31, 378-387.